

NORTHWESTERN UNIVERSITY

Mitochondrial Complex I Function in Leigh Syndrome and Aging.

A DISSERTATION

SUBMITTED TO THE GRADUATE SCHOOL
IN PARTIAL FULFILLMENT OF THE REQUIREMENTS

for the degree

DOCTOR OF PHILOSOPHY

Field of Driskill Graduate Training Program in Life Sciences

By

Gregory Scott McElroy

EVANSTON, ILLINOIS

September 2020

© Copyright by Gregory Scott McElroy 2020

All Rights Reserved

Abstract

Mitochondrial complex I is the primary entry point for electrons into the mitochondrial electron transport chain that is composed of 45 individual protein subunits that are encoded in both the nuclear and mitochondrial genomes. Mitochondrial complex I sits at an important nexus in the essential bioenergetic, biosynthetic, and signaling functions of mitochondria and is therefore a key regulator of metabolism and cellular and organismal function. Numerous previous studies have identified that severe reductions in mitochondrial complex I function through mutation or pharmacological inhibition can cause neurometabolic mitochondrial diseases such as Leigh syndrome and neurodegeneration in humans and animal models. Mitochondrial complex I function has been shown to decline with aging and is therefore associated with many aging-related pathologies including the common neurodegenerative diseases of aging such as Alzheimer's disease and Parkinson's disease. Despite these findings, numerous studies in small, short-lived model organisms have demonstrated that knockdown of mitochondrial complex I function can paradoxically increase lifespan. Furthermore, the anti-diabetic drug metformin, which is currently being investigated as a possible anti-cancer and anti-aging therapeutic, may mediate its effects through mild inhibition of mitochondrial complex I. Therefore, in this study, I sought to further explore the role of mitochondrial complex I function in malignancy, neurodegeneration, and aging with novel animal models and with a hypothesis that the toxic metabolite L-2-hydroxyglutarate may act as an effector of mitochondrial dysfunction-induced pathology. In the first set of experiments, I describe a novel mouse model in which tissue-specific expression of the yeast enzyme NDI1 is possible. I show that NDI1 complements loss of the supernumerary complex I subunit NDUFS4 in the brain of mice to prevent an early fatal phenotype but does not prevent motor impairment that is a hallmark of NDUFS4 loss. In the second set of experiments, I focus on the possible role of 2-hydroxyglutarate as a causative mechanism by which mitochondrial dysfunction can lead to cellular and organismal pathology using human cancer cell lines, genetically modified *Drosophila melanogaster*, and measurement of 2-hydroxyglutarate in mouse models. Finally, in the last set of experiments I seek to further characterize the impact of mild mitochondrial complex I function on lifespan, organismal function, and cellular gene expression in aged mice with ubiquitous loss of one allele of the essential complex I subunit NDUFS2.

Acknowledgements

There are many people to thank who have contributed to the projects described in this dissertation and who have supported me in my academic and personal journey. I thank the following core facilities at Northwestern University: Transgenic and Targeted Mutagenesis Laboratory (Rajeshwar Awatramani, Lynn Doglio), CTI Small Animal Imaging Core (Sol Misener, Daniele Procissi, Nicola Bertolino), Behavioral Phenotyping Core (Craig Weiss, Mary Kando), Pulmonary NextGen Sequencing Core (Hiam Abdala-Valencia, Kiwon Nam, Yuliya Politanska), RHLCCC Metabolomics Core (Peng Gao), Mouse Histology and Phenotyping Laboratory (Katherine Gruner, Hong Chang), Center for Advanced Microscopy, RHLCCC Flow Cytometry Core Facility. Histology services were provided by the Northwestern University Mouse Histology and Phenotyping Laboratory which is supported by NCI P30-CA060553 awarded to the Robert H Lurie Comprehensive Cancer Center. I thank Michele Hadhazy and Elizabeth McNally for the use of Whole-Body Plethysmography equipment. I thank the Center for Comparative Medicine animal husbandry and veterinary staff for their support of our experimental laboratory mouse colonies. I thank Paul Reyfman, Benjamin Singer, Kishore Anekalla, and Elizabeth Bartom for the use of their code and the Ceto pipeline for bioinformatic analyses. I thank Eric Dufour from the University of Tampere for reagent provision (NDI1 antibody). I thank the many co-workers, collaborators, and co-authors who have contributed directly and indirectly to this dissertation and who I have worked with closely over the past few years including: Divakar Mithal, Colleen Reczek, Inma Martinez-Reyes, Craig Horbinski, Ram Chakrabarty, Lauren Diebold Petrovich, Lizzie Steinert, Hyewon Kong, James Eisenbart, Josh Stoolman, Karthik Vasan, Leah Billingham, Sam Weinberg, Luzi Robles Cardona, Taylor Poor, Emma Baar, Ari Rodriguez, Paul Reyfman, Benjamin Signer, Jennifer Hu, Karen Ridge, Francisco Gonzalez, Scott Budinger, Ziyang Lu, Satoshi Watanabe, Sasha Misharin, Nikolay Markov, Luisa Morales-Nebreda, Nikita Joshi, Rachel Hunt, Lucy Granat, Ramya Ranganathan, and Joe Bateman. I thank the MSTP program and DGP staff and leadership for their support. I thank my thesis committee members Dr. Scott Budinger, Dr. Paul Schumacker, and Dr. James Surmeier for their time, support, and helpful suggestions and resources. I would especially like to thank my friends and family for their support during graduate school. Funding for this project was provided by the following NIH grants to

my mentor Navdeep Chandel NIH2PO1HL071643-11A1, NIH1R35CA197532-01, NIH1PO1AG049665-01. I was supported by three different NIH T32 training grants including the carcinogenesis training grant (5 T32 CA 9560-32), the pulmonary training grant (5 T32 HL 76139-13) and the MSTP training grant (5 T32 GM 008152-28).

List of Abbreviations

143B (human osteosarcoma cell line)
 2HG (2-hydroxyglutarate)
 AAV (adeno-associated virus)
 AD (Alzheimer's disease)
 ADP (adenosine diphosphate)
 ALS (amyotrophic lateral sclerosis)
 AMP (adenosine monophosphate)
 AMPK (AMP-activated protein kinase)
 AOA (aminooxyacetate)
 AOX (*Ciona intestinalis* alternate oxidase)
 ART (ADP ribosyltransferase)
 asyn (alpha-synuclein)
 ATF4 (activating transcription factor 4)
 ATF5 (activating transcription factor 5)
 ATP (adenosine triphosphate)
 ATPIF1 (ATP synthase inhibitory factor subunit 1)
 Bcl2 (B-cell lymphoma 2 apoptosis regulator)
 bZIP (basic leucine zipper domain)
 C (cytochrome c)
 Ca (calcium)
 Cas9 (CRISPR associated protein 9)
 cGAS (cyclic GMP-AMP synthase)
 CHOP (CCAAT/enhancer binding protein homologous protein)
 CMT (Charcot-Marie-Tooth disease)
 CNS (central nervous system)
 CO₂ (carbon dioxide)
 CoA (coenzyme A)
 CoQ (ubiquinone)
 CR caloric restriction (CR)
 CRAC (calcium release-activated channels)
 CRISPR (clustered regularly interspersed short palindromic repeats)
 CRP (C-reactive protein)
 CytB (cytochrome b)
 D-2HG (D/R enantiomer of 2 hydroxyglutarate)
 D2HGDH (D-2HG dehydrogenase)
 DDIT3 (DNA damage inducible transcript 3)
 DHODH (dihydroorotate dehydrogenase)
 DNA (deoxyribonucleic acid)
 E2F (E2 family transcription factors)
 ETC (electron transport chain)
 FADH₂ (flavin adenine dinucleotide – reduced form)
 FGF21 fibroblast growth factor 21 (FGF21)
 FH (fumarate hydratase)
 FIH (factor inhibiting HIF)
 FMN (flavin mononucleotide)
 FRTA (free-radical theory of aging)
 G2M (cell cycle phase G2 to mitosis transition/checkpoint)
 GABA (gamma-aminobutyric acid)
 Gad2 (glutamate decarboxylase 2)
 GDF15 (growth differentiation factor 15)
 GFAP (glial fibrillary acidic protein)
 GMP (guanosine monophosphate)

GP33 (LCMV glycoprotein 33)
 GSEA (Gene Set Enrichment Analysis)
 GTP (guanosine triphosphate)
 H₂O (water)
 HD (Huntington's disease)
 HIF (hypoxia inducible factor)
 HIV-TAT (human immunodeficiency virus trans-activator of transcription)
 HSC (hematopoietic stem cell)
 IDH (isocitrate dehydrogenase)
 IGF (insulin-like growth factor)
 IL-2 (interleukin 2)
 IL-6 (interleukin-6)
 iPSC (induced pluripotent stem cell)
 ISR (integrated stress response)
 K_m (Michaelis constant)
 KO (knock-out)
 Kras (Kirsten rat sarcoma virus oncogene)
 L-2HG (L/S enantiomer of 2hydroxyglutarate)
 L2HGDH (L-2HG dehydrogenase)
 lbNOX (*Lactobacillus brevis* NADH oxidase)
 LCMV (lymphocytic choriomeningitis virus)
 LDH (lactate dehydrogenase)
 LHON (Leber hereditary optic neuropathy)
 LS (Leigh syndrome)
 MAVS (mitochondrial antiviral signaling protein)
 MDa (megadaltons)
 MDH (malate dehydrogenase)
 MEF (mouse embryonic fibroblast)
 MELAS (mitochondrial myopathy encephalopathy lactic acidosis and stroke-like episodes)
 MERRF (myoclonic epilepsy with ragged red fibers)
 MPTP (1-methyl-4-phenyl-1,2,3,6-tetrahydropyridine)
 MSigDB (Molecular Signatures Database)
 MTHFD (Methylenetetrahydrofolate dehydrogenase)
 mTOR (mammalian target of rapamycin)
 mTORC1 (mammalian target of rapamycin complex I)
 mtUPR (mitochondrial unfolded protein response)
 MYC (avian virus myelocytomatosis oncogene)
 NAD⁺ (nicotinamide adenine dinucleotide – oxidized)
 NADH (nicotinamide adenine dinucleotide – reduced)
 NADP (nicotinamide adenine dinucleotide phosphate - oxidized)
 NADPH (nicotinamide adenine dinucleotide phosphate -reduced)
 NAM (nicotinamide)
 NAMPT (nicotinamide phosphoribosyltransferase)
 ND (NADH dehydrogenase)
 NDI1 (*Saccharomyces cerevisiae* NADH dehydrogenase internal I)
 NDUFS (NADH dehydrogenase iron-sulfur protein)
 NFAT (nuclear factor of activated T cells)
 NFκB (Nuclear factor kappa-light-chain-enhancer of activated B cells)
 NLRP3 (NOD-, LRR- and pyrin domain-containing protein 3)
 NMN (nicotinamide mononucleotide)
 NPC (neural progenitor cell)
 NR (nicotinamide riboside)
 NRF2 (nuclear factor erythroid 2-related factor 2)
 NSC (neural stem cell)

nuo (NADH ubiquinone oxidoreductase)
O₂ (molecular oxygen)
OGDH (oxoglutarate dehydrogenase)
OXPHOS (oxidative phosphorylation)
PARP (Poly-ADP ribose polymerase)
PC (pyruvate carboxylase)
PD (Parkinson's disease)
PDH (pyruvate dehydrogenase)
PGC-1 (Peroxisome proliferator-activated receptor gamma coactivator 1)
PHD (Prolyl hydroxylase domain enzyme)
PI3K (phosphoinositide 3-kinase)
POLG (mitochondrial DNA polymerase gamma)
Q (ubiquinol)
QH₂ (ubiquinone)
QPC (ubiquinol cytochrome c reductase)
qPCR (quantitative polymerase chain reaction)
RET (reverse electron transfer)
RISP (Reiske iron sulfur protein)
RNA (ribonucleic acid)
RNAi (RNA interference)
ROS (reactive oxygen species)
Rtg (retrograde regulation protein)
S3QELs (suppressors of site III_q0 electron leak)
SDH (succinate dehydrogenase)
SNc (substantia nigra pars compacta)
STING (stimulator of interferon genes)
TCA (tricarboxylic acid)
TERC (telomerase RNA component)
TERT (telomerase reverse transcriptase)
TET (ten-eleven-translocation)
TFAM (transcription factor A, mitochondrial)
TGF β (transforming growth factor beta)
TNF (tumor necrosis factor)
TOR (target of rapamycin)
Treg (regulatory T cell)
UV (ultraviolet light)
VEGF (vascular endothelial growth factor)
Vglut-2 (vesicular glutamate transporter 2)
VN (vestibular nuclei)
WNT (wingless and int-1)
 Δ CytB (cytochrome b null)

Table of Contents

Abstract.....	3
Acknowledgements.....	4
List of Abbreviations.....	6
Table of Contents.....	9
List of Tables and Figures.....	13
CHAPTER 1: Introduction.....	15
1.1) Author's Note.....	15
1.2) Mitochondria as signaling, bioenergetic and biosynthetic organelles.....	16
1.2.1) Mitochondria are a central hub in biosynthesis and bioenergetics.....	16
1.2.2) Mitochondrial complex I and the electron transport chain.....	21
1.2.3) NDI1 and other genetic manipulation of the electron transport chain.....	24
1.2.4) Mitochondria as signaling organelles.....	27
1.3) Mitochondria in aging.....	32
1.3.1) Theories of aging.....	32
1.3.2) A central role for mitochondria in aging.....	34
1.3.3) ETC function controls longevity in <i>Saccharomyces cerevisiae</i> , <i>Caenorhabditis elegans</i> , and <i>Drosophila melanogaster</i>	36
1.3.4) NAD ⁺ biology and aging mechanisms.....	40
1.3.5) Mitochondrial UPR and mitohormetic stress responses.....	42
1.3.6) Caloric restriction, insulin/IGF, mTOR, and exercise.....	44
1.3.7) Stem cell maintenance.....	46
1.3.8) Inflammaging.....	49
1.3.9) Mitochondria in age-related neurodegeneration.....	51
1.4) Primary mitochondrial disease.....	56
1.4.1) Overview of mitochondrial diseases.....	56
1.4.2) Leigh Syndrome or subacute necrotizing encephalomyelopathy.....	58

	10
1.4.3) The NDUFS4 mouse model of mitochondrial disease.....	59
1.4.4) Interventions that manipulate the NDUFS4 mouse model phenotype.....	63
1.5) L-2-hydroxyglutarate.....	65
1.5.1) D-2HG is an oncometabolite in IDH mutant cancer.....	65
1.5.2) L-2HG is produced during hypoxia and electron transport chain inhibition.....	67
1.5.3) L2HGDH deficiency resembles mitochondrial disease and may be a functional output of mitochondrial dysfunction in aging and neurodegeneration.....	68
CHAPTER 2: Methods.....	71
2.1) Introduction.....	71
2.2) Methods for expression of the yeast enzyme NDI1 is sufficient to rescue lifespan but not motor function in a model of mitochondrial disease.....	71
2.2.1) Key resources.....	71
2.2.2) Mouse models.....	72
2.2.3) Oxygen consumption and mitochondrial complex I sensitivity in cerebellar granule neurons.....	74
2.2.4) Open Field Test and Accelerating Rotarod Challenge.....	75
2.2.5) Magnetic Resonance Imaging.....	76
2.2.6) Histology.....	76
2.2.7) Metabolite measurement.....	77
2.2.8) U13C-Glucose Flux.....	78
2.2.9) RNA Sequencing.....	79
2.2.10) Protein and mRNA Quantification.....	80
2.2.11) NADH/NAD ⁺ Ratio.....	81
2.2.12) Whole Body Plethysmography.....	81
2.2.13) Electron transport chain diagram generation.....	81
2.2.14) Statistics.....	82
2.2.15) Data availability Statement.....	82

2.3) Methods for mitochondrial L-2-hydroxyglutarate accumulation is a determinant of mitochondrial dysfunction induced neuronal dysfunction.....	82
2.3.1) Animals and cell lines.....	82
2.3.2) CRISPR/cas9.....	83
2.3.3) Mitochondrial inhibitor treatments.....	83
2.3.4) Metabolomics.....	83
2.3.5) 2-hydroxyglutarate Chiral Derivatization.....	85
2.3.6) <i>Drosophila melanogaster</i> behavioral testing.....	85
2.3.7) Regulatory T cell isolation.....	86
2.3.8) Statistics.....	86
2.4) Methods for mild genetic reduction in mitochondrial complex I function does not significantly alter healthspan in amice despite significant gene expression changes.....	86
2.4.1) Animal studies.....	86
2.4.2) Protein and mRNA quantification.....	87
2.4.3) Glucose Tolerance Testing.....	88
2.4.4) RNA sequencing.....	88
2.4.5) Gene Network Analysis.....	89
2.4.5) Metabolite measurements.....	89
2.4.6) LCMV infection model.....	90
2.4.7) Flow cytometry.....	90
2.4.8) Open field behavioral test.....	91
2.4.9) Rotarod behavioral test.....	91
2.4.10) Grip strength behavioral test.....	92
2.4.11) Novel object recognition behavioral test.....	92
2.4.12) Metabolic treadmill behavioral test.....	93
2.4.13) Oxygen consumption measurements.....	94

CHAPTER 3: Expression of the yeast enzyme NDI1 is sufficient to rescue lifespan but not motor function in a model of mitochondrial disease.....	96
3.1) Introduction.....	96
3.2) Expression of yeast NDI1 protein is sufficient to prolong lifespan in a model of brain mitochondrial complex I dysfunction.....	98
3.3) Expression of yeast NDI1 is not sufficient to restore motor function.....	104
3.4) Expression of yeast NDI1 is sufficient to prevent MRI lesions and microglial activation.....	106
3.5) Expression of yeast NDI1 normalizes metabolite abundance and gene expression in the cerebellum.....	112
3.6) Discussion.....	117
CHAPTER 4: Mitochondrial L-2-hydroxyglutarate accumulation is a determinant of mitochondrial dysfunction induced neuronal dysfunction.....	119
4.1) Introduction.....	119
4.2) Mechanisms of 2-hydroxyglutarate accumulation.....	119
4.3) Mitochondrial stress signaling increases 2-HG in <i>Drosophila melanogaster</i>	123
4.4) Mitochondrial stress-induced L-2-HG regulates neuronal function.....	126
4.5) 2-hydroxyglutarate and aging.....	128
4.6) Discussion.....	130
CHAPTER 5: Mild genetic reduction in mitochondrial complex I function does not significantly alter healthspan in amice despite significant gene expression changes.....	132
5.1) Introduction.....	132
5.2) Loss of one allele of NDUFS2 does not significantly extend survival in mice.....	132
5.3) Loss of one allele of NDUFS2 does not significantly impact behavioral function.....	137
5.4) Loss of one allele of NDUFS2 leads to significant gene expression changes.....	139
5.5) Discussion.....	147
CHAPTER 6: Conclusions and future directions.....	148
CURRICULUM VITAE:.....	162

List of Tables and Figures

Figure 1.2.1.1. Mitochondria are signaling organelles and metabolic hubs.....	19
Figure 1.2.2.1. Mitochondrial complex I structure and functions.....	22
Figure 1.2.3.1. Mitochondrial electron transport chain modulators.....	26
Figure 1.3.2.1. Mitochondrial dysfunction is a hallmark of cancer and aging-related diseases.....	35
Figure 1.5.2.1. Mitochondrial metabolites control dioxygenase enzymes and epigenetics.....	67
Figure 1.5.3.1. Mitohormesis and survival.....	70
Table 2.2.1.1. Key Resources.....	71
Figure 3.2.1. Generation of NDI1 knock-in mice and confirmation of NDUFS4 knock-out and NDI1 knock-in.....	100
Figure 3.2.2. The yeast NDI1 protein is functional in mammalian neurons and is sufficient to rescue lifespan in a mitochondrial complex I-deficient mouse model.....	101
Figure 3.2.3. NDI1 expression is sufficient to prolong survival in mice deficient for NDUFS2 in the brain and deficiency for multiple components of the immune system is not sufficient to prolong lifespan in ubiquitous NDUFS4 deficient mice.....	103
Figure 3.3.1. NDI1 expression in the brain does not rescue progressive ataxia.....	105
Figure 3.3.2 NDI1 expression in the brain does not alter breathing parameters.....	106
Figure 3.4.1. NDI1 expression in NDUFS4-deficient brains prevents the formation of inflammatory glial activation and MRI lesions, and does not cause neurodegeneration.....	108
Figure 3.4.2. Representative histology images demonstrate microglial and astrocyte activation in the brain stem, olfactory bulb, and cerebellum.....	110
Figure 3.4.3. Characterization of persistently ataxic cKO+NDI1 muscle.....	111
Figure 3.5.1. Metabolic characterization of brain cells and brain metabolites.....	113
Figure 3.5.2. NDI1 expression in the brain partially restores metabolite abundance and gene expression in the cerebellum of NDUFS4-deficient mice.....	115
Figure 3.5.3. Gene ontology network analysis for cKO versus cKO+NDI1 cerebella.....	117

Figure 4.2.1. Determinants of mitochondrial 2-hydroxyglutarate production in cancer cells.....	120
Figure 4.2.2. Mitochondrial electron transport chain determinants of the metabolome.....	122
Figure 4.3.1. Mitochondrial stress signaling increases 2-HG levels via ATF4.....	124
Figure 4.3.2. 2-HG measured in heads from flies with pan-neuronal TFAM overexpression is predominantly the L enantiomer.....	125
Figure 4.4.1. Mitochondrial stress-induced L-2-HG regulates neuronal function.....	126
Figure 4.5.1. 2-Hydroxyglutarate measurements in mouse tissues correlate with pathology.....	129
Figure 5.2.1. NDUF52 protein and mRNA are mildly reduced while oxygen consumption is generally unaffected.....	133
Figure 5.2.2. NDUF52 does not significantly impact body weight, survival, or glucose tolerance.....	135
Figure 5.2.3. White blood cell differential of aged NDUF52 ^{+/-} and NDUF52 ^{+/+} mice.....	136
Figure 5.3.1. Longitudinal behavioral analysis of NDUF52 ^{+/-} and NDUF52 ^{+/+} mice.....	138
Figure 5.4.1. Metabolite measurements from NDUF52 ^{+/-} and NDUF52 ^{+/+} liver and kidney.....	140
Figure 5.4.2. Alveolar macrophage and alveolar type 2 cell RNA sequencing in NDUF52 ^{+/-} and NDUF52 ^{+/+} mice.....	142
Figure 5.4.3. Regulatory T cell RNA sequencing from NDUF52 ^{+/-} and NDUF52 ^{+/+} mice.....	144
Figure 5.4.4. Regulatory T cell gene ontology biological processes network analysis from NDUF52 ^{+/+} versus NDUF52 ^{+/-} mice.....	145
Figure 5.4.5. LCMV infection in NDUF52 ^{+/-} and NDUF52 ^{+/+} mice.....	146

CHAPTER 1: Introduction

1.1) Author's Note.

The work in this dissertation focuses on the role of mitochondrial complex I in aging and neurological dysfunction. The paradoxes of the effects of increasing and decreasing mitochondrial function during aging in model systems and the variable penetrance, expressivity, and pleiotropy of mitochondrial mutations are very big fundamental questions in biology which we currently do not have a complete grasp of, so while this introduction will attempt to summarize the state of the field in these areas, it is likely not comprehensive. Furthermore, with these broad questions in mind, the work described in subsequent chapters may lead to more questions than they answer, but I hope that this work and future work will continue to move the field forward, because there is a great unmet clinical need in addressing the mechanisms of mitochondrial disease and age-related disease.

The Chandel lab and others have demonstrated that, in addition to their role in cellular energetics, mitochondria serve as important signaling organelles. The production of ATP is intimately related to ROS production and metabolite flux through the tricarboxylic acid (TCA) cycle. Through these three key effects, mitochondria control diverse cellular functions. Our lab focuses on attempting to dissect and understand the relative contributions of the bioenergetic, biosynthetic, and signaling roles of. Based on recent work in our lab and others, we have become interested in the possibility that changes in the relative abundance of specific metabolites can contribute to the functional defects in cell populations by influencing the epigenetic state of the cell. For example, excessive accumulation of metabolites such as 2-hydroxyglutarate can inhibit the 2-oxoglutarate dependent dioxygenase family of enzymes and dramatically change the epigenetic state and function of hematopoietic stem cell and immune cell populations. Indeed, metabolites such as 2-hydroxyglutarate and lactate are both known to be dysregulated following mitochondrial respiratory chain manipulation and are known to potently influence immune-cell function. Studying the metabolites rescued in the novel NDI1 mouse introduced in this dissertation will provide further understanding of the roles of specific metabolites and their cell-specific sources which will aid in understanding the full downstream effects of complex I mutations that precipitate disease.

1.2) Mitochondria as signaling, bioenergetic and biosynthetic organelles

1.2.1) Mitochondria are a central hub in biosynthesis and bioenergetics

The colloquial definition of mitochondria as the “powerhouse of the cell” is well founded. Mitochondria are double-membrane-bound organelles that resemble alphaproteobacteria that are a prominent feature of the endosymbiotic theory on the origin of eukaryotic life and are therefore central to the evolution of all complex multicellular organisms [1]. Mitochondria are found in nearly all eukaryotic cells and play a central role in numerous metabolic processes [2]. The reason for the colloquial definition is that the mitochondria is best known as the site coupling the biochemical tricarboxylic acid cycle with the chemiosmotic gradient of the respiratory chain to produce oxidative phosphorylation (OXPHOS). The pioneering work of the twentieth century biochemists established adenosine triphosphate (ATP) as the primary energy currency of life, and established that mitochondrial OXPHOS was an important and efficient means of generating ATP [3]. However, the role of mitochondria goes well beyond its function as an efficient source of ATP (Figure 1.2.1.1).

Cells derive energy from the catabolism of macromolecules including carbohydrates, amino acids, and fatty acids to generate ATP and GTP which are in turn used to fuel cellular work. These macromolecules are broken down into a subset of metabolites that can be shuttled into the mitochondrial tricarboxylic acid where they are oxidized in a series of enzymatic steps that contribute electrons as reducing equivalents to the electron carriers NADH and FADH₂. These electron carriers then donate electrons to the inner mitochondrial membrane's electron transport chain (ETC) [2]. The electron transport chain consists of four large holoenzyme protein complexes (mitochondrial complexes I, II, III, and IV) which coordinate transition metal ions (iron and copper) to serve as the redox cores that shuttle electrons as well as the critical membrane delimited electron carrier metabolite ubiquinone (also known as coenzyme Q) and small hemeprotein cytochrome C that is loosely associated with the outer leaflet of the inner mitochondrial membrane. Complex IV, cytochrome c oxidase, passes electrons to the final electron receptor of the ETC: molecular oxygen, generating water [4]. The flow of electrons through the ETC is coupled to the translocation of protons which generates an electrochemical concentration gradient of hydrogen ions which is the cause of the mitochondrial membrane potential giving the mitochondrial matrix

a negative charge. This gradient is dissipated primarily through mitochondrial complex V, also known as ATP synthase, where the energy of the movement of hydrogen ions back across the inner mitochondrial membrane into the matrix (down their electrochemical gradient) is coupled to the synthesis of ATP from ADP and inorganic phosphate [2].

Pyruvate is one of the key metabolites that can enter the mitochondria to fuel TCA cycle flux. Major sources of pyruvate include glucose and glycogen catabolism through the glycolysis pathway, and lactate reduction by the reversible enzyme lactate dehydrogenase (LDH). During certain metabolic settings such as hypoxia and an increased glycolytic flux not balanced by an increase of pyruvate entry into mitochondria, pyruvate can be fermented to lactate by LDH. Alternatively, pyruvate can enter the mitochondria through the mitochondrial pyruvate carrier and can enter the TCA cycle by one of two enzymes: pyruvate dehydrogenase (PDH) to generate acetyl CoA, or pyruvate carboxylase (PC) to generate oxaloacetate. Entry of pyruvate via PC is one mechanism of anaplerosis, which is a term referring to the restoration of TCA intermediates that have been removed from the mitochondria typically for use in anabolic pathways. Two other important anaplerotic sources include the branched chain amino acid valine, and the most abundant amino acid glutamine, however these enter the TCA cycle at later steps. The classic TCA cycle pathway from 6-carbon glucose metabolism generates two molecules of 3-carbon pyruvate then uses PDH to generate two molecules of 2-carbon acetyl-CoA and 2 molecules of carbon dioxide. There are several other major sources of acetyl-CoA that can serve as the entry point to the TCA cycle. Examples of these include the branched chain amino acid catabolism from isoleucine and leucine, and β -oxidation for fatty acids which both occur in the mitochondrial matrix. All of the steps that produce acetyl-CoA also generate NADH. Regardless of the source, acetyl CoA will enter the TCA cycle by condensing with oxaloacetate to form citrate using the enzyme citrate synthase. The structure of citrate is a 6-carbon tricarboxylic acid, which is how the TCA cycle gets its name, but it is also sometimes referred to as the citric acid cycle or the Krebs cycle, after Hans Krebs who discovered the key biochemical steps in the 1930s. Once citrate has been generated, it can either continue to the next step of the TCA cycle or it can be exported and used to generate cytosolic acetyl-CoA which is essential for de novo fatty acid synthesis, cholesterol synthesis, and acetylation reactions including histone acetylation

which is an important epigenetic mechanism. To continue through the TCA, citrate is converted to isocitrate through a cis-aconitate intermediate using the enzyme aconitase. Next isocitrate dehydrogenase 2 (IDH2) converts isocitrate to the 5-carbon α -ketoglutarate, or 2-oxoglutarate, generating CO₂ and NADH. α -ketoglutarate is another important metabolite for entry and export of carbon intermediates to/from the TCA, since α -ketoglutarate can be converted to glutamate by glutamate dehydrogenase in a reversible step. The anaplerotic substrate glutamine can also generate glutamate and α -ketoglutarate using the enzyme glutaminase. These two metabolites are important for several transamination reactions to produce different amino acids and amino acid derivatives and play a key role in cell signaling. Next α -ketoglutarate is converted to the 4-carbon succinyl-CoA by the enzyme 2-oxoglutarate dehydrogenase (OGDH) producing NADH and CO₂. Succinyl-CoA is the entry point for the anaplerotic substrate valine. Next succinyl-CoA is converted to succinate generating GTP. Succinate then generates fumarate via the enzyme succinate dehydrogenase (SDH) which is in fact the membrane bound complex II of the ETC. This generates the electron carrier FADH₂. Next fumarate is reversibly converted to malate by the enzyme fumarate hydratase (FH). Finally, the enzyme MDH2 catalyzes the conversion of malate to oxaloacetate generating a final NADH. Oxaloacetate is an important source of the amino acid aspartate via aspartate transaminase. Oxaloacetate can then restart the TCA cycle with an additional acetyl-CoA as above [5], [2].

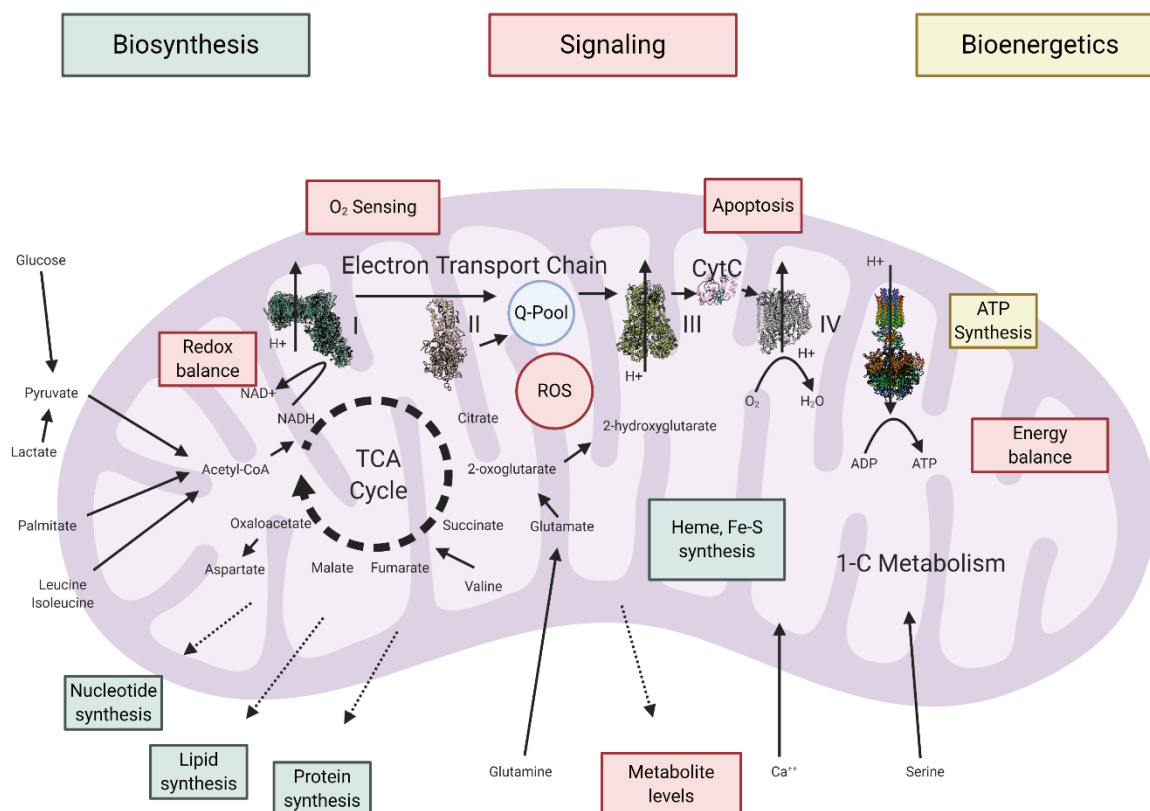


Figure 1.2.1.1. Mitochondria are signaling organelles and metabolic hubs. Mitochondria serve as bioenergetics, biosynthetic, and signaling organelles. Metabolites, superoxide-derived reactive oxygen species (ROS), and ATP produced in mitochondria are necessary for multiple cellular functions including epigenetic regulation and post-translational modifications. Heme, iron-sulfur cluster synthesis, 1-carbon metabolism, calcium regulation, nucleotide synthesis, lipid synthesis, protein synthesis, oxidative phosphorylation, oxygen sensing, apoptosis signaling, and the tricarboxylic acid cycle all involve mitochondrial function.

Transport of metabolites and reducing equivalents across the mitochondrial double membrane is an important and intricate process in cellular biology, and the search for specific transporters that allow influx and efflux of specific metabolite species is an ongoing area of research. There are several important transport mechanisms that are well defined and several transport mechanisms that recent and ongoing studies have implicated in dictating diverse cellular processes. For example, activity of the mitochondrial pyruvate carrier has been implicated in controlling cancer cell growth and maintaining stem cell function [6]. Transport of long-chain fatty acids across the mitochondrial membrane is the limiting step in fatty acid oxidation and also has been hypothesized to control cell function [2]. There are also several

mitochondrial transporters for balancing the levels of the essential reducing equivalents NAD/NADH and NADP/NADPH between the cytosol and the inner mitochondrial membrane. These include the malate-aspartate shuttle, the malate-citrate shuttle, the α -glycerophosphate shuttle, and the folate shuttle or 1-carbon metabolism pathway [5].

Other important pathways involving the mitochondria include 1-carbon metabolism, hydrogen sulfide metabolism, ammonia metabolism, reactive oxygen species production, heme metabolism, calcium buffering, and iron-sulfur cluster biogenesis [5], [2]. The recently discovered mitochondrial calcium uniporter is an important area of ongoing research, since the regulation of calcium levels in the cell and in the mitochondria contributes to significant cell physiology, particularly in electrically active cells like neurons and myocytes for action potentials, neurotransmitter release, and muscle contraction [7]. Calcium levels in the mitochondria regulate OXPHOS and release from the mitochondria is important for activation of caspases, which are calcium-activated proteases necessary for apoptosis [8]. Iron-sulfur clusters are another interesting example of the central role of mitochondria in physiology and pathophysiology. The iron-sulfur cluster is an evolutionarily ancient and flexible site of catalytic activity that is used within many enzymes across phyla [9]. Like heme synthesis, iron-sulfur clusters are generated *de novo* within mitochondria and are then incorporated into proteins within the mitochondria and elsewhere in the cell. The high reactivity of the iron-sulfur cluster is what allows it to be used in multiple enzymatic reactions, however that reactivity also can lead to damaging oxidative reactions. For example, recent evidence in a mouse model of the genetic neurodegenerative disease Friedreich's ataxia, also known as spinocerebellar degeneration, suggests that the mechanism of disease involves disruption of the mitochondrial iron-sulfur cluster biosynthetic process due to excessive oxidative damage to the very mitochondria enzymes that are responsible for iron-sulfur cluster biogenesis. In this recent study, it was found that reducing the oxygen available to react with the nascent iron-sulfur clusters within mitochondria, by treating mice with ambient hypoxic conditions, actually improved iron-sulfur cluster biogenesis and rescued the symptoms of neuronal dysfunction [10].

1.2.2) Mitochondrial complex I and the electron transport chain

The ETC consists of two primary entry points that are intimately linked to the TCA cycle as discussed above: these entry points are mitochondrial complex 1 and mitochondrial complex II. Both of these enzyme complexes accept electrons and pass them to ubiquinone forming ubiquinol. Ubiquinol is in turn oxidized back to ubiquinone by ETC complex III. Complex I is also known as NADH dehydrogenase or NADH:ubiquinone oxidoreductase. In mammalian cells, mitochondrial complex I is the largest complex in the ETC consisting of 45 individual protein subunits with a molecular weight approaching 1MDa [11], [12]. There are 14 core subunits that are highly evolutionarily conserved from bacteria to eukaryotes that make up the physical core of the mature assembled mitochondrial protein complex. These core subunits house the key redox-active cofactors such as FMN, heme, and iron-sulfur clusters. Seven of the core subunits are encoded in the mitochondrial DNA (ND1, ND2, ND3, ND4, ND4L, ND5, ND6) and reside in the membrane arm of the assembled complex. The remaining 7 core subunits and the 31 supernumerary subunits are all encoded in the nucleus and must be imported into the mitochondria with the dedicated mitochondrial protein import machinery [13]. For more than a decade it has been known that the general structure of complex I resembles an L or a chair with a prominent matrix arm which houses the NADH reaction site and an extended membrane arm [12]. However, in 2016 the first atomic resolution models were resolved using cryo-electron microscopy for full mitochondrial complex I from *Bos taurus* and *Ovis aries* [14], [15]. In the assembled complex, NADH dehydrogenase iron-sulfur protein 2 (NDUFS2), the 49 kDa core nuclear-encoded subunit, sits at an essential site at the interface of the membrane and matrix arms with an N-terminal loop in the membrane arm. NDUFS2 makes up a significant part of the site of ubiquinone binding and is therefore essential for the enzymatic activity of mitochondrial complex I [14], [15] (Figure 1.2.2.1). NDUFS4 is an 18kDa supernumerary accessory subunit that is required for the assembly of the full mature holoenzyme [16], [17]. In the complex I structure, NDUFS4 was found to exist at the interface between the NADH dehydrogenase domain and the rest of the complex [14], [15] (Figure 1.2.2.1).

Mitochondrial complex I has three essential functions, these include NADH turnover, proton translocation, and superoxide production (Figure 1.2.2.1). NADH can be generated in the mitochondria

from oxidative TCA cycle flux from the dehydrogenase enzymes as described earlier, from fatty acid oxidation, from branched chain amino acid oxidation, and from the reducing-equivalent transporters from cytosolic NADH mentioned earlier including serine catabolism [18]. Complex I is the dominant mechanism by which mitochondrial matrix NAD⁺ is regenerated for these reactions to continue, therefore it plays an important role in the ability of central carbon metabolism to proceed which is important for the central role of mitochondria in biosynthesis, catabolism, and cell signaling through the control of metabolite abundance. NAD⁺ is also consumed by enzymes such as the sirtuins for deacetylation reactions, the mono and poly-ADP ribosyltransferases (ARTs and PARPs) which are involved in DNA repair and accessibility, and NAD glycohydrolase which generates NAD-derived metabolites with pleiotropic effects [19]. Therefore, the appropriate ratio of NADH/NAD⁺ has a broad impact on cellular function even beyond its role in controlling metabolic flux in the mitochondrial matrix.

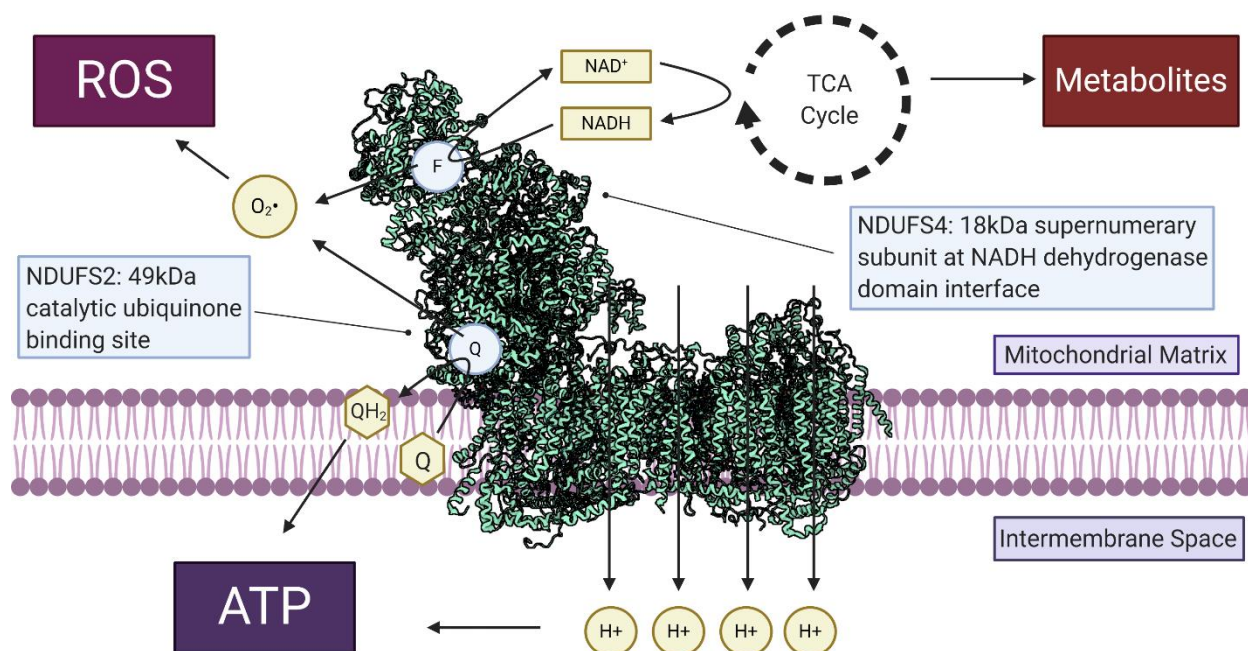


Figure 1.2.2.1. Mitochondrial complex I structure and functions. The full mammalian mitochondrial complex I is composed of 45 individual proteins. Mitochondrial complex I accepts electrons from NADH at

the flavin mononucleotide site of the matrix arm of the complex and transfers electrons through multiple redox centers to the electron carrier ubiquinone at the catalytic ubiquinone binding site. NADH turnover to NAD⁺ is required for oxidative TCA cycle flux and the generation of several essential metabolites for cell growth. Translocation of protons through the membrane arm contribute to mitochondrial membrane potential and ATP production. The approximate locations of superoxide production and the proteins NDUFS2 and NDUFS4 are indicated.

The two electrons from NADH are accepted at the FMN site of complex I in the matrix arm and are passed through a series of iron-sulfur clusters until they are donated to ubiquinone, generating ubiquinol [14], [15]. The process of electron transport or ubiquinol oxidation and protonation, is coupled (by a mechanism that is under active investigation that likely involves complex conformational changes) with the translocation of 4 protons across the inner mitochondrial membrane per 2 electrons from NADH through channels that are largely made of the conserved core subunits of complex I that are mtDNA-encoded in the membrane arm of the complex [5]. This proton translocation provides approximately 40% of the proton gradient that generates the negative mitochondrial membrane potential that drives OXPHOS with ATP-synthase used to generate ATP [20].

During the process of electron transport, there can be leak of single electrons from the reactive redox centers in enzymes to molecular oxygen, generating the negatively charged radical anion of dioxygen known as superoxide. Complex I is one of the major sites of superoxide production. Superoxide is a short-lived highly reactive species that is rapidly converted to the reactive oxygen species hydrogen peroxide by the enzyme superoxide dismutase (SOD) [5]. There are two sites of superoxide production in complex I, these are the I_F site which is the FMN redox center where NADH donates electrons, and the I_Q site, which is the site of ubiquinol reduction [21]. Some have argued that actually the I_F site is the only site of superoxide production and that different properties are attributable to superoxide production in forward vs reverse electron transfer (RET) states [22], [23], but the recent generation and characterization of site I_Q specific inhibitors of superoxide production suggests that both sites exist and are dominant producers of superoxide in different situations [24]. The rate of production of ROS from these sites is determined by the relative reduction of the FMN, which correlates closely with the NADH/NAD ratio, the proton-motive force, the relative reduction of the ubiquinone pool, and the oxygen concentration within the mitochondria. For example, multiple studies have identified that high levels of ROS are produced mainly from site I_Q in the setting of excessive succinate oxidation leading to a highly reduced Q-pool. During RET, in the setting

of a high proton-motive force and a highly reduced Q-pool, electrons from ubiquinol can be forced backwards through complex I and can generate NADH from NAD⁺ [25]. RET has been proposed to be an important driver of multiple physiological and pathophysiological processes including ischemia-reperfusion injury, [26], thermogenesis [27], and inflammation [28]. However, in other settings, such as in muscle during aerobic exercise, superoxide is produced more at site I_F than I_Q and is correlated mainly with a highly reduced NADH/NAD ratio [21]. In addition to settings which induce, reverse electron transfer, it has been observed that the function state of mitochondrial complex I can shift from an active to an inactive state during exposure to hypoxia [29], [14].

1.2.3) NDI1 and other genetic manipulation of the electron transport chain

There are several important genetic and pharmacological tools used to manipulate mitochondrial ETC function. Some of the classic pharmacological inhibitors of the ETC include hydrogen cyanide which inhibits ETC complex IV, antimycin A and myxothiazol which inhibit complex III, and piericidin A and rotenone which inhibit complex I (Figure 1.2.3.1). Antimycin A binds the Q_i site of complex III which prevents oxidation of cytochrome b heme groups which results in a high rate of superoxide production from semiquinone in the Q_o site due to internal electron backup within complex III [30]. Myxothiazol also inhibits complex III, but does so at the Q_o site preventing electron flow completely and thereby blocking Q_o site ROS production [31]. In addition, myxothiazol, but not antimycin, has an ETC-independent inhibitory effect on autophagy [32]. Piericidin A and rotenone bind the I_Q site of complex I, preventing electron transfer from complex I to ubiquinone, which can lead to lowered superoxide production from site I_Q, or can increase superoxide production, presumably from site I_F or dehydrogenase enzymes in the TCA depending on the metabolic state of the mitochondria [31]. Rotenone, but not piericidin, has been found to have microtubule destabilizing activity independent of ETC inhibition [33], [34]. There is some evidence of a dominant role of this microtubule destabilizing activity for limiting cell viability *in vitro*, for example, mesencephalic primary cultures from NDUFS4 deficient mice (which will be introduced in more detail later) were sensitive to rotenone but not piericidin [35]. Therefore, piericidin and antimycin are the inhibitors of choice in the Chandel laboratory for *in vitro* studies. Biguanides, including metformin and phenformin, also inhibit mitochondrial complex I [36]. Metformin binds complex I noncompetitively at an

uncharacterized site or sites that is not likely to be directly at or adjacent to the I_F or I_Q site, but that does limit the rate of ubiquinone reduction [36].

There are multiple single-gene-encoded enzymes in plants, fungi, bacteria, and simple animals that bypass different steps of the mitochondrial electron transport chain as it has evolved in mammals. Three important enzymes have been developed using these enzymes to experimentally rewire the mitochondrial electron transport chain. These include: 1) the *Saccharomyces cerevisiae* yeast NADH dehydrogenase internal 1 (NDI1) functions as an NADH dehydrogenase and ubiquinone reductase without the proton translocating activity of mitochondrial complex I, 2) the sea squirt *Ciona intestinalis* encodes an alternative ubiquinone oxidase (AOX) that directly passes electrons from the Q-pool to molecular oxygen, effectively bypassing the function of mitochondrial complex III and IV 3) The gram-positive *Lactobacillus brevis* bacteria encodes an NADH oxidase (IbNOX) that directly passes electrons from NADH to molecular oxygen, bypassing the role of the ETC complexes I, III, and IV and also not contributing to ATP production. There are cytosolic and mitochondrial targeted IbNOX constructs available for use in mammalian cells. NDI1, AOX, and IbNOX have all been confirmed to be functional in mammalian cells *in vitro* where they can functionally replace the respective mitochondrial complex functions described above and are becoming widely used tools for *in vitro* study particularly in cancer biology [37], [38], [39]. The Chandel lab and others have observed that it is possible *in vitro* to generate an electron transport chain *in vitro* without proton pumping that supports TCA flux by combining inhibitors or genetic knockout of mammalian ETC components with combined expression of NDI1 and AOX or with mitochondrial expression of IbNOX [38] (Figure 1.2.3.1).

Yeast NDI1 was first expressed in mammalian cells over twenty years ago [40]. Ectopic expression of NDI1 was confirmed to localize to the mitochondria and integrate into the ETC. NDI1 was found to support mitochondrial oxygen consumption and was resistant to rotenone, but sensitive to inhibition with flavone (a competitive inhibitor with structure similarity to ubiquinone), antimycin, and cyanide. Because NDI1 is a single protein it is insensitive to most complex I inhibitors, which bind in different locations within the complicated mammalian complex I with its 45 independent subunits. NDI1 is resistant to the classic I_Q inhibitors describe above (rotenone and antimycin), as well as metformin and

other biguanides (which will be described in more detail below). In addition to its metabolic role in the yeast ETC, in yeast NDI1 release can trigger apoptosis, similar to the mechanism of cytochrome C release leading to apoptosis in mammalian cells [41].

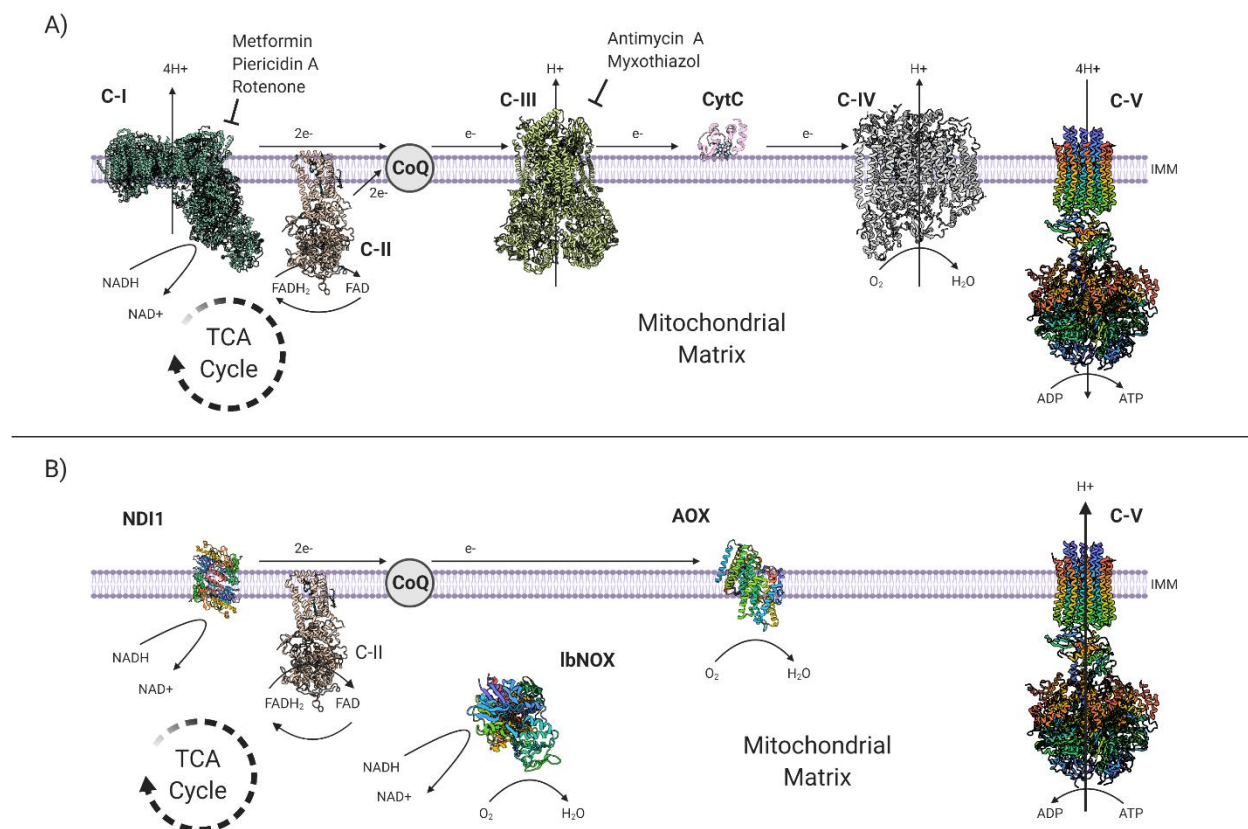


Figure 1.2.3.1. Mitochondrial electron transport chain modulators. A) Schematic of the mitochondrial electron transport chain. Electrons from electron carriers NADH and FADH₂ from the oxidative TCA cycle are transferred to the ubiquinone pool through mitochondrial complexes I and II, which in turn donates electrons to mitochondrial complex III, cytochrome C, mitochondrial complex IV, and finally molecular oxygen forming water. Proton translocation is coupled to ATP synthesis at complex V. Pharmacological inhibitors of complex I and III are indicated. B) Genetic tools from diverse phyla bypass the different steps of the electron transport chain. Yeast NADH dehydrogenase NDI1 bypasses mitochondrial complex I function without proton pumping. Sea squirt alternative oxidase AOX bypasses mitochondrial complexes III and IV to transfer electrons from ubiquinone to molecular oxygen without proton pumping. Bacterial NADH oxidase IbNOX transfers electrons from NADH directly to molecular oxygen. Imported cytosolic ATP can pump protons backwards through mitochondrial complex V to maintain mitochondrial membrane potential in the absence of electron transport chain proton pumping.

NDI1 has been expressed in multiple model organisms, most notably *Drosophila melanogaster*, which will be discussed in more detail in the later. NDI1 was also shown to rescue loss of function mitochondrial ETC mutations *in vitro* [42], which led to proposals that NDI1 could be used as a potential

gene therapy [43]. There are a number of studies in rodents that have explored NDI1 as a potential gene therapy using viral or recombinant protein delivery. Long-term expression of NDI1 in rat skeletal muscle was not found to induce autoimmunity despite the fungal origin of the NDI1 protein [44]. NDI1 delivery as a recombinant protein fused to HIV-TAT was found to be taken up in rat cardiomyocytes and be cardioprotective in an ischemia-reperfusion injury limiting infarction size [45], [46]. Viral NDI1 delivery by stereotactic injection of adeno-associated-virus (AAV) into the substantia nigra in the brains of rats was found to be neuroprotective in the rotenone model of induced Parkinsonism [47]. Similarly, in mice, AAV delivery of NDI1 to the substantia nigra demonstrated the causative role of complex I inhibition by the neurotoxin MPTP in dopaminergic cell death in the MPTP-induced mouse model of Parkinsonism [48], [49]. Intravitreal delivery of AAV-NDI1 has been found to be protective of neurons and visual function in two different models of retinal pathology; a rotenone-induced model of Leber hereditary optic neuropathy [50], and the experimental autoimmune encephalomyelitis mouse model of multiple sclerosis [51], [52].

1.2.4) Mitochondria as signaling organelles

Just prior to the turn of the 21st century the traditional view of mitochondria as passive metabolic hubs only used for ATP production drastically changed as mitochondria emerged as essential and active signaling organelles that control cell fate and function [53]. Arguably, the cause of this sea change in the perception of the mitochondrial role in signaling was triggered by the discovery that cytochrome c release from the mitochondria is a potent signal that initiates the apoptosis cascade resulting in cell death [54]. Several other discoveries at the same time period launched the field of mitochondrial signaling which has continued to develop over the past two decades. These other seminal findings include the localization of multiple signaling complexes to the mitochondrial outer membrane, the recognition that mitochondrial dysfunction could trigger an adaptive unfolded protein response and could modulate cytosolic calcium signaling, and that mitochondrial reactive oxygen species production was required for the initiation of hypoxic gene expression [53]. There are several canonical pathways that mitochondria can control based on their biosynthetic and bioenergetic roles, for example the ratio of AMP to ATP triggers activation of AMPK which can promote autophagy and limit anabolic metabolism and antagonize the pro-growth mTOR pathway. There are several NAD⁺ dependent pathways that were previously introduced, including

the sirtuins which can trigger signaling cascade changes due to their deacetylase activity. The number of signaling proteins and complexes that must localize to the mitochondrial outer membrane has continued to proliferate, perhaps most notably, the Bcl2 family proteins which are involved in regulation of apoptotic signaling [55], and multiple signaling pathways involved in controlling immune function such as the mitochondrial antiviral-signaling protein MAVS [56]. Mitochondrial DNA release from the mitochondria has also been shown to trigger inflammation, and there are several other connections between mitochondrial function and inflammation that will be discussed later [57]. The control of mitochondrial fission and fusion, and their role in mitochondrial turnover or mitophagy, have been an area of active investigation and has been implicated in modulating cell signaling in multiple contexts, particularly in neurodegenerative disorders such as Parkinson's, as several causal mutants have been identified in genes encoding components of the putative mitophagy machinery [58]. Mitochondrial contacts with the endoplasmic reticulum and other organelles have also received significant attention for their role in cell function and signaling particularly with regards to controlling lipid metabolism, ion exchange, and cellular stress signaling pathways [59]. ROS can control signaling via oxidation of susceptible protein thiols on cysteine residues that can alter protein function or interactions in cell signaling cascades [57]. In the following paragraphs I will expand more upon the role of metabolites in signaling and on the role of mitochondria in oxygen sensing.

Mitochondrial control of metabolite abundance has recently emerged as a major potential mechanism by which mitochondria control cell fate and function. Several metabolites from the mitochondrial TCA cycle have non-metabolic roles in signaling, particularly due to their role in post-translational modifications of proteins. Examples include the previously mentioned role of succinate in thermogenesis, the role of excessive accumulation of fumarate, succinate, and 2-hydroxyglutarate as oncometabolites that promote tumorigenesis in certain settings, the role of α -ketoglutarate in stem cell function, and the role of itaconate, succinate, lactate, and several other metabolites in the control of immune cell function [57]. One particular mechanism by which some of these effects may occur is the modulation of the epigenetic state of the nucleus. Histone acetylation is an important mechanism of marking active chromatin, and acetyl-CoA derived from mitochondrial citrate, is the substrate used by

histone acetyltransferases for histone acetylation [57]. The 2-oxoglutarate/ α -KG dependent enzymes are a diverse family of enzymes that require α -KG as a substrate and are involved in many functions in the cell, including collagen synthesis, carnitine synthesis, HIF signaling, protein hydroxylation, DNA demethylation, and histone demethylation [60]. There are several metabolites structurally similar to α -KG that can inhibit this family of enzymes, including fumarate, 2-hydroxyglutarate, and succinate (which is a product of the dioxygenase reaction formed from α -KG) [57]. Collectively the relative levels of these metabolites can alter epigenetics to determine cell fate, and can also interfere with many other cellular processes through control of the function of the α -KG-dependent dioxygenases [57]. The accumulation of individual metabolites has long been known to be toxic to certain cell types due to the discovery of severe pathologies in humans with inborn errors of metabolism [61]. The extent to which single metabolite accumulations can contribute to pathology in settings outside of the inborn errors of metabolism is an interesting question that needs to be further explored.

Oxygen utilization in the mitochondria primarily occurs at ETC complex IV (cytochrome c oxidase). At this site, O_2 serves as the terminal electron acceptor of the electron transport chain to form H_2O . However, there are multiple sites along the ETC at which electron leak can occur [62]. In this process a single electron is accepted by O_2 forming a superoxide radical which is rapidly converted to H_2O_2 through action of the enzyme superoxide dismutase (SOD). There are at least 12 putative sites of superoxide production in the mitochondria including sites within ETC complexes I, II, and III, and certain non-ETC mitochondrial dehydrogenases [23]. These sites contribute different amounts of ROS depending on the presence or absence of specific metabolic substrates and inhibitors, however sites at complex I and complex III provide the majority of mitochondrial ROS [63]. Different sites of ROS production have been implicated in a wide variety of physiological and pathophysiological processes [64]. Mitochondria are critical for the maintenance of biosynthetic and bioenergetic pathways mediated by the tricarboxylic acid (TCA) cycle and the mitochondrial membrane potential. The TCA produces important biosynthetic precursors in the mitochondria that are shuttled to the cytosol. Examples include the production of cytosolic acetyl Co-A from TCA-metabolite citrate for fatty acid synthesis, and the production of cytosolic aspartate from TCA-metabolite oxaloacetate for pyrimidine synthesis. Normal function of the TCA cycle

produces NADH and FADH₂, which are reducing equivalents that transfer electrons into the ETC. The mitochondrial membrane potential that is established by ETC complex proton pumping is used to generate ATP at complex V. The mitochondrial membrane potential is required for ROS production [65]. Mitochondria serve as signaling organelles through the release of ROS and the release of TCA cycle metabolites [66]. These two key mitochondrial signals can impinge on cytosolic signaling pathways. ROS can oxidize susceptible thiols in cysteine residues of signaling proteins. For example, the enzymatic site of protein phosphatases contains a candidate cysteine that can be modified by ROS oxidation [64]. The TCA-metabolite citrate is exported to the nucleus to create cytosolic acetyl CoA which is required for protein acetylation which can influence signaling pathways and the epigenetic state of the cell [67], [68], [65]. Mitochondrial ROS signals are required for diverse cellular functions such as differentiation, proliferation, and adaptation to stressors including hypoxia [69].

Due to its important role as the regulator of the NADH/NAD ratio to allow TCA flux, and its role in superoxide production, complex I has received attention recently as a potential target for cancer therapy [70], [20]. Over 10 recently FDA approved small molecule anti-cancer drugs have reported complex I inhibitory activity [20]. Treatment with the antidiabetic drug metformin was found to be associated with significant reductions in cancer incidence and mortality in retrospective analysis of observational and cohort studies [71]. As previously mentioned, metformin and other biguanides can act as inhibitors of mitochondrial complex I [36]. Metformin is primarily used as a first line therapy for its antidiabetic effects, which include inhibiting hepatic glucose output and increased peripheral glucose utilization. Although the precise mechanisms and tissue sites of metformin's action remain controversial, many of its pleiotropic effects are consistent with a mechanism in which complex I is mildly inhibited [72], [73]. For this reason, it is of interest to further understand the contribution of the complex I modulatory mechanism. While the Chandel lab have shown, using NDI1 in tumors, that complex I inhibition mediates an anti-cancer effect, the degree to which complex I inhibition in other tissues, and the degree to which it influences glucose metabolism to indirectly alter cancer behavior, are topics for future research and are motivating factors for generating a ubiquitous NDI1 expressing mouse model. Numerous clinical trials with metformin are

currently underway with metformin use as an adjuvant or combined therapy with some preliminary results suggesting efficacy in breast cancer [74], [72].

Cancer is an aging-related disease, in that the prevalence of most types of cancer increases dramatically with advanced age. There are numerous other diseases and conditions that are aging-related, including type-2 diabetes, susceptibility to pulmonary infections like community acquired pneumonia and influenza, interstitial lung diseases, sarcopenia, and neurodegenerative diseases such as Parkinson's disease and Alzheimer's disease. Mitochondrial dysfunction has been implicated in all of these processes and is frequently observed as an aspect of aging. Therefore, drugs that modulate mitochondrial function have been proposed as potential tools to target multiple aging-related diseases or modulate aging more generally. Metformin is one of these drugs since it already has significant beneficial effects in type-2 diabetes, a limited side-effect and well-established risk/safety profile from extensive use, and preliminary data on an anti-cancer effect [75]. Furthermore, work by our collaborators in a mouse model of air-pollution-induced lung injury, which is a major cause of mortality worldwide, treatment of mice with metformin was protective by inhibiting mitochondrial complex I in alveolar macrophages, which led to a decrease in mitochondrial ROS production from mitochondrial complex III due to its role in calcium release by limiting opening of calcium release-activated channels (CRAC) channels which limited release of the important proinflammatory cytokine interleukin-6 (IL-6) [76]. Since the control of inflammation is also widely implicated in cancer and aging-related diseases, this finding is potentially interesting as a mechanism by which metformin can influence multiple aging-related disorders. Some other major potential mechanisms by which metformin may influence healthspan and longevity include altering the microbiome, increasing adiponectin, inhibiting insulin and insulin-related growth factor 1 (IGF1) signaling, reducing obesity, inhibiting inflammation through NFkB signaling, antagonizing mTOR activity through AMPK activation, reducing oxidative stress, removing senescent cells, and activating stress responses and autophagy [75]. The role of complex I in many of these pleiotropic effects and how they relate to aging and neurodegenerative processes will be explored in more detail in the next section.

1.3) Mitochondria in aging

1.3.1) Theories of aging

The question of why and how we and other organisms age has been an enormous topic for philosophical and scientific inquiry that predates the modern scientific method. Some of the earliest theories of aging include the “rate-of-living” theories which conceptually tie in with the fundamental role of metabolic pathways and mitochondrial function in life [77], [78]. These theories posit that aging is determined by the rate at which biological entities change themselves by the conversion of raw material into biomass, and that faster conversion leads to faster aging [79], [80]. While these particular theories are no longer widely accepted, they share a conceptual framework with the widely discussed “free-radical theory of aging” (FRTA) that is associated with a landmark papers by Harman in the 1950s [81]. In this paper, a potential link between the effects of radiation damage and excessive reactive oxygen species production was established and hypothesized as an underlying mechanism of aging, since both high energy radiation and toxic reactive oxygen chemistry could lead to chemical damage to the macromolecules essential for life. Put simply, the FRTA posits that reactive oxygen species, as a toxic byproduct of oxidative metabolism, can damage biological macromolecules and the accumulation of this damage is manifest as the phenotypes and diseases of aging [82]. There are multiple other “accumulation of damage” theories of aging that grow from or are related to the FRTA. These include the idea that organisms, as imperfect biological systems, gradually accumulate damage by multiple means, not only ROS, and that this damage is not visible to natural selection and is the driver of aging [83]. An accumulation of negative mutations as a key driver of aging is part of this theory and is a well accepted concept and is frequently discussed as the link between aging and increased susceptibility to cancer.

Some recent modifications of the FRTA types of theories include a molecularly updated theory of how specific cell signaling pathways impact the rate of living control mechanistically through antagonism of pro-growth, pro-aging mTOR pathway versus the resistance pathways embodied by the FOXO pathway [84]. Another recent updated theory on the role of ROS and metabolic rate is the “uncoupling to survive” hypothesis: an idea that due to the increased time that a semiquinone of ubiquinone exists in the active site of complex III is linked to both ROS production rate and membrane potential, reducing ROS

could occur by mildly uncoupling of the electron transport chain either through expression of an uncoupling protein, or from proton leak through the adenine nucleotide translocase [85]. This theory suggests that higher metabolic rates with lower ROS production would protect against aging, which incorporates a similar logic as the FRTA but contrasts with the metabolic rate implications of the rate of living theories.

Another set of aging theories centers around that idea that aging is evolved or genetically programmed. One of the early formulations of this theory was laid out by Kirkwood in 1977 and is sometimes referred to as the “disposable soma theory” [86], [87]. This hypothesis, while still incorporating an aspect of FRTA damage induced aging, postulates that aging is an evolved energy saving strategy that involves a tradeoff of reduced error regulation in somatic cells. Similarly, the 1882 hypothesis by Weissman suggested that aging could be an evolved strategy for freeing up resources for younger animals in a population to facilitate evolution and reproductive fitness as different generations are required to provide variation for natural selection to function [78], [77]. A similar idea is the theory of “pleiotropic antagonism” which suggests that some genes that are beneficial in young organisms actually have a detrimental effect in aged organisms and this results in a genetically specified aging program [87]. Mechanisms of the concept of aging as a genetic program include the concepts of the detrimental effects of the accumulation of cells in the senescent state, shortening of telomeres with repetitive cell divisions leading to genome instability, endocrine signaling changes including the insulin/IGF-1 and mTOR growth promoting pathways being linked to aging, and the immunological theory that dysregulated immune responses occur due to signaling changes that lead to an increased innate immune inflammatory state with increased time that has a causal role in promoting age related diseases like cardiovascular disease, Alzheimer’s disease and cancer [78].

Clearly mitochondrial function is a central potential driver of aging through ROS in many of the above described theories. The extent to which the mitochondrial contribution to aging is due solely to the control of ROS as posited by the FRTA is unclear. There are significant data supporting and contradicting this idea, some of which will be reviewed below. It is clear, however, that despite epidemiological links on nutrition and aging, interventions specifically using antioxidants have so far been extremely unsuccessful

as a prevention or treatment strategy for human disease [88]. The data reviewed below will focus more on specifically manipulating electron transport chain function and its relationship to aging to incorporate both ROS-dependent and ROS-independent bioenergetic, biosynthetic, and signaling effects of mitochondrial function rather than focusing on the lens of evidence for and against the FRTA.

1.3.2) A central role for mitochondria in aging

Significant progress has been made in characterizing the molecular events that are common in aging, which is beginning to create targets for a potential understanding of causality in aging. Many studies have observed a decrease in mitochondrial content or function through multiple methods during aging and associated with numerous aging-associated diseases, perhaps most notably neurodegenerative diseases like Parkinson's disease, aging-related muscle functional declines or sarcopenia, pulmonary diseases [89], [87], [90], [91], [92], Figure 1.3.2.1). In the landmark conceptual review paper in 2013, "The Hallmarks of Aging," mitochondrial dysfunction was identified as one of 9 interrelated hallmarks of the aging process. The other hallmarks identified include cellular senescence, stem cell exhaustion, altered intercellular communication, genomic instability, telomere attrition, epigenetic alterations, loss of proteostasis, and deregulated nutrient signaling [93]. There are clear bi-directional mechanistic connections between mitochondrial function and all 8 of the other identified hallmarks. As previously described in detail, mitochondrial function controls organismal hypoxia responses and signaling, as well as controls various aspects of inflammation as just two examples of mitochondrial function influencing intercellular communication. Mitochondria have recently emerged as important determinants of stem cell maintenance and differentiation in multiple tissues [94]. There is a strong association between mitochondrial functional decline and the development of senescent cell phenotype, with manipulations that increase mitochondrial stress responses preventing senescence in several models [95], [94]. Nutrient sensing is intimately linked to mitochondrial function with its role as a central hub of catabolic metabolism which influences key sensing pathways such as mTOR, AMPK, and the insulin/IGF signaling axis [96]. The loss of proteostasis is linked to mitochondrial function through the intrinsic link between mitophagy and autophagy, the role of retrograde mitochondrial signaling influencing pro-translation pathways like MYC and mTOR, through induction of the mtUPR, through the pathways

that control the balance of mitochondrial/nuclear proteins, and mitochondrial proteins have been found to be overrepresented in the population of proteins that are prone to aggregation [97], [98]. As previously discussed in detail, epigenetic alterations can be controlled by mitochondrial function through the role of mitochondrial TCA metabolites as necessary cofactors for epigenetic mark addition and removal [57]. Telomere attrition can be influenced by mitochondrial function through mitochondria ROS production effects on TERT and TERC localization and function, and direct effects on telomeres [99]. Genomic instability is influenced by mitochondrial signaling at the level of pro- and anti-apoptotic signaling machinery, and mitochondrial ROS can potentially influence mutational burden [100].

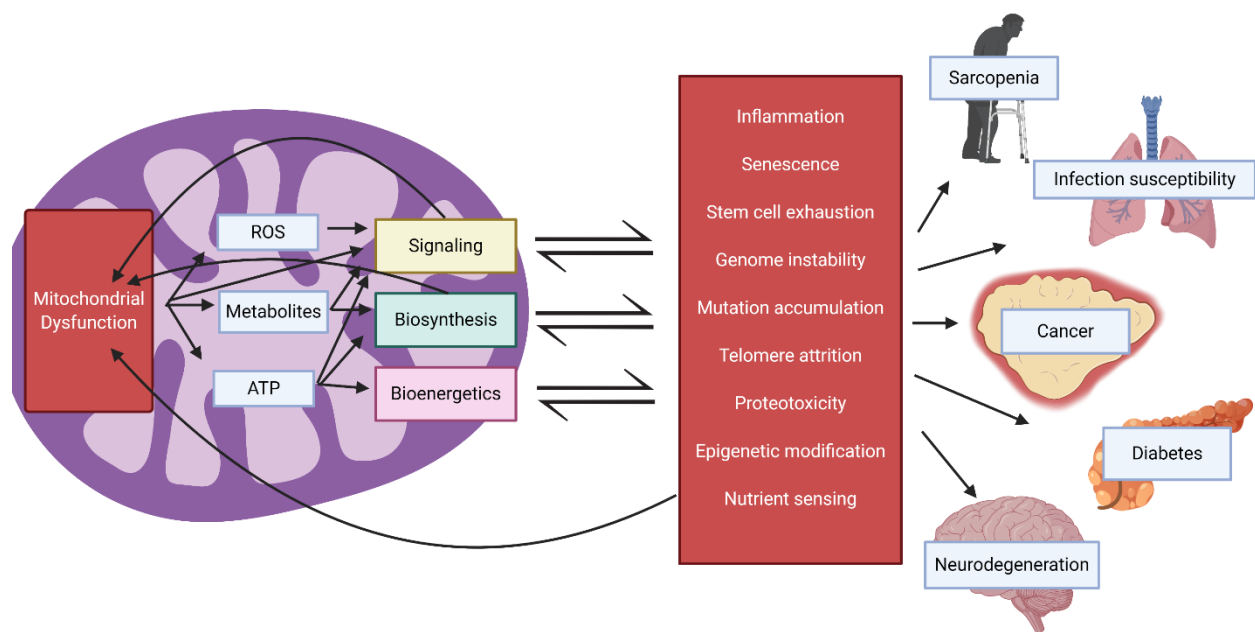


Figure 1.3.2.1. Mitochondrial dysfunction is a hallmark of cancer and aging-related diseases. Mitochondrial dysfunction is both a potential cause and effect of aging phenotypes through altered cell signaling, biosynthesis and bioenergetic demands.

1.3.3) ETC function controls longevity in *Saccharomyces cerevisiae*, *Caenorhabditis elegans*, and *Drosophila melanogaster*

Invertebrate model organisms, due to their rapid generation time and short lifespan have been used extensively to study aging and lifespan. Some common concerns raised about the use of these systems is that the results and mechanisms found will not be applicable to human aging due to the differences in time frame and complexity, and that measuring lifespan will not correlate with the concept of healthspan, that in addition to improving the length of time lived, that the quality of life is also improved and healthspan can be difficult to interpret in the setting of model organisms. Despite these concerns, most of what we know about the mechanisms and interventions that influence aging comes from model organisms and many factors have proved to be evolutionarily conserved across multiple organisms from fungi to invertebrates to mammals and even to primates and humans. One of the most consistent transcriptional changes associated with aging across model organisms is the downregulation of mitochondrial ETC and OXPHOS related gene.

The budding yeast *Saccharomyces cerevisiae* replicative aging model system is a widely used system to study aging in which a determination is made about how many times a mother cell can divide under asymmetric division to produce daughters. Yeast exhibit asymmetric inheritance of mitochondria based on age to produce rejuvenated daughter cells and mother cells that are limited to only a few more cell divisions [101]. Studies in yeast that increase longevity may be a valid model of stem cell maintenance and genes that extend yeast replicative lifespan share many genes that prolong lifespan in multicellular organisms [102], perhaps most notably reduced activity of the mTOR pathway (TOR in yeast) is associated with an increase in lifespan, with the famous rapamycin as an inhibitor of the TOR pathway increasing lifespan in multiple organisms [103]. One downstream target of mTOR inhibition is an increase in stress response pathways and mitochondrial biogenesis [102]. Aside from mTOR, mitochondria play an important role in determining aging in yeast. For example, the mitochondrial retrograde stress signaling response in yeast involving chromatin modifying complexes SAGA and SLIK has been shown to extend lifespan through a compensatory response in response to Rtg1 and Rtg3 translocation to the nucleus due to mitochondrial dysfunction [104].

Another example of potentially conserved mechanisms of aging-related dysfunction from yeast to mammals includes the interrelated role of lysosome function with mitochondrial function. Deterioration of the yeast lysosome-like vacuole is an early event in yeast replicative aging which precipitates age-related yeast mitochondria dysfunction [105]. Mitochondria and lysosomes are functionally related in numerous age-related disorders and the neurometabolic degenerative lysosomal storage disorders in humans [106], [107], [108], [109], [110], [111], [112]. While investigating the link between the lysosome-like yeast vacuole and yeast mitochondria, a recent report discovered a mechanism by which intracellular amino acid homeostasis disruption can drive age-related mitochondrial decline. Cysteine elevation and declining iron levels through an oxidant mediated mechanism, contribute to age-related mitochondrial functional decline in yeast [113]. Recent work in human cells identified that a similar mechanism may be possible. CRISPR-Cas9 screening in human cancer cells was carried out to identify the necessary pathways for which lysosomal acidity is required for cancer cell proliferation [114]. Necessity of iron uptake via lysosomal acidification is necessary for iron-sulfur cluster synthesis and electron transport chain function, therefore there is a potential mechanistic link between lysosomal dysfunction and mitochondrial dysfunction. These recent studies also highlight an idea about the potential toxicity of necessary intermediates of metabolism being potentially damaging, just as ROS is required for signaling, cysteine may be toxic in excess but is also required for protein, glutathione, and coenzyme A synthesis.

The roundworm *Caenorhabditis elegans* has been an important tool for studying the role of mitochondria in aging as a simple animal model system. An early and important finding in *C. elegans* that has upended the theories about mitochondrial functional decline causing aging has been that inhibition of components of the mitochondrial ETC with RNA interference (RNAi) increased lifespan while decreasing development, ATP production, and fertility [115], [116]. Specifically, subunits of mitochondrial complex I control lifespan in addition to several other proteins in other parts of the ETC. Specific complex I genes that increase lifespan when knocked down in *C. elegans* include *nuo-2* which is homologous to mammalian NADH dehydrogenase iron-sulfur protein 3 (NDUFS3) [116], [117], and D2030.4 which is homologous to mammalian NADH dehydrogenase 1 beta subcomplex subunit 7 (NDUFSB7) [116]. These worms tended to have approximately a 50% decrease in measured ATP concentrations, had decreased

oxygen consumption, and exhibited morphological changes in mitochondria [115], [116]. Importantly, in *C. elegans*, the timing of knock-down of ETC components during the larval L3 and L4 stages was determined to be essential for life span extension since knockdown in adults did not cause an increased lifespan despite similar levels of OXPHOS reduction [115].

Some of the lifespan extending manipulations of the *C. elegans* ETC with both RNAi and with mutations in ETC subunits that lead to hypomorphic ETC complexes require increased ROS levels, which argues against the primary role of ROS as a damaging agent limiting lifespan as proposed in the FRTA [118], [119]. For example, an RNAi screen for increased HIF activity featured ETC genes including *nuo-1* and increased lifespan [120]. As previously described, HIF activity requires mitochondrial ROS, and this raises the possibility of an idea of mitohormesis, in which a small amount of a potentially damaging entity like ROS can actually improve function within a specific window [121]. Another example of a well described mechanism of lifespan extension in *C. elegans*, is the mutation of complex I subunit *nuo-6* which mediates an increased lifespan through ROS-induced signaling through the intrinsic apoptosis path [122]. Therefore, ROS may not be a cause of aging, but may instead be correlated with aging due to its adaptive signaling role supporting stress response pathways. This concept is supported by additional work with *C. elegans* ROS control including the addition of pro-oxidants, knockdown of mtROS detoxification, and manipulations to increase mtROS generation [122].

The fruit fly *Drosophila melanogaster* has been used as a slightly more complicated animal model of aging [82]. Inhibition of the ETC in flies by several approaches, like in *C. elegans*, has been observed to increase lifespan, but with some important differences. For example, the drosophila homologs of several of the complex I subunits focused on in *C. elegans* life extension (*D. melanogaster* genes CG12709 and CG5548) exhibit developmental lethality when knocked down in flies [123]. Knockdown of the homologous gene of a different *C. elegans* complex 1 subunit (*nuo-1*), that extends lifespan upon knockdown in worms [124], in flies does not extend lifespan [125]. However, in drosophila, lifespan extension can be accomplished by knocking down other complex I subunits including CG9762 (mammalian homolog NADH dehydrogenase 1 b subcomplex 5, NDUF5B), CG9140 (mammalian homolog NADH dehydrogenase flavoprotein 1, NDUFV1), and CG9172 (mammalian homolog NADH

dehydrogenase iron-sulfur protein 7, NDUFS7) and CG2286 (mammalian homolog NADH dehydrogenase iron-sulfur protein 1, NDUFS1) [126], [125], [123]. These flies with complex I knockdown demonstrated increased lifespan and decreased fertility like in *C. elegans*, but the correlation with ATP levels and development was not as straightforward as in *C. elegans*. Different complex I subunits caused increases, decreases, or no change in ATP and development [125], [123]. Unlike in *C. elegans*, knockdown of complex I subunits only in adulthood was sufficient to extend lifespan [123]. The knockdowns of complex I that do extend lifespan in flies are also tissue specific. CG9763 and CG9162 knockdown in neurons alone is sufficient to extend lifespan [123]. CG2286 knockdown in muscles alone during development is sufficient to extend lifespan [126]. Furthermore, the correlations with ROS and lifespan in the ETC knockdowns is less straightforward in flies as compared to *C. elegans* [82]. There are also numerous genetic models of mitochondrial function in *D. melanogaster* in which decreased ETC component expression and decreased mitochondrial function is lined to decreased longevity and numerous other pathological consequences. For example RNAi of ND-49, the homolog of human NDUFS2, leads to TOR pathway activation and reduced survival [127].

In addition to the observation that knockdown of several components of the ETC can extend lifespan in *D. melanogaster*, studies have also found that interventions that increase mitochondria and/or mitochondrial complex I function are capable of extending *D. melanogaster* lifespan [82]. Increasing mitochondrial complex I by upregulating the *D. melanogaster* homolog of PGC-1, which is a key transcriptional coactivator that regulates mitochondrial biogenesis and function, was capable of increasing lifespan, but only when expressed in the intestine [128]. This lifespan extension was associated with increased mitochondria but decreased ROS and better overall tissue homeostasis.

Another approach to increasing mitochondrial complex I function is the expression of the yeast NDI1 protein as described previously. NDI1 expression with intact endogenous complex I leads to increased mitochondrial NADH dehydrogenase activity without significant changes in other ETC complexes [129], [130], [130]. NDI1 expression in flies was able to rescue loss of complex I function in a model of complex I assembly defects which leads to decreased stress resistance and decreased development [131]. NDI1 expression in the nervous system or the intestine increased lifespan while

global expression did not [130], [132]. The tissue specificity is fascinating and argues against a simple linear relationship between mitochondrial complex I function and physiology. Replicating similar studies in mammalian models is an important future direction to be discussed later.

The data on the role of ETC function in mammals and how it influences aging is complicated and somewhat contradictory. For example, the *NDUFS4* deficient mouse model demonstrates moderate reductions in complex I function that are associated with a significantly shortened lifespan [133]. We have found that complete knockout of *NDUFS2* is embryonic lethal in mice either with ubiquitous cre expression or with cre expression limited to the brain through use of the brain specific Nestin-cre. Whether an intermediate level of complex I knockdown in mammals can also result in increased lifespan is a major motivating question behind the present studies. Another interesting study of note was the finding from a large outbred mouse cohort study that increased metabolic activity with increased endogenous uncoupling was correlated with individual survival of mice [85]. Therefore, it is likely that tissue specific effects of different complex I manipulations and the extent of complex I manipulation in the context of expression of other mitochondrial proteins and metabolic state will all contribute to the relative positive and negative effects of complex I dysfunction on overall health and longevity (Figure 1.3.2.1).

1.3.4) NAD⁺ biology and aging mechanisms

Deficiency for vitamin B3, also known as niacin or nicotinic acid, leads to the disease pellagra which is defined by dermatitis, diarrhea, dementia, and death due to an inability of the body to supply sufficient NAD⁺ [134]. NAD⁺ precursor vitamins in the NAD⁺ salvage pathway such as nicotinamide (NAM), nicotinamide riboside (NR), and nicotinamide mononucleotide (NMN), have received significant attention as potential therapeutics to combat aging, as supplementation of in model organisms bolster NAD⁺ availability during aging and improves lifespan. As described previously, in addition to its role as a shuttle for reducing equivalents to the ETC, NAD⁺ is consumed by several enzymes resulting in the production of the salvage pathway intermediate NAM, these include the sirtuin deacetylases that have been implicated in regulating lifespan and mitochondrial metabolism, PARPs which are involved in regulating ER stress and DNA repair, and CD38/CD157 which is an NADase that is involved in cell adhesion and calcium signaling [134]. The sirtuins have received significant attention, due to the

increased activation of SIRT1 in particular, with protective benefits in several age-related tissue pathologies including neurodegeneration, cardiovascular disease, skeletal muscle function, and metabolic regulation of the liver and pancreas. Some of these effects are thought to be mediated by increased insulin sensitivity, increased fatty acid oxidation, and decreased inflammation which may all be related to increased mitochondrial biogenesis and improved function [135]. Neuronal overexpression of SIRT1 extends lifespan in mice [136].

One theory for the mechanism of a sirtuin and NAD⁺ mediated effect on mitochondrial function is that there is a decreased nuclear NAD⁺ with aging in mice which can lead to aberrant normoxic HIF signaling activation [137]. SIRT1 deletion accelerates the process while supplementation of NMN in aged mice decreased this HIF signaling, which lead to proposed a mechanism by which AMPK controlled different defects in mitochondrial homeostasis through SIRT1 declines secondary to NAD⁺ declines [137]. In the setting of low energy supply loss of SIRT1 function could lead to decreased activity of PGC1 α due to increased acetylation, while in the setting of high energy supply normoxic HIF stabilization prevented c-MYC from inducing TFAM expression, loss of either PGC1 α or TFAM could reduce mitochondrial biogenesis and function. As previously mentioned, PGCs (peroxisome proliferator-activated receptor gamma coactivators alpha and beta) along with NRF1 and NRF2 control and coordinate mitochondrial biogenesis. TFAM controls mtDNA transcription and replication. There are also mitochondrially localized sirtuins which may directly impact the mitochondrial OXPHOS and TCA enzymes by deacetylation [135], and may in turn be regulated by ETC function through the control of the NADH/NAD ratio.

Several studies have evaluated the impact of the NAD⁺ salvage pathway intermediates on mouse longevity and physiology, particularly NMN and NR due to their bioavailability [134]. NR supplementation protected against high fat diet induced obesity in mice and protected from diabetic neuropathy and hepatic dysfunction [138], [139]. NR supplementation has been found to increase oxidative metabolism in several tissues such as muscle, liver, and brown adipose tissue [138]. NR supplementation also improves muscle function in a model of muscular dystrophy [140]. NMN increases sensitivity to insulin in high fat diet treated mice [141]. NR and NMN have both been shown to increase lifespan and/or healthspan and reduce the development of metabolic diseases in mice [142], [143]. NAM

supplementation has been found to be protective from some hepatotoxic effects of high fat diet treatment in mice, while it did not extend lifespan. NAM supplemented mice showed lower inflammation, hepatic fat accumulation, and marker of oxidative stress [144]. Some studies find that the effects of NR and NMN supplementation are not solely due to sirtuin activation [139], [145]. One important theory on the mechanism by which NAD⁺ and sirtuins can have a positive impact on longevity is by activating mitochondrial stress pathways like the mitochondrial unfolded protein response (mtUPR) [146]. Indeed, it is possible that the reason why diverse mitochondrial perturbations in model organisms may have positive effects is that they all induce a protective stress response or responses.

1.3.5) Mitochondrial UPR and mitohormetic stress responses

The concept of hormesis is that a small amount of something harmful can paradoxically be helpful by inducing a protective homeostatic response that improves tolerance to stress. One of the major theories on why mitochondrial perturbations can improve longevity is this concept, and one of the most frequently cited mechanisms of mitohormesis is the mtUPR [121]. The mtUPR refers to a transcriptional response that can be activated by multiple types of mitochondrial insults and signals [97]. The mtUPR promotes repair and recovery of the mitochondrial network in order to promote cellular health and function. The interaction of the mtUPR with aging is complicated, on the one hand, mtUPR promotes mitochondrial repair and recovery from temporary insults, however excessive activation can have a negative impact on cellular function and can increase the accumulation of deleterious mutations in mtDNA [97]. mtUPR signaling can occur between cells and across tissues, which may have important implications for aging, for example ETC perturbations in neurons of *C. elegans* can lead to activation of the mtUPR in the intestine [147]. Mitochondrial insults that can activate the adaptive mtUPR include ROS, accumulation of unfolded proteins in the mitochondrial matrix, ETC inhibitors, mito-nuclear protein imbalance, and other genotoxic stress that perturbs OXPHOS activity. Key aspects of the response include activation of genes that promote OXPHOS recovery and biogenesis of mitochondria, mitochondrial proteostasis, antioxidant capacity, and the mitochondrial protein import machinery.

In mammals the details of the stress response are more complicated than in *C. elegans* and some of the key signaling proteins that induce the mtUPR include the bZIP transcription factors

CHOP/DDIT3, ATF4, and ATF5, which are also associated with the integrated stress response (ISR) [147]. The integrated stress response can also be triggered by ER stress, amino acid starvation, heme depletion, and infection leading to phosphorylation of eukaryotic translation initiation factor 2 subunit 1 (eIF2a) by the kinases PERK and GCN2 which slows protein production and selectively increases production of a specific subset of proteins that have upstream open reading frames. The precise mechanisms by which multiple perturbations of the mitochondria trigger the ISR and mtUPR remain an active area of research [148]. It has been observed that the mammalian hormones fibroblast growth factor 21 (FGF21) and growth differentiation factor 15 (GDF15) are potential signals of mitochondrial stress that can communicate and trigger adaptive stress responses across tissues. For example, ATF4 can trigger FGF21 production in response to mitochondrial dysfunction associated with skeletal muscle specific knockout of the autophagy regulating component ATG7, or in response to pharmacological mitochondrial inhibitors, [149] or in response to ectopic expression of uncoupling proteins in muscle [150]. FGF21, in turn, can protect from high fat diet induced obesity and improve insulin sensitivity and can lead to adipose tissue browning [149], [150]. GDF15 can be produced due to CHOP activation secondary to muscle mitochondrial proteotoxic stress and GDF15 can act to regulate food intake, weight gain, and insulin sensitivity [151]. Both FGF21 and GDF15 activity have been implicated in the protective metabolic effects of metformin treatment in mice [152, 153].

The role of complex I in the induction of stress responses has been explored in depth in *C. elegans*. Work from our collaborators in an unbiased longevity screen using RNAi in *C. elegans* revealed mitochondrial ETC components regulate the heat shock response to promote proteostasis and longevity in worms [154]. Proteomic studies in *C. elegans* have identified ETC components as being over-represented in peptides that are prone to misfolding and to insoluble inclusion body formation [98]. Therefore in addition to the previously described induction of stress responses, it is possible that knock-down of complex I and other ETC subunits may reduce the pool of aggregation prone proteins and therefore may reduce the seeding of further protein aggregation allowing proteostasis to be preserved with age [155]. RNAi knock down and mutation of complex I can induces mitohormesis through increased ROS production that leads to stress response pathway activation [120], [119], for example the hypoxia

response (discussed in more detail above), requires mitochondrial ROS and can increase autophagy [156] and decrease susceptibility to proteotoxic stress [157]. Due to the complicated assembly process of complex I, altered expression of single subunits may lead to imbalances in mitochondrial to nuclear protein levels which has been shown to induce mitochondrial stress mechanisms and may be both upstream and downstream of NAD biology [137]. The mtUPR is necessary for lifespan extension in the setting of some ETC knockdown genes [126], [158], [147]. But activation of the mtUPR alone is not sufficient to extend lifespan and is not required for lifespan extending effects of knockdown of all ETC subunits [159].

1.3.6) Caloric restriction, insulin/IGF, mTOR, and exercise

One of the most widely accepted interventions to increase longevity in model organisms is caloric restriction (CR) [160]. Mild reduction of caloric quantity without malnutrition is associated with increased lifespan and delayed disease onset in many organisms including *S. cerevisiae*, *C. elegans*, *D. melanogaster*, mice, rats, and non-human primates. Like in model organism some studies of lifespan and healthspan in primates has suggested a beneficial effect while some studies indicate some tradeoffs of healthspan for the increased lifespan such as a reduction in CNS volume [161], [162]. While nutritional studies and links to aging remain challenging in humans, there is some evidence that caloric restriction can have beneficial effects, particularly for reducing risk factors for the aging related diseases type 2 diabetes, cardiovascular disease, and cancer; and there is ample evidence that excessive caloric intake is harmful [163].

Studies in *C. elegans* indicate that glucose restriction increases lifespan by inducing OXPHOS and increasing ROS [164]. Studies in multiple tissues from mice indicate that caloric restriction results in transcriptional alterations that are suggestive of metabolic reprogramming including increased fatty acid oxidation, increased stress signaling pathways, and increased expression of genes related to redox balance [160]. Caloric restriction has also been shown to induce expression of uncoupling proteins, which may have a beneficial effect on longevity as mentioned previously.

Insulin resistance and the insulin-like growth factor (IGF) signaling axis are important aspects of type 2 diabetes and have been implicated in aging in numerous model systems. Caloric restriction may

act systemically via this axis by repressing insulin release and IGF signaling. Numerous studies in mice with high fat diet intake have demonstrated that manipulations of mitochondrial function can alter insulin sensitivity and prevent or exacerbate the negative effects of high fat diet treatment [160], [126]. Another impact of CR that is related to insulin signaling is the change of in body composition, as proportionally more fat mass is lost than lean mass during CR. This can lead to induction of the protective hormone adiponectin which can induce mitochondrial function and may be an important link between CR and mitochondrial function.

AMPK activation and its antagonism of the mTOR pathway has also been described as a potential mechanism by which CR has beneficial effects on longevity. Both the AMPK and mTOR signaling pathways are important nutrient sensors, with mTOR sensing amino acid abundance and triggering a pro-growth anabolic metabolic program when activated in sufficient nutrient environments, while AMPK can repress mTOR activity when energy deficits are detected. Inhibition of mTOR, specifically mTORC1-mediated signaling, by either caloric restriction or rapamycin can increase autophagy, promote stem cell function, and limit protein translation, which results in improved lifespans in model organisms [103].

As previously mentioned, muscle loss with aging is one of the most prominent, consistent, and well characterized features of aging in humans. The relative simplicity of obtaining and studying muscle biopsies (as compared with vital organs) and the highly metabolic nature of muscle cells have made them a major focus of the role of mitochondria in aging [103]. On average, humans exhibit declines in muscle strength at approximately 1% per year, with the rate of decline acceleration to 2-4% per year after 70 years of age [165], and the best intervention to prevent sarcopenia is physical exercise. In addition to the impact on skeletal muscle, cardiovascular and cognitive health also appear to be improved by exercise [166], [167], [168]. In a mouse model of mitochondrial dysfunction that results in early aging known as the mutator mouse, in which a mutation of the mitochondrial polymerase gamma causes a failure of proofreading-exonuclease activity resulting in the accumulation of mtDNA mutations, exercise prolonged lifespan and reversed several pathological phenotypes [169]. Exercise is now being explored as an intervention in aging mice and has been suggested to improve mouse cognition in a model of vascular

cognitive impairment [170], induce mtUPR in skeletal muscle of aged mice [171], improve muscle function in aging [172], [173], and protects against chronic inflammation and cancer [174]. Mechanistically, there are numerous adaptations to exercise, but increased mitochondrial biogenesis in multiple tissues seems to be a major factor perhaps through the activity of the PGC1 α /NRF/TFAM pathway [175], [166], [176]. Supply of the TCA intermediate citrate for acetyl-CoA through the activity of ATP-citrate-lyase also correlates with muscle mass, and increased ACL levels in mice increased mitochondrial function with aging [177].

1.3.7) Stem cell maintenance

Loss of stem cell function or stem cell exhaustion through depletion of stem cell pools or reduced capacity to proliferate and differentiate is a key hallmark of aging that has been well studied mechanistically and mitochondrial function has been strongly implicated in the appropriate maintenance of stem cell populations. There is also significant evidence that mitochondrial function can be causally related to the induction of the senescent cell state through provision of TCA metabolites and ROS [87]. Similarly, ROS and TCA metabolite levels have experimentally been shown to control the stemness, self-renewal, and capacity for differentiation of stem cells in several niches. For example, in mouse embryonic stem cells, the ratio of α KG/succinate has been experimentally demonstrated to control pluripotency [178]. The dioxygenase ten-eleven-translocation (TET) DNA demethylase enzymes were implicated for maintaining pluripotency by keeping key pluripotency epigenetically active and demethylated. ES cells were found to maintain high levels of α KG through glucose and glutamine catabolism to support self-renewal, while succinate caused the cells to differentiate and lose pluripotency [178]. There are several examples of ROS negatively impacting stem cell function and can lead to depletion from the niche, but there are also examples of the necessity of ROS for stem cells [179]. There is also some evidence for asymmetric inheritance of younger vs older mitochondria during stem cell division, like the asymmetric inheritance seen in yeast, which has been implicated in maintaining stemness [180].

Hematopoietic stem cells (HSC), which are multipotent stem cells residing in the bone marrow that provide the precursors for new blood cells throughout the lifespan, are characterized by low levels of mitochondrial activity in the quiescent state, with a reliance on glycolytic ATP. This state is thought to be

related to the existence of the HSCs in a hypoxic niche and may be an adaptation to limit flux through the TCA to prevent any possibility of ROS damage leading to mutation accumulation, since integrity of the genome is a major goal of the maintenance of stem cell pools [181]. Despite this observation, work from our lab has shown that ETC function is required for proper HSC differentiation and maintenance since deletion of an essential subunit of mitochondrial complex III, the Rieske iron sulfur protein (RISP), which resulted in proliferation of HSCs and prevented quiescence and differentiation leading to death due to an inability to produce sufficient blood cells [182]. The POLG mutator mouse also demonstrates accelerated HSC dysfunction as manifest by a reduction in lymphocytes and myeloid lineage skewing, which are features of changes to leukocyte populations with age, however the POLG mutant mice don't show a reduction in the HSC pool, but instead have arrested differentiation at immature stages of hematopoiesis and have mtDNA mutation rates that far exceed the amount of mtDNA mutations that accumulate with aging in normal mice, which have some implications for the validity of the model to study normal aging [183]. Data from the POLG mutator mice during embryogenesis, suggest that there are very early HSC and neural stem cell (NSC) defects that are partially reversible with the antioxidant n-acetyl-cysteine, suggesting that some of the observed deficits in this model are due to a negative role of ROS in stem cell function [184].

During brain development there are NSCs which are multipotent cells with the capacity for self-renewal and proliferation, and during adulthood in rodents, there are populations of radial-glia-like neural progenitor cells (NPCs) which continually undergo neurogenesis throughout the lifespan. The existence of adult neurogenesis in humans remains controversial [185]. Like NSCs, NPCs are also multipotent cells capable of differentiating down the 3 primary neural lineages to generate neurons, astrocytes, and oligodendrocytes. The primary locations where neural progenitor cells undergo neurogenesis in the adult mouse brain include the subventricular zone, which generates new neurons that migrate to the olfactory bulb, and the subgranular zone of the dentate gyrus of the hippocampus, due to the important role of the hippocampus in learning and memory, combined with the known functional decline of memory and cognition in aging and aging-related neurodegenerative disease, adult neurogenesis in the hippocampus

has received significant research attention. Brain regions with NPCs have been found to have increased rates of mitophagy [186].

NSCs are known to have a primarily glycolytic profile and the proliferative NPCs during embryogenesis also share this glycolytic profile. Loss of mitochondrial transcription factor A (TFAM), a protein that controls the expression and replication of mtDNA, leads to a complete loss of mitochondrial function by preventing the expression of several of the key OXPHOS genes encoded by mtDNA. Conditional deletion of TFAM in the hippocampus neural stem cells prevented neurogenesis at the intermediate progenitor stage, indicating that despite the glycolytic profile seen in proliferating neural stem cells, mitochondrial function is still essential [187]. Piracetam administration, a drug derived from the neurotransmitter GABA, that is related anticonvulsants such as levetiracetam, increased ATP concentrations in the hippocampus therefore increased mitochondrial function may correlate with increased neurogenesis [187]. Mitochondrial function may also help direct the fate of NPCs during differentiation. Loss of HK2 and LDHA is observed during differentiation from glycolytic NPCs to oxidative neurons and forced expression of HK2 and LDHA skews differentiation towards astrocytes and away from neurogenesis [188].

Limiting NAD⁺ levels in NPCs by deletion of the salvage pathway enzyme NAMPT can recapitulate a stem cell aging phenotype with decreased number of NPCs, decreased proliferation of NPCs, and decreased differentiation of NPCs especially to the oligodendrocyte lineage, while NMN supplementation was sufficient to sustain the NPC pool with aging in mice [189]. Furthermore, NDUFS2 function is required for NPC proliferation and differentiation [190]. NDUFS2 deficient NPCs showed impaired ATP production, proliferation, and differentiation into neurons and oligodendrocytes. NDUFS2 deficiency in this cell population was also associated with very early mortality by approximately 10 days of postnatal development [190]. Ubiquitous deletion of the enzyme L2HGDH, which recycles L-2-hydroxyglutarate back to α KG, in mice leads to impaired adult hippocampal neurogenesis presumably due to a direct effect of 2-HG accumulation and its ability to manipulate epigenetic state [191].

1.3.8) Inflammaging

Aging and many aging-related disease correlate with development of a state of chronic inflammation, particularly with mild elevation of the inflammatory serum markers interleukin 6 (IL-6) and C-reactive protein (CRP) in humans, with a skewing in leukocyte populations towards myeloid lineage cells [87]. Mitochondrial function may be involved in the control of inflammation during aging, since mitochondrial function has increasingly been identified as a central regulator of function in immune cells. One possible reason for the central role of mitochondria in immune function may be the evolutionary origin of bacteria from bacteria. Mitochondria still share several unique characteristics with potentially pathogenic bacteria, such as the circular mtDNA which resembles bacterial or viral DNA, and formylated peptides which also occur in bacteria but not nuclear encoded eukaryotic proteins. Immune cells evolved to identify these hallmarks of potential pathogens with immune proteins like the Toll-like receptor 9, the NLRP3 inflammasome, the cGAS-STING pathway, the mitochondrial antiviral signaling protein (MAVS), and the formyl peptide receptor 1 [87]. Therefore, increased release of mitochondrial-derived peptides and mtDNA, which are activators of these receptors, has been proposed as a potential mechanism by which declining mitochondrial function with age can trigger innate immune responses. Mitochondrial function in innate and adaptive immune cells also dictates the propensity and severity of immune response by controlling cell fate, signaling, and function in a variety of ways.

As previously mentioned, mtDNA release from the mitochondria (which occurs by an uncharacterized mechanism) can trigger innate immune inflammation through three pathways as previously mentioned; these include the Toll-like receptor 9 pathway, the NLRP3 inflammasome, and the cGAS-STING pathway. Toll-like receptor 9 recognizes extracellular or endosomal DNA, which leads to increased NF κ B signaling and results in elevated TNF α and IL-6 production. The downstream events of NLRP3 activation include caspase-1 activation which results in production of IL-1 β and IL-18. Finally, the cGAS-STING and MAVS pathway result in production of interferons. In addition to the possibility of mtDNA triggering these pathways, several of these mechanisms require mitochondrial function either due to ROS production or as a signaling platform, in order to stimulate inflammation. For example, MAVS signaling occurs and is coordinated at the outer mitochondrial membrane, and the NLRP3 inflammasome

requires ROS [87], [192], [56]. Furthermore, metabolites can influence immune cell functions, and lactate in particular has been shown to influence the inflammation through targeting of the MAVS signaling pathway [193].

A key aspect of innate immunity is the pro-inflammatory versus pro-repair polarization of macrophages. Pro-inflammatory macrophages are highly glycolytic but require mitochondrial function through a unique metabolic state to generate ROS from complex I RET through production of itaconate and succinate due to a disruption of IDH function [192]. ROS is required for IL-1b production, and the mitochondrial arginosuccinate shunt is used to generate nitric oxide. Anti-inflammatory or pro-resolving macrophages exhibit higher use of the classical TCA and ETC, producing less ROS, which has led to the oversimplified model in which inflammatory macrophages are glycolytic while anti-inflammatory macrophages are oxidative. This simple model is attractive since it would fit well with the observed correlation between declining mitochondrial function and increased inflammation and a reduction in repair. Indeed, the loss of healthy repair after tissue injury is a major feature and problem in aging, and therefore the metabolic factors controlling the pro-repair cells such as tissue macrophages and regulatory T cells (Tregs) is of great interest [194].

The adaptive immune system consists of T and B cells. B cells require mitochondrial function and mtROS for activation and proliferation, and changes in mitochondrial function, mitochondrial-derived metabolites and mtROS have been associated with the important B cell functions of class-switch recombination and plasma cell differentiation [192]. Long-lived antibody-secreting plasma cells rely on pyruvate entry into the mitochondria for long-term survival [195]. Naïve T cells are quiescent and exhibit low metabolic rates, however during activation of their T-cell receptors with appropriate co-stimulation, the cells become highly metabolically active with high rates of glycolysis and TCA cycle flux that requires both pathways and an intact ETC for robust activation which is dependent on the production of ROS for NFAT translocation to the nucleus and IL-2 production [196]. The production and levels of TCA metabolites, such as those controlling demethylation reactions, correlates with the formation of memory T cells and interferon responses through their ability to modulate epigenetics [192].

Recent work in the Chandel lab has identified that mitochondrial ETC function in Tregs is required for the suppressive function of Tregs that limits inflammation and autoimmunity [197]. Genetic deficiency of the mitochondrial complex III subunit RISP or QPC in mice leads to a fatal hyperinflammatory autoimmune phenotype. Although proliferation and survival of these Tregs in this model is unaffected, the loss of ETC activity leads to profound metabolic changes within the cell that prevent the cells from carrying out their key suppressive function. This defect causes the production of high levels of 2-HG, which is correlated with elevated DNA methylation, particularly at key genes necessary for the suppressive function of Tregs [197]. Whether a similar mechanism of decreased Treg suppressive function due to aging-related metabolic decreases in mitochondrial function is cause of chronic inflammation during normal aging remains to be determined.

1.3.9) Mitochondria in age-related neurodegeneration

Deficiencies in OXPHOS, reduced ETC complex function, and mtDNA mutations have been observed as prominent features of several neurodegenerative disorders and implicated as potential causes of neurodegeneration, including Alzheimer's disease (AD), amyotrophic lateral sclerosis (ALS), Huntington's disease (HD), Charcot-Marie-Tooth disease (CMT), and Parkinson's disease (PD) [198]. This led to the hypothesis that the cause of neuronal death in these diseases was a bioenergetic crisis due to a failure to provide sufficient ATP. However a study in mice directly testing the role of mitochondrial ATP synthesis by expressing the ATPase inhibitory factor in neurons found that, instead of promoting cell death, this led to a compensatory shift in neurons towards increased aerobic glycolysis that was actually protective in a model of neurotoxic exposure [199]. While this bioenergetic crisis hypothesis remains a possible contributing factor to neurodegeneration and the pathophysiology of defects observed in these and other diseases, the complex role of mitochondria in biosynthesis and signaling should not be overlooked.

Another important factor to consider, when analyzing mitochondrial function in the brain, is that there are both complicated intracellular and intercellular metabolic flexibilities that exist. The metabolic needs of the brain are very high, and glucose is used as the preferential substrate. While traditionally most research on brain metabolism has primarily focused on the neuron, more recently it has been

appreciated that the many supporting glial cells play a very important role in regulating neuron metabolism through the provision of specific substrates [200]. The relative importance of different metabolic pathways in different cell types and in different regions is therefore an important consideration that may drive the regional sensitivity to damage in neurodegenerative diseases. A common view of the cooperative metabolism between astrocyte and neuron metabolism is that astrocytes rely primarily on aerobic glycolysis while neurons rely heavily on OXPHOS with lactate produced by astrocytes feeding into neuronal OXPHOS [200]. Indeed, astrocyte-specific deletion of a subunit of mitochondrial complex IV, which significantly reduces OXPHOS, leads to the continued survival of astrocytes as glycolytic cells in mice without evidence of neurodegeneration [201]. Cellular mechanisms, such as phosphorylation of pyruvate dehydrogenase, exist to increase the relative energy contribution of glycolysis over OXPHOS during physiological events such as hypoxia, differentiation, and immune cell activation. Thus despite the existence of similar numbers of mitochondria in neurons and astrocytes, neurons are thought to be much more susceptible to deficits in OXPHOS since they are less capable of providing sufficient ATP for their requirements as they are either unable to significantly upregulate glycolysis or their energy needs are so high that they cannot be met by the relatively less efficient glycolytic pathway. In the brain, in addition to their metabolic and cell signaling roles, mitochondria-derived metabolites such as glutamate serve as neurotransmitters and precursors for neurotransmitters. Finally, mitochondria may help to coordinate the interaction between glia and neurons in the brain, For example fragmented mitochondrial release by activated microglia can lead to proinflammatory activation of astrocytes resulting in neuronal cell death [202].

Clinically, AD is characterized by cognitive impairment, especially with by loss of memory (dementia). Progressive cognitive deterioration leads to failure of language, attention, perception, and problem solving accompanied by irritability and emotional lability. Pathological features include gross atrophy of the cerebral cortex along with the accumulation of extracellular plaques of amyloid protein, intracellular neurofibrillary tangles, and gliosis. Clinically PD is characterized by progressive motor impairment with slow movements, a stooped body posture and shuffling gate, shaking of the hands, stiffness, and decreased balance, with later stages associated with cognitive impairment, hallucinations,

memory problems, and autonomic dysfunction. Pathological features include the loss of pigmented dopaminergic neurons in the ventral midbrain basal ganglia structure known as the substantia nigra pars compacta, intracellular proteinaceous Lewy body inclusions, and gliosis [198].

Origins of a causal hypothesis for mitochondrial dysfunction in neurodegenerative disease arise primarily from observations in AD and PD. In the 1980s it was discovered that 1-methyl-4-phenyl-1,2,3,6-tetrahydropyridine (MPTP) could induce an acute Parkinsonian phenotype in humans. It was determined that this was due to inhibition of mitochondrial complex I, and that other complex I inhibitors could recapitulate PD-like symptoms and dopaminergic toxicity in animal models. This led to the investigation and discovery of reduced mitochondrial complex I abundance and function in post-mortem PD patient brains and platelets. However, two key problems with this data included the fact that PD post-mortem brains had already lost the majority of the key neuronal type implicated in disease pathogenesis, dopaminergic neurons in the substantia nigra pars compacta, and the therapeutic drug used in PD, levodopa, was found to reduce OXPHOS activity in rodent brains despite its positive effect on PD-like symptoms. Around the same time, morphological changes in mitochondria were observed in postmortem brains from AD patients. Furthermore, fibroblasts from patients were found to have altered metabolic properties, [203] reduced glucose and glutamine oxidation, and increased calcium concentrations. Cybrid models (cytoplasmic hybrids) in which cells were depleted of mitochondria and then reconstituted with mitochondria from AD patient cells showed mitochondrial dysfunction, and reduction in the activity of mitochondrial complexes I and IV was found in platelets and brain tissue of AD patients, but the reductions were found to be mild and were observed in other neurodegenerative processes, and were not replicated in some studies leading to questions about the functional significance. Finally, in cell culture systems amyloid plaques were found to induce decreases in mitochondrial function, which called into question whether OXPHOS deficiency was a cause or effect of AD.

The observations that AD is associated with reduced expression and function of genes involved in the ETC in post-mortem tissues compared to controls [204], led to investigation of mtDNA integrity. Conflicting results with regards to the excessive accumulation of mtDNA mutations in patients with PD and AD, with some reports finding associations while other reports do not. For example, early reports

implicating mutations in the mitochondrially encoded complex I subunit ND2 (NADH dehydrogenase 2) in AD [198], but these results were not substantiated by other studies. As another example there is a common deletion of 4977bp of the mtDNA that has been associated with aging and also with AD, and ALS, so the lack of specificity makes it difficult to determine whether the correlation is primarily due to a correlation with age. There have been reports of an association of increased mitochondrial 5-methylcytosine with AD and PD pathology [205]. mtDNA methylation has recently been appreciated, but the functional effects and mechanisms are less well defined for mtDNA as compared with nuclear DNA methylation. Furthermore, some have hypothesized that observed changes in mtDNA could be due to neurodegenerative processes or attempts at repair leading to increased mitochondrial turnover. Therefore, despite significant work, whether mtDNA mutation are the cause or effect of neurodegenerative changes in PD and AD remains unproven

Currently there are two primary theories for explaining the loss of substantia nigra pars compacta (SNc) dopaminergic neurons in PD: Lewy body toxicity, and mitochondrial dysfunction. Lewy bodies are toxic proteinaceous intracellular inclusions with prominent involvement of the synaptic protein alpha-synuclein (asyn). Mutations and gene duplications for the gene encoding asyn increase the risk of PD. Furthermore, numerous studies have shown that asyn pathology can spread from distal sites and throughout the brain like a prion. Why the SNc dopaminergic neurons in particular would be sensitive to Lewy body pathology remains controversial, furthermore some cases of PD do not exhibit Lewy bodies in the SNc, or exhibit them after dopaminergic neuron loss has already commenced, and levels of asyn that have shown to be toxic to individual neurons in experimental models are typically not observed in PD patients. The link to mitochondrial dysfunction has been described above, but another important observation was that mutations in genes encoding PINK and Parkin, which have been shown to be required for triggering mitophagy as well as influencing several other aspects of mitochondria function including antioxidant pathways and OXPHOS, lead to inherited early onset forms of PD.

The current theories for the cell type specificity of the above mechanisms for selective SNc dopaminergic neuron loss include the unique calcium physiology of these neurons, their highly articulated axonal arbors, and the use of dopamine as a neurotransmitter. The activation physiology of these

neurons is relatively unique in the brain, with a slow, broad action potential that has high calcium entry, rhythmic pacemaking activity, and low expression of calcium binding proteins. For example, the nearby but not as susceptible dopaminergic neurons in the ventral tegmental area share the pacemaking activity and broad action potentials, but have lower calcium entry and much higher levels of calcium binding proteins. There is a feed-forward effect of calcium entry on increased OXPHOS and increased ROS production and elevated cytosolic calcium. Inhibition of calcium channels in dopaminergic neurons has been shown to decrease sensitivity to toxins. The projecting axons of SNc dopaminergic neurons are long and have highly articulated arbors that are not myelinated. It has been estimated that these axonal arbors in the mouse striatum have as many as 200,000 sites of vesicular release [206]. Markers of oxidative stress have been shown to increase in axons with increased size, and asyn, as a synaptic protein involved in neurotransmitter vesicle trafficking and release, is also increased with increasing axon size and branching. Other large highly branched neurons in the brain are not susceptible in PD, though, suggesting a combination of factors [206]. Dopamine is a redox active molecule that can become oxidized by mtROS, which can in turn reduce activity of the lysosomal enzyme glucocerebrosidase, leading to impaired lysosomal function and asyn accumulation; providing a potential mechanistic link between mitochondrial function and cellular pathology associated with PD [207]. Monoamine oxidase activity in SNc dopaminergic neurons limits cytosolic dopamine oxidation and, by localizing to the mitochondrial membrane, can shuttle electrons into the ETC rather than producing hydrogen peroxide, as a mechanism to both prevent ROS damage and also support the high bioenergetic demand of dopamine release in the dopaminergic neuron axon [208].

One area of active research is the role of mitochondrial-ER contacts. These inter-organelle contacts have been implicated in the regulation of lipid (including cardiolipin production and sphingolipid/ceramide metabolism) and calcium homeostasis which are both altered in neurodegenerative processes. Several precursors to insoluble protein aggregations characteristic to these disorders, like asyn, presenilins, amyloid precursor protein have been shown to localize to these sites [198]. Furthermore *C. elegans* proteomics studies revealed that ETC components, and complex I subunits in

particular, are over-represented in peptides that are prone to misfolding and to insoluble inclusion body formation [98].

The recent and prominent failure of several major clinical trials to limit amyloid accumulation in AD has led some to question the causative role of these accumulations and to reconsider other factors such as glucose metabolism and mitochondrial and immune function. Altered glucose and pyruvate metabolism has been described in AD and PD, and both disorders have been linked to type 2 diabetes [209], [210]. Recently, the role of inflammation and the immune system has gained some support as a predisposing or precipitating factor in AD and PD pathogenesis. AD has now been associated with detection of herpes virus in the brain [211]. PD has been suggested to be partially caused by changes in mitochondrial antigens leading to an autoimmune-like destruction of susceptible neurons [212]. Mice with deficiency for PINK and Parkin do not normally develop PD-like phenotypes, however it has been found that infection in the intestines can trigger PD like symptoms in these mice [213]. Finally, work with STING pathway deficient mice crossed to PINK and Parkin deficient mice has demonstrated that PINK and Parkin limit systemic inflammation caused by potential recognition of mtDNA through the STING pathway [214]. Together these findings implicate a potential interaction of mitochondrial function, systemic metabolism, and inflammation in the pathogenesis of the age-related neurodegenerative diseases, but the precise mechanisms of disease require further study.

1.4) Primary mitochondrial disease

1.4.1) Overview of mitochondrial diseases

Primary mitochondrial disorders are a heterogeneous group of diseases and syndromes that are caused by mutations in the nuclear and mitochondrial genomes that negatively impact aspects of mitochondrial function. Many of these diseases result in prominent dysfunction in the central nervous system (CNS), including motor dysfunction, seizures, ataxia, and movement disorders resembling Parkinsonism, as well as muscle pathology and dysfunction of other highly energetic tissues such as the kidneys, liver, intestines, and retina. Although features of primary mitochondrial disorders may resemble aspects of the common age-related neurodegenerative diseases, in primary mitochondrial disorders, these features rarely occur in isolation, but are typically part of a syndrome of multi-organ system

dysfunction [198]. Examples of these syndromes include the pediatric mitochondrial diseases which include Leigh syndrome (LS), Alpers-Huttenlocher syndrome, childhood myocerebrohepatopathy spectrum, ataxia neuropathy spectrum, myoclonic epilepsy myopathy sensory ataxia, Sengers syndrome, 3-methylglutaconic aciduria with deafness encephalopathy and Leigh like syndrome, Pearson syndrome, and congenital lactic acidosis, and the adult onset mitochondrial diseases which include Leber hereditary optic neuropathy (LHON), Kearns-Sayre syndrome, mitochondrial myopathy encephalopathy lactic acidosis and stroke-like episodes (MELAS), myoclonic epilepsy with ragged red fibers (MERRF), neurogenic muscle weakness ataxia and retinitis pigmentosa, chronic progressive external ophthalmoplegia, and mitochondrial neurogastrointestinal encephalopathy syndrome [215]. There is significant clinical and molecular heterogeneity in these syndromes. For example, some of these syndromes are associated with mutation in one or a few genes, some mutations can cause multiple of the syndromes, and mitochondrial heteroplasmy complicates the disease susceptibility and penetrance of these disorders, especially when they are associated with mtDNA gene mutations or deletions. Leigh syndrome can be caused by mutations in more than 75 different genes that are spread across both the mitochondrial and nuclear DNA. The currently accepted diagnostic algorithm for mitochondrial disease includes a clinical suspicion for mitochondrial disease based on clinical history and physical examination, measurement of lactate and pyruvate levels in the plasma and cerebrospinal fluid, measurement of plasma acylcarnitines, organic acids in urine, FGF21 and GDF15 levels in serum, neuroimaging, such as T2-weighted MRI imaging for Leigh syndrome, and evaluation of cardiovascular function. This clinical evaluation and testing is combined with genetic testing, either with specific panels for a known clinical syndrome, or mtDNA, exome, or whole genome sequencing with potential biopsy and analysis of affected tissue, especially muscle [215]. Mitochondrial diseases remain a very significant clinical challenge. While individually these diseases are rare, together diseases caused by mutations of mitochondrial-DNA-encoded and nuclear-gene-encoded mitochondrial proteins occur in approximately 1 in 4000 births, with much higher prevalence in certain populations [216]. Treatment options are very limited, perhaps due to an incomplete understanding of the pathogenesis of these diseases. The majority of primary

mitochondrial diseases are clinically challenging to diagnose and manage, and there are few effective disease-modifying therapies available for these diseases.

1.4.2) Leigh Syndrome or subacute necrotizing encephalomyelopathy

Leigh syndrome was first described by the physician Denis Leigh in a 1951 case report of an infant who succumbed to the disease at 7 months of age [217]. Due to pathological similarity to Wernicke's encephalopathy Leigh speculated that perhaps this disease was caused by a metabolic deficiency and he questioned the mechanism by which some regions of the brain are damaged while some are spared. This question is still an area of active research today. In the decades since Leigh's first report, it has become appreciated that Leigh syndrome is the most common of the pediatric mitochondrial diseases, affecting approximately 1 in 40,000 births [218].

Presentation of LS usually occurs within the first year, with developmental regression, seizures, blindness, dystonia, ataxia, hypotonia, and nystagmus as common neurological features eventually leading to death by 2-3 years of age [218]. Disease onset normally follows a period of normal development and cases of adult onset LS have been rarely reported. LS pathology reveals histological changes of increased vascularity, demyelination, and glial activation bilaterally in regions including the basal ganglia, brain stem, and cerebellum [218].

Defects in mitochondrial energy generation pathways are known to cause LS [219]. Mutations have been identified in over 50 genes encoded in both the nucleus and the mitochondria. These genes include electron transport chain complex protein subunits and assembly factors, mitochondrial dehydrogenase enzymes, and genes involved in the ubiquinone synthesis pathway [218]. Despite the identification of the genetic mutations that lead to many mitochondrial diseases including LS, the methods for treatment remain inadequate perhaps in part due to incomplete understanding of the disease mechanisms on a cellular level [220]. Studies of this disease may provide better understanding of the complex biology of cellular metabolism through specific defects in OXPHOS machinery that lead to profound and varied cellular defects.

One of the first nuclear genes identified to cause LS was *NDUFS4*. Novel mutations in *NDUFS4* continue to be identified in human populations to this day, and *NDUFS4* mutation frequently leads to a

relatively early onset and severe phenotype of LS with consistent brainstem involvement [221], [222, 223]. The assembly kinetics, subunit turnover, and precise structure of complex I remains a topic of research [224], [225]. As a nuclear encoded subunit, NDUFS4 contains an N-terminal mitochondrial localization sequence and is cleaved after mitochondrial import to form a mature protein [226]. Elevated cAMP levels increase mitochondrial accumulation of NDUFS4 through a C-terminal PKA-mediated phosphorylation event that prevents leak of NDUFS4 back into the cytosol [226]. NDUFS4 is incorporated into complex I fairly late during assembly and is required for the completion and stability of a functional complex I [227], [228]. Supramolecular interactions between complex I and complex III within super complexes lead to low levels of functional complex I in the absence of NDUFS4 [229].

1.4.3) The NDUFS4 mouse model of mitochondrial disease

In 2008, the first mouse model of LS was established by deletion of NDUFS4 [133]. A gene-targeting technique was used to generate lox-p sites flanking the second exon of the mouse NDUFS4 gene. Ubiquitous deletion of exon 2 was accomplished by expression of a cre recombinase in the epiblast stage of development [133]. Homozygous knockout of NDUFS4 in mice (NDUFS4^{-/-}) leads to a progressive encephalopathy that in many ways recapitulates the human disease [133]. These mice develop neurological symptoms of ataxia, blindness, seizures, regression of weight, and ultimately die by approximately 50-60 days of age with brain lesions in similar regions and with similar histopathological hallmarks as those observed in human LS [133]. An independently developed point mutant NDUFS4 mouse was developed in 2009, which removed the last 10 amino acids of NDFUS4 and reduced complex I function in heterozygous mice without LS clinical features. This construct was embryonic lethal in homozygous mice suggesting that this different construct may have had a type of dominant negative effect on complex I assembly [230]. A different method of NDUFS4 mutation in mice was accomplished by spontaneous B2 SINE retroviral insertion [231]. These NDUFS4^{fky/fky} mice also displayed features of the LS phenotype such as growth inhibition and ataxia that were similar but less severe than the NDUFS4 deficient mice [231]. Most mouse models of human disease are not perfect and it has been noted that while the NDUFS4 knockout mice display many of the features of human LS, the localization and severity of central nervous system lesions is slightly different with more damage in the cerebellum relative to the

basal ganglia in mice and more damage to the basal ganglia than the cerebellum in humans [232].

Despite this slight discrepancy, the NDUFS4 deficient mouse model has come to be accepted as a valid system for studying LS [232].

NDUFS4 mutation or deletion disrupts the normal function of the mitochondria which are important in myriad bioenergetic, biosynthetic, and signaling roles. Isolation of embryonic stem cells from NDUFS4^{fky/fky} mice revealed intact pluripotency and stability of the mitochondrial and nuclear genomes in these cell lines, however expression of mature glial and neuronal markers was reduced in NDUFS4^{fky/fky} derived cells [233]. A similar reduction of mature marker expression was observed during directed differentiation to neurons in human induced pluripotent stem cell lines with complex I deficiency [234]. Isolated mouse embryonic fibroblasts (MEFs) and cultured astrocytes and neurons from NDUFS4^{fky/fky} mice have undetectable levels of NDUFS4 protein, significantly reduced levels of complex I activity, and a slight reduction in ATP generation rate that was substrate dependent [235]. NDUFS4^{fky/fky} MEFs also had decreased mitochondrial membrane potential while astrocytes and neurons retained their mitochondrial membrane potential [235]. ATP synthesis using substrates that require OXPHOS in all of these isolated cells was abolished by the addition of the complex I inhibitor rotenone indicating that residual complex I activity contributes significantly to ATP production in NDUFS4^{fky/fky} cells [235]. Muscle and skin fibroblasts isolated from adult NDUFS4^{-/-} mice have inactive complex I, increased levels of reactive oxygen species (ROS), and an abnormal mitochondrial morphology with reduced branching [236]. Synaptic mitochondria from isolated synaptosomes of degeneration-prone regions of NDUFS4^{-/-} mouse brains exhibit decreased respiratory capacity relative to control and relative to isolated KO non-synaptic mitochondria and synaptic KO mitochondria from synaptosomes of regions of the brain that do not frequently show signs of neurodegeneration [237]. Surprisingly, comparisons of these susceptible and non-susceptible regions did not reveal detectable changes in ROS, glycolytic rate, or complex I stability [237]. Further research is needed to understand the cause of regional cellular sensitivity to loss of NDUFS4 and how this susceptibility leads to the neurodegenerative phenotype.

One of the key causes of death in NDUFS4 deficient mice and in certain LS patients with brainstem lesions is respiratory arrest [238]. NDUFS4^{-/-} mice display abnormal respiration with periods of

apnea and abnormal recorded responses to hypoxia in the ventral brainstem respiratory center. A major site of gliosis in *NDUFS4*^{-/-} mice, the brainstem vestibular nuclei (VN) are important for maintenance of balance. Damage or inflammation in this region contributes to ataxia. Notably, an injected viral cre was used to delete *NDUFS4* in the VN, which was sufficient to induce breathing abnormalities in mice with a slight decrease in survival rate. Furthermore, selective rescue of *NDUFS4* in the VN of *NDUFS4*^{-/-} mice was sufficient to improve median survival by approximately 2 weeks [231]. Consistent with a role of complex I function in oxygen sensing and breathing, *NDUFS4*^{-/-} mice, and mice treated with piericidin, were found to have impaired pulmonary vasoconstriction in a model of mainstem bronchus occlusion [239]. Recent studies have both supported and called into question the role of breathing dysfunction in *NDUFS4* mortality, with some evidence indicating that seizures are a major potential cause of death in the mouse model [240].

The availability of the floxed *NDUFS4* mouse has allowed further cell type specific definition of the *NDUFS4* mouse model by crosses with tissue- and cell-type-specific promoter-driven cre recombinases. For example, *NDUFS4* deficiency specifically in cardiomyocytes leads to the development of hypertrophic cardiomyopathy [241]. *NDUFS4* deficiency specifically in the myeloid lineage led to a skewing towards pro-inflammatory macrophages and shifted bone macrophage-osteoclast polarization away from a bone resorption phenotype [241]. Another tissue of interest in this model is the retina, as many LS patients exhibit optic nerve atrophy and retinal dystrophy, furthermore *NDUFS4* mutations, in addition to causing LS, can cause the mitochondrial eye disease LHON. The *NDUFS4*^{-/-} has been found to have a loss of retinal ganglion neurons and inflammation in the eye that leads to vision loss and atrophy of the optic nerve [242]. Follow up work on the retinal phenotype in these mice revealed that bipolar cell loss preceded and triggered the inflammation that led to ganglion cell loss [243]. Interestingly, several interventions have been shown to ameliorate this retinal phenotype by preventing inflammation and preventing retinal ganglion cell loss, including the donation of mitochondria from iPSCs, which may be due to an anti-inflammatory role for this intervention, as well as treatment with the immunosuppressive and mTOR inhibiting compound rapamycin, and treatment with the sedative zolpidem and the antispasmodic papaverine [243], [244]. In addition to optic nerve atrophy, it was found that *in vivo*

NDUFS4^{-/-} mice exhibited reduced light-evoked signaling in photoreceptors by electroretinography [245]. There was no observed photoreceptor degeneration or impaired regeneration of the visual pigment by the retinal pigment epithelium. Surprisingly, in *ex vivo* medium, isolated retinal photoreceptors were capable of normal light-evoked signaling by electroretinography, which indicates that rather than a developmental or cell intrinsic defect due to NDUFS4 deficiency, something about the *in vivo* microenvironment of the outer retina prevents normal photoreceptor function in NDUFS4 deficient mice [245].

NDUFS4^{-/-} mice and NDUFS4 deficiency restricted to excitatory glutamatergic neurons in mice have been found to have profoundly increased sensitivity to inhaled anesthetics, indicating a key role of mitochondrial function in anesthesia [246]. Interestingly, loss of NDUFS4 only in astrocytes using GFAP-cre, is not reported to lead to a fatal phenotype, but does alter anesthetic emergence. Mice without NDUFS4 in astrocytes had similar sensitivity to anesthetics, but had a significant delay in recovery from anesthesia [247].

Tissue specific deletion of NDUFS4 using a Nestin-promoter driven cre in neuron and glial cell precursors is sufficient to cause a nearly identical phenotype as ubiquitous deletion [248]. Recent studies using more specific cre-drivers have identified a more nuanced and neuron type specific understanding of NDUFS4 deficiency's effects on survival and neuronal function. Loss of NDUFS4 specifically in dopaminergic neurons demonstrated some evidence of non-motor symptoms of PD without resulting in motor dysfunction, ataxia, or loss of dopaminergic neurons [249]. Loss of NDUFS4 specifically in medium spiny neurons in the striatum led to long term progressive, but mild, motor impairment with no change in survival or evidence of cell death or inflammation [250]. Loss of NDUFS4 specifically in Purkinje neurons in the cerebellum was not found to be fatal or lead to motor dysfunction, despite evidence of inclusion formation in these cells in the fatal ataxic nestin-cre NDUFS4 model [248]. Use of an inducible ubiquitous cre resulted in the formation of an ataxic phenotype but took several months to develop, indicating an important role for NDUFS4 loss during development [248]. Finally, a recent paper has identified that NDUFS4 loss specifically in cholinergic neurons had no obvious effects, while loss of NDUFS4 in either glutamatergic or GABAergic neurons resulted in a fatal phenotype [240]. Loss of NDUFS4 in excitatory glutamatergic neurons using Vglut2-promoter-driven-cre resulted in progressive motor dysfunction,

brainstem inflammation, breathing abnormalities, and early mortality. Loss of NDUF54 in inhibitory GABAergic neurons using Gad2-promoter-driven-cre resulted in inflammation in the basal ganglia and seizure-induced mortality, earlier than in the excitatory neuron NDUF54 deficient mice, without motor dysfunction. This finding suggests a potential supremacy for seizures as an early cause of death in the nestin-cre NDUF54 deficient mice which also tend to die slightly earlier than the ubiquitous NDUF54^{-/-} mice [240].

1.4.4) Interventions that manipulate the NDUF54 mouse model phenotype

Several interventions in the literature have been described to reverse some or all of the phenotypes of the NDUF54 deficient mouse model, including pharmacological, gene therapy, and ambient environmental oxygen deprivation-based approaches. The protein Opa1 promotes mitochondrial fusion and helps to stabilize mitochondrial cristae by serving as a diffusion barrier. Opa1 is thought to improve the stability of respiratory chain complexes and super complexes and reduce ROS production by minimizing electron leak. Overexpression of Opa1 increases respiratory chain activity and oxygen consumption, improves the motor symptoms of NDUF54^{-/-} mice, and mildly increases lifespan by approximately 1 week [251]. Inhibition of poly-ADP-polymerase-1 (PARP), a DNA repair enzyme therapeutically targeted in certain cancers, by genetic and pharmacological means has been shown to increase aspects of mitochondrial function. PARP inhibitor treatment of NDUF54^{-/-} mice from day 30 until death improved the motor function and reduced gliosis in certain brain regions without effecting neuronal cell death or longevity [252]. Consistent with a mechanism of restoring NAD⁺ availability with PARP inhibitor treatment, a recent report found that direct supplementation of NAD⁺ precursor NMN extended lifespan, nearly doubling the median lifespan, in the NDUF54^{-/-} mice and reduced lactic acidosis [253]. NMN was observed to increase levels of α KG, so treatment of NDUF54^{-/-} mice with the cell-permeable dimethyl-ketoglutarate was attempted and also was found to extend lifespan by a slightly smaller margin than NMN supplementation.

The mTOR inhibitor rapamycin has been shown to improve longevity in mice by inhibiting the anabolic mTOR pathways. Remarkably, median survival of NDUF54^{-/-} mice was more than doubled with daily rapamycin treatment compared to vehicle treatment. Every-other-day dosing had a more modest

effect on longevity [254]. Treated mice have markedly reduced gliosis and significantly improved motor symptoms [254]. There was very high variability in lifespan with rapamycin treatment, with some individuals having lifespans comparable to vehicle treated controls and a minority of mice living over 200 days. The mice remain very small during the course of this treatment, most individuals were less than 10 grams, and this reduction in weight gain was dose dependent [254], [255]. Rapamycin treatment did not increase complex I expression, mitochondrial mass, or mtDNA content and did not consistently reduce markers of mTOR activity in the brain, but did improve cristae morphology in a similar manner as Opa1 overexpression [254]. In order to further test the clinical relevance of rapamycin as a treatment regimen for mitochondrial disease, rapamycin dosing was begun after symptom onset in *NDUFS4*^{-/-} mice [256]. Unfortunately waiting until symptom onset required a dose that is much higher than the comparable standard clinical dose for humans [256]. There was, however, a significant increase in median survival by approximately 25% [256]. Serine catabolism, which may be induced by this aberrant mTOR activation, which strongly induces serine catabolism, 1 carbon metabolism, and the mitochondrial enzyme MTHFD2 which recent evidence suggests can contribute to NADH accumulation in the mitochondria in the setting of ETC inhibition [257], [18]. A small molecule inhibitor of serine catabolism was shown to delay the onset of the clasping postural/spasticity phenotype of the *NDUFS4* deficient mice [18]. In a different model of mitochondrial dysfunction, mitochondrial myopathy, downregulation of anabolic mTOR signaling in muscle was capable to delay progression by preventing excessive activation of the integrated stress response, mitochondrial unfolded protein response, and one-carbon metabolism [257]. There is also a strong connection between excessive mTOR pathway activation and genetic epilepsy such as in the disease tuberous sclerosis [258], which may also contribute to the observed effects of mTOR regulation in mitochondrial neuropathies.

Another remarkable intervention that increased lifespan of *NDUFS4*^{-/-} mice was simply allowing the mice to live in a hypoxic environment [259]. This result is very surprising given the fact that these mice already exhibit hypoxemia under normoxic conditions with irregular breathing rates and irregular breathing reflexes. Nevertheless, maintenance of *NDUFS4*^{-/-} mice in 11% oxygen conditions drastically improved neuropathology, motor function, and longevity [259]. Long term exposure to hypoxia also was

found to prevent dysfunctional hypoxic pulmonary vasoconstriction in the model of mainstem bronchus occlusion *NDUFS4*^{-/-} mice [239]. Hypoxic *NDUFS4*^{-/-} mice had increased weights relative to normoxic mice and all survived past 160 days. Furthermore, ambient hyperoxia with 55% O₂ was universally fatal for *NDUFS4*^{-/-} mice at an earlier time point than normoxia implicating oxygen toxicity as a possible key factor in determining *NDUFS4*^{-/-} mouse lifespan [259], [260]. Given that oxygen is a necessary substrate for the impaired OXPHOS pathway, it may seem somewhat contradictory that limiting concentrations of oxygen are actually protective in this model, but the presence of evolutionarily conserved hypoxia responsive pathways that limit oxygen reliance on a cellular level; such as hypoxia inducible factor (HIF) activation, changes in ROS production, or changes in organ level physiology, may contribute to this protective benefit. This has led to the hypothesis that hypoxia, by activating some aspect of the protective hypoxia response or by reducing ROS, may provide a therapeutic benefit in patients with certain mitochondrial diseases. Follow up work by the same group found that interventions that limited oxygen delivery, including inducing severe anemia and exposure to carbon monoxide, were also beneficial in the *NDUFS4*^{-/-} mice, ameliorating behavioral defects, MRI lesions, and increasing survival [261]. These findings seemed to be independent of a hypoxia response and therefore implicated a potential role for direct oxygen toxicity in this model, raising the intriguing possibility that one of the reasons for mitochondrial disease CNS dysfunction is the inability of mitochondria to keep oxygen tension sufficiently low to prevent damaging effects.

1.5) L-2-hydroxyglutarate

1.5.1) D-2HG is an oncometabolite in IDH mutant cancer

Mutations in isocitrate dehydrogenase (IDH) genes 1 and 2 were identified in several types of human cancers starting with a case of colorectal cancer in 2007 [262], [263]. IDH1 and IDH2 mutations were subsequently found to be relatively common in glioblastoma [264], in this original paper IDH1 mutation was found to be associated with significantly increased survival. Further work has found that IDH mutations are associated with increased seizures in glioma patients, pointing to a potential role of 2-HG in the control of seizure threshold, perhaps due to structural similarity to the excitatory neurotransmitter glutamate [265]. Furthermore, IDH1 and IDH2 mutations were identified to occur

frequently in acute myeloid leukemia (AML). Other types of cancers with identified IDH mutations include chondrosarcoma, thyroid carcinoma, hepatic cholangiocarcinoma, angioimmunoblastic T-cell lymphoma, solid papillary carcinoma with reverse polarity, prostate adenocarcinoma, paraganglioma, and melanoma [263]. It was determined that the common mutations in these cancers occurred at specific sites in the IDH enzyme that lead to neomorphic enzyme activity that resulted in catalysis of the reduction of α KG to the D enantiomer of 2-hydroxyglutarate instead of IDH's normal enzymatic activity of oxidizing isocitrate to α KG. Although both enantiomer, L-2HG and D-2HG are made at low levels physiologically by promiscuous enzyme activity, the enzymes dehydrogenase enzymes L2HGDH and D2HGDH are normally able to convert 2-HG back to α KG. In the setting of IDH mutation, however, accumulation of supraphysiological levels of D-2HG allows this metabolite to act as an oncometabolite promoting cancer transformation and growth, primarily through its inhibitory effect on the TET enzymes leading to decreased DNA demethylation [266], [267] (Figure 1.5.2.1). It has been shown that L-2HG is actually a more potent inhibitor of the α KG-dependent dioxygenases like TET2 as compared with D-2HG, but there is some evidence that there are differential effects on different members of the dioxygenase family of enzymes with L-2HG inhibiting the PHD enzymes while D-2HG potentiates their activity [267], [268]. The above comparison was initially identified as a potential reason why D-2HG was observed as a causative oncometabolite, but L-2HG was not, however recent work in renal cell carcinomas has identified elevated L-2HG levels in several tumors, which was correlated with reduced expression of L2HGDH, decreased evidence of DNA demethylase activity (TET enzymes), and overexpression of L2HGDH *in vitro* was found to be suppressive of the phenotype of these cancer cells [269], [270]. Furthermore, a physiologically important role for 2-HG as a modulator of epigenetics has been demonstrated in *D. melanogaster* during normal larval development [271]. Upregulation of the fly homolog of lactate dehydrogenase was found to lead to significant accumulation of L-2HG during a specific stage of development, which was followed by upregulation of the fly homolog of L2HGDH to degrade L-2HG at subsequent stages of development. This raises the possibility of the physiological use of 2-HG as an epigenetic modifier to guide cell fate during development in animals [271].

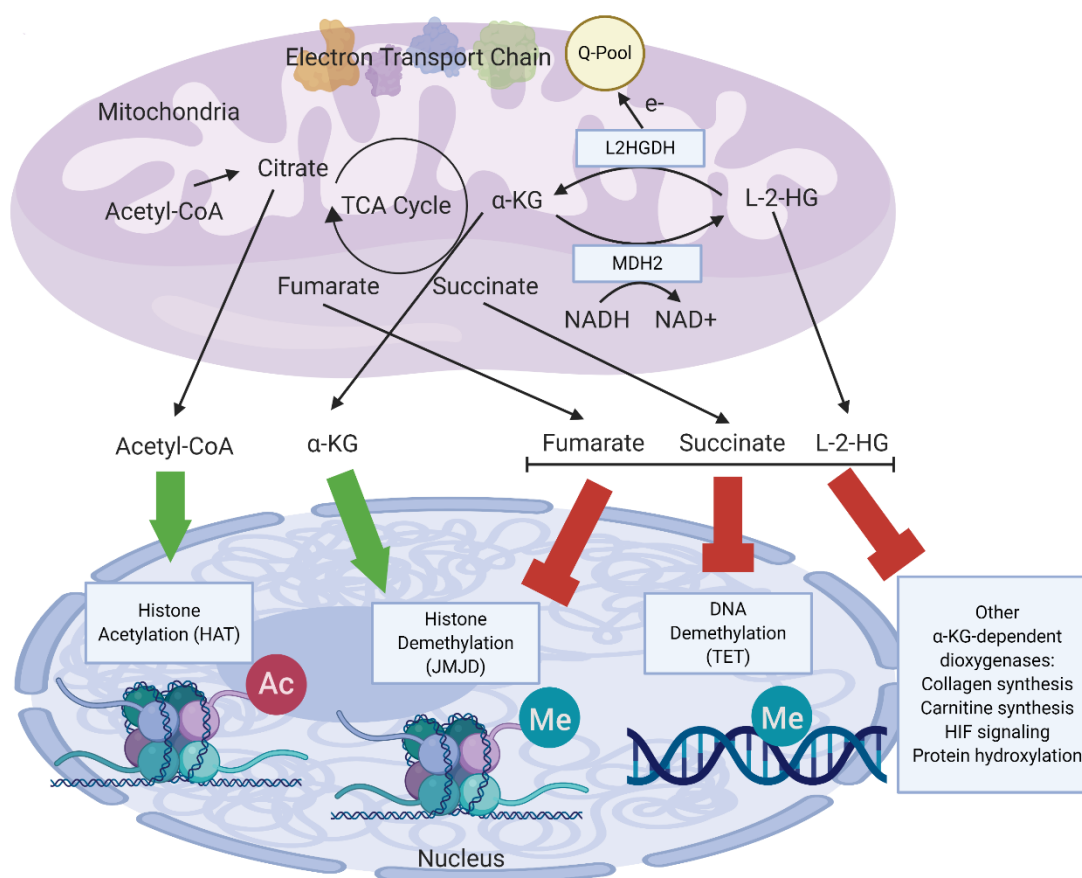


Figure 1.5.2.1. Mitochondrial metabolites control dioxygenase enzymes and epigenetics. 2-hydroxyglutarate, and other metabolites controlled by mitochondrial function, regulate the activity of numerous enzymes involved in epigenetics and other cellular processes.

1.5.2) L-2HG is produced during hypoxia and electron transport chain inhibition

The mechanisms of L-2HG production during physiological conditions in cells have received some attention. It was found that exposure to hypoxia can result in formation of L-2HG by reduction of α KG, that is catalyzed by promiscuous enzyme activity of lactate dehydrogenases and malate dehydrogenases and requires the conversion of NADH to NAD⁺ [272], [273]. This has led to the hypothesis that the production of L-2HG may serve as a type of metabolic release valve to deal with the increased reductive stress, or excess accumulation of NADH, that can occur with hypoxia [273]. It was also determined that acidic pH can favor the conversion to 2HG [274], [275], and that L-2HG can be further converted to L-2-hydroxyglutaramate by promiscuous enzymatic activity of glutamine synthetase, and that ω -amidase can convert L-2-hydroxyglutaramate back to 2-HG [276]. It was also determined that

mitochondrial ETC ablation, especially with loss of ETC complex III, which is another cause of elevated NADH, can lead to increased accumulation of 2-HG in cell lines and in mouse cells *in vivo* [277], [197], [182]. L2HGDH is an FAD-dependent mitochondrially localized enzyme, that is thought to transfer electrons from the oxidation of 2-HG to the electron transport chain via the electron-transferring flavoprotein (ETF) and ETF dehydrogenase to ubiquinone pool [278], which provides another mechanism by which ETC inhibition, particularly at complex III, can result in increased accumulation of L-2HG: preventing its oxidation back to α KG due to a highly reduced ubiquinone pool.

1.5.3) L2HGDH deficiency resembles mitochondrial disease and may be a functional output of mitochondrial dysfunction in aging and neurodegeneration

In the 1920s and 1930s, biochemists first identified 2-hydroxyglutarate as an intermediate of metabolism in extracts from animal tissues [279]. It was established that 2-HG was formed by the reduction of α KG as opposed to the oxidation reaction of α KG to succinyl-CoA and succinate. In 1980 a case report describing a child with severe developmental abnormalities and high L-2HG levels in the urine, established 2-hydroxyglutaric aciduria as an inborn error of metabolism in humans with severe neurological consequences due to elevated 2-HG levels [280]. Inborn errors of metabolism refer to developmental diseases in humans that are caused by loss of function of single metabolic enzymes. This class of disease include many of the primary mitochondrial diseases previously discussed as well as lysosomal storage disorders. While they are individually rare, with over 500 individual recognized disease entities, collectively inborn errors of metabolism have an incidence of approximately 1:1000 and while some are manageable with early recognition, many result in devastating neurological consequences and early mortality [61]. Several years after the first description of 2HG aciduria, a dehydrogenase enzyme for L-2HG was discovered in liver [281], and in 2004 the L2HGDH gene was identified as the cause of this disease [282]. Both L-, D-, and mixed L+D-2-hydroxyglutaric acidurias have since been described and manifest as a very rare, progressive neurometabolic disease featuring cerebellar ataxia, epilepsy, and neurodevelopmental delay and intellectual disability [283], [284], [285], [286], [287]. Several of these features are highly reminiscent of primary mitochondrial diseases and establish 2-HG as a neurotoxic molecule in humans. L2HGDH deficient mouse models have been developed, which recapitulate some

features of the human disease [287], [288]. These mouse models demonstrate a leukodystrophy, with progressive loss of white matter due to oligodendrocyte dysfunction, increased abundance of oligodendrocyte precursors, altered amino acid concentrations in the brain, increased susceptibility to seizures, reduced learning, impaired hippocampal neurogenesis in adults, increased methylation in tissues vacuolization in the brain including the cerebellum, gliosis, neuroinflammation, and early mortality [191], [288]. Since we also see 2-HG accumulate in several models of mitochondrial dysfunction, and 2-HG accumulation has direct neurotoxic consequences, we reasoned that 2-HG may contribute to the pathophysiology of mitochondrial dysfunction-induced neurodegeneration or neural dysfunction as a toxic metabolite. The effect of 2-HG in this mechanism may be through its influence on epigenetics [57], or other dioxygenase enzymes, or its effect on metabolism and transport of other amino acids and structurally related keto-acids in the brain.

In the following chapters of this dissertation, I will explore the role of mitochondrial complex I function or dysfunction, and potential role of 2-HG accumulation, on lifespan and organismal function (Figure 1.5.3.1). Complete loss of complex I subunits NDUFS2 and NDUFS4 results in significantly shortened survival in mice, but whether restoring NADH turnover without proton pumping to NDUFS4 and whether heterozygous loss of NDUFS2 might be beneficial through a hermetic response will be explored.

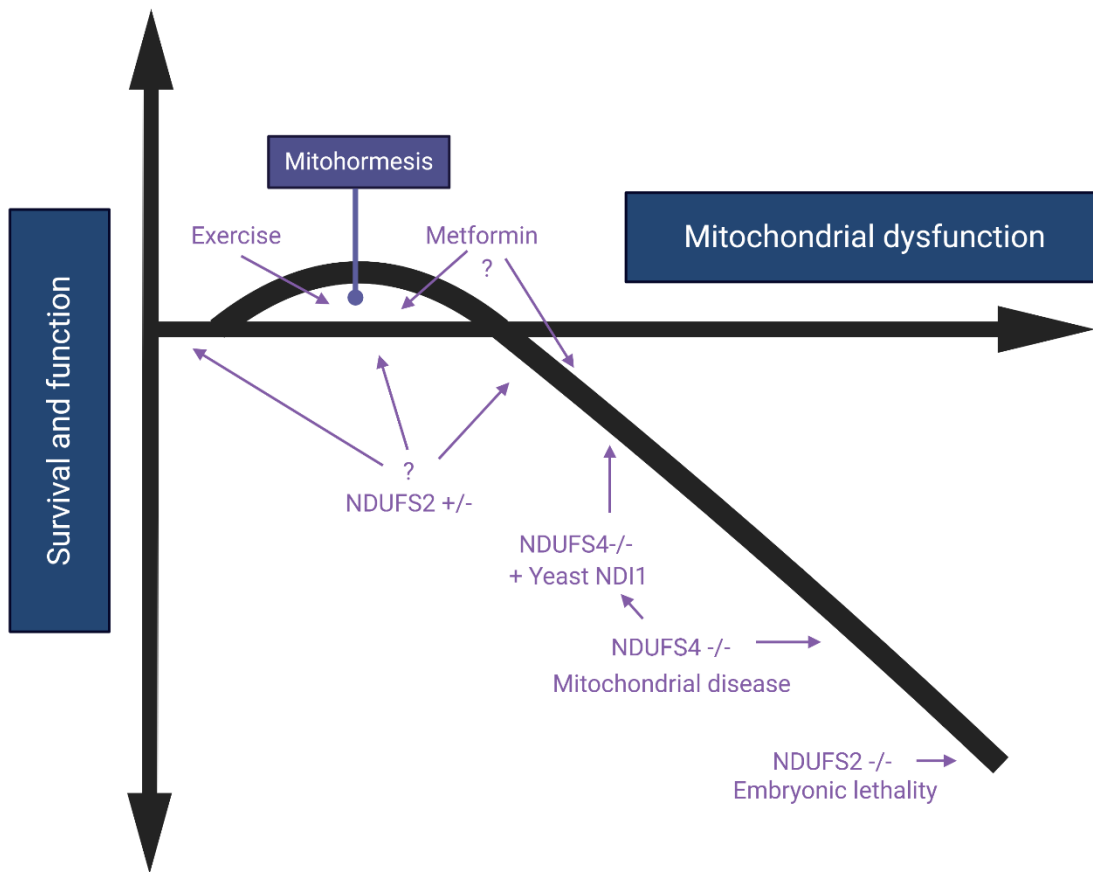


Figure 1.5.3.1. Mitohormesis and survival. Graphical representation of mitohormesis of complex I function, with mitochondrial dysfunction arising from exercise or metformin resulting in a beneficial response, while loss of complex I subunits NDUFS2 and NDUFS4 results in significantly reduced survival. Whether loss of just one copy of NDUFS2 has any benefits in survival and function is explored in this dissertation, as well as whether NDI1 expression in NDUFS4 deficient mice increases survival and function.

CHAPTER 2: Methods

2.1) Introduction

For simplicity, the methods sections have been separated by chapter. Significant portions of the methods section were written by myself or by my co-authors in manuscripts that I have co-authored [289].

2.2) Methods for expression of the yeast enzyme NDI1 is sufficient to rescue lifespan but not motor function in a model of mitochondrial disease

2.2.1) Key Resources Table

Table 2.2.1.1) Key resources table:

REAGENT or RESOURCE	SOURCE	IDENTIFIER
Antibodies		
IBA1	Wako	NC9288364
NDUFS4	Abcam	137064
NDI1	Eric Dufour – University of Tampere Finland	N/A
Vinculin	Cell Signaling	12901
Tubulin	Cell Signaling	2144
CD11b	eBioscience	48-0112-80
ACSA2	Milltenyi Biotec	130-102-365
CD45.2	eBioscience	56-0454-82
GFAP	Biocare	CP040A
Tyrosine Hydroxylase	Millipore Sigma	AB152
NeuN	Abcam	Ab104225
Chemicals, Peptides, and Recombinant Proteins		
Piericidin A	Sigma	A8674
Antimycin A	Sigma	P4368
Oligomycin A	Sigma	75351
U13C-Glucose	Cambridge Isotopes	CLM-1396-1
Critical Commercial Assays		
Seahorse XFe96 Flux Pack	Agilent	102416-100
Wes Simple Western System	Proteinsimple	SM-W004
RNeasy plus mini kit	QIAGEN	74134
CYBRFast 1-step RT-qPCR Lo-Rox Kit	Tonbo Biosciences	31-5201
Ambion DNase I	Invitrogen	AM2222
Papain Dissociation System	Worthington	LK003150
NAD/NADH Glo Assay	Promega	G9071
NEBNext Ultra II Kit	NEB	E7645
Octomacs C Tube	Milltenyi Biotec	130-093-237
Experimental Models: Organisms/Strains		
B6.129S4- <i>Ndufs4</i> ^{tm1Rpa/J}	The Jackson Laboratory	026963
B6.Cg-Tg(Nes-cre)1Kln/J	The Jackson Laboratory	003771
Rosa26 NDI1 knock-in C57bl6 background	This paper	N/A

Oligonucleotides		
CAG forward primer 5' – CAACGTGCTGGTTATTGTGC		
Neo reverse primer 5' – TCGCCTTCTTGACGAGTTCT		
NDI1 reverse primer 5' – AACCCAGTATCAGCACGTTTG		
Rosa B forward primer 5' – GAGTTCTCTGCTGCCTCCTG		
Rosa B reverse primer 5' – CCGACAAAACCGAAAATCTG		
WPRE B forward primer 5' – GACGAGTCGGATCTCCCTTT		
qPCR NDUF54 forward 5' GAGCACATCCACTTGGAAGC		
qPCR NDUF54 reverse 5' GATGTGCTCTTCTGGAACACC		
qPCR NDI1 forward 5' GCCGAAGAAGTCCAAATTCAC		
qPCR NDI1 reverse 5' CGACAGCCGTTCTCAGAT		
qPCR Actin forward 5' CTAAGGCCAACCGTGAAAAG		
qPCR Actin reverse 5' ACCAGAGGCATACAGGGACA		
Recombinant DNA		
<i>Rosa26</i> Lox-STOP-Lox NDI1 targeting cassette	This paper	N/A
Software and Algorithms		
Trimmomatic	Bolger et al., 2014	
STAR	Dobin et al., 2013	
HTSeq	Anders et al., 2015	
DESeq2	Love et al., 2014	
GSEA	Subramanian et al., 2005	
DropViz	Saunders et al., 2018	
MetaboAnalyst	Chong et al., 2018	
Tracefinder	Thermo Scientific	
Xcalibur	Thermo Scientific	
R	https://www.r-project.org/	
Mango	http://ric.uthscsa.edu/mango/	
Limelight	ActiMetrics	
Prism	GraphPad	
FinePointe	Buxco	

2.2.2) Mouse models

NDUF54 floxed and Nestin Cre mice were obtained from The Jackson Laboratory (B6.129S4-*Ndufs4^{flm1Rpa}*/J JAX stock #026963 and B6.Cg-Tg(Nes-cre)1Kln/J JAX stock #003771, respectively). NDI1 knock-in mice were generated at the Northwestern Transgenic and Targeted Mutagenesis Laboratory.

Briefly, we designed a targeting construct containing 5' and 3' *Rosa26* homology arms as well as a Lox-STOP-Lox cassette upstream of the *NDI1* gene from *Saccharomyces cerevisiae* (Fig. S1A). The targeting construct, which contains a neomycin resistance gene cassette, was electroporated into C57BL/6 embryonic stem cells. Neomycin-resistant ES clones were picked, and PCR was used to confirm proper incorporation of the targeting construct into the *Rosa26* locus. Two independent ES clones containing the *NDI1*-LSL allele were injected into blastocysts to produce germline-transformed heterozygous *NDI1*-LSL mice. For generation of Kaplan-Meier survival plots, mice that were determined to have severe ataxia, were moribund, or lost greater than 10% body weight were euthanized and included as events (deaths) while data points were censored when non-terminal animals were euthanized for experimentation and tissue analysis. All animal procedures were reviewed and approved by the Institutional Animal Care and Use Committee (IACUC) at Northwestern University.

NDI1 Genotyping Primers:

Confirmation of Cre recombination (LSL Excision/*NDI1* Expression) PCR:

NDI1 LSL allele 180bp, *NDI1* expressing allele 290bp

CAG forward primer 5' – CAACGTGCTGGTTATTGTGC

Neo reverse primer 5' – TCGCCTTCTTGACGAGTTCT

NDI1 reverse primer 5' – AACCCAGTATCAGCACGTTTG

NDI1-LSL allele PCR:

Rosa26 wt allele (no *NDI1*) 224bp, *NDI1*-LSL knock-in allele 509bp

Rosa B forward 5' – GAGTTCTCTGCTGCCTCCTG

Rosa B reverse 5' – CCGACAAAACCGAAAATCTG

WPRES forward 5' – GACGAGTCGGATCTCCCTTT

Genotyping primers and references for other mouse lines:

NDUFS2 genotyping primers: [290]

Forward primer: 5'-ATAAGAGTGGATAGGATGTTT-3'

Flox reverse primer: 5'-CATTTCTCCCTTCCCGTC-3'

Null allele reverse primer: 5'-AGTGGCAGAACAAATAGAGTGATCCAGGG-3'

NDUFS4 genotyping primers Jax labs: 026963

NDUFS4-1 5'-AGC CTG TTC TCA TAC CTC GG-3'

NDUFS4-2 5'-GTC CTC TAT GAG GGT ACA GAG-3'

NDUFS4-3 5'-GGT GCA TAC TTA TAC TAC TAG TAG-3'

Nestin Cre genotyping primer:, Jax labs # 3771

Cre Forward: 5'-GCAGAACCTGAAGATGTTGCGCCAT-3'

Cre Reverse: 5'-AGGTATCTCTGACCAGAGTCATCC-3'

Internal Control Forward: 5'-CTAGGCCACAGAATTGAAAGATCT-3'

Internal Control Reverse: 5'-GTAGGTGGAAATTCTAGCATCATCC-3'

RAG: Jax labs # 002216

RAG wt 5'-GAG GTT CCG CTA CGA CTC TG-3'

RAG Common 5'-CCG GAC AAG TTT TTC ATC GT-3'

RAG Mutant 5'-TGG ATG TGG AAT GTG TGC GAG-3'

IL6: Jax labs # 002650

IL6 fwd 5'-TTC CAT CCA GTT GCC TTC TTG G-3'

IL6 wt rev 5'-TTC TCA TTT CCA CGA TTT CCC AG-3'

IL6 Null reverse 5'-CCG GAG AAC CTG CGT GCA ATC C-3'

STING: Jax labs # 017537 (Sanger sequenced for genotype)

STING fwd – 5'-GAT CCG AAT GTT CAA TCA GC

STING rev – 5'-CGA TTC TTG ATG CCA GCA C

2.2.3) Oxygen consumption and mitochondrial complex I sensitivity in cerebellar granule neurons

Oxygen consumption of cerebellar granule neurons was carried out using a Seahorse XFe96 Analyzer.

Cultured neurons basal oxygen consumption was determined by 3 baseline measurements of oxygen consumption followed by the injection of 500nM Piericidin A (an inhibitor of mammalian mitochondrial complex I. 3 measurements were made after injection 1 and then a second combined injection of 1uM Antimycin A and Piericidin A to completely inhibit electron transport through combined mitochondrial complex I and III blockade. The residual oxygen consumption after Piericidin A and Antimycin A

combined injection (injection 2) was measured and subtracted from baseline and injection 1 measurements to determine the basal oxygen consumption and the complex I inhibitor-resistant oxygen consumption, respectively. Protocol for extraction and culture of early post-natal cerebellar granule neurons was adapted from previously published methods [291]. Prior to experimentation, mouse genotype was determined, and tissue culture plates were coated with poly-D-lysine (Fisher) at two different concentrations: 100µg/mL for pre-plating/glia dishes and 500µg/mL for cerebellar granule neuron plates. The following day the developing cerebellum of individual early postnatal mice was removed, and meninges were removed under a dissecting microscope. Next, tissue was incubated at 37°C for 15 minutes in Papain from the Papain Dissociation System Kit (Worthington) combined with 1mg/mL of DNase I. Tissue was then triturated using P1000 pipette tips pre-coated with serum and the suspension was allowed to settle for 30 seconds to 1 minute to allow large undissociated pieces to settle. Using serum-coated pipette tips, cells remaining in suspension were transferred to a new centrifuge vial and centrifuged at 200xg for 5 minutes. Cell pellets were resuspended in Minimum Essential Media + albumin-ovomucoid inhibitor. Resuspended cells were carefully layered over an additional 1mL of albumin-ovomucoid inhibitor solution in a new centrifuge vial and centrifuged at 70xg for 6 minutes, pelleting dissociated cells and leaving membrane fragments and lipid at the surface. Next, the cells were resuspended, passed through a 70-micron filter, and plated on pre-plating plates in Neurobasal A medium supplemented with 10% serum, glutamax, antibiotic/antimycotic, and KCl. Cells were allowed to settle for 20 minutes. After incubation, granule neurons and neuron progenitors were dislodged with gentle tapping while larger glia remained adhered. The pre-plating step for glial removal was repeated. Finally, an enriched population for cerebellar granule neurons was resuspended in serum-free media containing Neurobasal A Medium supplemented with 2% B-27, glutamax, antibiotic/antimycotic, and KCl and plated directly onto poly-D-lysine-coated Seahorse plates and cultured for 5 days prior to oxygen consumption analysis.

2.2.4) Open Field Test and Accelerating Rotarod Challenge

Spontaneous activity in an open field chamber (56 cm x 56 cm) was recorded with LimeLight4 animal tracing software to assess activity and exploratory behavior for 300 seconds. Distance travelled during

the test as well as the percentage time spent in the perimeter of the chamber as compared with the center (based on the central 9 boxes of a 5x5 grid of the open field) were recorded. The rotarod uses an accelerating rotating cylindrical rod upon which mice balance and walk forward to prevent themselves from falling. Mice were acclimated to the rotarod equipment for 2 days at a constant rate of 12 RPM for 60 seconds for 4 trials per day with at least 5 minutes between trials. Next, the mice were tested for 3 days with an accelerating program from 4 to 40 RPM over 300 seconds for 4 trials per day with at least 5 minutes between trials. Rotarod operation and automatic detection of falls was used with Rod software. Open Field Testing and Accelerating Rotarod Challenge were carried out using equipment at the Northwestern Behavioral Phenotyping Core Facility.

2.2.5) Magnetic Resonance Imaging

MRI imaging was performed at the Small Animal Molecular Imaging Lab of CTI (Feinberg School of Medicine, Northwestern University) on a ClinScan 7 T Scanner (Bruker, Germany) using a mouse head 4-channel phase array coil as receiver and a volume quadrature coil as transmitter. The imaging protocol included a 3D Flash multi-echo sequence (TR = 40 ms, TEs = 2.53, 6.09, 9.65, 13.21 ms, flip angle = 15, voxel size = 0.15x0.15x0.15 mm³) and a high resolution 2D T2-RARE (TR = 5940 ms, TE = 41 ms; voxel size = 0.09x0.09x0.5 mm³).

2.2.6) Histology

For histological analyses mice at approximately 7 weeks of age (late stage of disease for cKO mice) or over 12 months of age were selected. Mice were euthanized and perfused with cold PBS supplemented with heparin and either 4% paraformaldehyde or 10% neutral buffered formalin and tissues were post-fixed for >24 hours in paraformaldehyde or formalin. Spinal cords were then decalcified using 0.5M EDTA pH 8.0. Fixed brains, quadriceps muscles, and spinal cords were trimmed and embedded in Paraffin blocks and sectioned at the Northwestern Mouse Histology and Phenotyping Core facility. Tissues were stained with hematoxylin and eosin (H&E), Luxol fast blue (spinal cord only), and/or Gomori's Trichrome stain (muscle only) using 4 micron sections. Immunohistochemistry (IHC) was carried out on 4-micron sections using tyramide signal amplification and avidin-biotin complex methods (automated) and using 3,3'-Diaminobenzidine (DAB) chromogen. 3-4 individual mice were analyzed per group for astrocyte IHC,

microglia IHC, and spinal cord staining. 6 mice were analyzed per group for muscle and neuron quantification. Images were taken using a Nuance spectral camera on a Zeiss Axioskop upright microscope at the Northwestern Center for Advanced Microscopy. DAB staining quantification was carried out blinded in ImageJ using portions of 20x images with the number of cells determined using the Multi-point tool normalized to the analyzed area of pixels. For Purkinje neurons, the cell count was instead normalized to the analyzed linear pixel length rather than area. For quantification of tyrosine hydroxylase immunoreactivity in the striatum, the mean pixel intensities on a greyscale of uniformly DAB stained portions of 20x images of striatum were measured in ImageJ, then the inverse of this value was used as a proxy for immunoreactivity and each individual value was normalized as a percentage of the average of controls. Histology was reviewed by a trained neuropathologist.

2.2.7) Metabolite measurement

Mice were euthanized and cerebellum was rapidly isolated, and flash frozen in liquid nitrogen. Samples were stored at -80°C until extraction. Soluble metabolites were extracted directly from tissue using cold methanol/water (80/20, v/v) at approximately 1µL per 50µg of tissue. Tissue was disrupted for 15 seconds by ultrasonication for brain (Branson Sonifier 250), or by rotor-stator homogenization for muscle (QIAGEN TissueRuptor II). Protein was precipitated by incubation at -80°C. Debris were pelleted by centrifugation at 18,000xg for 15 min at 4°C. The supernatant was transferred to a new tube and evaporated to dryness using a SpeedVac concentrator (Thermo Savant). Metabolites were reconstituted in 50% acetonitrile in analytical-grade water, vortex-mixed, and centrifuged to remove debris. Samples were analyzed by Ultra-High-Performance Liquid Chromatography and High-Resolution Mass Spectrometry and Tandem Mass Spectrometry (UHPLC-MS/MS). Specifically, the system consisted of a Thermo Q-Exactive in line with an electrospray source and an Ultimate3000 (Thermo) series HPLC consisting of a binary pump, degasser, and auto-sampler outfitted with an Xbridge Amide column (Waters; dimensions of 4.6mm x 100mm and a 3.5µm particle size). Mobile phase A contained 95% (vol/vol) water, 5% (vol/vol) acetonitrile, 10mM ammonium hydroxide, 10mM ammonium acetate, pH = 9.0; and mobile phase B was 100% Acetonitrile. The gradient was as follows: 0 min, 15% A; 2.5 min, 30% A; 7 min, 43% A; 16 min, 62% A; 16.1-18 min, 75% A; 18-25 min, 15% A with a flow rate of 400µL/min. The capillary of the ESI source was set to 275°C,

with sheath gas at 45 arbitrary units, auxiliary gas at 5 arbitrary units, and the spray voltage at 4.0kV. In positive/negative polarity switching mode, an m/z scan range from 70 to 850 was chosen and MS1 data was collected at a resolution of 70,000. The automatic gain control (AGC) target was set at 1×10^6 and the maximum injection time was 200 ms. The top 5 precursor ions were subsequently fragmented, in a data-dependent manner, using the higher energy collisional dissociation (HCD) cell set to 30% normalized collision energy in MS2 at a resolution power of 17,500. Data acquisition and analysis were carried out by Xcalibur 4.1 software and Tracefinder 4.1 software, respectively (both from Thermo Fisher Scientific). The peak area for each detected metabolite was normalized by the total ion current which was determined by integration of all of the recorded peaks within the acquisition window. Downstream analysis was carried out using Microsoft Excel and R. The list of the top 50 candidate metabolites for differential abundance between Cre and cKO cerebella was created by sorting metabolites by p value of a t-test comparing 6 Cre and 6 cKO mice (3 male and 3 female mice of each genotype) at approximately 7 weeks of age which is the late stage of cKO disease. Heatmaps generated using R package Pheatmap after transformation of peak areas for each metabolite to Z scores (for brain) and using MetaboAnalyst 4.0 for muscle. Pathway analysis of KEGG compound IDs, principal components analysis score plots, and multiple comparisons adjusted T-tests for muscle were performed using MetaboAnalyst 4.0 [292]

2.2.8) U13C-Glucose Flux

Cultured astrocyte-enriched primary cultures from the cerebellum and brainstem from mice less than 7 days of age were extracted and cultured for 7 days. Astrocyte-enriched primary cultures were then trypsinized and plated at 500,000 cells per mouse in 6-well plates. The following day, normal growth media was replaced with glucose flux media (Glucose-free DMEM powder supplemented with sodium bicarbonate, HEPES, antibiotics and 10% serum with 5mM U13C-Glucose and 2mM glutamine, pH 7.4) for 6 hours. After incubation, cells were rinsed with ice cold 0.9% NaCl, then 80% methanol was added to plates at a ratio of 700 cells per μL . Plates were then incubated at -80°C for 20 minutes. Cells were then extracted and homogenized using cell scrapers, vortexed for 1 minute, and centrifuged in a refrigerated table-top microcentrifuge at maximum speed for 10 minutes. Metabolite-containing supernatants were then processed and measured by mass-spectrometry as described above.

2.2.9) RNA Sequencing

6 mice per group (3 male and 3 female) were euthanized at approximately 7 weeks of age and the cerebellum was rapidly dissected and flash frozen in liquid nitrogen. Whole cerebellum RNA was extracted using a QIAGEN RNeasy Plus Mini Kit. Tissues were homogenized in RLT Plus Buffer + BME with a QIAGEN TissueRuptor II handheld rotor-stator homogenizer. After tissue homogenization, QIAshredder spin columns were used followed by gDNA elimination columns and an on-column DNase digestion with Ambion RNase-free Dnase during the RNeasy RNA preparation manufacturer protocol. RNA was quantified and QC was checked using an Agilent 4200 TapeStation RNA ScreenTape. mRNA libraries were prepared using NEBNext Ultra Kit with polyA selection (New England BioLabs). Libraries were sequenced using a Next-Seq 500 High Output for 75 cycles (Illumina). Raw BCL read files were demultiplexed and FASTQ files were generated using bcl2fastq and trimmed using Trimmomatic [293]. Next, the reads were aligned to the mouse mm10 reference genome using STAR to generate BAM files [294]. HTSeq was used to count reads in the exons of genes [295]. Likelihood ratio tests for all samples and all detected transcripts and pairwise differential gene expression analyses were carried out using the R package DESeq2 [296]. Gene set enrichment analysis was carried out using the Broad Institute GSEA software after conversion to human homologue gene symbols [297]. The pairwise differential gene expression output generated from DESeq2 was submitted as a pre-ranked list based on the DESeq2 Wald Statistic (stat column) output sorting genes from significantly upregulated to significantly downregulated. GSEA was performed on Hallmark Gene Sets from the GSEA Molecular Signatures Database (Liberzon et al., 2015). Publicly available Drop-seq data from the mouse brain was accessed and a graph of NDUFS4 gene expression by cell type cluster in the cerebellum was generated through the DropViz platform (Saunders et al., 2018). Gene Set Enrichment Analysis software and Cytoscape software were used to generate gene network analysis plots. Preranked lists were analyzed for gene set enrichment for all 7350 Gene Ontology (GO) Biological Process gene sets on the Molecular Signatures Database. Next, GSEA results were loaded into the Enrichment Map Visualization tool [298] in GSEA and Cytoscape software with enrichment map parameters set to a P-value cutoff of 0.005 and an FDR Q-value cutoff of 0.05 of 0.1 as noted in figure legends, a similarity cutoff using an overlap coefficient of 0.5.

2.2.10) Protein and mRNA Quantification

Protein quantification was carried out on protein extracts from whole brain tissue from approximately 7-week-old mice and from mice >6 months of age and on muscle of mice >12 months of age. Mice were euthanized and tissue was flash frozen in liquid nitrogen. Protein was extracted using lysis buffer (Cell Signaling 9803S) and ultrasonication (Branson Sonifier 250) for brain and rotor-stator homogenization (QIAGEN TissueRuptor II) for muscle. Protein was quantified using the Pierce BCA assay (Thermo Fisher Scientific) and NDI1 and NDUFS4 were measured using a ProteinSimple Wes Simple Western System, an automated capillary-based immunoassay. Approximately 30µg of total protein was loaded for each sample and antibodies were loaded at 1:100 (NDUFS4), 1:500 (NDI1), 1:200 (Vinculin), and 1:1000 (Tubulin). There is not a commercially available Anti-NDI1 antibody; however, we received a small amount of an Anti-NDI1 antibody from Dr. Eric Dufour from the University of Tampere, Finland to confirm the detection of NDI1 in brain tissue. Furthermore, we used the Anti-NDUFS4 antibody (Abcam 137064), the Anti-Vinculin antibody (Cell Signaling 12901), and the Anti-Tubulin antibody (Cell Signaling 2144). Virtual blot images were created within ProteinSimple Compass software. Peak area was normalized to loading control peak area and plotted in GraphPad Prism. mRNA was measured in cell types sorted from adult mouse brain to confirm the specific and appropriate Cre recombination in brain cell types. Nestin Cre should cause recombination in all adult brain cell types except for microglia. Therefore, we measured NDUFS4 and NDI1 mRNA in microglia and astrocytes from mice expressing NDI1 and conditional NDUFS4 knockout due to Nestin Cre expression. Brains from adult mice >7 weeks of age were dissociated for 30 minutes using the Papain Dissociation System Kit (Worthington) and Octomacs C Tube (Milltenyi Biotec) tissue homogenization. Cells were separated using a 27% Percoll centrifugation step to remove myelin debris. Cells were sorted directly into cell lysis buffer RLT+BME using a BD FACS Aria II Flow Cytometer at the Northwestern RHLCCC Flow Cytometry Core Facility. Antibody panel for cell selection consisted of CD11b and CD45.2 for microglia and ACSA2 for astrocytes. Specifically, we used an Anti-CD11b antibody (eBioscience 48-0112-80), an Anti-CD45.2 antibody (eBioscience 56-0454-82), and an Anti-ACSA2 antibody (Milltenyi Biotec 130-102-365). RNA was extracted using a QIAGEN RNeasy Plus Micro Kit following manufacturer protocol and qPCR was carried out using a CYBRFast 1-

step RT-qPCR Lo-Rox Kit (Tonbo Biosciences) following manufacturer protocol with a BioRad CFX384 Real Time System.

qPCR Primers:

NDUFS4 forward 5'-GAGCACATCCACTTGGAAGC

NDUFS4 reverse 5'-GATGTGCTCTTCTGGAACACC

NDI1 forward 5'-GCCGAAGAAGTCCAAATTCAC

NDI1 reverse 5'-CGACAGCCGTTCTCAGAT

Actin forward 5'-CTAAGGCCAACCGTGAAAAG

Actin reverse 5'-ACCAGAGGCATACAGGGACA

2.2.11) NADH/NAD⁺ Ratio

NADH/NAD⁺ ratio was determined on enriched astrocyte primary cultures from post-natal mouse cerebellum using the NAD/NADH Glo Assay (Promega) following the manufacturer-supplied protocol. Primary cultures enriched for cerebellar astrocytes were derived using a protocol adapted from the Cerebellar Granule Neuron culture protocol detailed in the section on oxygen consumption and mitochondrial complex I sensitivity in cerebellar granule neurons and Schildge et al. (2013). Pre-plating plates after cerebellar granule neuron culture were maintained as mixed cultures and enriched for astrocytes by providing astrocyte-selective media (DMEM supplemented with 10% serum) for 7 days followed by trypsinization and replating of the confluent astrocyte layer.

2.2.12) Whole Body Plethysmography

A Buxco Finepointe 4-site whole body plethysmography apparatus was used to record the breathing pattern and ventilation dynamics of awake, unrestrained mice. Frequency, tidal volume, and minute ventilation were recorded during a 20-minute period after 120 minutes of acclimation in the calibrated cylindrical chambers.

2.2.13) Electron transport chain diagram generation

The diagram was generated using BioRender software, and NDI1 crystal structure representation was derived from Iwata et al. 2012.

2.2.14) Statistics

Statistical analyses and graph generation were carried out using GraphPad Prism 8 and R. Figure alignment was carried out using Adobe Illustrator. Statistical tests are referenced in the figure legends. All T-tests were two-tailed. ANOVA refers to an ordinary one-way ANOVA carried out with Dunnett's multiple comparisons test comparing all groups to control unless otherwise indicated in the figure legend. Error bars indicate SEM. N refers to biological replicates (individual animals).

2.2.15) Data Availability Statement

All data is freely available. RNA-seq data will be deposited in the GEO repository prior to publication while all other intermediate file types in analysis including normalized gene count tables are available upon request or will be provided as supplementary information. Metabolite abundance raw data tables are available upon request or will be provided as supplementary information.

2.3) Methods for mitochondrial L-2-hydroxyglutarate accumulation is a determinant of mitochondrial dysfunction induced neuronal dysfunction

2.3.1) Animals and cell lines

Flies were maintained by our collaborators at King's College London on standard yeast, glucose, cornmeal, and agar food at 25°C in a 12-h light/dark cycle unless stated otherwise. Details of fly stocks are listed in Table S7. Fly stocks were from the Bloomington Drosophila Stock Center; the Vienna Drosophila Resource Center [299]; the NIG-Fly Stock Center, Japan; and FlyORF. Pan-neuronal TFAM overexpression causes late pupal lethality, so to obtain viable adults, TFAM was pan-neuronally overexpressed in a *TFAM* loss-of-function heterozygous mutant background (*nSyb-Gal4, TFAM^{c01716}*). For imaging experiments, embryos were laid over a 24-h period at 25°C, incubated for a further 24 h at 25°C, and then incubated at 29°C for 3 d before analysis, unless stated otherwise.

Mice were housed at Northwestern University Center for Comparative Medicine as previously described. All animal procedures were reviewed and approved by the Institutional Animal Care and Use Committee (IACUC) at Northwestern University.

143B-Cytb-WT and 143B-Cytb- Δ cells were previously described [300]. Cells were grown in Dulbecco's Modified Eagle's Medium containing 4.5 g/L glucose, 4 mM L-glutamine, 10% fetal bovine serum, 1 mM methyl pyruvate, 400 μ M uridine, 1% HEPES and 1% antibiotic-antimycotic (Gibco) at 37°C with 5% CO₂.

2.3.2) CRISPR/cas9

L2HGDH, AOX, NDI1, LbNOX-Mito, LbNOX-Cyto and control pWPI and pLV vectors containing GFP or RFP, were transfected into 293T cells using jetPRIME along with pMD2.G and psPAX2 packaging vectors to produce Control-GFP, Control-RFP, AOX-GFP, NDI1-RFP, LbNOX-Mito-RFP, LbNOX-Cyto-RFP, lentivirus. 3 days after infection, cell lines were sorted for GFP and RFP-positive cells using a BD FACS Aria cell sorter. The cells were continuously sorted to maintain high GFP and RFP expression. 143B-Cytb- Δ -NDUFS2_KO and MDH2_KO cells were generated using the pSpCas9(BB)-2A-GFP (PX458) plasmid from Addgene, which expresses Cas9 along with the gene-specific RNA guides (gRNAs) listed below as previously described.

sgRNA ID	Sequence
sgNDUFS2_1	GGTCACTCACCATTCCAAGG
sgNDUFS2_2	CTGCAGCCGGAGTAAGATGG
sgMDH2	CACCGGCGCCAGTACCTTTCACAG
sgNon-targeting	GTAGCGAACGTGTCCGGCGT

2.3.3) Mitochondrial inhibitor treatments

Cells were treated for the indicated times with Piericidin A (Sigma A8674) or Antimycin A (P4368) added to the normal growth media at 500nM-1 μ M.

2.3.4) Metabolomics

For tissue culture: Subconfluent culture dishes were incubated for 2 h, 8h, or 24h in DMEM that contained 15 mM glucose and 2 mM glutamine supplemented with 10% dialyzed FBS in the presence or absence of 1 mM pyruvate and/or 400 μ M uridine. Following this, cells were washed with ice-cold saline and then

overlaid with cold methanol/water (80/20, v/v). Plates were incubated at -80°C for 20 min. Cells were transferred to an Eppendorf tube and pelleted by centrifugation at 16,000 × g for 15 min at 4°C. The supernatant was transferred to a new tube and evaporated to dryness using a SpeedVac concentrator (Thermo Savant). Metabolites were reconstituted in 50% acetonitrile in analytical-grade water, vortex-mixed, and centrifuged to remove debris. For *Drosophila melanogaster* tissue, 20 2–5-d-old adult flies (equal numbers of males and females) were snap-frozen on liquid nitrogen in a 15-ml Falcon tube and then vortexed for 5 s five times to decapitate. Heads were then quickly separated and stored at -80°C. Soluble metabolites were extracted directly from tissue using cold methanol/water (80/20, vol/vol) at 1 µl per 10 µg of tissue. Tissue was disrupted for 15 s by ultrasonication (Branson Sonifier 250). Debris were pelleted by centrifugation at 18,000 × g for 15 min at 4°C. The supernatant was transferred to a new tube and evaporated to dryness using a SpeedVac concentrator (Thermo Fisher Scientific). Metabolites were reconstituted in 50% acetonitrile in analytical-grade water, vortex-mixed, and centrifuged to remove debris. Samples were analyzed by HPLC and high-resolution mass spectrometry and tandem mass spectrometry (MS/MS). Specifically, the system consisted of a Q-Exactive in line with an electrospray source and an Ultimate3000 (Thermo Fisher Scientific) series HPLC consisting of a binary pump, degasser, and auto-sampler outfitted with an Xbridge Amide column (dimensions of 4.6 × 100 mm and a 3.5-µm particle size; Waters). Mobile phase A contained 95% (vol/vol) water, 5% (vol/vol) acetonitrile, 10 mM ammonium hydroxide, and 10 mM ammonium acetate, pH 9.0; and mobile phase B was 100% acetonitrile. The gradient was as follows: 0 min, 15% A; 2.5 min, 30% A; 7 min, 43% A; 16 min, 62% A; 16.1–18 min, 75% A; 18–25 min, and 15% A with a flow rate of 400 µl/min. The capillary of the electrospray ionization (ESI) source was set to 275°C, with sheath gas at 45 arbitrary units, auxiliary gas at 5 arbitrary units, and the spray voltage at 4.0 kV. In positive/negative polarity switching mode, a mass-to-charge ratio scan range from 70 to 850 was chosen, and MS1 data were collected at a resolution of 70,000. The automatic gain control target was set at 10⁶, and the maximum injection time was 200 ms. The top five precursor ions were subsequently fragmented in a data-dependent manner, using the higher energy collisional dissociation cell set to 30% normalized collision energy in MS2 at a resolution power of 17,500. Data acquisition and analysis were performed by Xcalibur 4.1 software and Tracefinder 4.1

software, respectively (both from Thermo Fisher Scientific). The peak area for each detected metabolite was normalized by the total ion count.

2.3.5) 2-hydroxyglutarate Chiral Derivatization

Resolution of enantiomers of 2-HG was accomplished by derivatization with diacetyl-L-tartaric anhydride (DATAN) in acetic acid after the above SpeedVac step and measured by HPLC-MS/MS as previously described. For separation of DATAN derivatized D- and L-2-HG, samples were analyzed by HPLC-MS/MS, which consisted of a TSQ in line with an electrospray source and an Vanquish (Thermo Fisher Scientific) series HPLC consisting of a binary pump, degasser, and auto-sampler outfitted with an Ascentis Express C18 column (dimensions of 2.1 × 150 mm and a 2.7- μ m particle size; Supelco). Liquid chromatography was performed using a 98% buffer A (water with 2 mM ammonium formate, pH 3.5, adjusted by formic acid) and 2% buffer B (methanol) isocratic elution of 10 min per sample. In negative mode, the capillary of the ESI source was set to 325°C, with sheath gas at 50 arbitrary units, auxiliary gas at 10 arbitrary units, and the spray voltage at 2,500 V. S-lens values were 37 V and reactions monitored, and collision energies were mass-to-charge ratio 363.06 \rightarrow 147.03 (20 V). 2-HG chromatograms were generated with Xcalibur software with spectral smoothing algorithm boxcar 15.

2.3.6) *Drosophila melanogaster* behavioral testing

Our collaborators at King's College London carried out all *Drosophila melanogaster* behavioral testing. For all assays using flies with neuronal dysfunction, vials were placed on their sides during eclosion to prevent flies from becoming stuck in the food. For climbing assays, male flies of appropriate genotype were selected under CO₂ anesthesia, within 24 h of eclosion. Assays were undertaken 24–48 h later to allow the flies to recover from the anesthetic, 1–3 h after morning illumination. Individual flies were aspirated from a vial into a 10-ml serological pipette (Falcon). Flies were relocated to the base of the pipette by tapping against the bench. The height obtained in three continuous 10-s climbs was measured for each fly, and the mean computed to give the data point for that insect. Wandering (i.e., nonvertical) or discontinuous climbs were excluded.

For wing inflation assays, all flies that eclosed from each cross were collected under CO₂ anesthesia, and stored at 25°C for ≥24 h to ensure that an uninflated wing phenotype was not due to young age. The numbers of flies with inflated, semi-inflated, and uninflated wings were then counted.

Viability assays were performed by counting the number of pupae containing flies that failed to eclose and empty pupal cases from which viable flies have successfully eclosed.

2.3.7) Regulatory T cell isolation

Splenic T-regs were isolated using a Stemcell Technologies EasySep Mouse CD4+CD25+ Regulatory T Cell Isolation Kit II following manufacturer protocols.

2.3.8) Statistics

Statistical analyses and graph generation were carried out using GraphPad Prism 8 and R. Figure alignment was carried out using Adobe Illustrator. Statistical tests are referenced in the figure legends. All T-tests were two-tailed. ANOVA refers to an ordinary one-way ANOVA carried out with Dunnett's multiple comparisons test comparing all groups to control unless otherwise indicated in the figure legend. Error bars indicate SEM. N refers to biological replicates (individual animals or independent experiments).

2.4) Methods for mild genetic reduction in mitochondrial complex I function does not significantly alter healthspan in amice despite significant gene expression changes

2.4.1) Animal studies

Generated NDUFS2 heterozygous mice by crossing NDUFS2 floxed and Sox2-Cre mice references below. We sent samples from the NDUFS2 floxed mice that we used to generate NDUFS2 global heterozygote to Jackson labs for SNP analysis. This came back as approximately 95% B6/J and 5% 129S1/SvImJ. The SOX2 cre mice from Jackson that we used to generate the NDUFS2 global het background are on a mixed C57BL/6J/N background (according to Jackson: "In 2011, a 32 SNP (single nucleotide polymorphism) panel analysis, with 27 markers covering all 19 chromosomes and the X chromosome, as well as 5 markers that distinguish between the C57BL/6J and C57BL/6N substrains, was performed on the rederived living colony at The Jackson Laboratory Repository. While the 27 markers throughout the genome suggested a C57BL/6 genetic background, 1 of 5 markers that determine C57BL/6J from C57BL/6N were found to be segregating. These data suggest the mice sent to The

Jackson Laboratory Repository were on a C57BL/6N genetic background. The SOX2 cre mice were backcrossed for 3 generations to C57b6/J in house prior to breeding with the NDUFS2 floxed mice. Then following the generation of the global heterozygous mice there were 3 more backcross generations to C57b6/J to generate the mice in the cohort. Mice were housed at Northwestern University Center for Comparative Medicine as previously described. All animal procedures were reviewed and approved by the Institutional Animal Care and Use Committee (IACUC) at Northwestern University.

NDUFS2 genotyping primers:

Forward primer: 5'-ATAAGAGTGGATAGGATGTTT-3'

Flox reverse primer: 5'-CATTTCTCCCTTCCCGTC-3'

Null allele reverse primer: 5'-AGTGGCAGAACAAATAGAGTGATCCAGGG-3'

Cre genotyping primers (Jax labs strain # 008454) – Sox2 cre

Cre Forward: 5'-GCAGAACCTGAAGATGTTTCGCCAT-3'

Cre Reverse: 5'-AGGTATCTCTGACCAGAGTCATCC-3'

Internal Control Forward: 5'-CTAGGCCACAGAATTGAAAGATCT-3'

Internal Control Reverse: 5'-GTAGGTGGAAATTCTAGCATCATCC-3'

2.4.2) Protein and mRNA quantification

Whole cell lysate extracts were prepared from the indicated cell lines by harvesting and lysing cells in 1x cell lysis buffer (Cell Signaling) containing the Halt protease inhibitor cocktail (Thermo Scientific). The Pierce BCA Protein Assay kit (Thermo Scientific) was used to quantify the protein concentrations. 50-100 µg of whole cell lysate was resolved on an SDS-PAGE gel (Bio-Rad) and transferred to a nitrocellulose membrane using the Trans-Blot Turbo Transfer System (Bio-Rad). Membranes were blocked using 5% milk for 1 h and then incubated in the primary antibody overnight. Antibodies used were: anti-NDUFS2 (Abcam; catalogue number: ab96160; used at a 1:500 dilution), anti-Tubulin (Cell Signaling; catalog number: 2144, used at a 1:1000 dilution). IRDye 800CW goat anti-rabbit (LI-COR #926-32211) and IRDye 680RD goat anti-mouse (LI-COR #926-68070) were used as secondary antibodies. Image Studio Lite version 3.1 (LI-COR) was used for the analysis of protein levels.

RNA was extracted using a QIAGEN RNeasy Plus Micro Kit following manufacturer protocol and qPCR was carried out using a CYBRFast 1-step RT-qPCR Lo-Rox Kit (Tonbo Biosciences) following manufacturer protocol with a BioRad CFX384 Real Time System.

NDUFS2 qPCR Primers:

5'-TTTCGGGAGCTGTCATGTACC-3'

5'-TGGTCACCGCTTTTTCCTTCA-3'

2.4.3) Glucose Tolerance Testing

Mice were fasted overnight. A small incision was made at the tail base for blood glucose measurements, and fasting glucose was measured using a glucometer. Mice were given a glucose bolus by oral gavage at a dose of 2 grams per kilogram of body weight from a 0.2mg/μL stock solution of glucose in sterile water. Glucose measurements were recorded at 15 minutes, 30 minutes, 45 minutes, 60 minutes, and 120 minutes after glucose bolus delivery.

2.4.4) RNA sequencing

Mice were euthanized. Lungs were perfused with PBS and then instilled with Dispase and DNase, minced, and digested, then filtered, and centrifuged, red blood cells were lysed, and cells were stained for sorting. Alveolar macrophages and alveolar type 2 cells were isolated as previously described [76].

Splenic T-reg cells were isolated using a Stemcell Technologies EasySep Mouse CD4+CD25+ Regulatory T Cell Isolation Kit II following manufacturer protocols. RNA was extracted using Qiagen All-Prep DNA/RNA extraction kits following manufacturer protocols. RNA was quantified and QC was checked using an Agilent 4200 TapeStation RNA ScreenTape. mRNA libraries were prepared using NEBNext Ultra Kit with polyA selection (New England BioLabs). Libraries were sequenced using a Next-Seq 500 High Output for 75 cycles (Illumina). Raw BCL read files were demultiplexed and FASTQ files were generated using bcl2fastq and trimmed using Trimmomatic. Next, the reads were aligned to the mouse mm10 reference genome using STAR to generate BAM files. HTSeq was used to count reads in the exons of genes.

Pairwise differential gene expression analyses were carried out using the R package DESeq2. Gene set enrichment analysis was carried out using the Broad Institute GSEA software after conversion to human homologue gene symbols. The pairwise differential gene expression output generated from DESeq2 was

submitted as a pre-ranked list based on the DESeq2 Wald Statistic (stat column) output sorting genes from significantly upregulated to significantly downregulated. GSEA was performed on Hallmark Gene Sets from the GSEA Molecular Signatures Database.

2.4.5) Gene Network Analysis

Gene Set Enrichment Analysis software and Cytoscape software were used to generate gene network analysis plots. Preranked lists were analyzed for gene set enrichment for all 7350 Gene Ontology (GO) Biological Process gene sets on the Molecular Signatures Database. Next, GSEA results were loaded into the Enrichment Map Visualization tool in GSEA and Cytoscape software with enrichment map parameters set to a P-value cutoff of 0.005 and an FDR Q-value cutoff of 0.05 or 0.1 as noted in figure legends, a similarity cutoff using an overlap coefficient of 0.5.

2.4.5) Metabolite measurements

Mice were euthanized and tissues were rapidly isolated, and flash frozen in liquid nitrogen. Samples were stored at -80°C until extraction. Soluble metabolites were extracted directly from tissue using cold methanol/water (80/20, v/v) at approximately 1µL per 50µg of tissue. Tissue was disrupted for 15 seconds by rotor-stator homogenization (QIAGEN TissueRuptor II). Protein was precipitated by incubation at -80°C. Debris were pelleted by centrifugation at 18,000xg for 15 min at 4°C. The supernatant was transferred to a new tube and evaporated to dryness using a SpeedVac concentrator (Thermo Savant). Metabolites were reconstituted in 50% acetonitrile in analytical-grade water, vortex-mixed, and centrifuged to remove debris. Samples were analyzed by Ultra-High-Performance Liquid Chromatography and High-Resolution Mass Spectrometry and Tandem Mass Spectrometry (UHPLC-MS/MS). Specifically, the system consisted of a Thermo Q-Exactive in line with an electrospray source and an Ultimate3000 (Thermo) series HPLC consisting of a binary pump, degasser, and auto-sampler outfitted with an Xbridge Amide column (Waters; dimensions of 4.6mm × 100mm and a 3.5µm particle size). Mobile phase A contained 95% (vol/vol) water, 5% (vol/vol) acetonitrile, 10mM ammonium hydroxide, 10mM ammonium acetate, pH = 9.0; and mobile phase B was 100% Acetonitrile. The gradient was as follows: 0 min, 15% A; 2.5 min, 30% A; 7 min, 43% A; 16 min, 62% A; 16.1-18 min, 75% A; 18-25 min, 15% A with a flow rate of 400µL/min. The capillary of the ESI source was set to 275°C, with sheath gas at 45 arbitrary units,

auxiliary gas at 5 arbitrary units, and the spray voltage at 4.0kV. In positive/negative polarity switching mode, an m/z scan range from 70 to 850 was chosen and MS1 data was collected at a resolution of 70,000. The automatic gain control (AGC) target was set at 1×10^6 and the maximum injection time was 200 ms. The top 5 precursor ions were subsequently fragmented, in a data-dependent manner, using the higher energy collisional dissociation (HCD) cell set to 30% normalized collision energy in MS2 at a resolution power of 17,500. Data acquisition and analysis were carried out by Xcalibur 4.1 software and Tracefinder 4.1 software, respectively (both from Thermo Fisher Scientific). The peak area for each detected metabolite was normalized by the total ion current which was determined by integration of all of the recorded peaks within the acquisition window. Downstream analysis was carried out using Microsoft Excel and R. Statistical analysis using multiple comparisons adjusted T-tests, and plot generation were performed using MetaboAnalyst 4.0 (Chong et al., 2018).

2.4.6) LCMV infection model

Mice were infected with lymphocytic choriomeningitis virus (LCMV) by intraperitoneal injection at 2×10^5 PFU. Blood was collected retro-orbitally, red blood cells were lysed, leukocytes were antibody-stained and analyzed by flow cytometry.

2.4.7) Flow cytometry

Blood was collected from mice and red blood cells were lysed. An antibody panel for a white blood cell differential was used to stain leukocytes, which were subsequently analyzed on a BD FACS Symphony at the Northwestern Flow Cytometry Core Facility. Antibody panels shown below:

White Blood Cell Differential:

Laser	Laser	Filter	Dye	Antigen	Clone	Vendor
Violet	405	450/50	eFluor450	CD11b	M1/70	Biolegend
		525/50	V500	CD45	30-F11	BD
Green	552	575/25	PE	CD115	AFS98	BD
		780/60	PECy7	CD62L	MEL-14	eBio
Red	640	670/30	APC	CD43	S11	Biolegend
		780/60	ACPCy7	Ly6C	HK1.4	Biolegend
Far Red	690	730/45	Alexa 700	Ly6G	18A	BD

LCMV Panels:

Day 0:

APC- gp33 tetramer

Pecy7- CD8a

APCef780 - CD45.2

BV785- CD44

Day 7+:

APC- gp33 tetramer

Pecy7- CD8a

PerCPcy5.5- CD62L

BV785- CD44

2.4.8) Open field behavioral test

The open field test is used to assess general activity, anxiety and exploratory behavior in rodents. On the day of testing, mice were acclimated in the testing room 30 minutes prior to testing. To test, mouse was placed in the open arena (acrylic box: 44cmx44cmx44cm) and allowed to explore the area in the box for 10 minutes. Activity in the open field was recorded by digital video camera and Any-maze software (Stoelting Inc.) was used to score behavior in open-field testing. Parameters analyzed include total distance travelled, mean speed, time spent in the central and peripheral zones and duration of the immobility (resting time in seconds) in the arena. Statistical analysis was performed using one-way ANOVA (followed by Tukey's honest significant difference post-hoc test for multiple comparisons), using GraphPad Prism 7 software (GraphPad Software, La Jolla California USA). Data were considered significant for $p < 0.05$. Data are expressed as mean \pm SEM.

2.4.9) Rotarod behavioral test

Mice were placed on a rotating rod apparatus (Ugo Basile) that accelerates linearly from 4 to 40 rotations per minute over a 5-minute period. Mice were subjected to 4 trials per day for 4 consecutive days, each trial lasting to a maximum of ten minutes, with at least ten minutes of rest between each trial. The average performances for each day were plotted, and statistical differences between the different groups

were analyzed using repeated measures two-way ANOVA (followed by Tukey's honest significant difference post-hoc test for multiple comparisons). All statistical analyses here and elsewhere were performed using GraphPad Prism 7 software (GraphPad Software, La Jolla California USA). Data were considered significant for $p < 0.05$. Data are expressed as mean \pm SEM.

2.4.10) Grip strength behavioral test

Forelimb skeletal muscle strength was assessed using a digital grip strength meter (Columbus Instruments, Columbus, OH). The mice were picked up by the tail from the cage and then allowed to rest on a hard surface with all four paws on the flat surface. Then the mouse was lifted by its tail and was gently and slowly lowered over the top of the horizontal mesh grid attached to the grip meter, such that only its front paws can grip the grid. The mouse was allowed to grasp the mesh grid with its forelimbs and will then be gradually pulled backward steadily along a horizontal plane until the grid is released. When the animal releases the grid, the maximal grip strength will be recorded on the meter. Grip strength was measured in each animal six successive times, and the average of the values for each mouse was used to calculate muscle strength, normalized to mouse body weights. Statistical analysis was performed using one-way ANOVA (followed by Tukey's honest significant difference post-hoc test for multiple comparisons), using Graphpad Prism 7 software (GraphPad Software, La Jolla California USA). Data were considered significant for $p < 0.05$. Data are expressed as mean \pm SEM

2.4.11) Novel object recognition behavioral test

Mice were acclimated in the testing room 30 minutes prior to the testing. Novel object testing was performed in the same apparatus used for open-field testing. One day before testing (Day 0), animals were habituated for 5 min, 3 times a day for adaptation. For familiar trial (Day 1), mice will be placed in the open arena and allowed to explore for 1 minute. Mice were then briefly returned to their home cage while the arena was cleaned, and two identical objects are placed into the field. Mice were given 10 min of object-exploration time to investigate the arena. After this exposure trial, mice were returned to their home cage, and the arena and objects were cleaned with 70% ethanol to remove all olfactory cues. For the novel object test trial (Day 2), one of the familiar objects was replaced with a novel object, and mice were re-introduced to the arena after 24 hours. Mice were given 10 min of object-exploration time to

investigate the arena. To quantify the amount of time the mice spent exploring the novel object, a ratio was computed whereby the total time spent exploring the novel object was divided by the total time spent exploring both the novel and familiar objects. Behavior was recorded using Any-maze software and later scored offline by trained scorers blind to experimental groups. Statistical analysis was performed using one-way ANOVA (followed by Kruskal-Wallis non-parametric test for multiple comparisons), using Graphpad Prism 7 software (GraphPad Software, La Jolla California USA). Data were considered significant for $p < 0.05$. Data are expressed as mean \pm SEM.

2.4.12) Metabolic treadmill behavioral test

Mice were weighted and acclimated in the testing room 30 minutes prior to the testing. Before each testing session, Oxymax software (Columbus Instruments, Columbus, OH, USA) and open circuit indirect calorimetry treadmills (Metabolic Modular Treadmill, Columbus Instruments, Columbus, OH) were calibrated and checked for hardware malfunctions according to manufacturer instructions. Prior to calibration, sample pump was turned on with flow indicator showing flow set at 4–5 LPM. Pressure reading was set at ~800mmHg and gas tank output pressure was set at 5-10psi. Gas calibration was performed and adjusted when necessary using the GAIN and FINE knobs to set reading at 0.50% CO₂ and 20.5% O₂. Drierite (Calcium Sulfate with Indicator, Sigma-Aldrich; St. Louis, MO, USA) was changed constantly to maintain accurate gas readings and to assure that moisture accumulating during testing could properly be absorbed. During experiments, system sample pump maintained a constant sample flow reading of 0.63 L/min and sample drier a purge gas flow reading of 1.5 L/min. Mice were placed in the chamber with 20° incline and with shock grid supplying with small current (3Hz and 1.5mA). We used incremental treadmill protocol for testing, consisted of 7 stages: stage 1: 2.5m/min for 3 min, stage 2: 5 m/min for 3 min, stage 3: 10 m/min for 2 min, stage 4: 15 m/min for 2 min, stage 5: 20 m/min for 2 min, stage 6, 25 m/min for 2 min, stage 7: 30 m/min for 2 min, with stage 7 can be continued to exhaustion by increasing the speed by 2.5 m/min for 2 min. Oxymax computer software collected gas concentrations and flow to calculate oxygen consumption (VO₂), carbon dioxide expiration (VCO₂), and RER (VCO₂/VO₂) from the treadmill every 15 sec. Maximum run speed (meter/min) and time until exhaustion (min) were also recorded. Statistical analysis was performed using one-way ANOVA (followed by Tukey's

honest significant difference post-hoc test for multiple comparisons), using Graphpad Prism 7 software (GraphPad Software, La Jolla California USA). Data were considered significant for $p < 0.05$. Data are expressed as mean \pm SEM.

2.4.13) Oxygen consumption measurements

Oxygen consumption measurements were carried out using a Seahorse XFe96 Analyzer. Synaptosomes were isolated using a ThermoFisher Syn-PER Synaptic Protein Isolation Reagent and manufacturer protocols. Isolated mitochondria were isolated from tissue by dounce homogenization and differential centrifugation using following Agilent Seahorse manufacturer protocols. Cerebellar granule neurons and glia measurements were made from cultured primary cells as described above. The residual oxygen consumption after 1 μ M Piericidin A and Antimycin A combined injection was measured and subtracted from oxygen consumption measurements to determine the basal mitochondrial oxygen consumption. Protocol for extraction and culture of early post-natal cerebellar granule neurons was adapted from previously published methods [291]. Prior to experimentation, mouse genotype was determined, and tissue culture plates were coated with poly-D-lysine (Fisher) at two different concentrations: 100 μ g/mL for pre-plating/glial dishes and 500 μ g/mL for cerebellar granule neuron plates. The following day the developing cerebellum of individual early postnatal mice was removed, and meninges were removed under a dissecting microscope. Next, tissue was incubated at 37°C for 15 minutes in Papain from the Papain Dissociation System Kit (Worthington) combined with 1mg/mL of DNase I. Tissue was then triturated using P1000 pipette tips pre-coated with serum and the suspension was allowed to settle for 30 seconds to 1 minute to allow large undissociated pieces to settle. Using serum-coated pipette tips, cells remaining in suspension were transferred to a new centrifuge vial and centrifuged at 200 \times g for 5 minutes. Cell pellets were resuspended in Minimum Essential Media + albumin-ovomucoid inhibitor. Resuspended cells were carefully layered over an additional 1mL of albumin-ovomucoid inhibitor solution in a new centrifuge vial and centrifuged at 70 \times g for 6 minutes, pelleting dissociated cells and leaving membrane fragments and lipid at the surface. Next, the cells were resuspended, passed through a 70-micron filter, and plated on pre-plating plates in Neurobasal A medium supplemented with 10% serum, glutamax, antibiotic/antimycotic, and KCl. Cells were allowed to settle for 20 minutes. After incubation, granule

neurons and neuron progenitors were dislodged with gentle tapping while larger glia remained adhered. The pre-plating step for glial removal was repeated. Finally, an enriched population for cerebellar granule neurons was resuspended in serum-free media containing Neurobasal A Medium supplemented with 2% B-27, glutamax, antibiotic/antimycotic, and KCl and plated directly onto poly-D-lysine-coated Seahorse plates and cultured for 5 days prior to oxygen consumption analysis.

CHAPTER 3: Expression of the yeast enzyme NDI1 is sufficient to rescue lifespan but not motor function in a model of mitochondrial disease

3.1) Introduction

Mitochondrial complex I regenerates NAD⁺ and proton pumps for TCA cycle function and ATP production, respectively. Mitochondrial complex I dysfunction has been implicated in many brain pathologies including Leigh Syndrome and Parkinson's disease. We sought to determine whether NAD⁺ regeneration or proton pumping is the dominant function of mitochondrial complex I in protection from brain pathology. We generated a mouse that conditionally expresses the yeast NDI1 protein, a single enzyme that can replace the NAD⁺ regeneration capability of the 45-subunit mammalian mitochondrial complex I without proton pumping. NDI1 expression was sufficient to dramatically prolong lifespan without significantly improving motor function in a mouse model of Leigh Syndrome. Therefore, mitochondrial complex I activity in the brain supports organismal survival through its NAD⁺ regeneration capacity, while optimal motor control requires the bioenergetic function of mitochondrial complex I.

Mitochondria are essential bioenergetic, biosynthetic, and signaling organelles within eukaryotic cells. The electron transport chain is a key component of mitochondria because it provides the proton-motive force that drives oxidative phosphorylation as well as the oxidation of NADH to NAD⁺ to allow the tricarboxylic acid (TCA) cycle to proceed [5]. The TCA cycle provides the building blocks for many of the cell's macromolecules, including amino acids, nucleic acids, carbohydrates, lipids, and their derivatives such as neurotransmitters. In mammalian mitochondria, a 45-subunit complex known as mitochondrial complex I couples the oxidation of NADH to proton pumping for the generation of ATP [16]. Dysfunction of mitochondrial complex I has been implicated in neurodegenerative diseases, such as the age-related Parkinson's Disease and the inherited genetic disorder Leigh Syndrome [198]. Given the essential role of mitochondrial complex I in both NAD⁺ regeneration and ATP production, it is difficult to parse out which of these functions controls the effects of mitochondrial complex I dysfunction in the setting of complex tissues like the brain.

Perturbations to the mitochondrial electron transport chain, particularly at mitochondrial complex I, can decrease the ability of mitochondria to produce ATP as well as the biosynthetic precursors

necessary for macromolecule generation. Under normal circumstances, the bioenergetic and biosynthetic roles of mitochondrial complex I are not separable, because the oxidation of NADH and the subsequent transfer of electrons to the Q pool is linked to the translocation of protons across the inner mitochondrial membrane to generate the mitochondrial membrane potential. To dissect these two key functions of mitochondrial complex I *in vivo*, we made use of the single subunit yeast enzyme NADH dehydrogenase internal 1 (NDI1). In yeast, the NDI1 protein serves as the major entry point into the electron transport chain, catalyzing the oxidation of NADH in the matrix in a manner similar to mammalian mitochondrial complex I. However, unlike mammalian mitochondrial complex I, NDI1 is unable to proton pump and contribute to the production of ATP. Previously, NDI1 has been expressed in mammalian cells, both *in vitro* and through viral delivery [40], [50], [73], and it has been shown to increase the lifespan of *Drosophila* when ectopically expressed [129].

To test the effect of restoring NADH oxidation in the setting of mitochondrial complex I dysfunction, we used a Cre/Lox approach to conditionally delete the NDUF54 protein and express the yeast NDI1 protein in mice. NDUF54 is an 18 kDa accessory subunit of mitochondrial complex I required for the proper assembly and stable formation of the complex. Mice with deletion of NDUF54, either globally or specifically in the brain with Nestin-Cre driven recombination, are frequently used to model the mitochondrial diseases Leigh Syndrome and Leber Hereditary Optic Neuropathy [133], [248]. The NDUF54 subunit is the most frequently mutated mitochondrial complex I gene found in humans with Leigh Syndrome [301]. Deletion of the NDUF54 protein in mice recapitulates many features of human Leigh Syndrome, including the development of bilateral hyperintense lesions on a T2-weighted MRI in the brainstem and cerebellum, glial activation, seizures, ataxia, growth regression, and early mortality. It is important to note that deletion of NDUF54 does not result in a complete loss of mitochondrial complex I function, and that the reduction in the enzymatic activity of mitochondrial complex I varies from tissue to tissue [133], [237], [229]. Interestingly, previous studies have shown that treatment with rapamycin and hypoxia improves the lifespan and motor function of global NDUF54 knockout mice [259], [254], and interventions more specifically targeting NADH elevation such as NAD-precursor supplementation, dimethyl-ketoglutarate treatment, and inhibition of mitochondrial serine catabolism all demonstrated

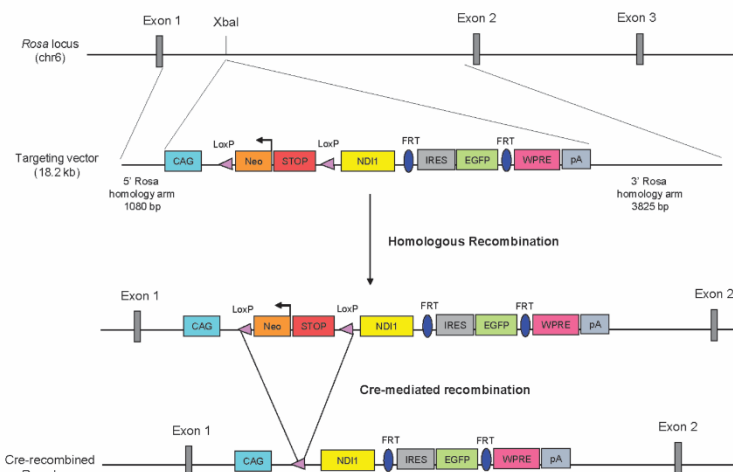
benefits [253], [18]. Recently, conditional deletion of NDUFS4 in specific neuronal subpopulations showed that either GABAergic neurons (Gad2-cre) or glutamatergic neurons (Vglut2-cre) are sufficient to drive a fatal phenotype, but that brainstem and cerebellar glutamatergic neurons are likely the drivers of ataxia while GABAergic neurons are likely the drivers of seizures [240].

3.2) Expression of yeast NDI1 protein is sufficient to prolong lifespan in a model of brain mitochondrial complex I dysfunction.

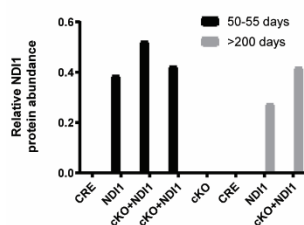
In order to conditionally express yeast NDI1 *in vivo*, we generated NDI1 knock-in mice using the *Rosa26* locus. Specifically, we designed a targeting construct containing 5' and 3' *Rosa26* homology arms, as well as a Lox-STOP-Lox (LSL) cassette upstream of the NDI1 gene (Figure 3.2.1 A). Thus, NDI1 is only expressed following Cre recombination and removal of the Lox-STOP-Lox cassette. The NDI1-LSL targeting construct was electroporated into C57BL/6 embryonic stem (ES) cells. Two independent ES clones harboring the NDI1-LSL allele were injected into blastocysts to produce germline-transformed heterozygous NDI1-LSL mice. To express NDI1 in the setting of mitochondrial complex I dysfunction in the brain, we bred our NDI1-LSL mice to NDUFS4-floxed Nestin-Cre (cKO) mice. This generated NDI1-LSL NDUFS4-floxed Nestin-Cre (cKO + NDI1) mice, where NDI1 is expressed and NDUFS4 is lost specifically in the brain. Nestin is an intermediate filament protein that is activated at approximately embryonic day 11 in all mature neural lineage cells, including astrocytes, oligodendrocytes, and neurons. Notably, microglia do not arise from a Nestin-positive precursor; therefore, Cre recombination does not occur in these cells. To assess Cre-dependent recombination of the NDI1-LSL and NDUFS4-floxed alleles, we measured NDI1 and NDUFS4 protein abundance in the brain (Figure 3.2.1. B, C). At all ages measured, the NDI1 protein was properly expressed and the NDUFS4 protein was properly lost. Additionally, we examined the mRNA levels of NDI1 and NDUFS4 in various cell types of adult mouse brains. As expected, NDI1 expression and NDUFS4 deletion was observed in astrocytes, but not in microglia (Figure 3.2.1. D-F).

Recent single cell RNA-sequencing of the mouse brain suggests that in the cerebellum the NDUFS4 transcript is most highly expressed in granule neurons (Figure 3.2.1 G). To evaluate the metabolic function of mitochondrial complex I and NDI1, we isolated cerebellar granule neurons and

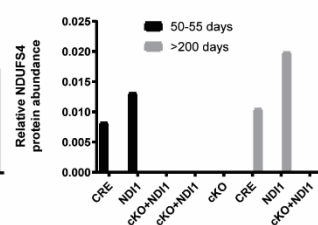
A.



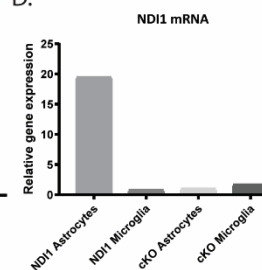
B.



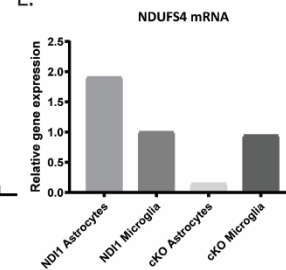
C.



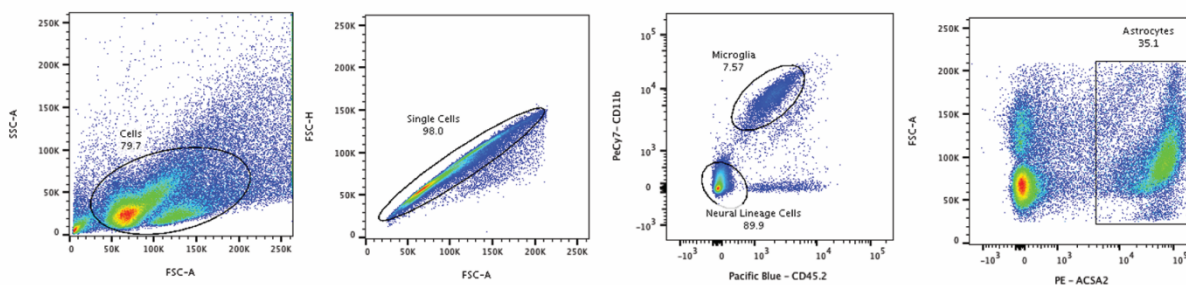
D.



E.



F.



G.

Clusters With Highest Expression of NDUFSA (top 10 results)

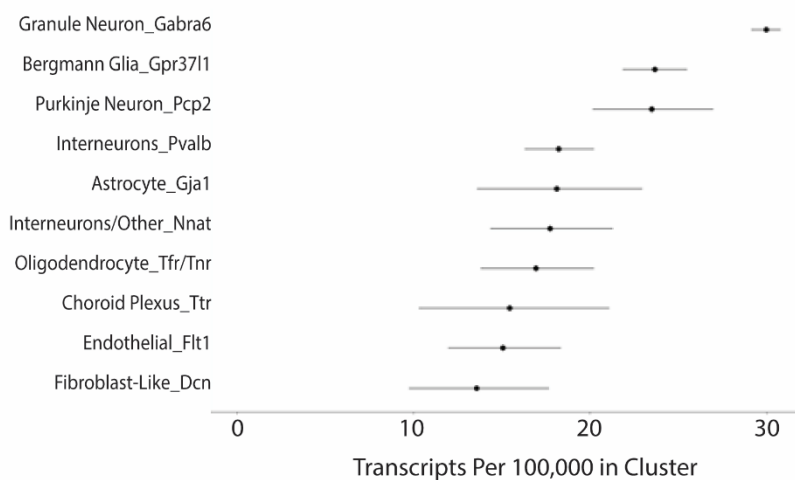


Figure 3.2.1. Generation of NDI1 knock-in mice and confirmation of NDUFS4 knock-out and NDI1 knock-in. (A) Schematic of the NDI1-LSL targeting construct for knock-in at the mouse *Rosa26* locus. Homologous recombination in embryonic stem cells after electroporation allows the generation of mice with the NDI1-LSL allele in their germline. Cre-mediated recombination of LoxP sites leads to deletion of the STOP cassette and expression of the yeast enzyme NADH Dehydrogenase Internal 1 (NDI1). (B) NDI1 protein quantification in whole brain tissue using a Wes automated capillary-based fluorescent immunoassay system. The area of fluorescent peaks detected at 58 kDa (predicted NDI1 molecular weight) divided by the area of peaks detected at 111 kDa (predicted Vinculin molecular weight) as a loading control were used to generate bar graphs of relative protein abundance of NDI1 at 7 weeks of age and at greater than 6 months of age to demonstrate that NDI1 protein remains detectable in adult brain tissue. (C) NDUFS4 protein quantification in whole brain tissue using a Wes automated capillary-based fluorescent immunoassay system. The area of fluorescent peaks detected at 26 kDa (predicted NDUFS4 molecular weight) divided by the area of peaks detected at 52 kDa (predicted Tubulin molecular weight) as a loading control were used to generate bar graphs of relative protein abundance of NDUFS4 at 7 weeks of age and at greater than 6 months of age to demonstrate appropriate depletion of NDUFS4 gene in adult brain tissue. (D) NDI1 and (E) NDUFS4 mRNA measured by qPCR from astrocytes and microglia were sorted from adult NDI1 expressing mice and NDUFS4 cKO mice to confirm appropriate recombination by Nestin Cre in neural lineage cells (astrocytes) but not microglia. (F) Sort layout and gating strategy for mRNA analysis of astrocytes and microglia. (G) DropViz data suggests that in the mouse cerebellum the relative NDUFS4 expression is highest in cerebellar granule neurons. Publicly available Drop-seq data on the DropViz online platform was used to query NDUFS4 expression by putative cell type cluster in the mouse cerebellum.

analyzed their basal oxygen consumption rate (Figure 3.2.2 A-B) as well as their oxygen consumption after treatment with the ATP synthase inhibitor oligomycin A (Figure 3.2.2 C) and the mitochondrial complex I inhibitor piericidin A (Figure 3.2.2 D). Cerebellar granule neurons expressing NDI1 demonstrated a mild increase in basal oxygen consumption and were resistant to mitochondrial complex I inhibition (Figure 3.2.2 B). Loss of NDUFS4 in cerebellar granule neurons caused a significant decrease in both basal and coupled respiration that was rescued by NDI1 expression (Figure 3.2.2 B, C). Moreover, the cerebellar granule neurons from mice expressing NDI1 demonstrated significant resistance to oxygen consumption reduction upon treatment with the mitochondrial complex I inhibitor piericidin A (Figure 3.2.2 B). These data suggest that the yeast NDI1 protein is expressed and functional in the brains of our mice.

Mice with NDUFS4 deletion, whether it be a global NDUFS4 knockout mouse or a mouse with NDUFS4 lost specifically in the brain (cKO mouse), show pathologic changes resembling Leigh Syndrome, including reactive gliosis in the brainstem, abnormal breathing pattern, seizures, and ataxia [133], [248]. It has been reported by us and others that NDUFS4-floxed Nestin-Cre (cKO) mice die between the ages of postnatal day 45 and postnatal day 60 [248] (Figure 3.2.2 E). Interestingly, when mice express NDI1 in the cKO background (cKO + NDI1) their lifespan is drastically increased by a full

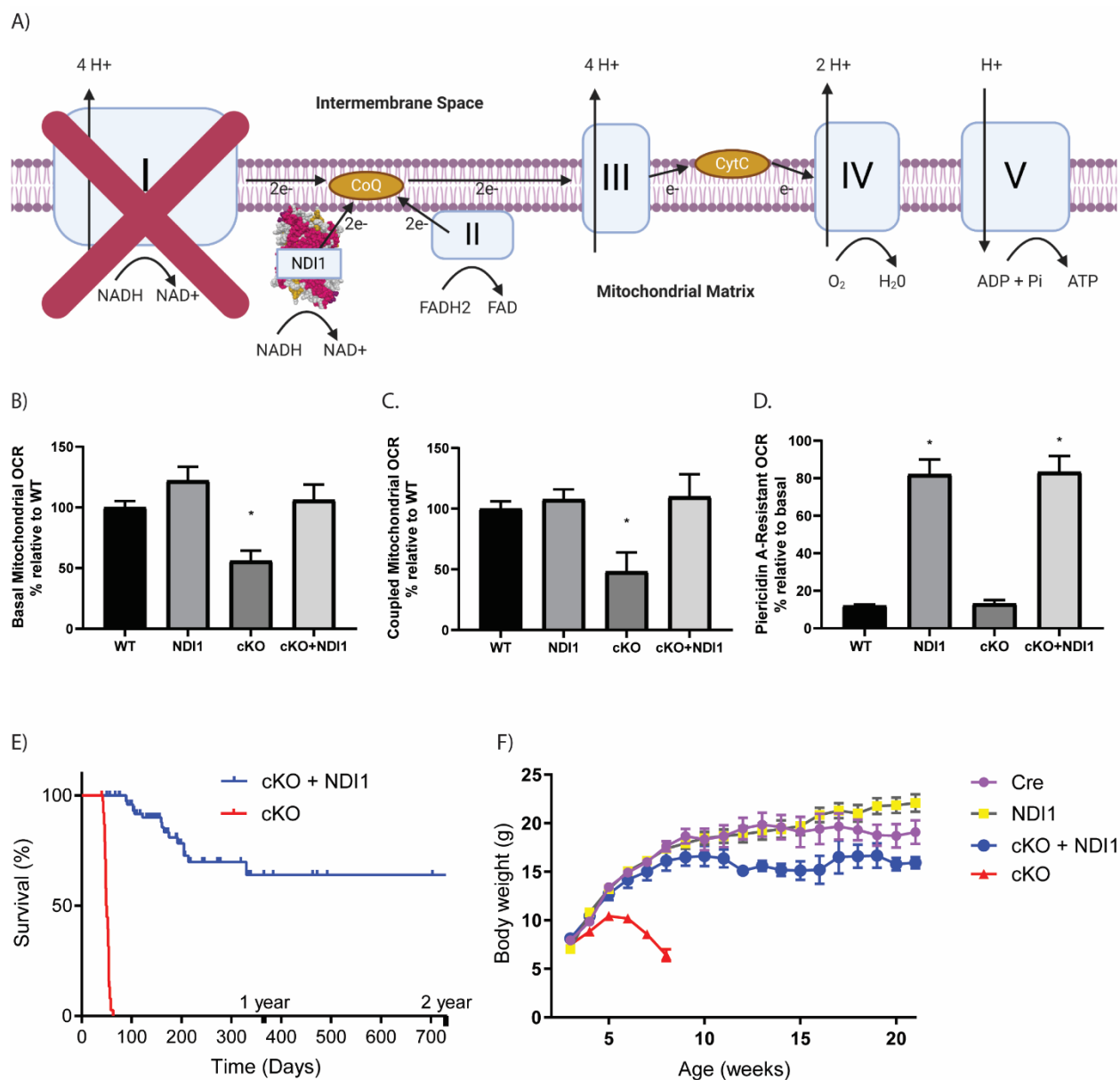


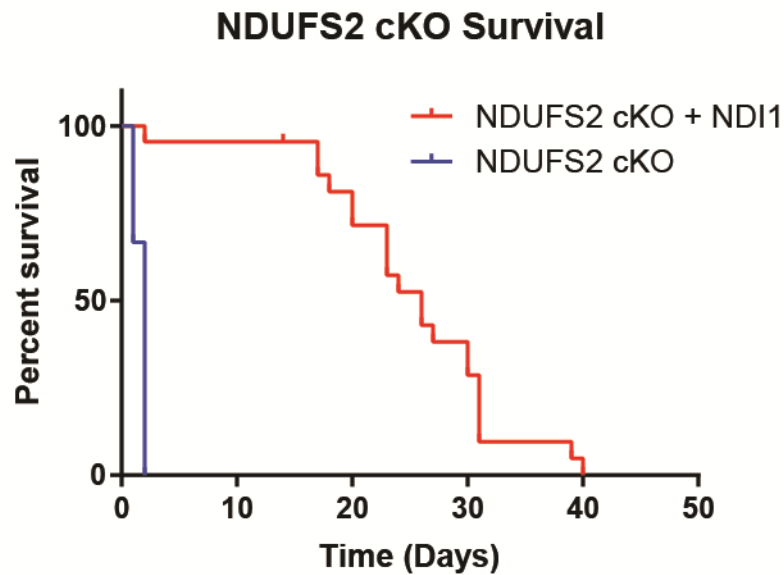
Figure 3.2.2. The yeast NDI1 protein is functional in mammalian neurons and is sufficient to rescue lifespan in a mitochondrial complex I-deficient mouse model. (A) A schematic drawing of the mammalian mitochondrial electron transport chain. When mammalian mitochondrial complex I is not functional, the yeast NDI1 protein can transport electrons and regenerate NAD⁺ like mammalian mitochondrial complex I; however, NDI1 cannot proton pump. **(B)** The basal oxygen consumption rate (OCR) of cerebellar granular neurons from postnatal day 2-7 mice was measured. Nestin Cre positive and negative littermate control (wildtype, WT) mice were examined as well as mice expressing yeast NDI1 in the brain (NDI1), mice with loss of NDUFS4 (mitochondrial complex I) in the brain (cKO), and mice with loss of NDUFS4 but expression of NDI1 in the brain (cKO + NDI1). The data were pooled from 6 independent experiments (N=7-14 per genotype, ANOVA P=0.0008, Dunnett's multiple comparisons test WT vs cKO *P<0.05). **(C)** ATP-coupled oxygen consumption in cerebellar granular neurons was measured with the ATPase inhibitor Oligomycin A. The data were pooled from 4 independent

experiments (N=4-11 per genotype, ANOVA $P=0.0008$, Dunnett's multiple comparisons test WT vs cKO $*P<0.05$). **(D)** Percentage of basal oxygen consumption that is resistant to treatment with the mitochondrial complex I inhibitor Piericidin A at 500nM. (N=3-5 per group, ANOVA $P<0.0001$, * denotes $P<0.05$ Dunnett's multiple comparisons test vs WT). **(E)** Kaplan-Meier curves of brain-specific NDUFS4-deficient mice with and without transgenic expression of yeast NDI1. (cKO N=40 and cKO + NDI1 N=59, Log-rank test $P<0.0001$). **(F)** Body weight in grams over time for the various mouse genotypes, cKO + NDI1 indicates 2 alleles of NDI1. (N=21-38 per group, ANOVA $P<0.0001$, Dunnett's multiple comparisons test comparing Nestin Cre positive control to cKO $P<0.0001$).

order of magnitude in some individuals, with a median survival greater than 1 year of age (Figure 3.2.2 E). Thus, a single yeast enzyme is sufficient to prolong the lifespan of a mouse in which the 45 subunit-containing mitochondrial complex I is dysfunctional. Consistent with previous reports, the cKO mice reached an average weight of approximately 11g by 30-40 days of age and then, during the late stage of disease, exhibited growth regression (Figure 3.2.2 F). In contrast, the cKO + NDI1 mice did not exhibit growth regression, but rather attained a body weight closer to their littermate controls (Figure 3.2.2 F). Our data demonstrate an intriguing concordance of the timing of behavioral deficits, along with a plateau or slight regression of weight gain in cKO + NDI1 at the critical period of 7-10 weeks (Figure 3.2.2 F), during which cKO mice exhibit weight loss, rapid decline in motor function, seizures, and early mortality. It is unclear why this time period is so consistent in this model and what specifically triggers this change. Similarly, in human Leigh Syndrome, the etiology of the precise timing of onset and the rate of decline are important challenges for future studies.

We carried out some additional genetic crosses to further evaluate the role of NDI1 in survival and the role of several components of the innate and adaptive immune pathway on the survival of ubiquitous NDUFS4 deficient mice. Loss of the mitochondrial complex I subunit NDUFS2 in the brain is lethal perinatally with either embryonic lethality and still-birth or is fatal by 1-2 days after birth. Expression of NDI1 in these mice was sufficient to allow for survival until approximately 4-5 weeks of age, with severe motor and growth impairments (Figure 3.2.3 A). Generation of NDUFS4 deficient mice that were also deficient for T cells (RAG deficient), the IL-6 cytokine (IL-6 deficient), or the cGAS-STING innate cytosolic DNA sensing pathway (STING-deficient), were not sufficient to prolong survival compared to NDUFS4 deficient control mice (Figure 3.2.3 B).

A)



B)

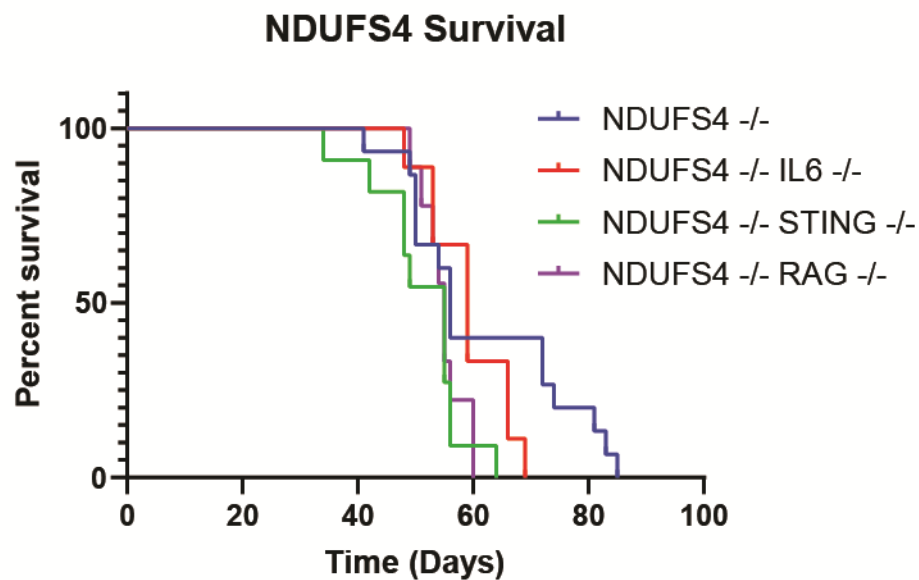


Figure 3.2.3. NDI1 expression is sufficient to prolong survival in mice deficient for NDUFS2 in the brain and deficiency for multiple components of the immune system is not sufficient to prolong lifespan in ubiquitous NDUFS4 deficient mice. (A) Kaplan-Meier curves of brain-specific NDUFS2-deficient mice with and without transgenic expression of yeast NDI1. (N=6 NDUFS2 cKO and 22 NDUFS2

cKO+NDI1, Survival Curve Comparison: Log-rank (Mantel-Cox) test $P < 0.0001$) **(B)** Kaplan-Meier curves of ubiquitous NDUFS4-deficient mice with and without ubiquitous loss of RAG, IL6, and STING (N=9-15 per genotype, Survival Curve Comparison: Log-rank (Mantel-Cox) test $P = 0.0273$).

3.3) Expression of yeast NDI1 is not sufficient to restore motor function.

To determine whether the NAD⁺ regeneration capability of NDI1 is sufficient to improve the progressive ataxia observed in the well-established NDUFS4-deficient mouse model, we measured coordination, balance, and ambulation in our cKO + NDI1 mice by two classic tests of mouse behavior, the rotarod and the open field test. As shown in Figure 3.3.1 A, cKO + NDI1 mice (> than 2 months of age) are almost completely incapable of performing the rotarod task due to severe coordination and impaired balance. This result is similar to what we and others have observed for the cKO mice [248]. NDI1 expression in the brain, in the absence of NDUFS4 deletion (NDI1 mice), does not impair the balance or coordination of the mice (Figure 3.3.1 A). Moreover, when we examined the distance traveled using an open field task, we found that cKO + NDI1 mice, like late stage cKO mice, have a diminished distance traveled compared to control mice (Figure 3.3.1 B). Due to a combination of ataxia and visual impairment cKO mice exhibit a high amount of variability in location preference in the open field test, with some mice spending significant proportions of time near the center, while others remain closer to the walls at the periphery (Figure 3.3.1 C, D). This contrasts with control mice, which spend the majority of their time at the periphery (Figure 3.3.1 C, D). Interestingly, expression of NDI1 in the cKO mice has no effect on their pattern of activity. Thus, cKO + NDI1 mice display a high variance of location preference, with such mice spending time in both the center of the open field as well as the periphery (Figure 3.3.1 C, D).

It is thought that early mortality in global NDUFS4-deficient mice is due to brainstem dysfunction which ultimately leads to respiratory failure [302]. In partial support of this idea, a recent report suggested that brainstem dysfunction-mediated breathing abnormalities in glutamatergic neuron-specific NDUFS4-deficient mice led to death but did so at a slightly later time point than the seizure-mediated death in GABAergic neuron-specific NDUFS4-deficient mice [240]. Indeed, we have observed tonic-clonic seizures in our Nestin-Cre-specific cKO mice, but not the cKO + NDI1 mice; however, the cause of death for the cKO + NDI1 mice that died prematurely remains unknown and may be due to a delayed disruption of

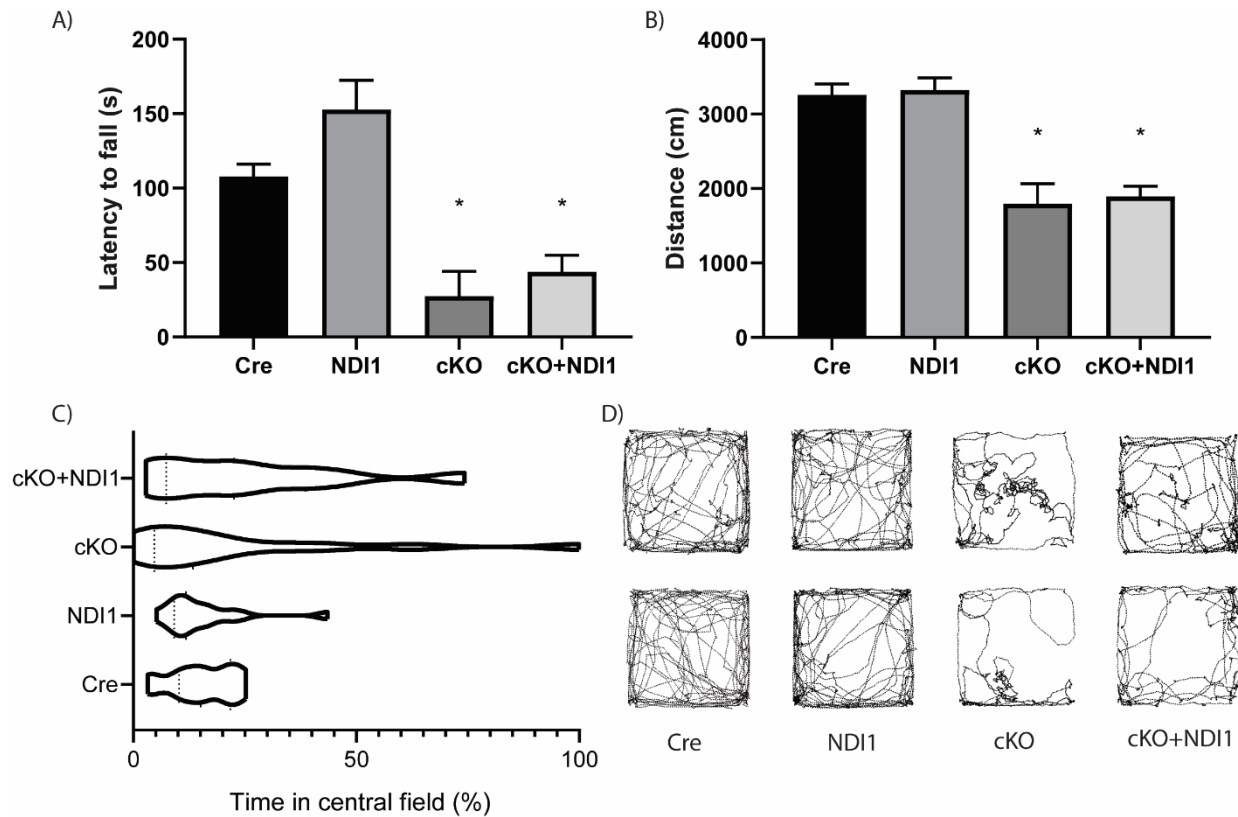
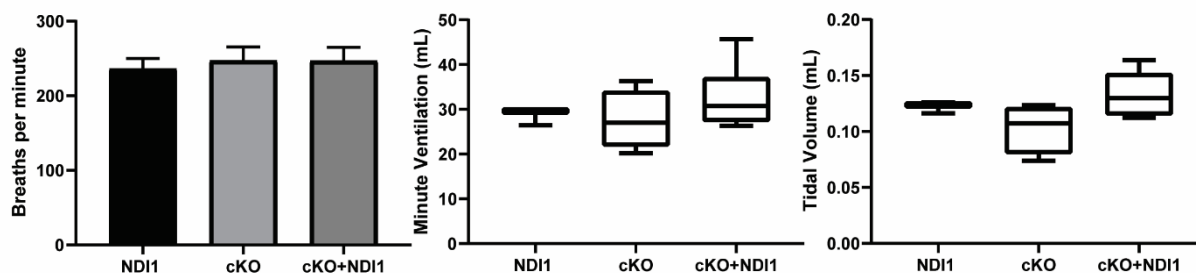


Figure 3.3.1. NDI1 expression in the brain does not rescue progressive ataxia (A) Latency to fall in an accelerating rotarod challenge in seconds (s). The average trial duration of 4 trials per day for 3 consecutive days, after 2 days of habituation at constant speed (N=8-22 per genotype, ANOVA $P < 0.0001$, Dunnett's multiple comparisons test compared to Cre control $*P < 0.01$). **(B)** Distance the mouse traveled in 300 seconds in a novel open field environment (N=12-22 per genotype, ANOVA $P < 0.0001$, Dunnett's multiple comparisons test compared to Cre control $*P < 0.0001$). **(C)** Percent time spent in the central zone of a novel open field environment. Central zone is defined as the central 9 squares of a 5x5 grid overlaid on the total area. (Bartlett's test $P < 0.0001$). **(D)** Two representative path images of the open field test for each mouse genotype examined is shown.

breathing patterns. However, we found that the average breathing frequency, tidal volume, and minute ventilation plethysmography parameters of both cKO mice and cKO + NDI1 mice were not significantly different compared to littermate control mice. However, these mice may have an increase in variability of these parameters (Figure 3.3.2 A). Furthermore, we did not observe any prolonged apneas in either cKO + NDI1 or cKO mice, despite some evidence of abnormal breathing patterns (Figure 3.3.2 B). Therefore, we would speculate that seizures are the dominant cause of death in the Nestin Cre model, since we do not observe profound breathing differences between the fatal cKO genotype and the surviving cKO + NDI1 genotype. Perhaps GABAergic neurons in the basal ganglia, which have recently been identified as

an important cell population driving seizure-induced mortality, are a key population of cells that mediates the observed survival of cKO + NDI1 mice.

A)



B)

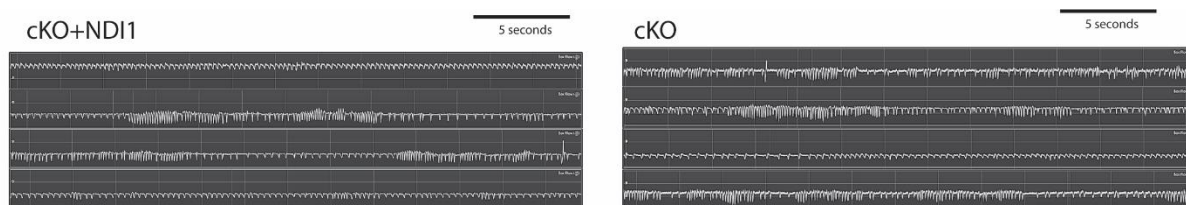


Figure 3.3.2 NDI1 expression in the brain does not alter breathing parameters (A) Breathing parameters, including frequency, minute ventilation, and tidal volume, from whole body plethysmography of unrestrained mice. (N=3-6 per genotype, ANOVA not significant). **(B)** Representative whole-body plethysmography breathing patterns of cKO+NDI1 (left) and cKO (right) mice at over 7 weeks of age with times of regular and irregular breathing patterns in both groups. No apneas were observed in either group.

3.4) Expression of yeast NDI1 is sufficient to prevent MRI lesions and microglial activation.

Since a key diagnostic feature of human mitochondrial disease is the presence of symmetric bilateral hyperintense T2-weighted MRI lesions, researchers have used MRI to assess disease severity in the NDUFS4-deficient mouse model [303]. MRI imaging of late stage cKO mice (8 weeks of age) revealed bilateral hyperintensities in the olfactory bulb and cerebellum near the fourth ventricle (Figure 3.4.1 A). cKO + NDI1 mice, on the other hand, did not develop detectable MRI lesions in the cerebellum or brainstem, and only developed hyperintensities in the olfactory bulb at 6 months of age (Figure 3.4.1 A). Pathological analyses of mouse brains at 7 weeks of age showed regions of microglial activation in the olfactory bulb, cerebellum, and brainstem of cKO mice, but not in age-matched cKO + NDI1 and control mice (Figure 3.4.1 B). Moreover, the cKO mice had an accumulation of microglia with shortened

processes compared to cKO + NDI1 and control mice (Figure 3.4.1 C, Figure 3.4.2 B). Recall that in cKO mice *NDUFS4* is not deleted in microglia following Nestin-driven Cre recombination; thus, the observed microglial activation is likely not a cell-intrinsic feature but rather a response to damage to or signals from *NDUFS4*-deficient neural lineage cells. We also immunostained for the activated astrocyte marker GFAP, and observed an increase in an activated phenotype in the brainstem, olfactory bulb, and cerebellum of cKO mice, with a non-statistically significant increase in GFAP+ cell numbers in these regions (Figure 3.4.2 A, Figure 3.4.1 C).

Since numerous mitochondrial disorders cause muscle dysfunction, and Nestin Cre can lead to recombination in skeletal muscle satellite cells, we sought to investigate the possibility that the persistent motor deficits observed in our model were due to loss of *NDUFS4* in the muscle. To that end, we profiled the quadriceps muscle from ataxic cKO + NDI1 mice at 12 months of age or older and compared to age-matched littermate controls expressing NDI1 that do not develop ataxia. We reasoned that if there were muscle changes leading to this ataxic phenotype, they would be progressive and more likely to be observed robustly in aged mice. Large proximal muscles, including the quadriceps, are frequent sites of involvement in certain types of human mitochondrial disease such as Myoclonic Epilepsy with Ragged Red Fibers (MERRF), in which pathognomonic histological changes known as “ragged red fibers” are frequently observed. We therefore stained fixed muscle tissues from cKO + NDI1 and NDI1 mice using H&E and trichrome stain (Figure 3.4.3 A-B). The average cross-sectional fiber diameter was not significantly changed, and we saw no evidence of central nuclei (a marker of muscle regeneration after damage) or ragged red fibers (Figure 3.4.3 A-C). Moreover, we found no significant change in the level of *NDUFS4* protein in homogenized quadricep tissue (Figure 3.4.3 D). We also found no statistically significant changes in soluble metabolites extracted from homogenized quadriceps of cKO + NDI1 and NDI1 mice (Figure 3.4.3 E-G). These data do not support the hypothesis that muscle dysfunction contributes to the behavioral phenotype.

To attempt to explain the persistent ataxia in cKO + NDI1 mice, we sought to quantify neuron abundance in several regions of motor control in mice that survive over one year of age. These regions

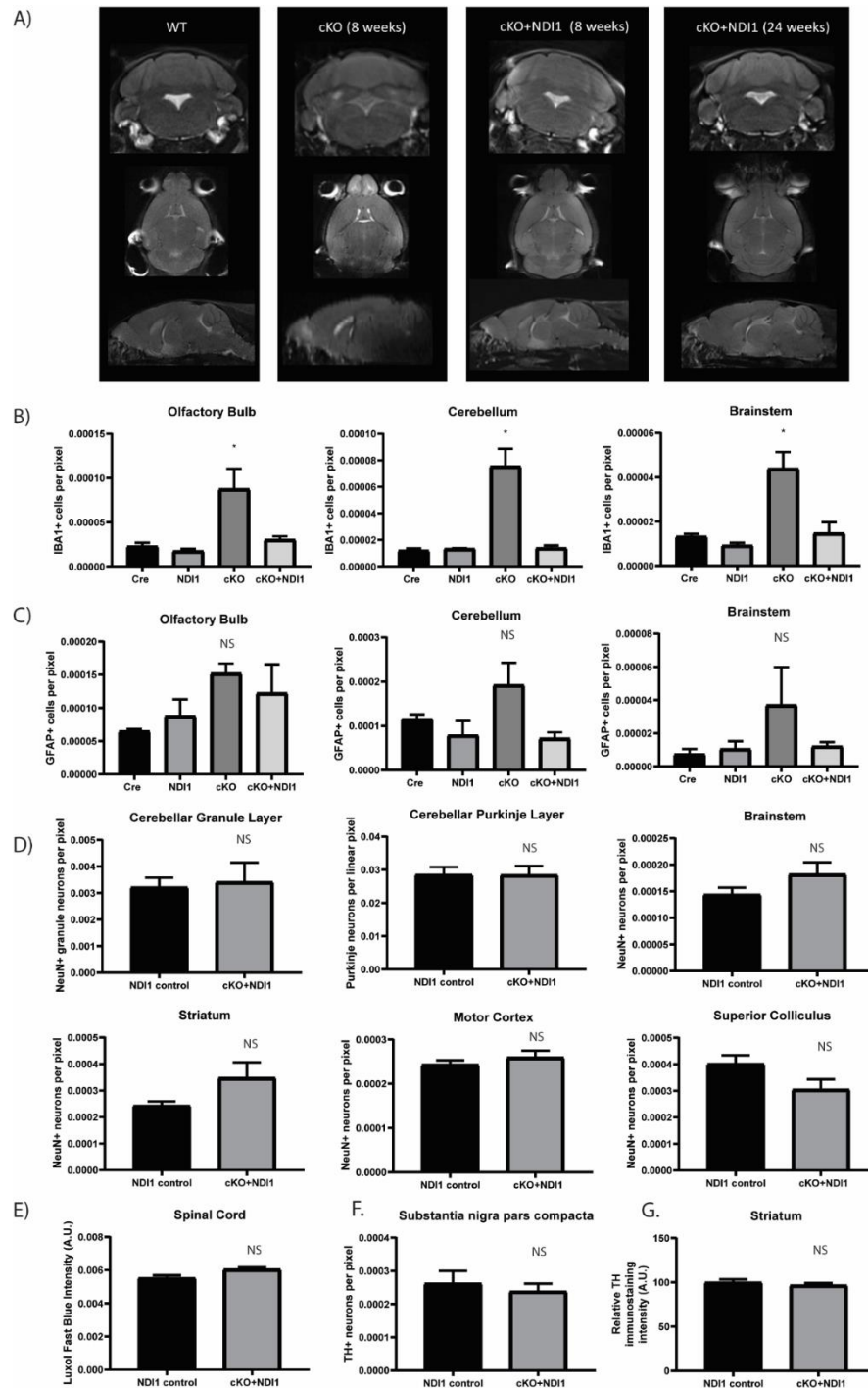


Figure 3.4.1 NDI1 expression in NDUFS4-deficient brains prevents the formation of inflammatory glial activation and MRI lesions, and does not cause neurodegeneration. (A) Representative images from a magnetic resonance imaging (MRI) T2-weighted turbo spin echo sequence. The coronal, horizontal, and sagittal planes for each mouse genotype are shown at the approximate level where cKO mice exhibit bilateral hyperintense lesions in the olfactory bulb, brainstem, and cerebellum. **(B)** Quantification of IBA1+ microglia from DAB IBA1 positive microglia in brain regions demonstrating cKO inflammation at 7-8 weeks of age quantified in 20x image fields normalized to pixel area. (N=3-4 per

genotype, * denotes ANOVA $P < 0.05$ with Dunnett's multiple comparisons test vs WT $P < 0.05$). See also Fig. S3. **(C)** Quantification of GFAP+ DAB-stained activated astrocytes in 20x image fields normalized to pixel area at 7-8 weeks of age (N=3 per genotype, ANOVA not significant). See also Fig. S3. **(D)** Quantification of NeuN+ DAB-stained neurons in 20x image fields normalized to pixel area from motor control brain regions or for Purkinje neurons quantification of cells from H&E stained per linear pixel of the cerebellar Purkinje layer at over 1 year of age (N=6 per genotype, T-test not significant). **(E)** Spinal cord Luxol fast blue staining quantified as average of the white matter mean grey-scale pixel intensity at 3 randomly selected spinal levels (N=3 per genotype, T-test not significant). **(F)** Substantia nigra tyrosine hydroxylase+ DAB stained dopaminergic neurons quantified in 20x image fields normalized to pixel area (N=6 per genotype, T-test not significant). **(G)** Tyrosine hydroxylase+ DAB immunoreactivity of dopaminergic neuron projection to the striatum quantified by inverse grey-scale pixel intensity normalized to control average from 20x image fields (N=5-6 per genotype, T-test not significant).

include the cerebellar Purkinje neuron layer, the cerebellar granule neuron layer, and NeuN+ neurons in the brainstem, the superior colliculus of the midbrain, the striatum, and the motor cortex (Figure 3.4.1. D).

There were no significant changes in cell number between ataxic mice (cKO + NDI1) and NDI1 controls, and there was no gross evidence of inflammation or neurodegeneration by H&E staining. We also evaluated the spinal cord by H&E and Luxol fast blue staining (the classic stain to measure myelination) and saw no significant changes between the genotypes (Figure 3.4.1 E). Finally, we used tyrosine hydroxylase (TH) to quantify dopaminergic neurons in the substantia nigra pars compacta and found no evidence of significant changes between cKO + NDI1 mice and controls (Figure 3.4.1 F). There was also equal TH immunoreactivity in the striatum (Figure 3.4.1 G). Ultimately, we were unable to find definitive evidence of significant neurodegeneration or neuroinflammation in the brain regions involved in motor function in the cKO + NDI1 mice that would explain their dramatic motor phenotype. We hypothesize that this is because of a functional (rather than structural) deficit in cerebellar or brainstem circuits containing glutamatergic neurons, due to a decrease in ATP production, in turn due to the lack of proton-pumping by NDI1. However, we do not have direct evidence of this *in situ*.

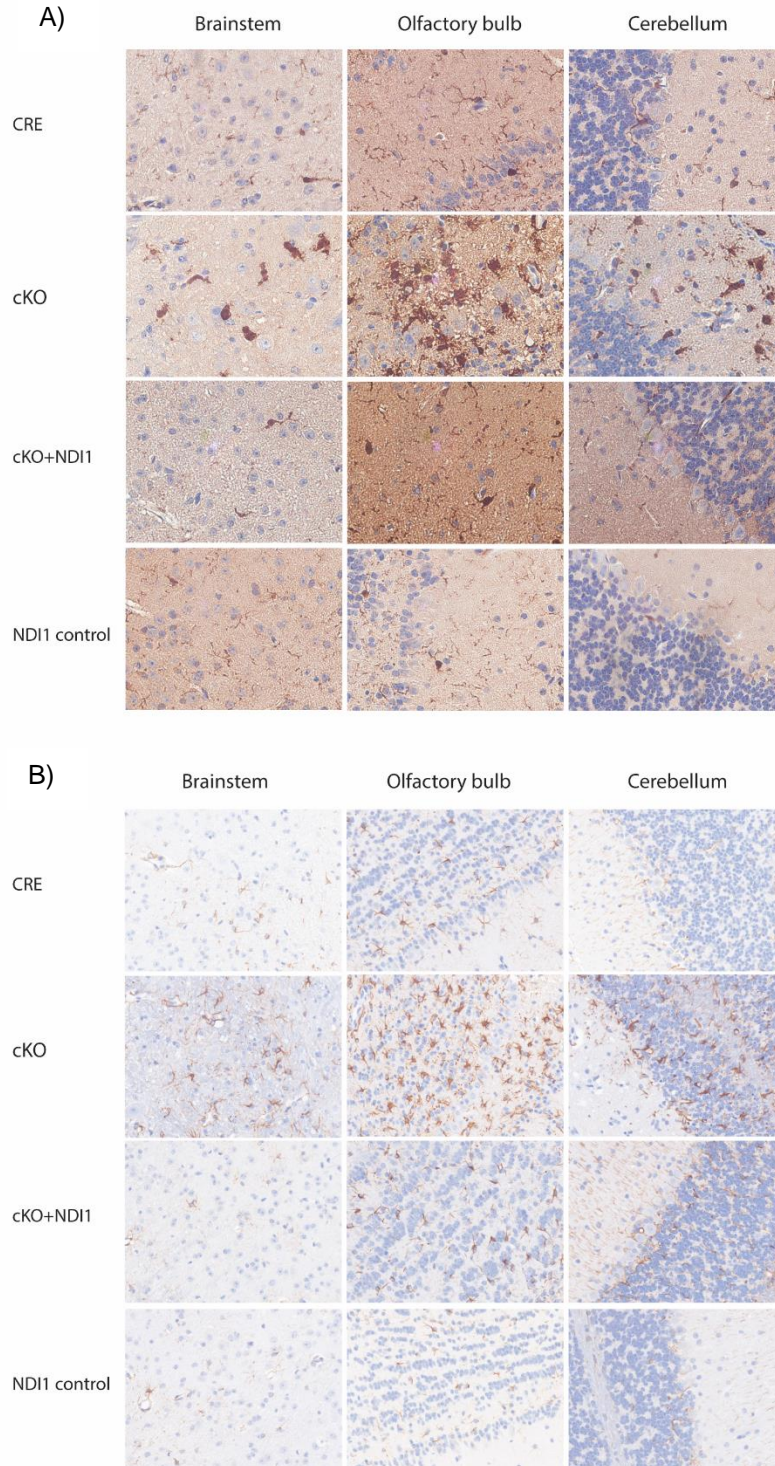


Figure 3.4.2. Representative histology images demonstrate microglial and astrocyte activation in the brain stem, olfactory bulb, and cerebellum. (A) DAB staining of IBA1 for microglial abundance and morphology as an indicator of neuroinflammation. 63x representative images of mouse olfactory bulb,

brainstem, and cerebellum cut in horizontal section. **(B)** DAB staining of GFAP for astrocyte abundance and activation morphology as an indicator of neuroinflammation. 40x representative images of mouse olfactory bulb, brainstem, and cerebellum cut in horizontal section.

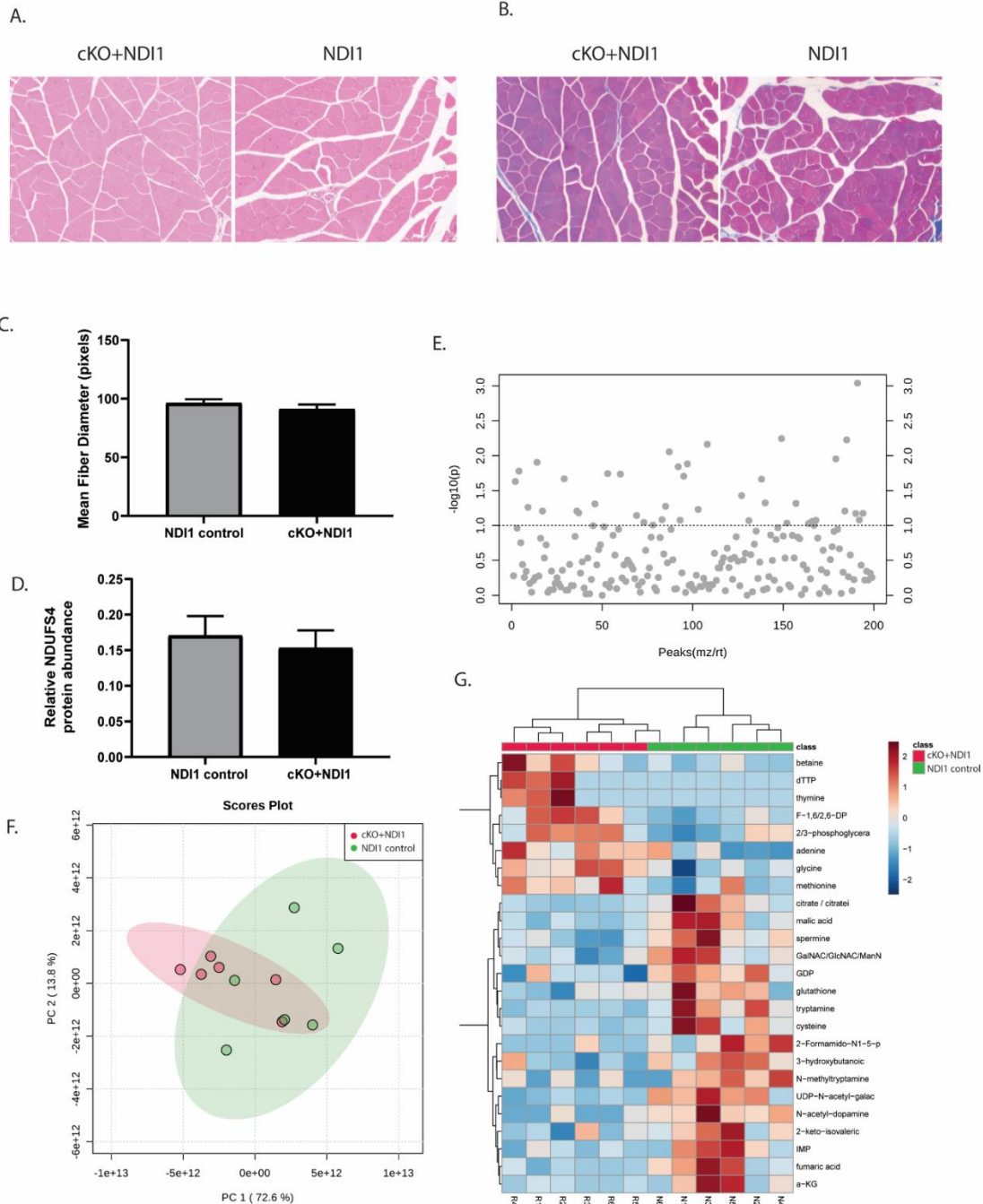


Figure 3.4.3. Characterization of persistently ataxic cKO+NDI1 muscle. **(A)** Representative Hematoxylin and Eosin (H&E) and **(B)** trichrome staining of quadriceps cross section in both NDI1 control and cKO + NDI1 ataxic mice over 1 year of age. No central nuclei or ragged-red-fibers are observed. **(C)** Quantification of relative mean fiber diameter in quadriceps muscle (N=6 per genotype, T-test not significant). **(D)** Quantification of NDUFS4 protein abundance in quadriceps muscle using a Wes automated capillary-based fluorescent immunoassay system. The area of fluorescent peaks detected at

26 kDa (predicted NDUFS4 molecular weight) divided by the area of peaks detected at 52 kDa (predicted Tubulin molecular weight) as a loading control were used to generate bar graphs of relative protein abundance of NDUFS4 at over 1 year of age (N=6 per genotype, T-test not significant). **(E-G)** Soluble metabolite measurements of quadriceps muscles at over 1 year of age. **(E)** Multiple T-tests with multiple hypothesis adjustment to 0.1 resulted in no discoveries of significantly different metabolite levels (N=6 per genotype). **(F)** Principal component analysis scores plot of muscle metabolite profile. **(G)** Heatmap of top 25 candidate metabolites ranked by T-test P-value Z-scores calculated by row.

3.3.5. Expression of yeast NDI1 normalizes metabolite abundance and gene expression in the cerebellum

Since the cerebellum is frequently the source of ataxia in pediatric disease, and we observed cerebellar pathology in our mouse model, we molecularly characterized this region of the brain by performing whole cerebellum tissue metabolomic and transcriptomic analyses (Figure 3.5.1, 3.5.2). Using our soluble metabolite profile, we compared cKO and Cre control mice and identified the top 50 metabolites with altered relative abundance (Figure 3.5.2 A). Additionally, we generated heatmaps, to assess trends in the soluble metabolite profiles (Figure 3.5.2 A). As expected, given the ability of NDI1 to regenerate NAD⁺ and allow flux through the TCA cycle, we observed that cKO + NDI1 cerebella, unlike cKO cerebella, trended towards metabolite level normalization. Of note, the cerebella of cKO mice have increased lactate levels compared to the cerebella of control mice (Figure 3.5.2 B), consistent with previous models of mitochondrial dysfunction in which lactate is increased as a result of compensatory increases in oxidative glycolysis. To further characterize the ability of NDI1 expression to alter central carbon metabolism, we used heavy isotope-labeled glucose tracing in astrocyte-enriched primary hindbrain culture (Figure 3.5.1 A). Comparison of wildtype astrocytes to cKO revealed small but statistically significant decreases in the labeling of glutamate and citrate without significant changes in the labeling of lactate, glycolytic intermediates, or other TCA cycle intermediates (Figure 3.5.1 A). This finding of minimal changes in glucose tracing between wildtype and cKO is consistent with recent *in vivo* metabolic tracing experiments in global NDUFS4 deficient mice [18]. Expression of NDI1, however, with or without deletion of NDUFS4, did cause significant changes in flux to the TCA cycle without significantly altering labeling of the early steps of glycolysis. NDI1-expressing astrocytes showed significantly increased labeling of citrate, aspartate, malate, succinate, and glutamate, while demonstrating decreased labeling of pyruvate and alanine (Figure 3.5.1 A). Therefore, NDI1 expression is sufficient to alter carbon

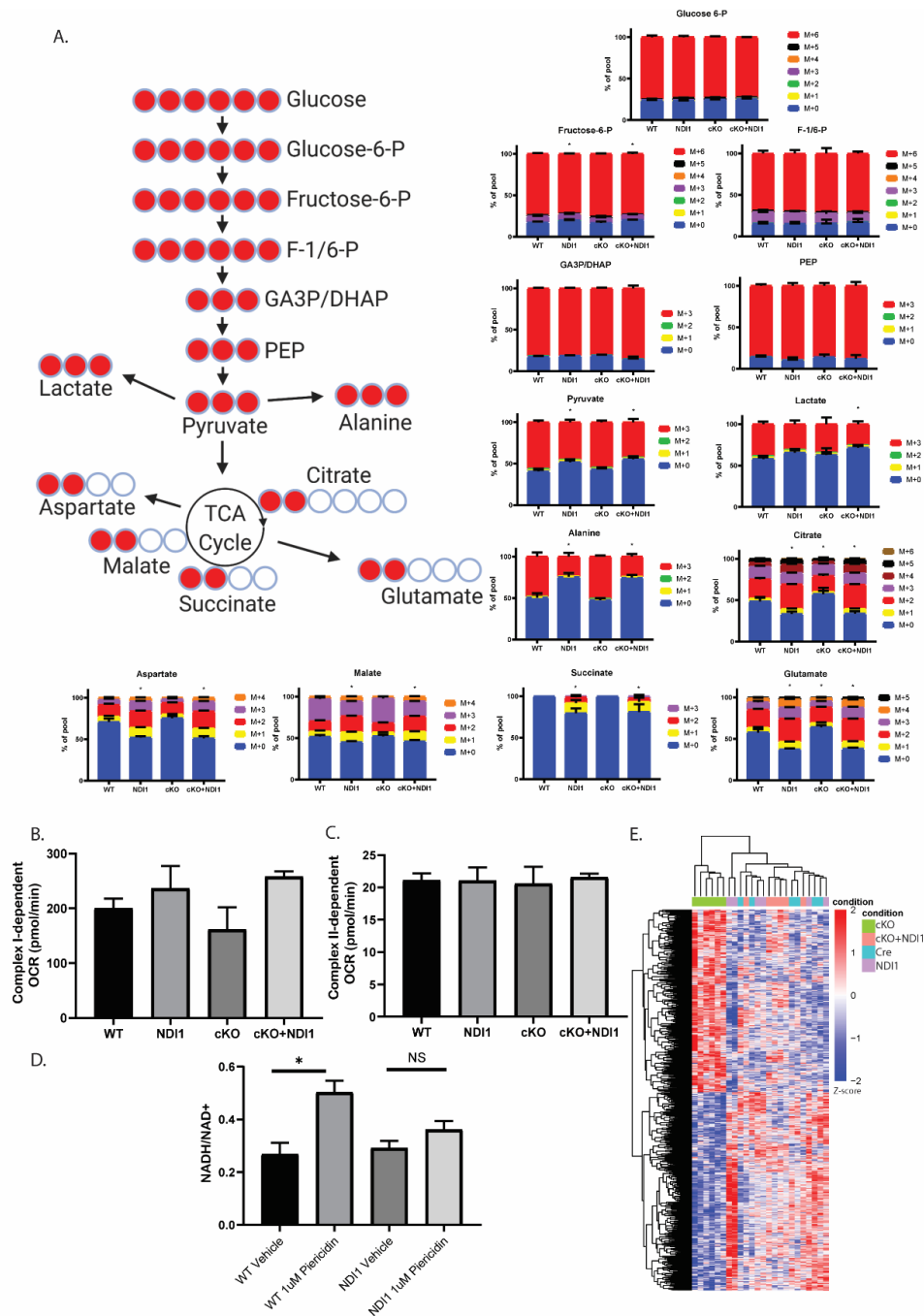
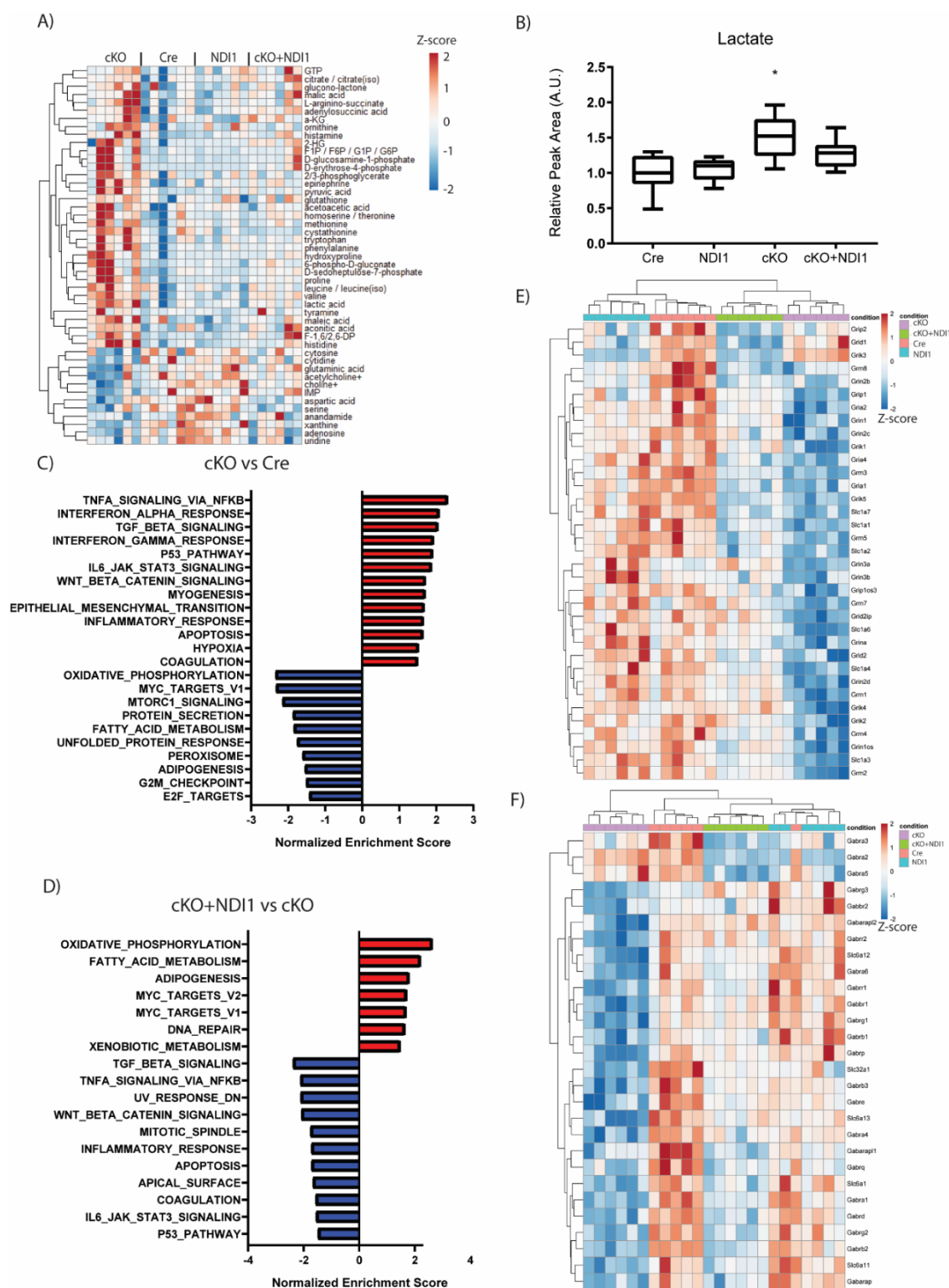


Figure 3.5.1. Metabolic characterization of brain cells and brain metabolites. (A) Uniformly labeled ^{13}C -glucose metabolite tracing in cultured astrocyte-enriched primary cells from early post-natal mice for 6 hours. The percentage of the total pool was calculated for each condition ($N=3-7$ per group, * indicates significant two-way-ANOVA $P<0.05$ with Tukey's multiple comparisons test vs WT adjusted $P<0.05$ for $M+0$ peak, ANOVAs calculated independently for each metabolite). **(B)** Mitochondrial complex I-dependent ADP stimulated respiration in permeabilized astrocyte-enriched primary brain cultures. Cells were permeabilized and provided the complex I substrates pyruvate and malate. ($N=3-7$ per group, ANOVA not significant). **(C)** Mitochondrial complex II-dependent ADP-stimulated respiration in permeabilized astrocyte-enriched primary brain cultures. Cells were permeabilized and provided the

complex II substrate succinate along with ADP and complex I inhibitors. (N=3-7 per group, ANOVA not significant). **(D)** NADH/NAD⁺ ratio in cultured astrocyte-enriched primary cells from early post-natal WT vs NDI1 expressing mice. NDI1 expression prevents a significant increase in the NADH/NAD⁺ ratio following mitochondrial complex I inhibition with Piericidin A. (N=3 per group, * indicates one-way ANOVA P=0.0003 with Tukey's multiple comparisons tests WT Vehicle vs WT 1 μ M Piericidin A adjusted P=0.0003). **(E)** RNA sequencing analysis of whole cerebellum tissue. Significantly differentially expressed genes between Cre, NDI1, cKO, and cKO+NDI1 samples were determined with a likelihood ratio test using a threshold adjusted P value of 0.05 and then clustered.

flux from glucose into the TCA cycle in cultured astrocytes. Next we used mitochondrial complex I- versus complex II-specific substrates with ADP stimulation to drive oxygen consumption in permeabilized astrocyte cultures. The mitochondrial complex I substrates pyruvate and malate demonstrated a comparable pattern of oxygen consumption among the astrocytes of the various genotypes as that shown for cerebellar granule cells, with trends toward increased oxygen consumption in NDI1-expressing cells and decreased oxygen consumption in cKO cells, however, these changes were not statistically significant (Figure 3.5.1 B). The complex II substrate succinate was also given to astrocytes along with complex I inhibition to assess complex II-dependent respiration. As shown in Figure 3.5.1 C, complex II-dependent oxygen consumption was equivalent in the astrocytes of all four genotypes. We also directly evaluated the ability of NDI1 to regulate the NADH/NAD⁺ ratio in astrocyte cultures upon inhibition with the mitochondrial complex I inhibitor piericidin A. The NADH/NAD⁺ ratio was significantly increased following mitochondrial complex I inhibition in wildtype cells while NDI1-expressing cells were resistant to significant NADH/NAD⁺ ratio elevation following mitochondrial complex I inhibition (Figure 3.5.1 D).

Using mRNA extracted from whole mouse cerebellum, we performed RNA-sequencing and differential gene expression analysis. Among the various mouse genotypes, we found numerous significant (adjusted P value <0.05) changes in gene expression using a likelihood ratio test of all samples (Figure 3.5.1 E). Complete-linkage clustering dendrograms of samples (columns) and genes (rows) was carried out and revealed independent clustering of cKO samples, while cKO + NDI1 samples were interspersed among the Cre and NDI1 controls (Figure 3.5.1 E). Pairwise differential gene expression analysis, followed by Gene Set Enrichment Analysis (GSEA), suggested that expression of a number of key pathways that are dysregulated in the cerebella of cKO mice is significantly enriched in the cerebella of cKO + NDI1 mice compared with cKO mice (Figure 3.5.2 C, D). This implies that the function of these pathways is fully or partially restored in cKO + NDI1 mice compared with cKO mice. For example, the



spectrometry (UHPLC MS/MS). The top 50 candidate metabolites ranked by T-test P values comparing Cre to cKO are shown. See also Fig. S4. **(B)** The relative abundance of whole tissue cerebellum lactate normalized to the mean of Cre control. Data is combined from 2 independent UHPLC MS/MS runs (N=6-11 per genotype, ANOVA $P=0.0003$, Dunnett's multiple comparisons test Cre compared to cKO $*P=0.002$). **(C-F)** RNA sequencing analysis of whole cerebellum tissue. Gene set enrichment analysis (GSEA) comparing Cre to cKO **(C)** and cKO to cKO + NDI1 **(D)** of MSigDB Hallmark gene sets using DESeq2-derived pre-ranked gene lists. **(E)** Heatmap of glutamate receptor and transporter gene expression. **(F)** Heatmap of GABA receptor and transporter gene expression. For A and C-F, N=6 per genotype: 3 male and 3 female mice at approximately 7 weeks of age.

gene sets for Oxidative Phosphorylation, MYC Targets, and Fatty Acid Metabolism are significantly downregulated pathways in cKO cerebella compared to Cre control cerebella (Figure 3.5.2 E), yet GSEA analysis revealed that these same pathways are significantly upregulated in cKO + NDI1 cerebella compared to cKO cerebella (Figure 3.5.2 F). We noticed that several of the top dysregulated genes identified by the among-group likelihood ratio test included GABA receptor genes. Given the recent publication of conditional *NDUFS4* deficiency in GABAergic and glutamatergic neurons causing seizure-mediated mortality versus ataxia and breathing-dysfunction-mediated mortality respectively [240], we decided to specifically interrogate the transcriptomic data for GABA and glutamate receptors and channels. Using unsupervised clustering based on these genes, we found that glutamate receptor and transporter genes were significantly downregulated in cKO mice compared with controls, and although cKO + NDI1 mice trended towards control levels, cKO and cKO + NDI1 mice clustered separately from controls (Figure 3.5.2 E). GABA receptor and transporter genes were also downregulated in cKO mice compared with controls; however, for these genes, cKO + NDI1 mice clustered more closely with NDI1 controls than with the cKO mice (Figure 3.5.2 F). Given the recent data on the role of glutamatergic and GABAergic neurons in the fatal and ataxic phenotype of *Vglut2-Cre* and *Gad2-Cre* conditional *NDUFS4*-deficient mice [240], we think this provides intriguing preliminary data about the relative degree of rescue and continued impairment of different neuron types due to NDI1 expression. In the future, it will be of interest to continue genetically dissecting the cell type specificity of the observed fatal and ataxic phenotypes. Since *Gad2-Cre* conditional *NDUFS4* deficient mice exhibit seizure-induced-mortality at a time point consistent with *Nestin-Cre* mortality, a reduction in seizure burden due to NDI1 expression in GABAergic neurons in the midbrain may be a key mechanism by which lifespan is prolonged in our model. We believe our data suggest that it is a population of glutamatergic neurons in the brainstem

and/or cerebellum that remain impaired in our model and cause the persistent ataxia despite a dramatic rescue of lifespan and *ex vivo* oxygen consumption.

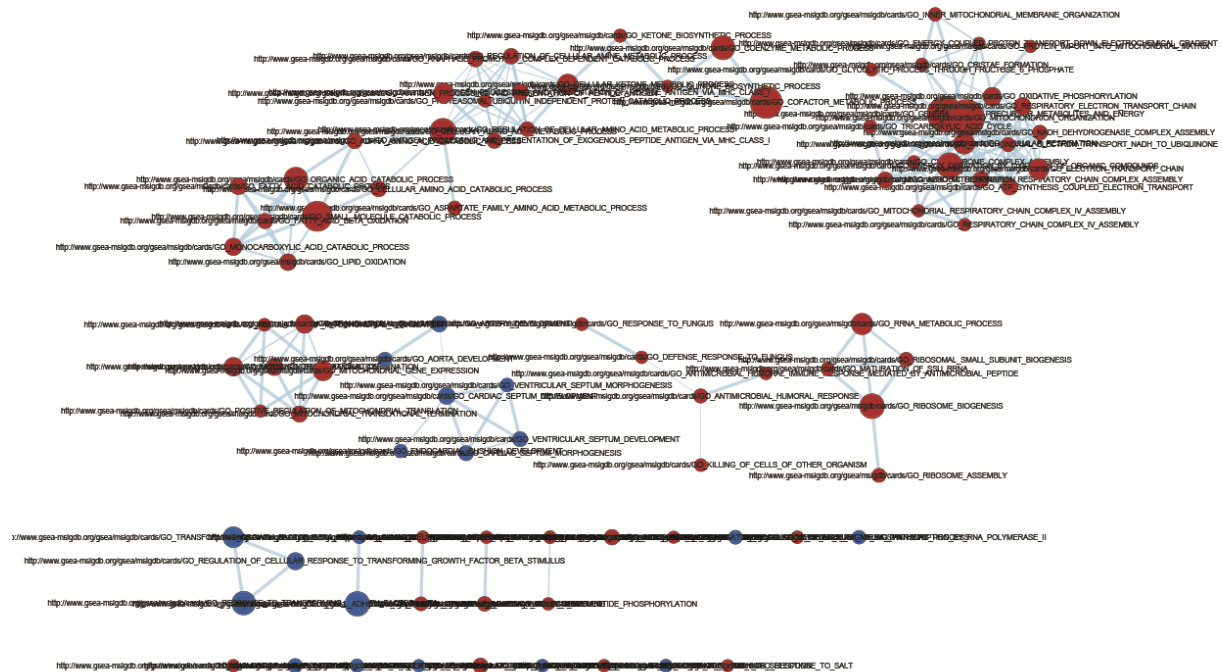


Figure 3.5.3. Gene ontology network analysis for cKO versus cKO+NDI1 cerebella. Gene set enrichment analysis was carried out on a preranked list of differentially expressed genes for all 7350 Gene Ontology Biological Process gene sets from the MSigDB and a network analysis was carried out with the following parameters a P-value cutoff of 0.005 and an FDR Q-value cutoff of 0.05, a similarity cutoff using an overlap coefficient of 0.5. Enriched in cKO+NDI1 are red, while depleted are blue, and the size of the circle indicates the size of the gene set.

To further analyze the RNA sequencing data from *NDUFS4* cKO versus cKO+NDI1 cerebellum, we carried out gene ontology network analysis on all biological process gene sets archived in the Molecular Signatures Database (MSigDB). Prominent networks of enriched gene sets in cKO+NDI1 included mitochondrial TCA and OXPHOS processes, amino acid, ketone, and lipid catabolic processes, translational machinery, and immune function markers; while depleted gene sets were largely gene sets mostly involved in abnormal developmental processes and transforming growth factors (Figure 3.5.3).

3.6) Discussion

Overall, our results indicate that a single yeast enzyme capable of regenerating mitochondrial NAD⁺ from NADH is sufficient to significantly prolong the lifespan, but not maintain the motor function, of mice with impairment of the 45-subunit mammalian mitochondrial complex I in the brain. It is possible that

a very metabolically active subset of neurons is dependent on mitochondrial complex I ATP for proper function. Perhaps restoration of NADH oxidation combined with a compensatory increase in glycolysis is sufficient to prevent reactive glial inflammation, but fails to completely restore neuronal function, as the latter may require ATP from mitochondrial complex I. Further genetic dissection of the cell-type specificity of our observed lifespan extension with NDI1 will be of interest in future studies, particularly with the use of Vglut2-Cre and Gad2-Cre to more directly determine the relative impact of these two key neuron populations in the prevention of seizures versus breathing abnormalities and ataxia.

One limitation of this study is our inability to definitively demonstrate the *in situ* mitochondrial NADH/NAD⁺ ratio or ATP production rates that are likely central to the mechanism of rescue in this model. We think that technical limitations, including the rapid changes that occur post-mortem, the relative instability of these metabolites, and the inability to rapidly isolate mitochondria in this model have contributed to our inability to detect them in tissue. Recent work in the literature has also demonstrated that the changes in whole tissue NADH/NAD⁺ ratio are quite subtle in global NDUF54 deficient mice; reportedly less than a twofold change [18]. A second limitation is that we have not definitively identified the mechanism by which cKO + NDI1 mice remain ataxic. We do not observe significant neuroinflammation or neurodegeneration in our mouse model, and do not see any evidence of muscle or spinal cord pathology.

CHAPTER 4: Mitochondrial L-2-hydroxyglutarate accumulation is a determinant of mitochondrial dysfunction induced neuronal dysfunction

4.1) Introduction

Some of the text and figures are derived from work and experiments done by collaborators and is from manuscripts which I co-authored and that are published and in preparation [289]. As described in Chapter 1, 2-hydroxyglutarate (2HG) is a neurotoxic oncometabolite that can accumulate to high levels as a potential result of mitochondrial electron transport chain dysfunction to dissipate high levels of NADH and as a result of reduced conversion back to α KG when mitochondrial complex III is inhibited or when the dehydrogenase enzyme L2HGDH is mutated or deficient.

4.2) Mechanisms of 2-hydroxyglutarate accumulation

It has previously been reported that 2-hydroxyglutarate accumulates in the setting of mitochondrial complex III mutation as a result of α KG reduction and promiscuous enzyme activity of LDH and MDH (See Chapter 1). In order to genetically and pharmacologically confirm the proposed mechanisms of mitochondrial 2-HG accumulation, we used the 143B human osteosarcoma cell line. Treatment with the mitochondrial complex III inhibitor antimycin A (500nM) consistently results in elevated 2HG levels that are detectable by mass spectrometry (Figure 4.2.1 A-B). Treatment with the mitochondrial complex I inhibitor piericidin A leads to less consistent accumulation of 2HG (Figure 4.2.1. A-B). This is presumably because inhibition of mitochondrial complex I only causes one of the two necessary factors for 2HG accumulation: that is increasing NADH to promote 2HG production, but unlike antimycin, piericidin does not decrease the oxidation of 2HG back to α KG. Surprisingly, however, L2HGDH overexpression was sufficient to decrease the accumulation of 2HG in antimycin treated cells (Figure 4.2.1. B). This was not anticipated since it is assumed that L2HGDH requires mitochondrial complex III function since it should donate the electrons from the conversion of 2HG to α KG to ETF and the Q pool, which would then require mitochondrial complex III function for ubiquinol oxidation. This finding requires further investigation to determine how L2HGDH can continue to function in the absence of mitochondrial complex III function. Genetic mitochondrial complex III deficiency using a cytochrome B null 143B cell line also demonstrates 2HG accumulation (Figure 4.2.1. C). The mitochondrial enzyme MDH2 is the only

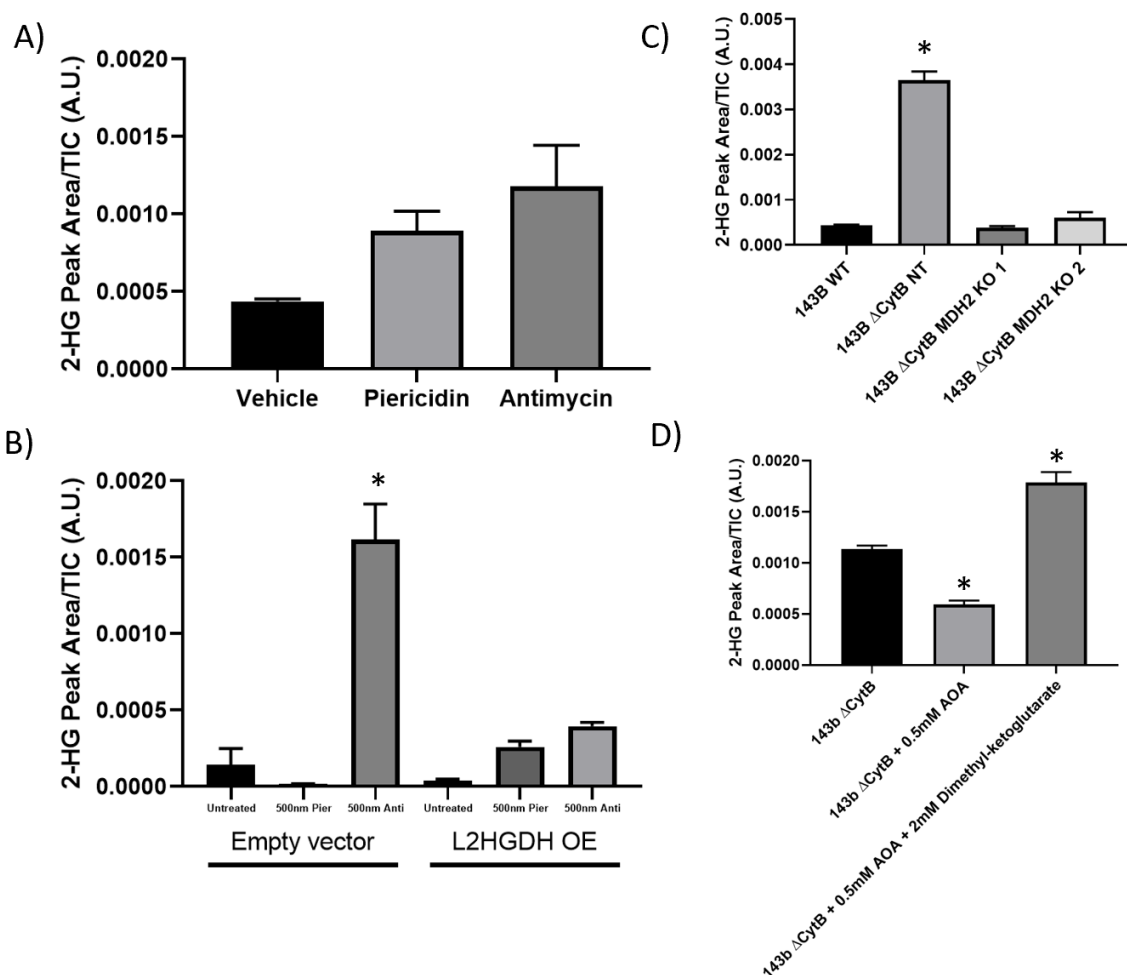


Figure 4.2.1. Determinants of mitochondrial 2-hydroxyglutarate production in cancer cells. (A) WT human 143B osteosarcoma cell 2-hydroxyglutarate measurement. One-way ANOVA $P = 0.0558$, $N=3$. **(B)** 2-hydroxyglutarate measurements in WT and cytochrome B (CytB - mitochondrial complex III) deficient and malate dehydrogenase 2 deficient 143B cell lines. $N=3$ per group, One-way ANOVA $P<0.0001$ Dunnett's multiple comparisons test Untreated vs antimycin $p<0.0001$ **(C)** 2-hydroxyglutarate measurements in empty vector and L-2-hydroxyglutarate dehydrogenase (L2HGDH) overexpressing 143B cells. One-way ANOVA $P<0.0001$, $N = 3$ per group, Dunnett's multiple comparisons test WT vs CytB null $P<0.0001$ **(D)** 2-hydroxyglutarate measurement in CytB null 143B cells when treated with aminotransferase inhibitor aminooxyacetate (AOA) and supplemented with cell permeable dimethyl ketoglutarate. One-way ANOVA $P<0.0001$, Dunnett's multiple comparisons test CytB null vs AOA $P=0.0022$, CytB null vs AOA and DMK $P=0.0008$, $N=3$ per group.

putative L-2HG producing enzyme in the mitochondrial matrix since LDH and MDH1 reside in the cytosol.

Therefore, using CRISPR/cas9, *MDH2* was deleted in 143B ΔCytB cells, which resulted in decreased

accumulation of 2HG (Figure 4.2.1. C). Finally, 143B ΔCytB cells were treated with vehicle, the

aminotransferase inhibitor aminooxyacetate (AOA) to prevent glutaminolysis as a source of α KG, or a combination of AOA and the cell permeable α KG source dimethyl-ketoglutarate (Figure 4.2.1). These results identified that 2HG, in the setting of mitochondrial complex III inhibition or mutation, is produced predominantly in the mitochondrial matrix as a result of MDH2 promiscuous enzyme activity that is driven by high levels of NADH and α KG which is supported by glutaminolysis.

As part of a more comprehensive study of the role of mitochondrial Q-pool regulation in cancer cell growth, we measured soluble metabolites in several genetically manipulated 143B cell lines. In addition to 2HG, several soluble metabolites are significantly altered by loss of mitochondrial complex III (Figure 4.2.2. A). Restoration of ubiquinol oxidation in 143B Δ CytB cells by ectopic expression of AOX normalizes multiple metabolite levels, including 2HG, towards WT 143B cells as compared with Δ CytB cells and empty vector controls (Figure 4.2.2. B). Expression of IbNOX in the cytosol had larger effects overall on the soluble metabolome than expression of IbNOX in the mitochondria, but mitochondrial IbNOX decreased 2HG levels relative to cytosolic IbNOX (Figure 4.2.2. C-D). Abundance of NADH is elevated in Δ CytB cells lacking NDUFS2 and decreased by expression of NDI1 or IbNOX in the mitochondria or the cytosol (Figure 4.2.2. D). These results point towards the role of NADH accumulation in the mitochondrial matrix in the accumulation of 2HG.

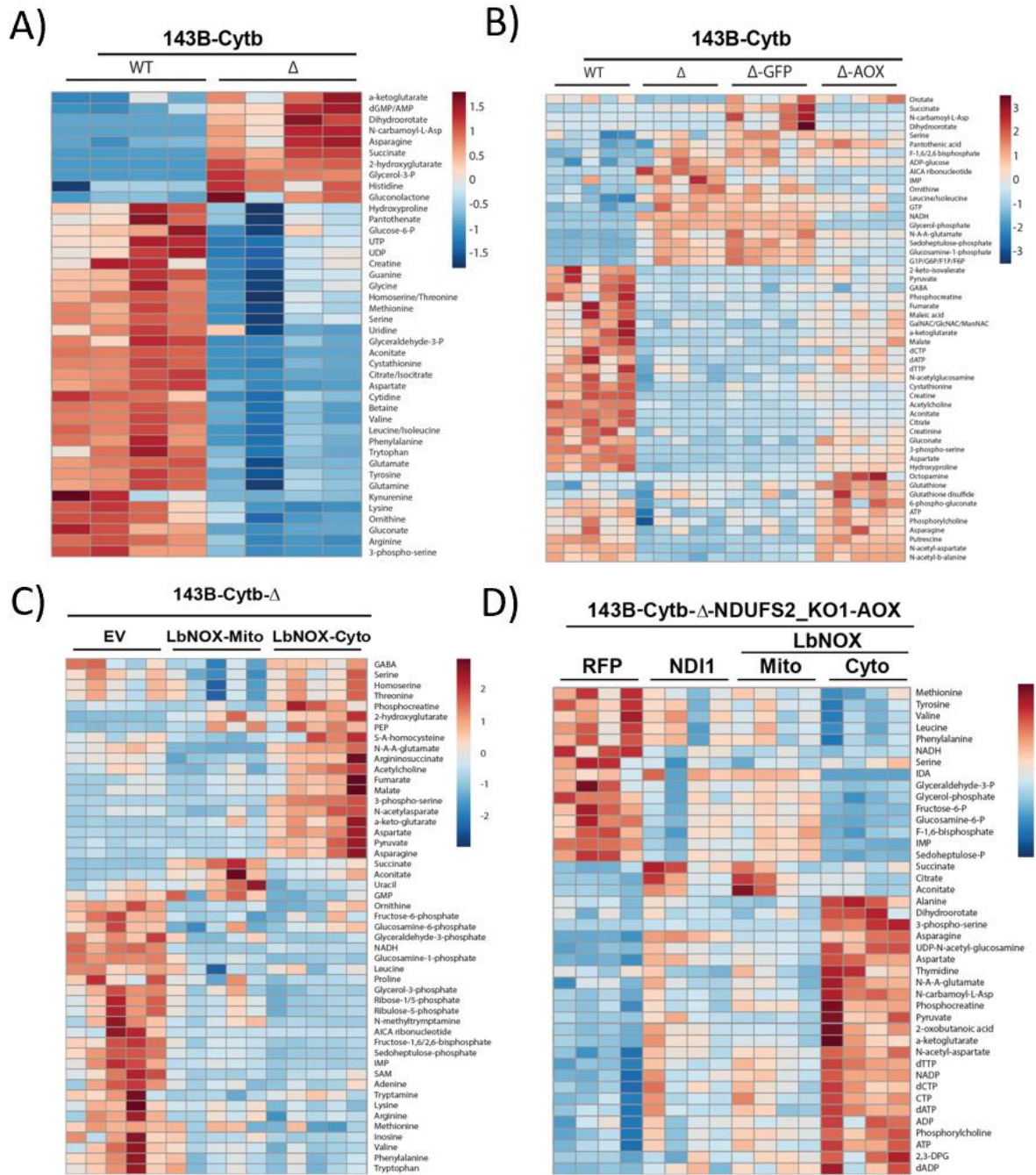


Figure 4.2.2. Mitochondrial electron transport chain determinants of the metabolome. (A) WT and cytochrome B (Cytb - mitochondrial complex III) deficient 143B human osteosarcoma cell lines significantly altered soluble metabolites with a threshold adjusted P value of 0.05. Z-score scaled by metabolite with red representing higher abundance and blue representing lower abundance. (B) WT, cytochrome B (mitochondrial complex III) deficient, empty vector, and alternate oxidase (AOX)-expressing human osteosarcoma cell lines significantly altered soluble metabolites with a threshold adjusted P value of 0.05. Z-score scaled by metabolite with red representing higher abundance and blue representing lower abundance. (C) Cytochrome B (mitochondrial complex III) deficient, and LbNOX expressing human

osteosarcoma cell lines significantly altered soluble metabolites with a threshold adjusted P value of 0.05. Z-score scaled by metabolite with red representing higher abundance and blue representing lower abundance. **(D)** NDUFS2 (mitochondrial complex I) deficient cytochrome B (mitochondrial complex III) deficient human osteosarcoma cell lines expressing empty vector, yeast ND11, and IbNOX significantly altered soluble metabolites with a threshold adjusted P value of 0.05. Z-score scaled by metabolite with red representing higher abundance and blue representing lower abundance.

4.3) Mitochondrial stress signaling increases 2-HG in *Drosophila melanogaster*

Our collaborators at King's College London have a model of mitochondrial stress induced neuronal dysfunction in *Drosophila melanogaster* by overexpression of TFAM. Due to our interest in a potential role of 2HG as a toxic metabolite effector of mitochondrial dysfunction, we measured soluble metabolites in *D. melanogaster* heads sent to us by our collaborators (Figure 4.3.1. A-G). Several metabolites demonstrated differential abundance, including 2HG which was elevated in the TFAM overexpressing flies and knockdown of ATF4 decreased 2HG accumulation (Figure 4.3.1. G). We confirmed that it was the L enantiomer of 2HG in these flies by chiral derivatization (Figure 4.3.2. A-I).

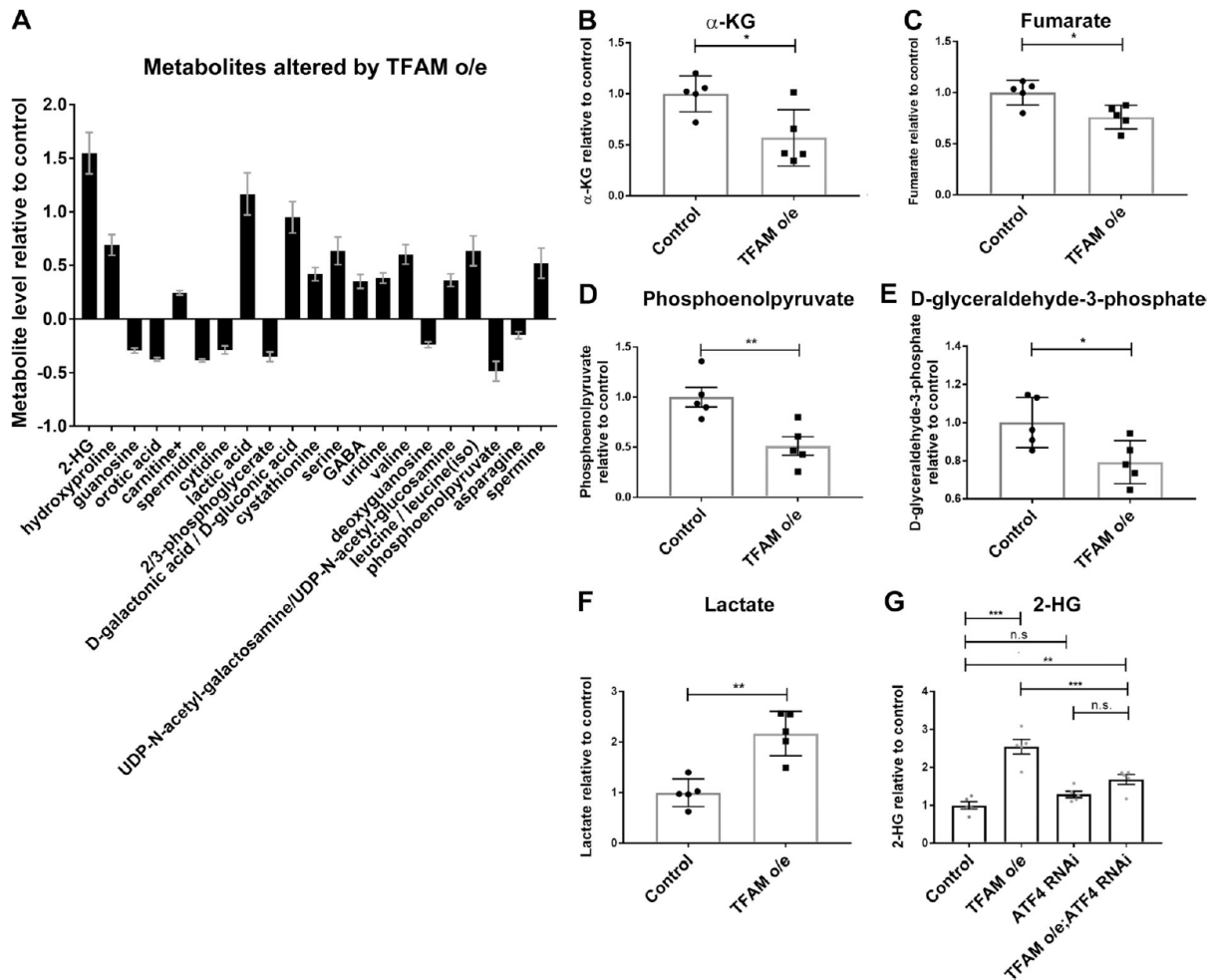


Figure 4.3.1. Mitochondrial stress signaling increases 2-HG levels via ATF4. (A) Metabolites whose levels are significantly changed (5% false discovery rate) in adult heads from flies with pan-neuronal TFAM overexpression (o/e) using nSyb-Gal4. (B–F) Levels of individual TCA cycle and glycolytic metabolites in adult heads from flies with pan-neuronal TFAM overexpression using nSyb-Gal4. (G) Knockdown of ATF4 reduces the increase in 2-HG levels caused by pan-neuronal TFAM overexpression using nSyb-Gal4. Controls are nSyb-Gal4 hemizygotes. Data are represented as mean \pm SEM. $n = 5$ for all genotypes. ns, not significant; *, $P \leq 0.05$; **, $P \leq 0.01$; ***, $P \leq 0.001$.

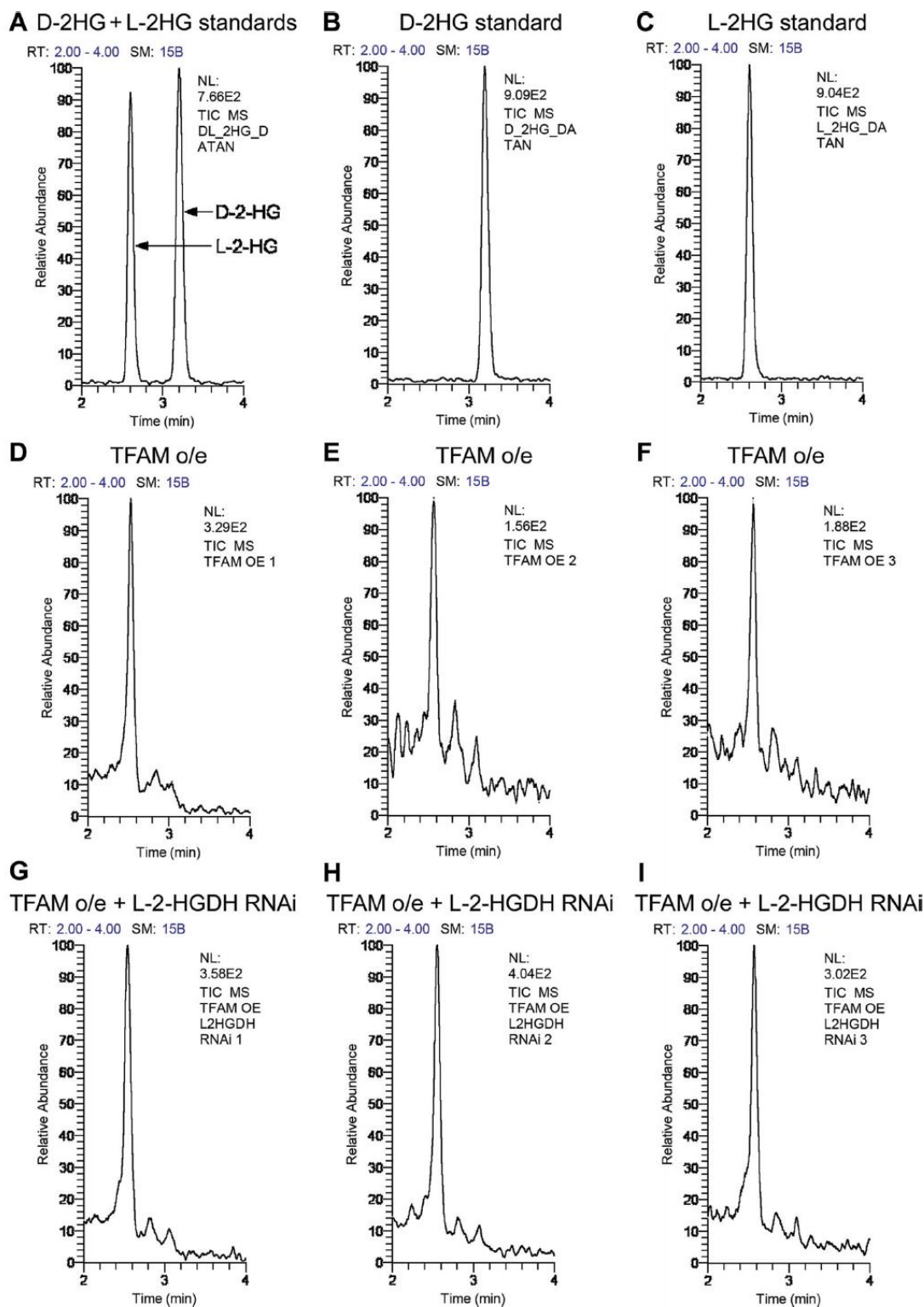


Figure 4.3.2. 2-HG measured in heads from flies with pan-neuronal TFAM overexpression is predominantly the L enantiomer. HPLC-MS/MS was used to determine the enantiomers of 2-HG present. (A) Derivatization of a racemic mixture of standards of D and L enantiomers of 2-HG with DATAN

allows separation of 2-HG enantiomer derivatives by HPLC retention time. (B) Derivatization of D-2-HG standard with DATAN. (C) Derivatization of L-2-HG standard with DATAN. (D–F) DATAN derivatization of 2-HG extracted from heads from flies overexpressing TFAM with nSyb-Gal4 ($n = 3$) shows that the majority of 2-HG present is the L-2-HG enantiomer, based on the retention time (compare D–F to C). (G–I) DATAN derivatization of 2-HG extracted from flies overexpressing TFAM and L-2-HGDH RNAi with nSyb-Gal4 ($n = 3$) shows that the majority of 2-HG present is the L-2-HG enantiomer, based on the retention time (compare G–I to C). In D–I, HPLC-MS/MS was performed using independent biological replicates, shown in each panel.

4.4) Mitochondrial stress-induced L-2-HG regulates neuronal function

Together with our collaborators, we confirmed that knockdown of L2HGDH in flies increased 2HG accumulation in the TFAM overexpressing fly model (Figure 4.4.1. A) and that overexpression of L2HGDH in flies decreased 2HG accumulation in the TFAM overexpressing fly model (Figure 4.4.1. D). Our collaborators then found that the neural and neuromuscular-developmental phenotypes of decreased climbing ability and decreased wing inflation in TFAM overexpressing flies were dependent of 2HG levels, as knockdown of L2HGDH worsened the phenotypes and overexpression of L2HGDH ameliorated the phenotypes (Figure 4.4.1. B-C, E-F). This data clearly suggests a causative link between mitochondrial-dysfunction-induced 2HG accumulation and phenotypes of neural dysfunction in flies. Our collaborators went on to link this finding with ATF4 induced LDH upregulation as a mechanism of 2HG accumulation in this particular model [289].

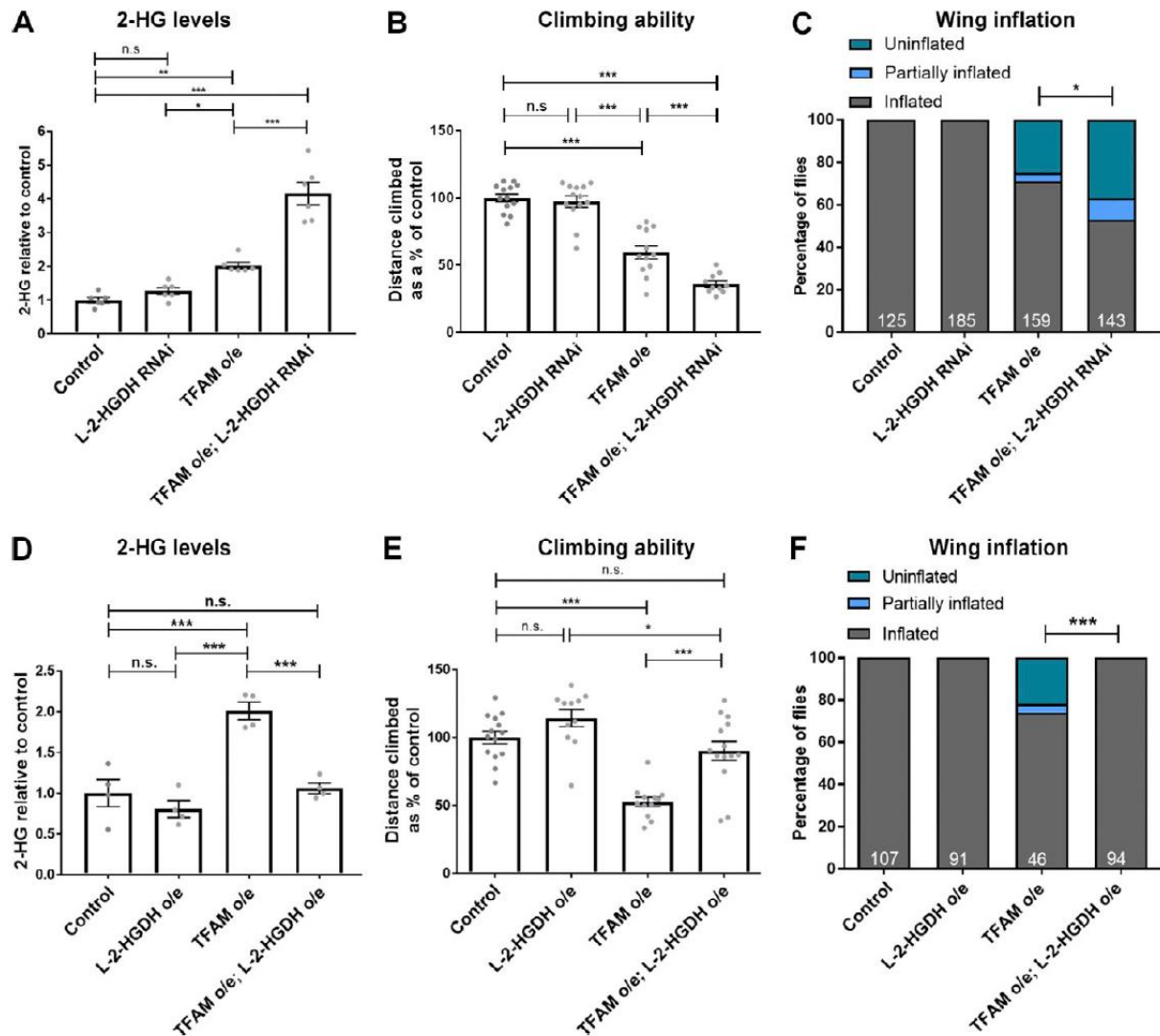


Figure 4.4.1. Mitochondrial stress-induced L-2-HG regulates neuronal function. (A) The increase in 2-HG levels caused by pan-neuronal TFAM overexpression (o/e) is exacerbated by L-2-HGDH knockdown. $n = 6$ for all genotypes. (B) L-2-HGDH knockdown enhances the climbing defect caused by pan-neuronal TFAM overexpression. Control $n = 13$, L-2-HGDH RNAi $n = 13$, TFAM overexpression $n = 12$, TFAM overexpression + L-2-HGDH RNAi $n = 10$. (C) L-2-HGDH knockdown enhances the wing inflation defect caused by pan-neuronal TFAM overexpression. Numbers of flies are shown in white. (D) L-2-HGDH overexpression prevents the increase in 2-HG levels caused by TFAM overexpression. $n = 4$ for all genotypes. (E) L-2-HGDH overexpression alleviates the climbing defect caused by pan-neuronal TFAM overexpression. Control $n = 14$, L-2-HGDH overexpression $n = 11$, TFAM overexpression $n = 12$, TFAM overexpression + L-2-HGDH overexpression $n = 14$. (F) L-2-HGDH overexpression alleviates the wing inflation defect caused by pan-neuronal TFAM overexpression. Numbers of flies are shown in white. nSyb-Gal4 was used for pan-neuronal expression. Controls are nSyb-Gal4 hemizygotes. Data are represented as mean \pm SEM. n.s., not significant; *, $P \leq 0.05$; **, $P \leq 0.01$; ***, $P \leq 0.001$.

4.5) 2-hydroxyglutarate and aging

In the NDUFS4 cKO and NDI1 expressing mouse models described in Chapter 3, we also found a significant elevation of 2HG in the cerebellum in the ataxic cKO mice compared to Cre controls (Figure 4.5.1. A). Surprisingly, we did not see that this level of 2HG was significantly ameliorated in the cKO+NDI1 mice. Instead, there was not a statistically significant trend towards elevated 2HG levels in the cKO+NDI1 mice compared to Cre controls (Figure 4.5.1. A). Furthermore, in the NDUFS2 cKO + NDI1 mice, preliminary data from the cerebellum of 2 mice compared to 2 littermate controls at approximately 3 weeks of age demonstrated a trend towards increased 2HG in the ataxic NDUFS2 cKO+NDI1 mice (Figure 4.5.1. B). Finally, we know that genetic deletion of ETC component genes can result in 2HG accumulation, but whether the comparatively milder mitochondrial dysfunction induced by aging can also result in significant 2HG accumulation is currently unknown. We measured metabolites in regulatory T cells isolated from 6 month versus 18-month C57Bl6j mice and found a trend towards increased 2HG levels which correlates with previous studies that have identified increased methylation with aging (Figure 4.5.1. C). However, a replication study failed to detect 2HG in Tregs from either young or aged mice, so this preliminary data requires further validation.

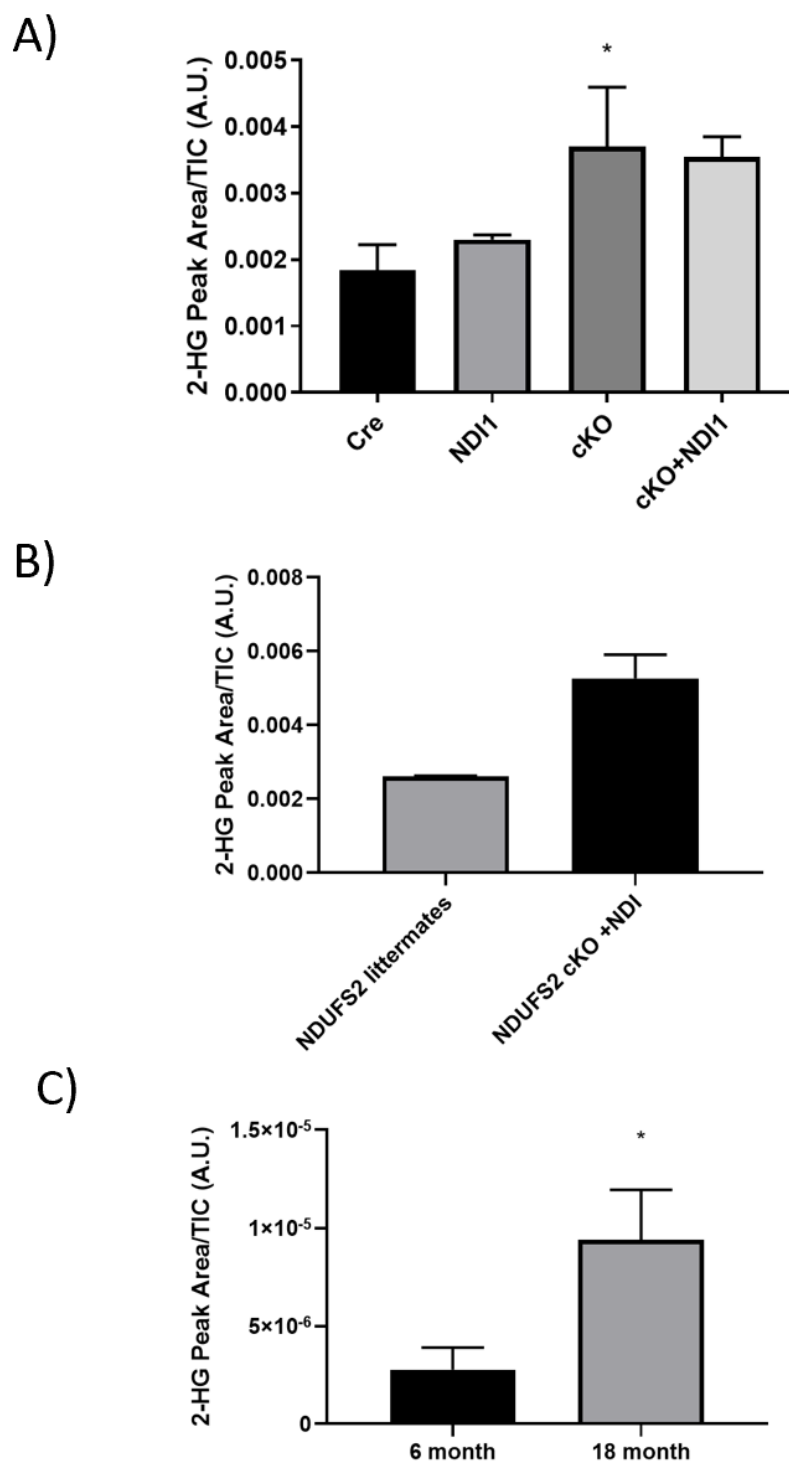


Figure 4.5.1. 2-Hydroxyglutarate measurements in mouse tissues correlate with pathology. (A) 2-hydroxyglutarate measurement in cerebellum tissue of mice at approximately 7 weeks of age. NDUF54 and Nestin cre mice as described in chapter 3. One-way ANOVA $P=0.0429$, Dunnett's Multiple

Comparisons test Cre vs cKO *Adjusted P value = 0.0454, N = 6 per genotype. **(B)** 2-hydroxyglutarate measurement in cerebellum tissue of mice at approximately 3 weeks of age. NDUF52 and Nestin cre mice as described in chapter 3. T-test P = 0.0533, N = 2 per genotype. **(C)** 2-hydroxyglutarate measurement in regulatory T cells isolated from 6 and 18-month-old wildtype C57Bl6J mice obtained from the National Institute on Aging. T-test *P = 0.0448, N = 5.

4.6) Discussion

We confirmed most of the described mechanisms of 2HG production in cancer cells in the setting of mitochondrial dysfunction using 143B cells. Increased NADH and α KG concentrations favor formation of 2HG in the mitochondrial matrix through the promiscuous action of MDH2. Surprisingly we found that L2HGDH overexpression is capable of decreasing 2HG abundance even in the setting of mitochondrial complex III inhibition, by a mechanism that requires further validation since ubiquinol oxidation at complex III was assumed to be necessary for L2HGDH enzymatic function. It is possible that superoxide generation by electron leak is one potential mechanism that could allow L2HGDH to continue to function, this could occur directly from L2HGDH's flavin group, or could occur at ETF or from other inputs into the Q pool by reverse electron transfer. Alternatively, a previously undescribed transfer of electrons across the inner mitochondrial membrane, either directly or through other electron carriers, to cytochrome C may be occurring to lead to a low level of oxygen consumption at complex IV.

Our published work in flies indicates that, at least in this model, 2HG is an effector of mitochondrial dysfunction that causes neurological and developmental defects. We also found that 2HG correlates with pathology in mice in several settings. In our NDUF54 Nestin-cre mice, we found 2HG to be elevated in brain tissue. By expressing NDI1, we reasoned that increased NADH turnover would decrease the accumulation of 2HG just as it had for lactate and several other metabolites as discussed in Chapter 3. However, at the time point of approximately 7 weeks, the persistently ataxic, but prolonged surviving, cKO+NDI1 mice demonstrated a trend towards increased 2HG levels compared to Cre control that was not statistically significant. Therefore, one possible interpretation of this data is that 2HG levels correlate with behavioral dysfunction and ataxia rather than correlating with survival. This may be consistent with our published data in flies in which 2HG accumulation is necessary for the observed neurological deficits, and in our more severe mouse model of neurological dysfunction, the NDUF52 cKO + NDI1 mice which are severely ataxic and only survive for 3-4 weeks. These data may also suggest that

NDI1 expression described in Chapter 3 is not sufficient to completely restore mitochondrial NADH turnover, or it may suggest that, like in the flies, there is increased cytosolic production of 2HG by LDH or MDH1 perhaps due to a compensatory change in glycolytic machinery or flux in these models.

CHAPTER 5: Mild genetic reduction in mitochondrial complex I function does not significantly alter healthspan in amice despite significant gene expression changes

5.1) Introduction

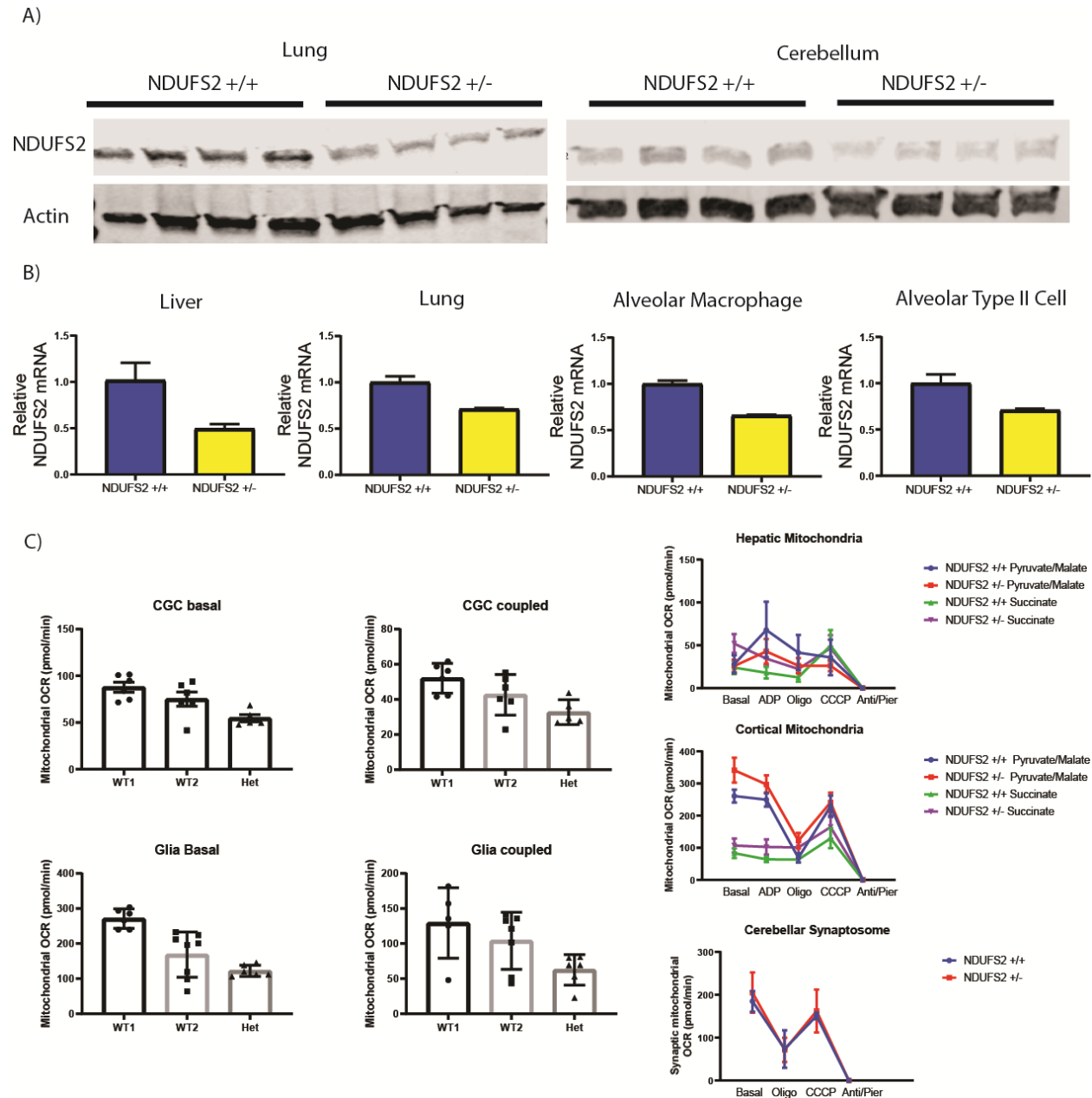
One of the most consistent changes that occurs in aging animals is a decline in mitochondrial function. Mutations in genes encoding mitochondrial proteins that lead to severe decreases in mitochondrial function cause dramatic multi-system pathology and a shortened lifespan in model organisms and in human patients with mitochondrial diseases. Paradoxically, however, several studies have indicated that knockdown of components of the electron transport chain, and in particular mitochondrial complex I, in model organisms such as *C. elegans* and *D. melanogaster*, can have a significant life extending effect. Furthermore, the widely used antidiabetic drug metformin has been identified as a possible anti-aging medication that may mediate its preventative effects on several aging-related pathologies through mild inhibition of mitochondrial complex I. To explore the role of mild genetic impairment of mitochondrial complex I on lifespan and healthspan in mammals, we aged cohorts of mice heterozygous for a null allele of the essential mitochondrial complex I gene *Ndufs2* intermixed and co-housed with their WT littermates and longitudinally measured several behavioral markers of healthspan and analyzed gene expression and metabolite levels in several tissues and cell types of interest.

5.2) Loss of one allele of NDUFS2 does not significantly extend survival in mice

NDUFS2 is a nuclear-encoded enzymatic subunit of mitochondrial complex I that is the core subunit that makes up the ubiquinone binding site and is therefore required for mitochondrial complex I function. Ubiquitous deletion of *Ndufs2* is embryonic lethal in mice, and mutations in *NDUFS2* have been identified to cause mutations in humans with mitochondrial diseases such as Leigh Syndrome [304]. We obtained *Ndufs2* floxed mice from Dr. Lopez-Barneo at the University of Seville [290] and crossed them to Sox2-Cre ubiquitous expressing Cre mice to generate a global null allele of *Ndufs2*. These mice were backcrossed to C57Bl6j WT mice for several generations and all cohorts were derived from the same backcross number with >95% C57Bl6j genetic identity based on SNP analysis by the Jackson laboratory. We first wanted to validate the NDUFS2 +/- mouse model by measuring mRNA and protein in several

tissues. This revealed an expected mild decrease of NDUFS2 message and protein (Figure 5.2.1. A-B).

Oxygen consumption, however, was not significantly impacted by NDUFS2 genotype (Figure 5.2.1 C).



liver and brain cortex oxygen consumption supplemented with either mitochondrial complex I substrates (pyruvate and malate) or mitochondrial complex II substrate (succinate). Cerebellar synaptosome oxygen consumption. Oxygen Consumption Rate (OCR) are all normalized to Antimycin and Piericidin inhibited respiration by subtraction. Isolated mitochondria and synaptosomes N=3 per group.

We measured oxygen consumption in primary neuron and astrocyte cultures, which showed a trend towards a lower basal oxygen consumption and ATP coupled oxygen consumption in one *NDUFS2* +/- mice compared to two *NDUFS2* +/+ mice, but isolated mitochondria from liver and brain tissue and isolated synaptosomes did not demonstrate significant decreases in basal, coupled, or uncoupled OCR in *NDUFS2* +/- mice (Figure 5.2.1. C). These results require further validation, but the preliminary findings suggest that the impairment of mitochondrial complex I is very mild and is perhaps cell and tissue type specific.

We observed a trend towards a slightly higher body weight on average in both male and female *NDUFS2* +/- mice compared to *NDUFS2* +/+ mice that arose at approximately 6 months of age and continued for several months but then the average body weights converged rather than continuing to diverge after 18 months of age (Figure 5.2.2. C). While our study was not powered to detect a small difference in lifespan, we did not observe any significant changes in early mortality between *NDUFS2* +/+ mice and *NDUFS2* +/- mice (Figure 5.2.2. B-C). This was, however, sufficient to exclude the possibility of dramatic increases in lifespan in the *NDUFS2* +/- mice. Glucose tolerance testing was carried out in mice younger than 6 months, and older than 20 months to determine whether *NDUFS2* genotype had an effect on whole body glucose disposal. While no significant changes were observed in the younger time points, aged females had a trend towards a slight decrease in peak glucose concentrations in *NDUFS2* +/- mice which could point towards more rapid glucose disposal, however this was not observed in male *NDUFS2* +/- mice (Figure 5.2.2. D).

Next, we measured a white blood cell differential for aged (27 month old) *NDUFS2* +/+ vs *NDUFS2* +/- mice to determine whether *NDUFS2* genotype had any effect on the steady state levels of leukocyte populations, or changed the skewing of leukocytes towards myeloid lineages with aging, but we observed no significant changes in the percentage of monocyte or neutrophil populations (Figure 5.2.3 A-B)

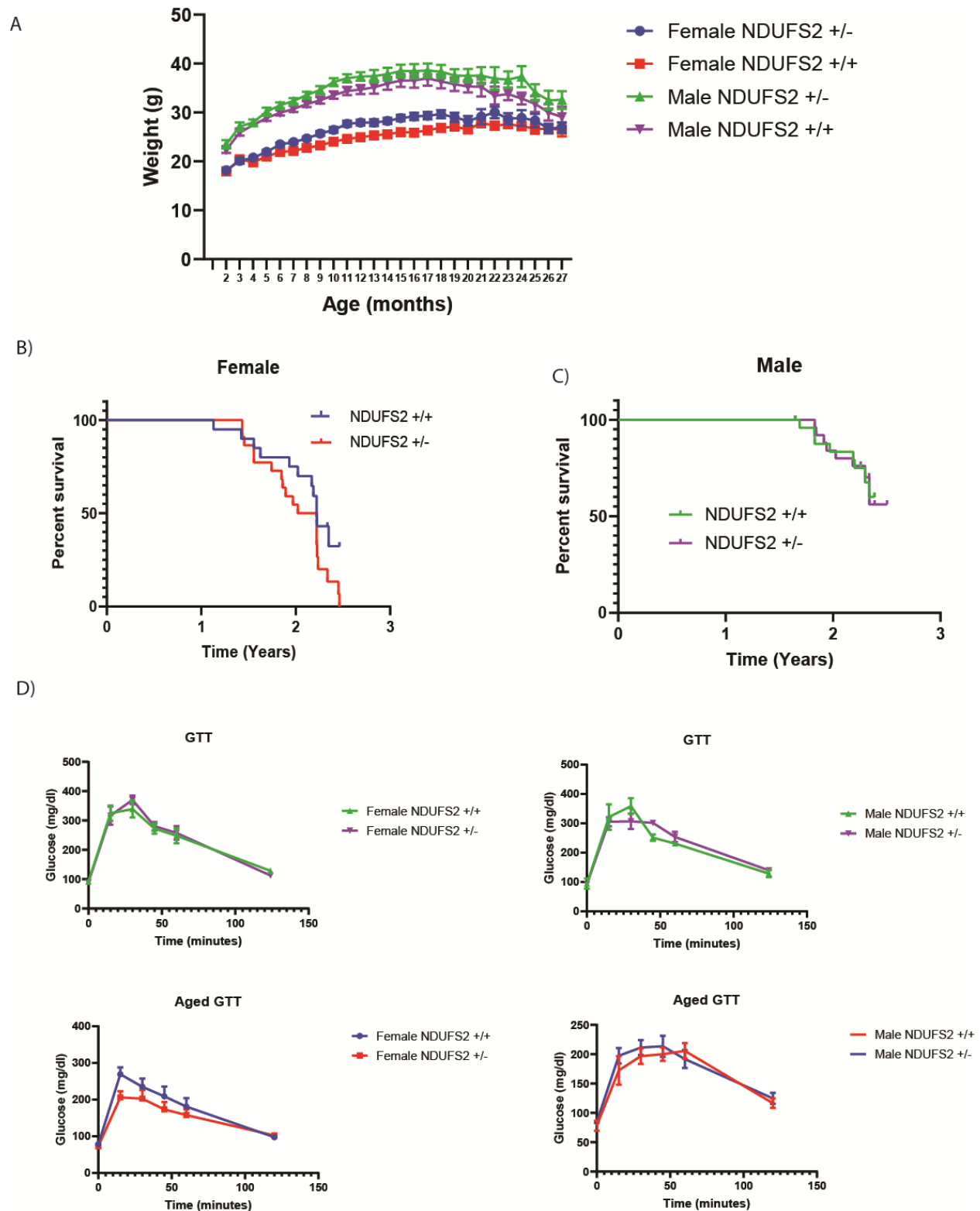
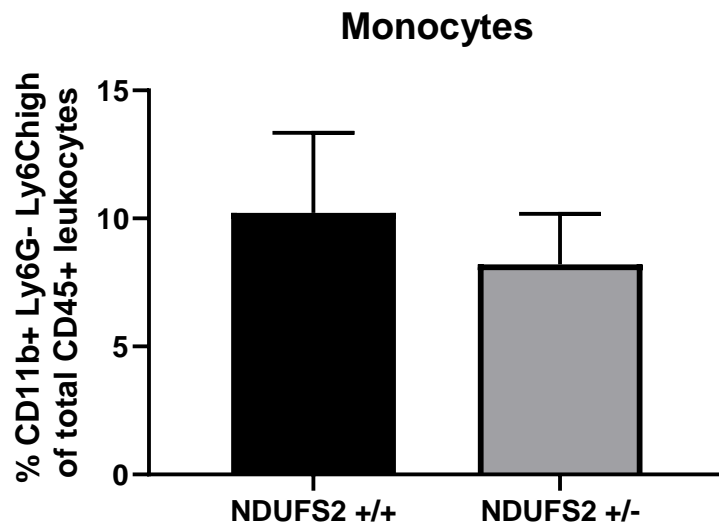


Figure 5.2.2. NDUFS2 does not significantly impact body weight, survival, or glucose tolerance.

(A) Average body weight by month for NDUFS2 +/- and NDUFS2 +/+ mouse cohorts, separated by sex. Multiple T-tests adjusted P value <0.01: Female NDUFS2 +/- vs Female NDUFS2 +/+ months 6-12 and

16. N=22-34 per group **(B)** Survival of N = 20-22 per group Log-rank (Mantel-Cox) test P = 0.0791 **(C)** N = 28-29 per group. Log-rank (Mantel-Cox) test P = 0.9842 **(D)** Glucose tolerance tests for young (Mice < 6 months of age) and old (Mice > 20 months of age) mice. Young females N = 4-6 per group, young males N = 2-3 per group, old females N = 7-11 per group, old males N = 5-7 per group.

A)



B)

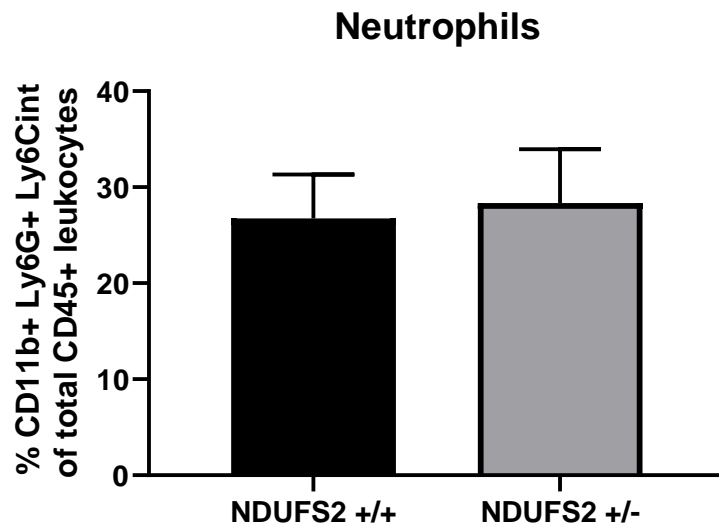


Figure 5.2.3. White blood cell differential of aged NDUF2S2^{+/-} and NDUF2S2^{+/+} mice. NDUF2S2^{+/+} and NDUF2S2^{+/-} 27-month-old mice CD11b⁺, Ly6G⁻, and Ly6C high monocytes (A) and CD11b⁺, Ly6G⁺, Ly6C intermediate neutrophils (B) as a percentage of total CD45⁺ cells were measured by flow cytometry. N=4, T-tests not significant.

5.3) Loss of one allele of NDUFS2 does not significantly impact behavioral function

We longitudinally measured several classic mouse behavioral tests in our cohorts of NDUFS2 $+/+$ and NDUFS2 $+/-$ mice at 3, 6, 12, 18, and 24 months of age, separated by sex. These tests included the open field behavior test, grip strength, rotarod, novel object recognition, and maximal forced treadmill challenge to assess several aspects of motor and cognitive function. Declines in motor and cognitive function were observed with advancing age on all tests with all groups however there were not significant or consistent changes between NDUFS2 $+/+$ and NDUFS2 $+/-$ mice in any of these behavioral tests across ages and sexes (Figure 5.3.1. A-E).

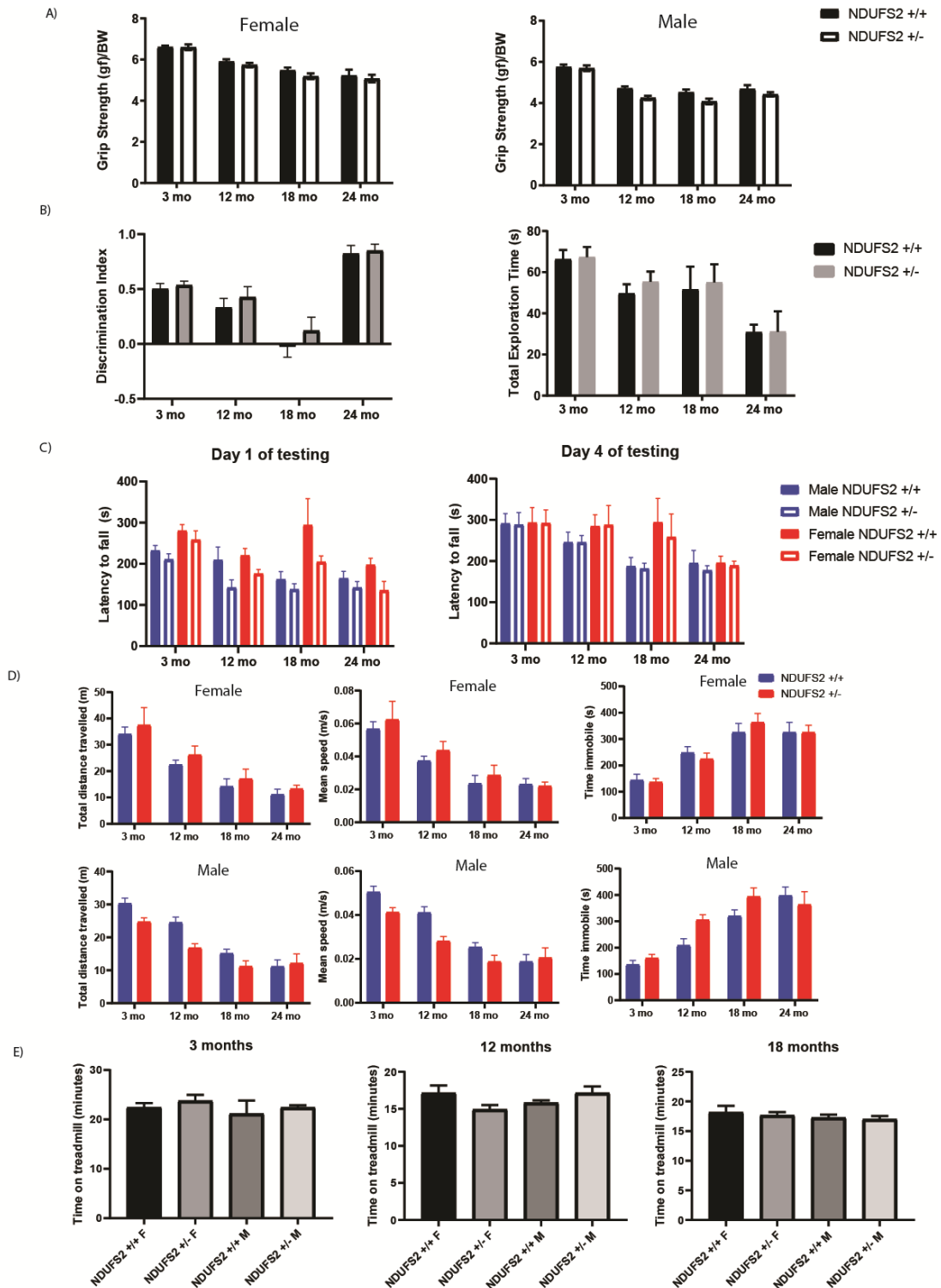


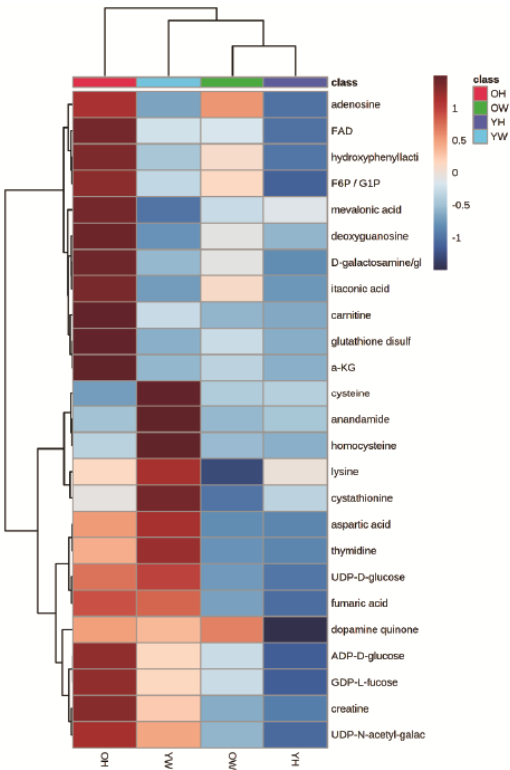
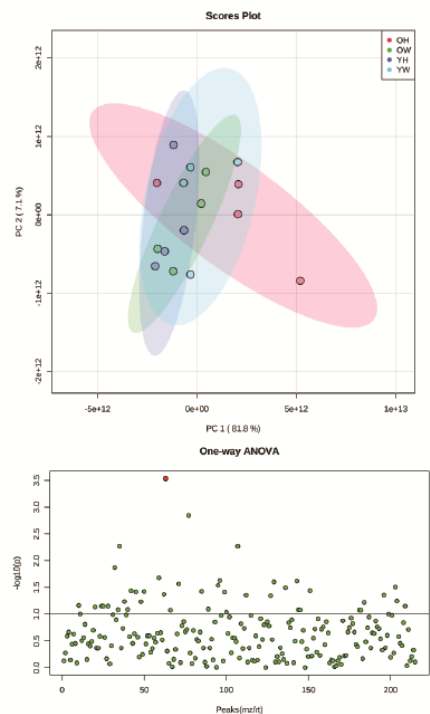
Figure 5.3.1) Longitudinal behavioral analysis of NDUFS2 +/- and NDUFS2 +/+ mice. (A) Grip strength grams of force normalized to body weight. N = 4-18 per group. Multiple T-tests not significant: Two-stage linear step-up procedure of Benjamini, Krieger and Yekutieli, with Q=1% NDUFS2+/+ vs NDUFS2+/- independently for each sex at each time point. **(B)** Novel object recognition test discrimination

index and total exploration time. Male and female data combined. N = 7-25 per group, Multiple T-tests not significant: Two-stage linear step-up procedure of Benjamini, Krieger and Yekutieli, with $Q=1\%$ $NDUFS2^{+/+}$ vs $NDUFS2^{+/-}$ independently for each time point. **(C)** Rotarod latency to fall at first and fourth day of testing. N=4-18 per group, Multiple T-tests not significant: Two-stage linear step-up procedure of Benjamini, Krieger and Yekutieli, with $Q=1\%$ $NDUFS2^{+/+}$ vs $NDUFS2^{+/-}$ independently for each sex at each time point. **(D)** Open field behavior test total distance travelled in 10 minutes, average speed, and time spent immobile. N=4-18 per group. Multiple T-tests not significant: Two-stage linear step-up procedure of Benjamini, Krieger and Yekutieli, with $Q=1\%$ $NDUFS2^{+/+}$ vs $NDUFS2^{+/-}$ independently for each sex at each time point. **(E)** Forced maximal exercise on accelerating treadmill challenge. 3 months: N = 2-8 per group, 12 months N = 4-6, 18 months N = 4 per group. Multiple T-tests not significant: Two-stage linear step-up procedure of Benjamini, Krieger and Yekutieli, with $Q=1\%$ $NDUFS2^{+/+}$ vs $NDUFS2^{+/-}$ independently for each sex at each time point.

5.4) Loss of one allele of *NDUFS2* leads to significant gene expression changes

We measured young (less than 6 months of age) and old (greater than 20 months of age) tissue soluble metabolites from liver and kidney in 4 male mice per genotype. PCA plots of the metabolite profiles were not segregating by groups. Multiple one way ANOVAs with an adjusted P value for multiple comparisons of 0.1 revealed only 1 significant alerted metabolite among groups in liver, that is cysteine, which was found to be elevated in young $NDUFS2^{+/+}$ mice compared to $NDUFS2^{+/-}$ young and old mice and $NDUFS2^{+/+}$ old mice (Figure 5.4.1. A). While not statistically significant at this threshold, we generated heatmaps of the top 25 metabolites by P value, which in liver demonstrated a trend towards accumulation of several TCA intermediates and mitochondrial metabolites in the aged $NDUFS2^{+/-}$ livers as compared with other groups, for example α KG was elevated in old $NDUFS2^{+/-}$ mice. Based on the heatmap, aged $NDUFS2^{+/-}$ mice are the most different from the rest of the groups. In the kidney, only the polyamine spermidine was found to be statistically significant at an adjusted threshold of 0.05 (Figure 5.4.1. B). With a threshold of 0.1, both 3,4-dihydroxyphenylacetaldehyde (DOPAL) and guanidinoacetate are significantly different between groups. DOPAL was elevated in young $NDUFS2^{+/+}$ kidney, while guanidinoacetate a toxic, seizure-inducing metabolite that is a precursor of creatine synthesized in the kidney by glycine and arginine producing ornithine, was found to be elevated in the $NDUFS2^{+/-}$ kidney. DOPAL is also a toxic dopamine metabolite, but another dopamine metabolite dopamine quinone, was found to be elevated in $NDUFS2^{+/-}$ kidney but was not statistically significant. Based on the heatmap, aged $NDUFS2^{+/-}$ mice are the most different from the rest of the groups. 2HG was not found to be significantly altered in any of the groups in either tissue.

A) Liver



D) Kidney

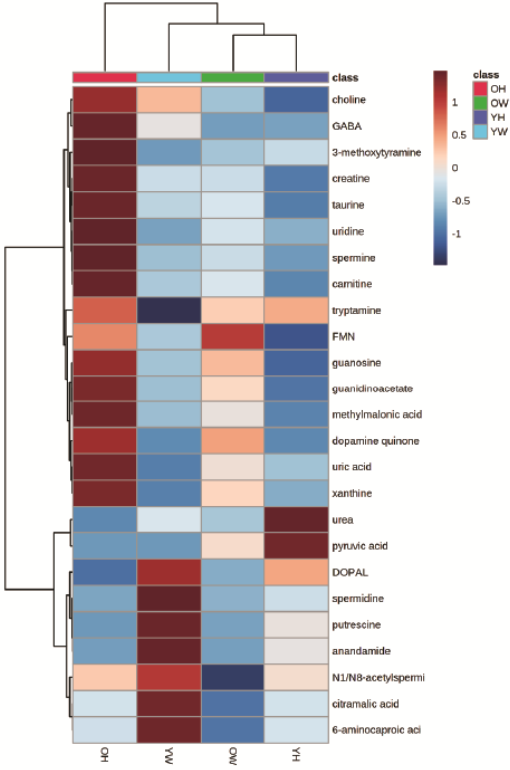
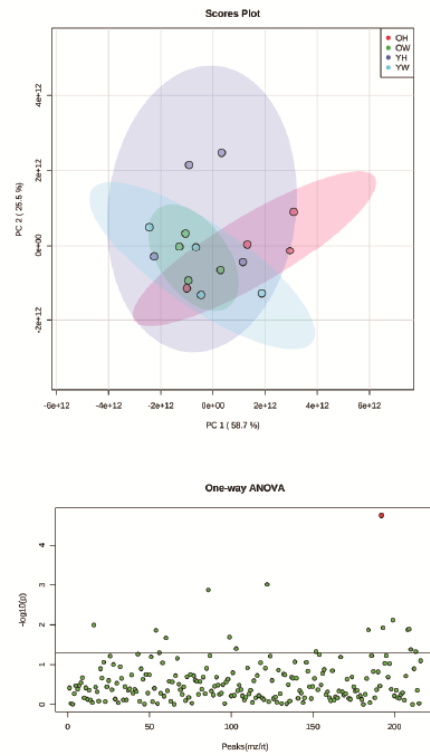
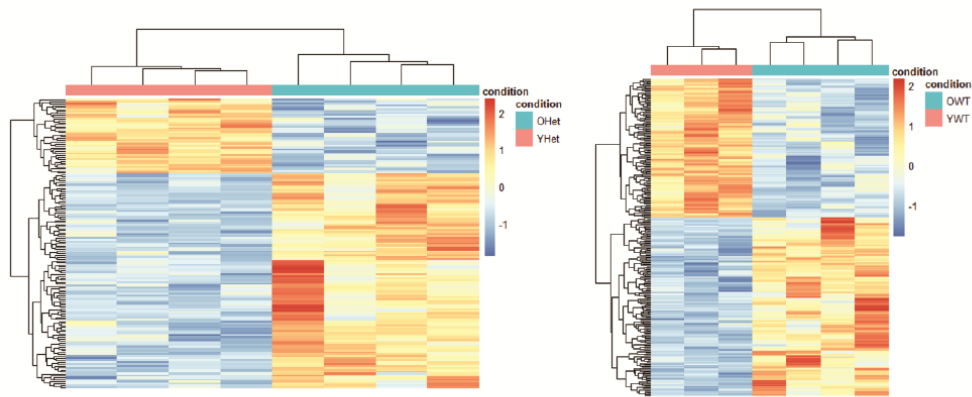


Figure 5.4.1) Metabolite measurements from NDUFS2 +/- and NDUFS2 +/- liver and kidney. (A) Liver tissue metabolite measurements. Principal component analysis scores plot, one-way ANOVA

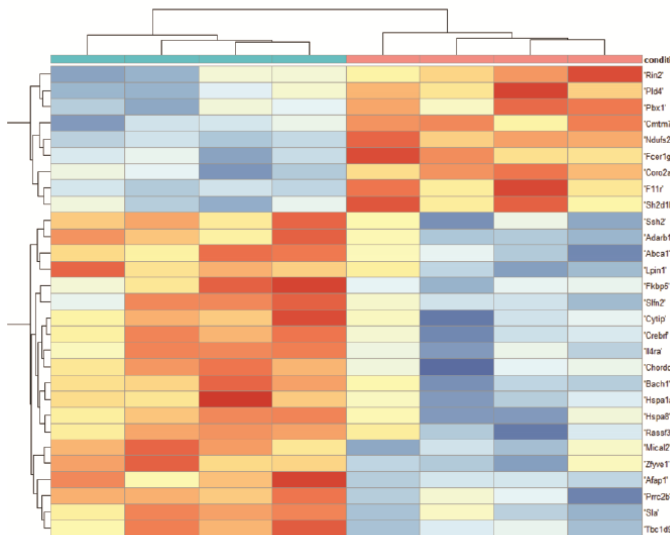
results, with adjusted P value < 0.1 highlighted in red (cysteine), heatmap of top 25 metabolites by ANOVA P value plotted as Z-score group averages by row and clustered. OW old NDUFS2^{+/+}, OH old NDUFS2 ^{+/-}, YW young NDUFS2 ^{+/+}, YH, young NDUFS2 ^{+/-}. N = 4 per group. **(B)** Kidney tissue metabolite measurements. Principal component analysis scores plot, one-way ANOVA results, with adjusted P value < 0.05 highlighted in red (spermidine), heatmap of top 25 metabolites by ANOVA P value plotted as Z-score group averages by row and clustered. OW old NDUFS2^{+/+}, OH old NDUFS2 ^{+/-}, YW young NDUFS2 ^{+/+}, YH, young NDUFS2 ^{+/-}. N = 4 per group.

Next we carried out RNA sequencing of alveolar macrophages, alveolar type II cells, and regulatory T cells isolated from NDUFS2 ^{+/+} and NDUFS2 ^{+/-} mice at young (<6 months of age) and old (20 months of age) time points. Consistent with previous work by our collaborators, several hundred genes were significantly differentially expressed in alveolar macrophages between young and old mice in both the NDUFS2 ^{+/+} and NDUFS2 ^{+/-} genotypes (Figure 5.4.2. A). Direct comparison of 20-month-old NDUFS2 ^{+/+} to NDUFS2 ^{+/-} alveolar macrophages (Figure 5.4.2. B) or alveolar type II cells (Figure 5.4.2. C) revealed far fewer significantly differentially expressed genes relative to the comparison of young versus old cells. Despite relatively few genes individually meeting the threshold of significance, gene set enrichment analysis revealed that there were several pathways differentially expressed between NDUFS2 ^{+/+} and NDUFS2 ^{+/-} cells. In NDUFS2 ^{+/-} alveolar macrophages, gene sets involved in proliferation and differentiation were enriched, including the G2M checkpoint, E2F targets, mitotic spindle, hedgehog signaling, and WNT/ β catenin hallmark gene sets (Figure 5.4.2. D). In NDUFS2 ^{+/+} alveolar macrophages the top enriched gene sets included oxidative phosphorylation, reactive oxygen species, MYC targets, interferon alpha, and the unfolded protein response hallmark gene sets (Figure 5.4.2. D). In NDUFS2 ^{+/-} alveolar type II cells enriched gene sets were involved in inflammation pathways including allograft rejection, NFkB/TNF signaling, epithelial mesenchymal transition, complement, IL2 signaling, inflammatory response, heme metabolism and protein secretion hallmark gene sets (Figure 5.4.2. E). In NDUFS2 ^{+/+} alveolar type II cells displayed gene set enrichment for reactive oxygen species and Kras signaling hallmark gene sets (Figure 5.4.2. E). Together these results indicate that there may be complex cell and tissue type specific responses to mild impairment of mitochondrial complex I during aging. These data, with enrichment of the reactive oxygen species response pathway and the unfolded protein response pathway in NDUFS2 ^{+/+} cells, indicates that the hypothesis that loss of one allele of *Ndufs2* would trigger a beneficial unfolded protein response through induction of ROS is not correct.

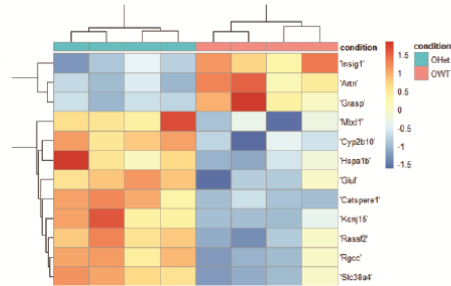
A) Alveolar Macrophages Young vs Old



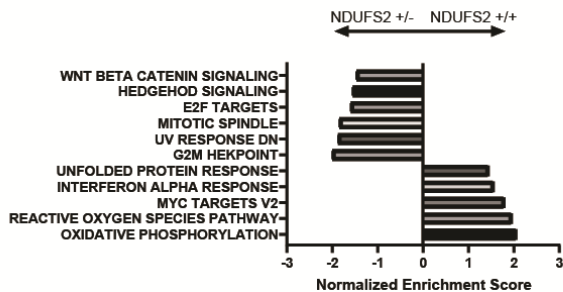
B) Alveolar Macrophages Old NDUF2 +/+ vs NDUF2 +/-



C) Alveolar Type II Cells Old NDUF2 +/+ vs NDUF2 +/-



D) Alveolar Macrophages Old NDUF2 +/+ vs NDUF2 +/-



E) Alveolar Type II Cells Old NDUF2 +/+ vs NDUF2 +/-

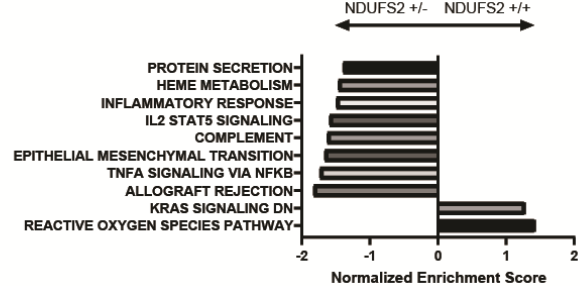


Figure 5.4.2. Alveolar macrophage and alveolar type 2 cell RNA sequencing in NDUF2 +/- and NDUF2 +/+ mice. (A) Young (<6 months) vs old (20 months) alveolar macrophage RNA sequencing results for NDUF2 +/- (left) and NDUF2 +/+ (right). Adjusted P value <0.05 by pairwise differential gene expression analysis. Z-scores scaled by gene with red indicating higher expression and blue indicating lower expression. **(B)** 20-month-old alveolar macrophage RNA sequencing results for NDUF2 +/- versus

NDUFS2 +/+ . Adjusted P value <0.05 by pairwise differential gene expression analysis. Z-scores scaled by gene with red indicating higher expression and blue indicating lower expression. **(C)** 20 months old alveolar type II cell RNA sequencing results for NDUFS2+/- versus NDUFS2 +/+. Adjusted P value <0.05 by pairwise differential gene expression analysis. Z-scores scaled by gene with red indicating higher expression and blue indicating lower expression. **(D)** Hallmark gene set enrichment analysis for 20-month-old alveolar macrophages for differential gene expression between NDUFS2+/- and NDUFS2+/+. Hallmark gene set FDR threshold set at 0.1. **(E)** Hallmark gene set enrichment analysis for 20-month-old alveolar type II cells for differential gene expression between NDUFS2+/- and NDUFS2+/+. Hallmark gene set FDR threshold set at 0.1. Ohet = Old NDUFS2 +/-, OWT = Old NDUFS2 +/+, Yhet = Young NDUFS2 +/-, YWT = Young NDUFS2 +/+. N=3-4 per group

We next focused on the RNA sequencing results from Tregs. At the young time-point, NDUFS2 +/+ and NDUFS2 +/- Tregs had relatively fewer significant changes in gene expression as compared with the older time-point. For Tregs we carried out gene set enrichment analysis for both gene ontology biological processes gene sets and hallmark gene sets (Figure 5.4.3. A-B). Network analysis of the gene ontology biological processes for differentially expressed genes between NDUFS2 +/+ and NDUFS2 +/- Tregs at <6 months of age revealed no significant enriched gene set networks for NDUFS2 +/-, but a few networks involved in translation/mRNA processing, the inner mitochondrial membrane, and cytochrome C regulation in NDUFS2 +/+ Tregs (Figure 5.4.3. A). Hallmark gene set enrichment mirrored these results. Gene sets enriched in NDUFS2 +/- included NFkB/TNF signaling, UV response, TGFβ signaling, and protein secretion (Figure 5.4.3. B). Some of these enriched hallmark gene sets were shared with the alveolar macrophages and alveolar type II cells (Figure 5.4.2. D-E). Hallmark gene sets enriched in NDUFS2 +/+ Tregs included reactive oxygen species signaling, OXPHOS, E2F, IL6, mTOR, glycolysis, and the unfolded protein response (Figure 5.4.3. B). In 20-month-old Tregs, the differences between NDUFS2 +/+ and NDUFS2 +/- were far more pronounced (Figure 5.4.4. A-B). Network analysis of gene ontology biological process gene sets revealed an extensive network of overlapping gene sets significantly enriched in aged NDUFS2 +/+ Tregs compared to NDUFS2 +/- Tregs that included pathways involved in mitochondrial metabolism and biogenesis, cell proliferation, DNA repair, RNA processing, and immunity, while the networks of gene sets significantly enriched in NDUFS2 +/- Tregs were pathways involved in methylation and demethylation (Figure 5.4.4. B). Hallmark gene set enrichment between age NDUFS2 +/+ and NDUFS2 +/- Tregs was largely similar to that described in younger Tregs, with the notable addition of enrichment of a hypoxia hallmark gene set in NDUFS2 +/- Tregs (Figure 5.4.4. B).

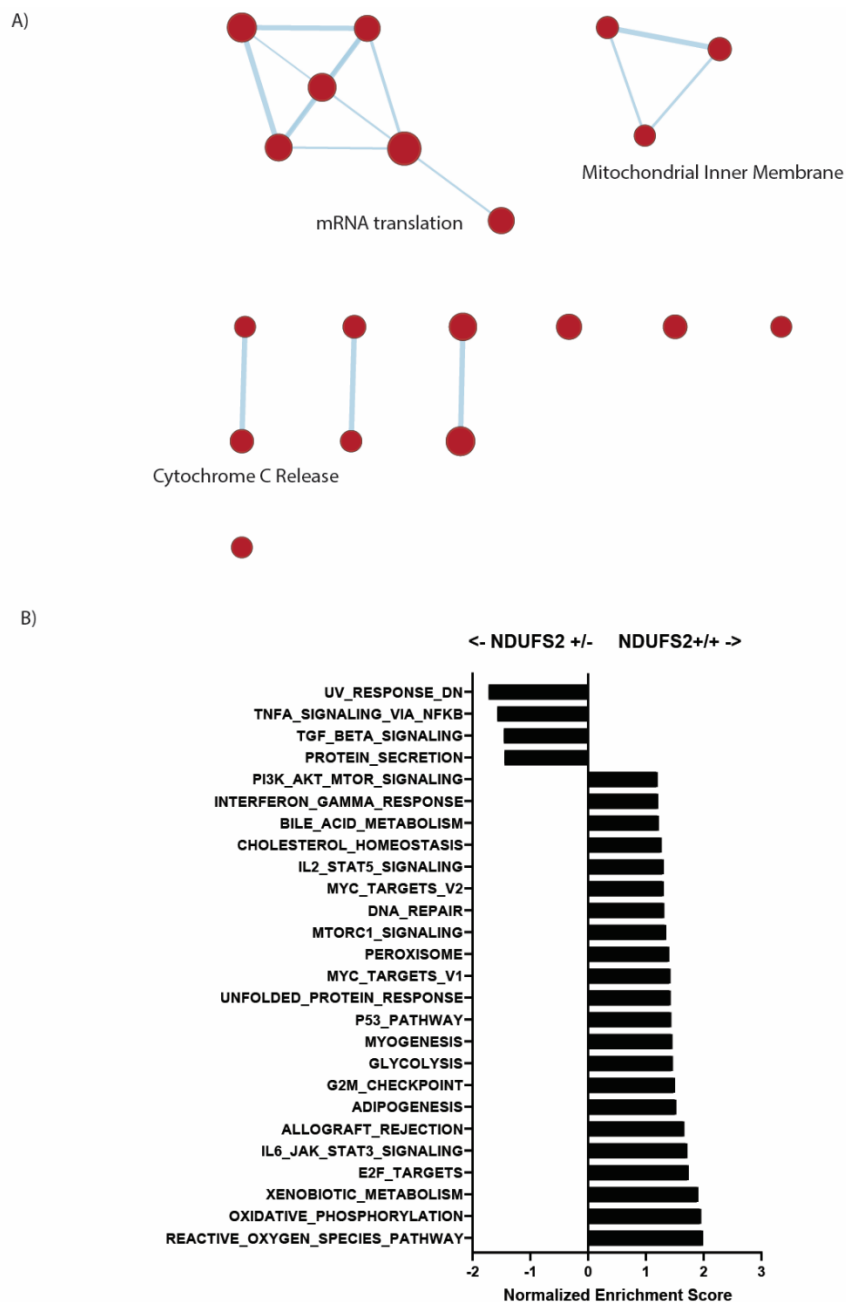


Figure 5.4.3) Regulatory T cell RNA sequencing from NDUF2 +/- and NDUF2 +/+ mice. (A) Network analysis for gene ontology biological process gene set enrichment analysis of differential gene expression between <6-month-old regulatory T cells from NDUF2 +/- versus NDUF2 +/+ mice. Key networks are identified. Red represents gene sets enriched in NDUF2 +/+. Circle size represents gene set size. Adjusted P value threshold 0.05. **(B)** Hallmark gene set enrichment analysis for <6-month-old regulatory T cells for differential gene expression between NDUF2 +/- and NDUF2 +/+. Gene set FDR <0.25.

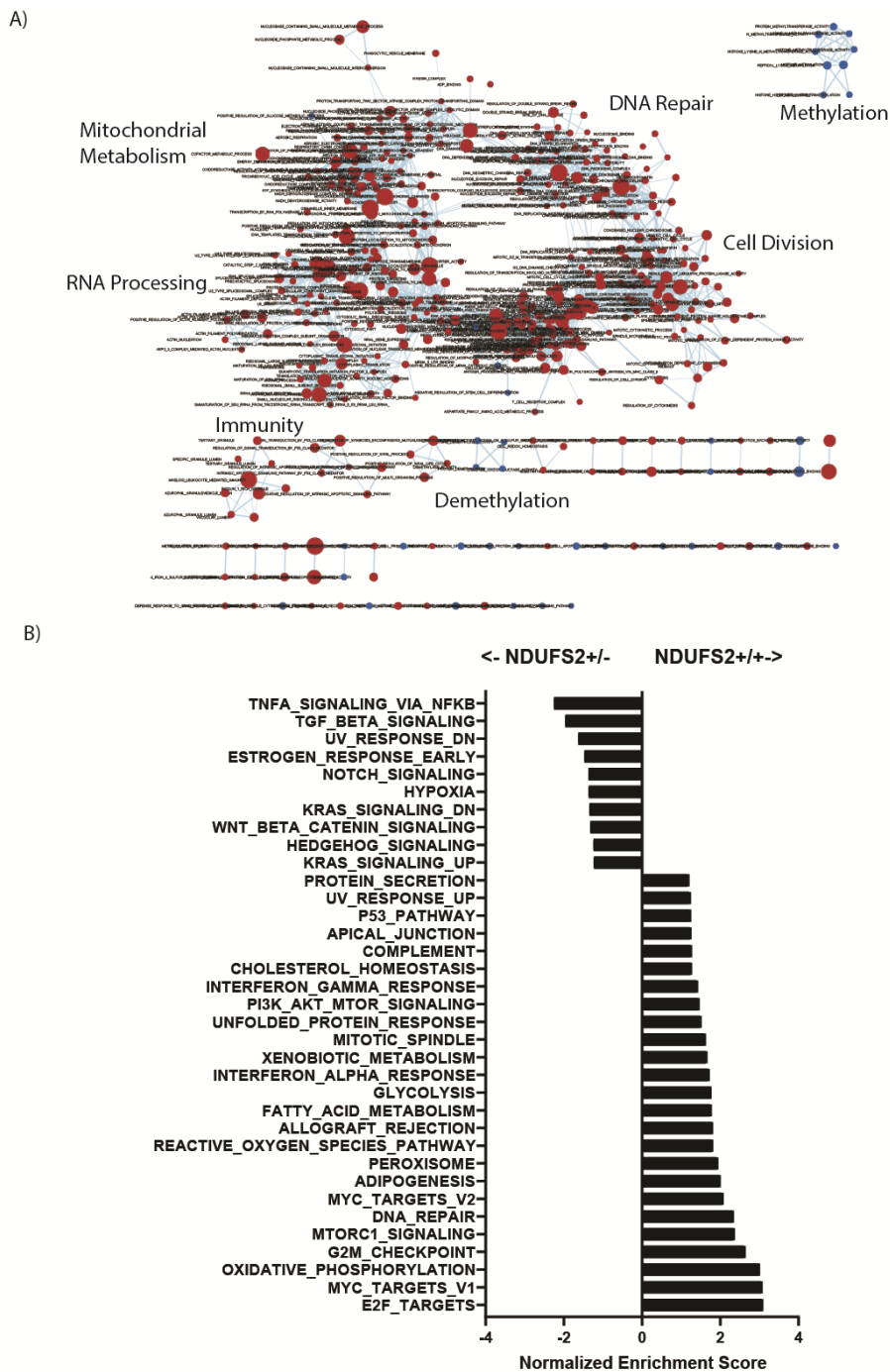


Figure 5.4.4) Regulatory T cell gene ontology biological processes network analysis from NDUF2 +/+ versus NDUF2 +/- mice. (A) Network analysis for gene ontology biological process gene set enrichment analysis of differential gene expression between 20-month-old regulatory T cells from NDUF2 +/+ versus NDUF2 +/- mice. Key networks are identified. Red represents gene sets enriched in NDUF2 +/+ and blue represents gene sets enriched in NDUF2 +/- . Circle size represents gene set size. Adjusted P value threshold 0.05. **(B)** Hallmark gene set enrichment analysis for 20-month-old

regulatory T cells for differential gene expression between *NDUFS2*^{+/-} and *NDUFS2*^{+/+}. Gene set FDR <0.25.

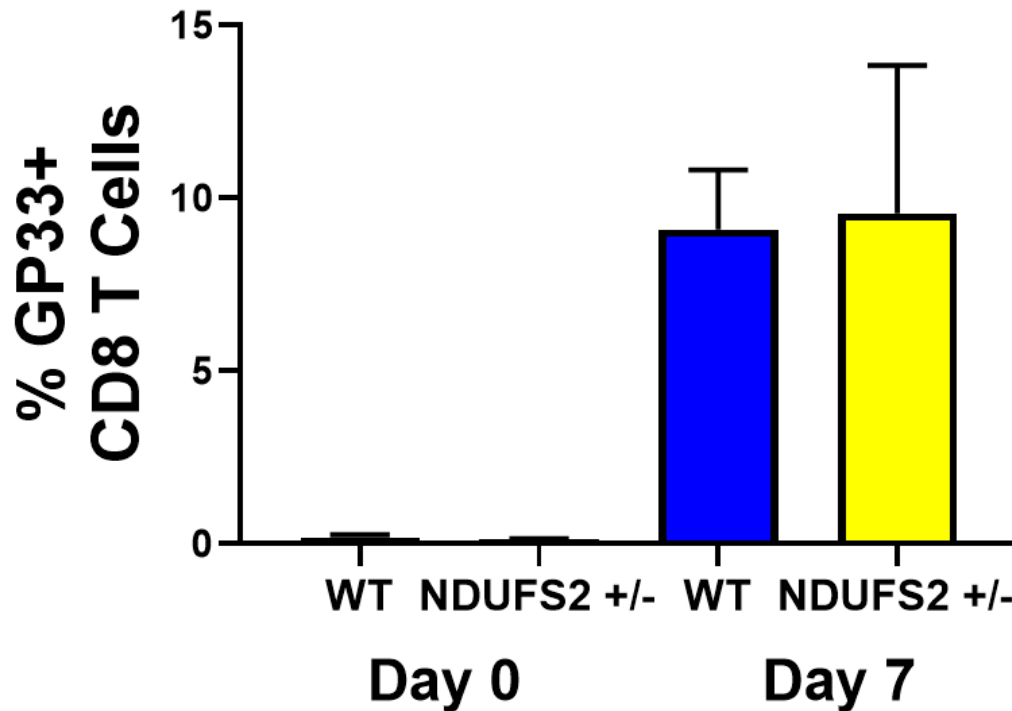


Figure 5.4.5. LCMV infection in *NDUFS2*^{+/-} and *NDUFS2*^{+/+} mice. Percentage of GP33 tetramer binding CD8 T cells was determined by flow cytometry. N = 4 mice per group. T tests not significant. WT=*NDUFS2*^{+/+}. Mice were 20 months of age at time of infection.

Due to the observed changes in gene expression in two different immune cell types involved in regulating inflammation and immunity during the aging process, we wanted to test whether there were dramatic differences in an infection model between *NDUFS2*^{+/+} and *NDUFS2*^{+/-} mice at 20 months of age. Therefore, we infected aged (20-month-old) *NDUFS2*^{+/+} and *NDUFS2*^{+/-} mice with lymphocytic choriomeningitis virus (LCMV) and measured their response to infection by measuring the percentage of epitope specific CD8 T cells that bound to GP33 tetramer one week after infection. There were no significant differences between *NDUFS2*^{+/+} and *NDUFS2*^{+/-} in their response to this viral infection (Figure 5.4.5).

5.5) Discussion

Overall our data indicate that our attempt to mildly inhibit mitochondrial complex I activity by genetic loss of one allele of *Ndufs2* in mice did not result in significant benefits for lifespan or healthspan. Although the preliminary oxygen consumption data and scarcity of metabolite changes in the highly metabolic liver and kidney tissues do not suggest a significant impairment of mitochondrial complex I function, there are significant gene expression changes in several cell types caused by loss of one allele of *Ndufs2*. This indicates that there clearly is a cellular response to slight reduction in this essential complex I component. In Tregs, which we have previously identified as a cell type dysregulated in aging and that may be particularly prone to 2HG accumulation, it is very interesting that we see enrichment of genes involved in demethylation, as we think that 2HG would inhibit demethylation, it is possible that the very minor buildup of 2HG or other inhibitors of α KG-dependent dioxygenase enzymes in *NDUFS2* +/- cells over the course of the lifetime does elicit a compensatory upregulation of these demethylation processes to overcome metabolite inhibition. It is possible that this impingement of complex I function was not sufficient to induce lifespan or healthspan extending effects even with aging, and that any slight differences in this model might require a more aggressive perturbation or a much higher power to uncover.

Chapter 6: Conclusions and future directions

The data described in chapters 3-5 lead to a few interesting conclusions and many more potential avenues for future research. From the data described in chapter 3, it is clear that expression of the yeast enzyme NDI1 in the brains of mice is able to significantly prolong the lifespan, but not restore motor function, in a mouse model of the human disease Leigh Syndrome caused by loss of the mitochondrial complex I subunit NDUFS4. From the data described in chapter 4, it is clear that, at least in flies, 2HG can serve as an effector of mitochondrial dysfunction resulting in neurological dysfunction. Finally, from the data in chapter 5, it is clear that loss of one allele of *Ndufs2* in mice is not sufficient to dramatically increase or decreases healthspan or lifespan in mice. The links between these three stories require further validation, and each raises its own set of future experiments and possibilities.

One clear project for future research involves further genetic determination of the cell types responsible for death and dysfunction in the NDUFS4 mouse model using the NDI1 conditionally expressing mouse. For example, crossing NDUFS4 and NDI1 to the *Gad2* and *Vglut2* reporter driven Cre recombinase lines would provide interesting results that would complement the study that was performed using the Nestin Cre mice in chapter 3. Our preliminary results indicate that it may be that GABAergic neurons are the predominant driver of death through seizure induction in the Nestin-Cre model, and that it is NDI1 expression in these cells that is predominantly responsible for the lifespan-extending effects that we observed, while glutamatergic neurons in the brainstem and cerebellum may require the extra ATP from mitochondrial complex I in order to prevent ataxia. The NDI1 mouse can also be used to test the role of mitochondrial complex I function in other neurodegenerative models, as well as the role of complex I inhibition in metformin's mechanism of action for its antidiabetic, anti-cancer, and proposed anti-aging effects. It would also be of interest to follow up the preliminary findings of NDUFS4 ubiquitous deficiency being unaffected by loss of multiple components of the inflammation response including STING, RAG, and IL6. It may be that the neuroinflammation observed in NDUFS4 deficient models is not necessary for the disease pathogenesis but is a reactive byproduct of the primary disease pathophysiology. Direct comparison of NDI1 expression's effect on longevity in mice versus flies, independent of mitochondrial complex I mutations, is another area of potential future research. Recall from chapter 1, that studies have

indicated that NDI1 expression in *Drosophila melanogaster* is sufficient to increase lifespan in WT flies only when NDI1 is expressed in the brain or in the intestine, not ubiquitously. It would be interesting to directly compare NDI1 expressing mice and Cre mice described in chapter 3 over the course of the mouse lifespan to see if NDI1 expression in the setting of normal complex I function could result in beneficial or deleterious effects. Our preliminary data in chapter 3 indicate that NDI1 expression in the brain of mice is well tolerated. It would also be interesting to use the NDI1 mice to further explore the disease mechanisms of LHON in the retina of the ubiquitous NDUFS4 deficient mice.

Due to our results in *Drosophila melanogaster* described in chapter 4, we have begun developing a novel mouse model that can conditionally overexpress the L2HGDH enzyme in mice. Crossing this mouse to NDUFS4 deficient mice and RISP or QPC deficient mice to reduce accumulation of 2HG is of great interest to determine the necessity of 2HG accumulation in these and other disease pathologies *in vivo*.

Measurement of 2HG levels in NDUFS2 +/- Tregs and other cell types is of interest during the aging process due to our preliminary observation of 2HG levels increasing with age in WT Tregs and due to the finding that demethylation gene sets were highly enriched in NDUFS2 +/- Tregs. Further characterization of Treg function in these mice, including T cell repression assays, DNA methylation analysis, tumor rejection studies, and more aggressive infection challenges such as influenza A infection and recovery are warranted.

References

1. Roger, A.J., S.A. Munoz-Gomez, and R. Kamikawa, *The Origin and Diversification of Mitochondria*. Curr Biol, 2017. **27**(21): p. R1177-R1192.
2. Spinelli, J.B. and M.C. Haigis, *The multifaceted contributions of mitochondria to cellular metabolism*. Nat Cell Biol, 2018. **20**(7): p. 745-754.
3. Pagliarini, D.J. and J. Rutter, *Hallmarks of a new era in mitochondrial biochemistry*. Genes Dev, 2013. **27**(24): p. 2615-27.
4. Xu, W., T. Barrientos, and N.C. Andrews, *Iron and copper in mitochondrial diseases*. Cell Metab, 2013. **17**(3): p. 319-28.
5. Chandel, N.S., *Navigating metabolism*. 2015, Cold Spring Harbor, New York: Cold Spring Harbor Laboratory Press. xv, 248 pages.
6. Schell, J.C., et al., *A role for the mitochondrial pyruvate carrier as a repressor of the Warburg effect and colon cancer cell growth*. Mol Cell, 2014. **56**(3): p. 400-13.
7. De Stefani, D., M. Patron, and R. Rizzuto, *Structure and function of the mitochondrial calcium uniporter complex*. Biochim Biophys Acta, 2015. **1853**(9): p. 2006-11.
8. Tantral, L., et al., *Intracellular calcium release is required for caspase-3 and -9 activation*. Cell Biochem Funct, 2004. **22**(1): p. 35-40.
9. Cardenas-Rodriguez, M., A. Chatzi, and K. Tokatlidis, *Iron-sulfur clusters: from metals through mitochondria biogenesis to disease*. J Biol Inorg Chem, 2018. **23**(4): p. 509-520.
10. Ast, T., et al., *Hypoxia Rescues Frataxin Loss by Restoring Iron Sulfur Cluster Biogenesis*. Cell, 2019. **177**(6): p. 1507-1521 e16.
11. Lenaz, G., et al., *Mitochondrial complex I defects in aging*. Mol Cell Biochem, 1997. **174**(1-2): p. 329-33.
12. Clason, T., et al., *The structure of eukaryotic and prokaryotic complex I*. J Struct Biol, 2010. **169**(1): p. 81-8.
13. Wiedemann, N. and N. Pfanner, *Mitochondrial Machineries for Protein Import and Assembly*. Annu Rev Biochem, 2017. **86**: p. 685-714.
14. Zhu, J., K.R. Vinothkumar, and J. Hirst, *Structure of mammalian respiratory complex I*. Nature, 2016. **536**(7616): p. 354-358.
15. Fiedorczuk, K., et al., *Atomic structure of the entire mammalian mitochondrial complex I*. Nature, 2016. **538**(7625): p. 406-410.
16. Stroud, D.A., et al., *Accessory subunits are integral for assembly and function of human mitochondrial complex I*. Nature, 2016. **538**(7623): p. 123-126.
17. Lazarou, M., et al., *Analysis of the assembly profiles for mitochondrial- and nuclear-DNA-encoded subunits into complex I*. Mol Cell Biol, 2007. **27**(12): p. 4228-37.
18. Yang, L., et al., *Serine Catabolism Feeds NADH when Respiration Is Impaired*. Cell Metab, 2020. **31**(4): p. 809-821 e6.
19. Audrito, V., et al., *NAD-Biosynthetic and Consuming Enzymes as Central Players of Metabolic Regulation of Innate and Adaptive Immune Responses in Cancer*. Front Immunol, 2019. **10**: p. 1720.
20. Urra, F.A., et al., *The Mitochondrial Complex(I)ty of Cancer*. Front Oncol, 2017. **7**: p. 118.
21. Wong, H.S., et al., *Production of superoxide and hydrogen peroxide from specific mitochondrial sites under different bioenergetic conditions*. J Biol Chem, 2017. **292**(41): p. 16804-16809.
22. Pryde, K.R. and J. Hirst, *Superoxide is produced by the reduced flavin in mitochondrial complex I: a single, unified mechanism that applies during both forward and reverse electron transfer*. J Biol Chem, 2011. **286**(20): p. 18056-65.
23. Brand, M.D., *Mitochondrial generation of superoxide and hydrogen peroxide as the source of mitochondrial redox signaling*. Free Radic Biol Med, 2016. **100**: p. 14-31.
24. Wong, H.S., P.A. Monternier, and M.D. Brand, *S1QELs suppress mitochondrial superoxide/hydrogen peroxide production from site IQ without inhibiting reverse electron flow through Complex I*. Free Radic Biol Med, 2019. **143**: p. 545-559.

25. Chance, B. and G. Hollunger, *The interaction of energy and electron transfer reactions in mitochondria. VI. The efficiency of the reaction.* J Biol Chem, 1961. **236**: p. 1577-84.
26. Chouchani, E.T., et al., *Ischaemic accumulation of succinate controls reperfusion injury through mitochondrial ROS.* Nature, 2014. **515**(7527): p. 431-435.
27. Mills, E.L., et al., *Accumulation of succinate controls activation of adipose tissue thermogenesis.* Nature, 2018. **560**(7716): p. 102-106.
28. Mills, E.L., et al., *Succinate Dehydrogenase Supports Metabolic Repurposing of Mitochondria to Drive Inflammatory Macrophages.* Cell, 2016. **167**(2): p. 457-470 e13.
29. Galkin, A., et al., *Lack of oxygen deactivates mitochondrial complex I: implications for ischemic injury?* J Biol Chem, 2009. **284**(52): p. 36055-61.
30. Quinlan, C.L., et al., *The mechanism of superoxide production by the antimycin-inhibited mitochondrial Q-cycle.* J Biol Chem, 2011. **286**(36): p. 31361-72.
31. Brand, M.D., *The sites and topology of mitochondrial superoxide production.* Exp Gerontol, 2010. **45**(7-8): p. 466-72.
32. Ma, X., et al., *Mitochondrial electron transport chain complex III is required for antimycin A to inhibit autophagy.* Chem Biol, 2011. **18**(11): p. 1474-81.
33. Passmore, J.B., et al., *The respiratory chain inhibitor rotenone affects peroxisomal dynamics via its microtubule-destabilising activity.* Histochem Cell Biol, 2017. **148**(3): p. 331-341.
34. Barrientos, A. and C.T. Moraes, *Titration of the effects of mitochondrial complex I impairment in the cell physiology.* J Biol Chem, 1999. **274**(23): p. 16188-97.
35. Choi, W.S., R.D. Palmiter, and Z. Xia, *Loss of mitochondrial complex I activity potentiates dopamine neuron death induced by microtubule dysfunction in a Parkinson's disease model.* J Cell Biol, 2011. **192**(5): p. 873-82.
36. Vial, G., D. Demaille, and B. Guigas, *Role of Mitochondria in the Mechanism(s) of Action of Metformin.* Front Endocrinol (Lausanne), 2019. **10**: p. 294.
37. Hakkaart, G.A., et al., *Allotopic expression of a mitochondrial alternative oxidase confers cyanide resistance to human cell respiration.* EMBO Rep, 2006. **7**(3): p. 341-5.
38. Perales-Clemente, E., et al., *Restoration of electron transport without proton pumping in mammalian mitochondria.* Proc Natl Acad Sci U S A, 2008. **105**(48): p. 18735-9.
39. Titov, D.V., et al., *Complementation of mitochondrial electron transport chain by manipulation of the NAD⁺/NADH ratio.* Science, 2016. **352**(6282): p. 231-5.
40. Seo, B.B., et al., *Molecular remedy of complex I defects: rotenone-insensitive internal NADH-quinone oxidoreductase of Saccharomyces cerevisiae mitochondria restores the NADH oxidase activity of complex I-deficient mammalian cells.* Proc Natl Acad Sci U S A, 1998. **95**(16): p. 9167-71.
41. Cui, Y., et al., *Mitochondrial release of the NADH dehydrogenase Ndi1 induces apoptosis in yeast.* Mol Biol Cell, 2012. **23**(22): p. 4373-82.
42. Bai, Y., et al., *Lack of complex I activity in human cells carrying a mutation in MtDNA-encoded ND4 subunit is corrected by the Saccharomyces cerevisiae NADH-quinone oxidoreductase (NDI1) gene.* J Biol Chem, 2001. **276**(42): p. 38808-13.
43. Yagi, T., et al., *Possibility of transkingdom gene therapy for complex I diseases.* Biochim Biophys Acta, 2006. **1757**(5-6): p. 708-14.
44. Marella, M., et al., *No immune responses by the expression of the yeast Ndi1 protein in rats.* PLoS One, 2011. **6**(10): p. e25910.
45. Mentzer, R.M., Jr., et al., *Reduction of infarct size by the therapeutic protein TAT-Ndi1 in vivo.* J Cardiovasc Pharmacol Ther, 2014. **19**(3): p. 315-20.
46. Perry, C.N., et al., *Xenotransplantation of mitochondrial electron transfer enzyme, Ndi1, in myocardial reperfusion injury.* PLoS One, 2011. **6**(2): p. e16288.
47. Marella, M., et al., *Protection by the NDI1 gene against neurodegeneration in a rotenone rat model of Parkinson's disease.* PLoS One, 2008. **3**(1): p. e1433.
48. Richardson, J.R., et al., *Obligatory role for complex I inhibition in the dopaminergic neurotoxicity of 1-methyl-4-phenyl-1,2,3,6-tetrahydropyridine (MPTP).* Toxicol Sci, 2007. **95**(1): p. 196-204.
49. Barber-Singh, J., et al., *Neuroprotective effect of long-term NDI1 gene expression in a chronic mouse model of Parkinson disorder.* Rejuvenation Res, 2009. **12**(4): p. 259-67.

50. Chadderton, N., et al., *Intravitreal delivery of AAV-NDI1 provides functional benefit in a murine model of Leber hereditary optic neuropathy*. Eur J Hum Genet, 2013. **21**(1): p. 62-8.
51. Talla, V., et al., *NADH-dehydrogenase type-2 suppresses irreversible visual loss and neurodegeneration in the EAE animal model of MS*. Mol Ther, 2013. **21**(10): p. 1876-88.
52. Talla, V., R. Koilkonda, and J. Guy, *Gene Therapy with Single-Subunit Yeast NADH-Ubiquinone Oxidoreductase (NDI1) Improves the Visual Function in Experimental Autoimmune Encephalomyelitis (EAE) Mice Model of Multiple Sclerosis (MS)*. Mol Neurobiol, 2020. **57**(4): p. 1952-1965.
53. Chandel, N.S., *Mitochondria as signaling organelles*. BMC Biol, 2014. **12**: p. 34.
54. Liu, X., et al., *Induction of apoptotic program in cell-free extracts: requirement for dATP and cytochrome c*. Cell, 1996. **86**(1): p. 147-57.
55. Aouacheria, A., et al., *Connecting mitochondrial dynamics and life-or-death events via Bcl-2 family proteins*. Neurochem Int, 2017. **109**: p. 141-161.
56. Jacobs, J.L. and C.B. Coyne, *Mechanisms of MAVS regulation at the mitochondrial membrane*. J Mol Biol, 2013. **425**(24): p. 5009-19.
57. Martinez-Reyes, I. and N.S. Chandel, *Mitochondrial TCA cycle metabolites control physiology and disease*. Nat Commun, 2020. **11**(1): p. 102.
58. Pickles, S., P. Vigie, and R.J. Youle, *Mitophagy and Quality Control Mechanisms in Mitochondrial Maintenance*. Curr Biol, 2018. **28**(4): p. R170-R185.
59. Murley, A. and J. Nunnari, *The Emerging Network of Mitochondria-Organelle Contacts*. Mol Cell, 2016. **61**(5): p. 648-653.
60. Islam, M.S., et al., *2-Oxoglutarate-Dependent Oxygenases*. Annu Rev Biochem, 2018. **87**: p. 585-620.
61. El-Hattab, A.W., *Inborn errors of metabolism*. Clin Perinatol, 2015. **42**(2): p. 413-39, x.
62. Murphy, M.P., *How mitochondria produce reactive oxygen species*. Biochemical Journal, 2009. **417**: p. 1-13.
63. Quinlan, C.L., et al., *The determination and analysis of site-specific rates of mitochondrial reactive oxygen species production*. Methods Enzymol, 2013. **526**: p. 189-217.
64. Holmstrom, K.M. and T. Finkel, *Cellular mechanisms and physiological consequences of redox-dependent signalling*. Nat Rev Mol Cell Biol, 2014. **15**(6): p. 411-21.
65. Martinez-Reyes, I., et al., *TCA Cycle and Mitochondrial Membrane Potential Are Necessary for Diverse Biological Functions*. Molecular Cell, 2016. **61**(2): p. 199-209.
66. Chandel, N.S., *Evolution of Mitochondria as Signaling Organelles*. Cell Metab, 2015. **22**(2): p. 204-6.
67. Wellen, K.E., et al., *ATP-citrate lyase links cellular metabolism to histone acetylation*. Science, 2009. **324**(5930): p. 1076-80.
68. McDonnell, E., et al., *Lipids Reprogram Metabolism to Become a Major Carbon Source for Histone Acetylation*. Cell Rep, 2016. **17**(6): p. 1463-1472.
69. Schieber, M. and N.S. Chandel, *ROS function in redox signaling and oxidative stress*. Curr Biol, 2014. **24**(10): p. R453-62.
70. Weinberg, S.E. and N.S. Chandel, *Targeting mitochondria metabolism for cancer therapy*. Nat Chem Biol, 2015. **11**(1): p. 9-15.
71. Franciosi, M., et al., *Metformin therapy and risk of cancer in patients with type 2 diabetes: systematic review*. PLoS One, 2013. **8**(8): p. e71583.
72. Mallik, R. and T.A. Chowdhury, *Metformin in cancer*. Diabetes Res Clin Pract, 2018. **143**: p. 409-419.
73. Wheaton, W.W., et al., *Metformin inhibits mitochondrial complex I of cancer cells to reduce tumorigenesis*. Elife, 2014. **3**: p. e02242.
74. Roshan, M.H., Y.K. Shing, and N.P. Pace, *Metformin as an adjuvant in breast cancer treatment*. SAGE Open Med, 2019. **7**: p. 2050312119865114.
75. Barzilai, N., et al., *Metformin as a Tool to Target Aging*. Cell Metab, 2016. **23**(6): p. 1060-1065.
76. Soberanes, S., et al., *Metformin Targets Mitochondrial Electron Transport to Reduce Air-Pollution-Induced Thrombosis*. Cell Metab, 2019. **29**(2): p. 335-347 e5.

77. Sergiev, P.V., O.A. Dontsova, and G.V. Berezkin, *Theories of aging: an ever-evolving field*. Acta Naturae, 2015. **7**(1): p. 9-18.
78. Jin, K., *Modern Biological Theories of Aging*. Aging Dis, 2010. **1**(2): p. 72-74.
79. Rubner, M., *Volksernährungsfragen*. 1908, Leipzig.: Akademische Verlagsgesellschaft m.b.H. iv, 143 p.
80. Pearl, R., *The rate of living, being an account of some experimental studies on the biology of life duration*. 1928, New York,: A.A. Knopf. 8 p.l., 185, 1 p.
81. Harman, D., *Aging: a theory based on free radical and radiation chemistry*. J Gerontol, 1956. **11**(3): p. 298-300.
82. Hur, J.H., D.A. Stork, and D.W. Walker, *Complex-I-ty in aging*. J Bioenerg Biomembr, 2014. **46**(4): p. 329-35.
83. Gladyshev, V.N., *The origin of aging: imperfectness-driven non-random damage defines the aging process and control of lifespan*. Trends Genet, 2013. **29**(9): p. 506-12.
84. Rollo, C.D., *Aging and the Mammalian regulatory triumvirate*. Aging Dis, 2010. **1**(2): p. 105-38.
85. Speakman, J.R., et al., *Uncoupled and surviving: individual mice with high metabolism have greater mitochondrial uncoupling and live longer*. Aging Cell, 2004. **3**(3): p. 87-95.
86. Kirkwood, T.B., *Evolution of ageing*. Nature, 1977. **270**(5635): p. 301-4.
87. Sun, N., R.J. Youle, and T. Finkel, *The Mitochondrial Basis of Aging*. Mol Cell, 2016. **61**(5): p. 654-666.
88. Steinhubl, S.R., *Why have antioxidants failed in clinical trials?* Am J Cardiol, 2008. **101**(10A): p. 14D-19D.
89. Herbener, G.H., *A morphometric study of age-dependent changes in mitochondrial population of mouse liver and heart*. J Gerontol, 1976. **31**(1): p. 8-12.
90. Short, K.R., et al., *Decline in skeletal muscle mitochondrial function with aging in humans*. Proc Natl Acad Sci U S A, 2005. **102**(15): p. 5618-23.
91. Stocco, D.M. and J.C. Hutson, *Quantitation of mitochondrial DNA and protein in the liver of Fischer 344 rats during aging*. J Gerontol, 1978. **33**(6): p. 802-9.
92. Mora, A.L., M. Bueno, and M. Rojas, *Mitochondria in the spotlight of aging and idiopathic pulmonary fibrosis*. J Clin Invest, 2017. **127**(2): p. 405-414.
93. Lopez-Otin, C., et al., *The hallmarks of aging*. Cell, 2013. **153**(6): p. 1194-217.
94. Zhang, H., K.J. Menzies, and J. Auwerx, *The role of mitochondria in stem cell fate and aging*. Development, 2018. **145**(8).
95. Korolchuk, V.I., et al., *Mitochondria in Cell Senescence: Is Mitophagy the Weakest Link?* EBioMedicine, 2017. **21**: p. 7-13.
96. Jesinkey, S.R., et al., *Mitochondrial GTP Links Nutrient Sensing to beta Cell Health, Mitochondrial Morphology, and Insulin Secretion Independent of OxPhos*. Cell Rep, 2019. **28**(3): p. 759-772 e10.
97. Shpilka, T. and C.M. Haynes, *The mitochondrial UPR: mechanisms, physiological functions and implications in ageing*. Nat Rev Mol Cell Biol, 2018. **19**(2): p. 109-120.
98. David, D.C., et al., *Widespread protein aggregation as an inherent part of aging in C. elegans*. PLoS Biol, 2010. **8**(8): p. e1000450.
99. Zheng, Q., J. Huang, and G. Wang, *Mitochondria, Telomeres and Telomerase Subunits*. Front Cell Dev Biol, 2019. **7**: p. 274.
100. Sullivan, L.B. and N.S. Chandel, *Mitochondrial reactive oxygen species and cancer*. Cancer Metab, 2014. **2**: p. 17.
101. Klecker, T. and B. Westermann, *Asymmetric inheritance of mitochondria in yeast*. Biol Chem, 2020.
102. He, C., C. Zhou, and B.K. Kennedy, *The yeast replicative aging model*. Biochim Biophys Acta Mol Basis Dis, 2018. **1864**(9 Pt A): p. 2690-2696.
103. Saxton, R.A. and D.M. Sabatini, *mTOR Signaling in Growth, Metabolism, and Disease*. Cell, 2017. **168**(6): p. 960-976.
104. Jazwinski, S.M., J.C. Jiang, and S. Kim, *Adaptation to metabolic dysfunction during aging: Making the best of a bad situation*. Exp Gerontol, 2018. **107**: p. 87-90.

105. Hughes, A.L. and D.E. Gottschling, *An early age increase in vacuolar pH limits mitochondrial function and lifespan in yeast*. *Nature*, 2012. **492**(7428): p. 261-5.
106. Assali, E.A., et al., *Nanoparticle-mediated lysosomal reacidification restores mitochondrial turnover and function in beta cells under lipotoxicity*. *FASEB J*, 2019. **33**(3): p. 4154-4165.
107. Audano, M., A. Schneider, and N. Mitro, *Mitochondria, lysosomes, and dysfunction: their meaning in neurodegeneration*. *J Neurochem*, 2018. **147**(3): p. 291-309.
108. Colacurcio, D.J. and R.A. Nixon, *Disorders of lysosomal acidification-The emerging role of v-ATPase in aging and neurodegenerative disease*. *Ageing Res Rev*, 2016. **32**: p. 75-88.
109. de la Mata, M., et al., *Mitochondrial Dysfunction in Lysosomal Storage Disorders*. *Diseases*, 2016. **4**(4).
110. Ferguson, S.M., *Beyond indigestion: emerging roles for lysosome-based signaling in human disease*. *Curr Opin Cell Biol*, 2015. **35**: p. 59-68.
111. Nixon, R.A., D.S. Yang, and J.H. Lee, *Neurodegenerative lysosomal disorders: a continuum from development to late age*. *Autophagy*, 2008. **4**(5): p. 590-9.
112. Plotegher, N. and M.R. Duchen, *Mitochondrial Dysfunction and Neurodegeneration in Lysosomal Storage Disorders*. *Trends Mol Med*, 2017. **23**(2): p. 116-134.
113. Hughes, C.E., et al., *Cysteine Toxicity Drives Age-Related Mitochondrial Decline by Altering Iron Homeostasis*. *Cell*, 2020. **180**(2): p. 296-310 e18.
114. Weber, R.A., et al., *Maintaining Iron Homeostasis Is the Key Role of Lysosomal Acidity for Cell Proliferation*. *Mol Cell*, 2020. **77**(3): p. 645-655 e7.
115. Dillin, A., et al., *Rates of behavior and aging specified by mitochondrial function during development*. *Science*, 2002. **298**(5602): p. 2398-401.
116. Lee, S.S., et al., *A systematic RNAi screen identifies a critical role for mitochondria in C. elegans longevity*. *Nat Genet*, 2003. **33**(1): p. 40-8.
117. Rea, S.L., N. Ventura, and T.E. Johnson, *Relationship between mitochondrial electron transport chain dysfunction, development, and life extension in Caenorhabditis elegans*. *PLoS Biol*, 2007. **5**(10): p. e259.
118. Yang, W. and S. Hekimi, *Two modes of mitochondrial dysfunction lead independently to lifespan extension in Caenorhabditis elegans*. *Aging Cell*, 2010. **9**(3): p. 433-47.
119. Yang, W. and S. Hekimi, *A mitochondrial superoxide signal triggers increased longevity in Caenorhabditis elegans*. *PLoS Biol*, 2010. **8**(12): p. e1000556.
120. Lee, S.J., A.B. Hwang, and C. Kenyon, *Inhibition of respiration extends C. elegans life span via reactive oxygen species that increase HIF-1 activity*. *Curr Biol*, 2010. **20**(23): p. 2131-6.
121. Yun, J. and T. Finkel, *Mitohormesis*. *Cell Metab*, 2014. **19**(5): p. 757-66.
122. Yee, C., W. Yang, and S. Hekimi, *The intrinsic apoptosis pathway mediates the pro-longevity response to mitochondrial ROS in C. elegans*. *Cell*, 2014. **157**(4): p. 897-909.
123. Copeland, J.M., et al., *Extension of Drosophila life span by RNAi of the mitochondrial respiratory chain*. *Curr Biol*, 2009. **19**(19): p. 1591-8.
124. Tsang, W.Y., et al., *Mitochondrial respiratory chain deficiency in Caenorhabditis elegans results in developmental arrest and increased life span*. *J Biol Chem*, 2001. **276**(34): p. 32240-6.
125. Rera, M., V. Monnier, and H. Tricoire, *Mitochondrial electron transport chain dysfunction during development does not extend lifespan in Drosophila melanogaster*. *Mech Ageing Dev*, 2010. **131**(2): p. 156-64.
126. Owusu-Ansah, E., W. Song, and N. Perrimon, *Muscle mitohormesis promotes longevity via systemic repression of insulin signaling*. *Cell*, 2013. **155**(3): p. 699-712.
127. Perez-Gomez, R., et al., *Downregulation of respiratory complex I mediates major signalling changes triggered by TOR activation*. *Sci Rep*, 2020. **10**(1): p. 4401.
128. Rera, M., et al., *Modulation of longevity and tissue homeostasis by the Drosophila PGC-1 homolog*. *Cell Metab*, 2011. **14**(5): p. 623-34.
129. Sanz, A., et al., *Expression of the yeast NADH dehydrogenase Ndi1 in Drosophila confers increased lifespan independently of dietary restriction*. *Proc Natl Acad Sci U S A*, 2010. **107**(20): p. 9105-10.
130. Bahadorani, S., et al., *Neuronal expression of a single-subunit yeast NADH-ubiquinone oxidoreductase (Ndi1) extends Drosophila lifespan*. *Aging Cell*, 2010. **9**(2): p. 191-202.

131. Cho, J., et al., *Expression of yeast NDI1 rescues a Drosophila complex I assembly defect*. PLoS One, 2012. **7**(11): p. e50644.
132. Hur, J.H., et al., *Increased longevity mediated by yeast NDI1 expression in Drosophila intestinal stem and progenitor cells*. Aging (Albany NY), 2013. **5**(9): p. 662-81.
133. Kruse, S.E., et al., *Mice with mitochondrial complex I deficiency develop a fatal encephalomyopathy*. Cell Metab, 2008. **7**(4): p. 312-20.
134. Canto, C., K.J. Menzies, and J. Auwerx, *NAD(+) Metabolism and the Control of Energy Homeostasis: A Balancing Act between Mitochondria and the Nucleus*. Cell Metab, 2015. **22**(1): p. 31-53.
135. Haigis, M.C. and D.A. Sinclair, *Mammalian sirtuins: biological insights and disease relevance*. Annu Rev Pathol, 2010. **5**: p. 253-95.
136. Satoh, A., et al., *Sirt1 extends life span and delays aging in mice through the regulation of Nk2 homeobox 1 in the DMH and LH*. Cell Metab, 2013. **18**(3): p. 416-30.
137. Gomes, A.P., et al., *Declining NAD(+) induces a pseudohypoxic state disrupting nuclear-mitochondrial communication during aging*. Cell, 2013. **155**(7): p. 1624-38.
138. Canto, C., et al., *The NAD(+) precursor nicotinamide riboside enhances oxidative metabolism and protects against high-fat diet-induced obesity*. Cell Metab, 2012. **15**(6): p. 838-47.
139. Trammell, S.A., et al., *Nicotinamide Riboside Opposes Type 2 Diabetes and Neuropathy in Mice*. Sci Rep, 2016. **6**: p. 26933.
140. Ryu, D., et al., *NAD+ repletion improves muscle function in muscular dystrophy and counters global PARylation*. Sci Transl Med, 2016. **8**(361): p. 361ra139.
141. Yoshino, J., et al., *Nicotinamide mononucleotide, a key NAD(+) intermediate, treats the pathophysiology of diet- and age-induced diabetes in mice*. Cell Metab, 2011. **14**(4): p. 528-36.
142. Zhang, H., et al., *NAD(+) repletion improves mitochondrial and stem cell function and enhances life span in mice*. Science, 2016. **352**(6292): p. 1436-43.
143. Mills, K.F., et al., *Long-Term Administration of Nicotinamide Mononucleotide Mitigates Age-Associated Physiological Decline in Mice*. Cell Metab, 2016. **24**(6): p. 795-806.
144. Mitchell, S.J., et al., *Nicotinamide Improves Aspects of Healthspan, but Not Lifespan, in Mice*. Cell Metab, 2018. **27**(3): p. 667-676 e4.
145. Zhou, C.C., et al., *Hepatic NAD(+) deficiency as a therapeutic target for non-alcoholic fatty liver disease in ageing*. Br J Pharmacol, 2016. **173**(15): p. 2352-68.
146. Mouchiroud, L., et al., *The NAD(+)/Sirtuin Pathway Modulates Longevity through Activation of Mitochondrial UPR and FOXO Signaling*. Cell, 2013. **154**(2): p. 430-41.
147. Durieux, J., S. Wolff, and A. Dillin, *The cell-non-autonomous nature of electron transport chain-mediated longevity*. Cell, 2011. **144**(1): p. 79-91.
148. D'Amico, D., V. Sorrentino, and J. Auwerx, *Cytosolic Proteostasis Networks of the Mitochondrial Stress Response*. Trends Biochem Sci, 2017. **42**(9): p. 712-725.
149. Kim, K.H., et al., *Autophagy deficiency leads to protection from obesity and insulin resistance by inducing Fgf21 as a mitokine*. Nat Med, 2013. **19**(1): p. 83-92.
150. Keipert, S., et al., *Skeletal muscle mitochondrial uncoupling drives endocrine cross-talk through the induction of FGF21 as a myokine*. Am J Physiol Endocrinol Metab, 2014. **306**(5): p. E469-82.
151. Chung, H.K., et al., *Growth differentiation factor 15 is a myomitokine governing systemic energy homeostasis*. J Cell Biol, 2017. **216**(1): p. 149-165.
152. Kim, E.K., et al., *Metformin ameliorates experimental-obesity-associated autoimmune arthritis by inducing FGF21 expression and brown adipocyte differentiation*. Exp Mol Med, 2018. **50**(1): p. e432.
153. Coll, A.P., et al., *GDF15 mediates the effects of metformin on body weight and energy balance*. Nature, 2020. **578**(7795): p. 444-448.
154. Labbadia, J., et al., *Mitochondrial Stress Restores the Heat Shock Response and Prevents Proteostasis Collapse during Aging*. Cell Rep, 2017. **21**(6): p. 1481-1494.
155. Ben-Zvi, A., E.A. Miller, and R.I. Morimoto, *Collapse of proteostasis represents an early molecular event in Caenorhabditis elegans aging*. Proc Natl Acad Sci U S A, 2009. **106**(35): p. 14914-9.

156. Bohensky, J., et al., *HIF-1 regulation of chondrocyte apoptosis: induction of the autophagic pathway*. Autophagy, 2007. **3**(3): p. 207-14.
157. Mehta, R., et al., *Proteasomal regulation of the hypoxic response modulates aging in C. elegans*. Science, 2009. **324**(5931): p. 1196-8.
158. Houtkooper, R.H., et al., *Mitochondrial protein imbalance as a conserved longevity mechanism*. Nature, 2013. **497**(7450): p. 451-7.
159. Bennett, C.F., et al., *Activation of the mitochondrial unfolded protein response does not predict longevity in Caenorhabditis elegans*. Nat Commun, 2014. **5**: p. 3483.
160. Anderson, R.M. and R. Weindruch, *Metabolic reprogramming, caloric restriction and aging*. Trends Endocrinol Metab, 2010. **21**(3): p. 134-41.
161. Colman, R.J., et al., *Caloric restriction delays disease onset and mortality in rhesus monkeys*. Science, 2009. **325**(5937): p. 201-4.
162. Pifferi, F., et al., *Promoting healthspan and lifespan with caloric restriction in primates*. Commun Biol, 2019. **2**: p. 107.
163. Most, J., et al., *Calorie restriction in humans: An update*. Ageing Res Rev, 2017. **39**: p. 36-45.
164. Schulz, T.J., et al., *Glucose restriction extends Caenorhabditis elegans life span by inducing mitochondrial respiration and increasing oxidative stress*. Cell Metab, 2007. **6**(4): p. 280-93.
165. Goodpaster, B.H., et al., *The loss of skeletal muscle strength, mass, and quality in older adults: the health, aging and body composition study*. J Gerontol A Biol Sci Med Sci, 2006. **61**(10): p. 1059-64.
166. Rowe, G.C., A. Safdar, and Z. Arany, *Running forward: new frontiers in endurance exercise biology*. Circulation, 2014. **129**(7): p. 798-810.
167. Willis, B.L., et al., *Midlife fitness and the development of chronic conditions in later life*. Arch Intern Med, 2012. **172**(17): p. 1333-40.
168. Chakravarty, E.F., et al., *Reduced disability and mortality among aging runners: a 21-year longitudinal study*. Arch Intern Med, 2008. **168**(15): p. 1638-46.
169. Safdar, A., et al., *Endurance exercise rescues progeroid aging and induces systemic mitochondrial rejuvenation in mtDNA mutator mice*. Proc Natl Acad Sci U S A, 2011. **108**(10): p. 4135-40.
170. Trigiani, L.J., et al., *Benefits of physical exercise on cognition and glial white matter pathology in a mouse model of vascular cognitive impairment and dementia*. Glia, 2020.
171. Cordeiro, A.V., et al., *Aerobic Exercise Training Induces the Mitochondrial Imbalance and UPRmt in the Skeletal Muscle of Aged Mice*. J Gerontol A Biol Sci Med Sci, 2020.
172. Zhao, Y., et al., *Lifelong treadmill training improves muscle function detected by a modified grip strength test during aging in BALB/c mice*. Life Sci, 2020. **251**: p. 117603.
173. Muhammad, M.H. and M.M. Allam, *Resveratrol and/or exercise training counteract aging-associated decline of physical endurance in aged mice; targeting mitochondrial biogenesis and function*. J Physiol Sci, 2018. **68**(5): p. 681-688.
174. Nilsson, M.I., et al., *Lifelong aerobic exercise protects against inflammaging and cancer*. PLoS One, 2019. **14**(1): p. e0210863.
175. Arany, Z., et al., *Transcriptional coactivator PGC-1 alpha controls the energy state and contractile function of cardiac muscle*. Cell Metab, 2005. **1**(4): p. 259-71.
176. Steiner, J.L., et al., *Exercise training increases mitochondrial biogenesis in the brain*. J Appl Physiol (1985), 2011. **111**(4): p. 1066-71.
177. Das, S., et al., *ATP citrate lyase improves mitochondrial function in skeletal muscle*. Cell Metab, 2015. **21**(6): p. 868-76.
178. Carey, B.W., et al., *Intracellular alpha-ketoglutarate maintains the pluripotency of embryonic stem cells*. Nature, 2015. **518**(7539): p. 413-6.
179. Bigarella, C.L., R. Liang, and S. Ghaffari, *Stem cells and the impact of ROS signaling*. Development, 2014. **141**(22): p. 4206-18.
180. Katajisto, P., et al., *Stem cells. Asymmetric apportioning of aged mitochondria between daughter cells is required for stemness*. Science, 2015. **348**(6232): p. 340-3.
181. Suda, T., K. Takubo, and G.L. Semenza, *Metabolic regulation of hematopoietic stem cells in the hypoxic niche*. Cell Stem Cell, 2011. **9**(4): p. 298-310.

182. Anso, E., et al., *The mitochondrial respiratory chain is essential for haematopoietic stem cell function*. Nat Cell Biol, 2017. **19**(6): p. 614-625.
183. Norddahl, G.L., et al., *Accumulating mitochondrial DNA mutations drive premature hematopoietic aging phenotypes distinct from physiological stem cell aging*. Cell Stem Cell, 2011. **8**(5): p. 499-510.
184. Ahlqvist, K.J., et al., *Somatic progenitor cell vulnerability to mitochondrial DNA mutagenesis underlies progeroid phenotypes in Polg mutator mice*. Cell Metab, 2012. **15**(1): p. 100-9.
185. Kumar, A., et al., *ADULT NEUROGENESIS IN HUMANS: A Review of Basic Concepts, History, Current Research, and Clinical Implications*. Innov Clin Neurosci, 2019. **16**(5-6): p. 30-37.
186. Sun, N., et al., *Measuring In Vivo Mitophagy*. Mol Cell, 2015. **60**(4): p. 685-96.
187. Beckervordersandforth, R., et al., *Role of Mitochondrial Metabolism in the Control of Early Lineage Progression and Aging Phenotypes in Adult Hippocampal Neurogenesis*. Neuron, 2017.
188. Zheng, X., et al., *Metabolic reprogramming during neuronal differentiation from aerobic glycolysis to neuronal oxidative phosphorylation*. Elife, 2016. **5**.
189. Stein, L.R. and S. Imai, *Specific ablation of Namp1 in adult neural stem cells recapitulates their functional defects during aging*. EMBO J, 2014. **33**(12): p. 1321-40.
190. Cabello-Rivera, D., et al., *Mitochondrial Complex I Function Is Essential for Neural Stem/Progenitor Cells Proliferation and Differentiation*. Front Neurosci, 2019. **13**: p. 664.
191. Ma, S., et al., *L2hgdh Deficiency Accumulates l-2-Hydroxyglutarate with Progressive Leukoencephalopathy and Neurodegeneration*. Mol Cell Biol, 2017. **37**(8).
192. Mehta, M.M., S.E. Weinberg, and N.S. Chandel, *Mitochondrial control of immunity: beyond ATP*. Nat Rev Immunol, 2017. **17**(10): p. 608-620.
193. Zhang, W., et al., *Lactate Is a Natural Suppressor of RLR Signaling by Targeting MAVS*. Cell, 2019. **178**(1): p. 176-189 e15.
194. Singer, B.D. and N.S. Chandel, *Immunometabolism of pro-repair cells*. J Clin Invest, 2019. **129**(7): p. 2597-2607.
195. Lam, W.Y., et al., *Mitochondrial Pyruvate Import Promotes Long-Term Survival of Antibody-Secreting Plasma Cells*. Immunity, 2016. **45**(1): p. 60-73.
196. Sena, L.A., et al., *Mitochondria are required for antigen-specific T cell activation through reactive oxygen species signaling*. Immunity, 2013. **38**(2): p. 225-36.
197. Weinberg, S.E., et al., *Mitochondrial complex III is essential for suppressive function of regulatory T cells*. Nature, 2019. **565**(7740): p. 495-499.
198. Area-Gomez, E., et al., *Mitochondria, OxPhos, and neurodegeneration: cells are not just running out of gas*. J Clin Invest, 2019. **129**(1): p. 34-45.
199. Formentini, L., et al., *In vivo inhibition of the mitochondrial H⁺-ATP synthase in neurons promotes metabolic preconditioning*. EMBO J, 2014. **33**(7): p. 762-78.
200. Belanger, M., I. Allaman, and P.J. Magistretti, *Brain energy metabolism: focus on astrocyte-neuron metabolic cooperation*. Cell Metab, 2011. **14**(6): p. 724-38.
201. Supplie, L.M., et al., *Respiration-deficient astrocytes survive as glycolytic cells in vivo*. J Neurosci, 2017.
202. Joshi, A.U., et al., *Fragmented mitochondria released from microglia trigger A1 astrocytic response and propagate inflammatory neurodegeneration*. Nat Neurosci, 2019. **22**(10): p. 1635-1648.
203. Peterson, C. and J.E. Goldman, *Alterations in calcium content and biochemical processes in cultured skin fibroblasts from aged and Alzheimer donors*. Proc Natl Acad Sci U S A, 1986. **83**(8): p. 2758-62.
204. Liang, W.S., et al., *Alzheimer's disease is associated with reduced expression of energy metabolism genes in posterior cingulate neurons*. Proc Natl Acad Sci U S A, 2008. **105**(11): p. 4441-6.
205. Blanch, M., et al., *Altered Mitochondrial DNA Methylation Pattern in Alzheimer Disease-Related Pathology and in Parkinson Disease*. Am J Pathol, 2016. **186**(2): p. 385-97.
206. Surmeier, D.J., *Determinants of dopaminergic neuron loss in Parkinson's disease*. FEBS J, 2018. **285**(19): p. 3657-3668.

207. Burbulla, L.F., et al., *Dopamine oxidation mediates mitochondrial and lysosomal dysfunction in Parkinson's disease*. Science, 2017. **357**(6357): p. 1255-1261.
208. Graves, S.M., et al., *Dopamine metabolism by a monoamine oxidase mitochondrial shuttle activates the electron transport chain*. Nat Neurosci, 2020. **23**(1): p. 15-20.
209. Hu, G., et al., *Type 2 diabetes and the risk of Parkinson's disease*. Diabetes Care, 2007. **30**(4): p. 842-7.
210. Arvanitakis, Z., et al., *Diabetes mellitus and risk of Alzheimer disease and decline in cognitive function*. Arch Neurol, 2004. **61**(5): p. 661-6.
211. Itzhaki, R.F., *Corroboration of a Major Role for Herpes Simplex Virus Type 1 in Alzheimer's Disease*. Front Aging Neurosci, 2018. **10**: p. 324.
212. Fahmy, A.M., et al., *Mitochondrial antigen presentation: a mechanism linking Parkinson's disease to autoimmunity*. Curr Opin Immunol, 2019. **58**: p. 31-37.
213. Matheoud, D., et al., *Intestinal infection triggers Parkinson's disease-like symptoms in Pink1(-/-) mice*. Nature, 2019. **571**(7766): p. 565-569.
214. Sliter, D.A., et al., *Parkin and PINK1 mitigate STING-induced inflammation*. Nature, 2018. **561**(7722): p. 258-262.
215. Gorman, G.S., et al., *Mitochondrial diseases*. Nat Rev Dis Primers, 2016. **2**: p. 16080.
216. DiMauro, S., et al., *The clinical maze of mitochondrial neurology*. Nat Rev Neurol, 2013. **9**(8): p. 429-44.
217. Leigh, D., *Subacute necrotizing encephalomyelopathy in an infant*. J Neurol Neurosurg Psychiatry, 1951. **14**(3): p. 216-21.
218. Lake, N.J., et al., *Leigh syndrome: neuropathology and pathogenesis*. J Neuropathol Exp Neurol, 2015. **74**(6): p. 482-92.
219. Budde, S.M., L.P. van den Heuvel, and J.A. Smeitink, *The human complex I NDUF54 subunit: from gene structure to function and pathology*. Mitochondrion, 2002. **2**(1-2): p. 109-15.
220. DiMauro, S. and M. Mancuso, *Mitochondrial diseases: therapeutic approaches*. Biosci Rep, 2007. **27**(1-3): p. 125-37.
221. Ortigoza-Escobar, J.D., et al., *Ndufs4 related Leigh syndrome: A case report and review of the literature*. Mitochondrion, 2016. **28**: p. 73-8.
222. Lamont, R.E., et al., *A novel NDUF54 frameshift mutation causes Leigh disease in the Hutterite population*. Am J Med Genet A, 2017. **173**(3): p. 596-600.
223. Leshinsky-Silver, E., et al., *NDUF54 mutations cause Leigh syndrome with predominant brainstem involvement*. Mol Genet Metab, 2009. **97**(3): p. 185-9.
224. Guaras, A.M. and J.A. Enriquez, *Building a Beautiful Beast: Mammalian Respiratory Complex I*. Cell Metab, 2017. **25**(1): p. 4-5.
225. Dieteren, C.E., et al., *Subunit-specific incorporation efficiency and kinetics in mitochondrial complex I homeostasis*. J Biol Chem, 2012. **287**(50): p. 41851-60.
226. De Rasmo, D., et al., *cAMP-dependent protein kinase regulates the mitochondrial import of the nuclear encoded NDUF54 subunit of complex I*. Cell Signal, 2008. **20**(5): p. 989-97.
227. Ogilvie, I., N.G. Kennaway, and E.A. Shoubridge, *A molecular chaperone for mitochondrial complex I assembly is mutated in a progressive encephalopathy*. J Clin Invest, 2005. **115**(10): p. 2784-92.
228. Kahlhofer, F., et al., *Accessory subunit NUYM (NDUF54) is required for stability of the electron input module and activity of mitochondrial complex I*. Biochim Biophys Acta, 2017. **1858**(2): p. 175-181.
229. Calvaruso, M.A., et al., *Mitochondrial complex III stabilizes complex I in the absence of NDUF54 to provide partial activity*. Hum Mol Genet, 2012. **21**(1): p. 115-20.
230. Ingraham, C.A., et al., *NDUF54: creation of a mouse model mimicking a Complex I disorder*. Mitochondrion, 2009. **9**(3): p. 204-10.
231. Leong, D.W., et al., *Proteomic and metabolomic analyses of mitochondrial complex I-deficient mouse model generated by spontaneous B2 short interspersed nuclear element (SINE) insertion into NADH dehydrogenase (ubiquinone) Fe-S protein 4 (Ndufs4) gene*. J Biol Chem, 2012. **287**(24): p. 20652-63.

232. Breuer, M.E., et al., *Cellular and animal models for mitochondrial complex I deficiency: a focus on the NDUF54 subunit*. IUBMB Life, 2013. **65**(3): p. 202-8.
233. Johnson, J., et al., *Deletion of the Complex I Subunit NDUF54 Adversely Modulates Cellular Differentiation*. Stem Cells Dev, 2016. **25**(3): p. 239-50.
234. Yokota, M., et al., *Mitochondrial respiratory dysfunction disturbs neuronal and cardiac lineage commitment of human iPSCs*. Cell Death Dis, 2017. **8**(1): p. e2551.
235. Bird, M.J., et al., *Neuronal and astrocyte dysfunction diverges from embryonic fibroblasts in the Ndufs4^{flky/flky} mouse*. Biosci Rep, 2014. **34**(6): p. e00151.
236. Valsecchi, F., et al., *Primary fibroblasts of NDUF54(-/-) mice display increased ROS levels and aberrant mitochondrial morphology*. Mitochondrion, 2013. **13**(5): p. 436-43.
237. Kayser, E.B., M.M. Sedensky, and P.G. Morgan, *Region-Specific Defects of Respiratory Capacities in the Ndufs4(KO) Mouse Brain*. PLoS One, 2016. **11**(1): p. e0148219.
238. Quintana, A., et al., *Fatal breathing dysfunction in a mouse model of Leigh syndrome*. J Clin Invest, 2012. **122**(7): p. 2359-68.
239. Schleifer, G., et al., *Impaired hypoxic pulmonary vasoconstriction in a mouse model of Leigh syndrome*. Am J Physiol Lung Cell Mol Physiol, 2019. **316**(2): p. L391-L399.
240. Bolea, I., et al., *Defined neuronal populations drive fatal phenotype in a mouse model of Leigh Syndrome*. Elife, 2019. **8**.
241. Chouchani, E.T., et al., *Complex I deficiency due to selective loss of Ndufs4 in the mouse heart results in severe hypertrophic cardiomyopathy*. PLoS One, 2014. **9**(4): p. e94157.
242. Yu, A.K., et al., *Mitochondrial complex I deficiency leads to inflammation and retinal ganglion cell death in the Ndufs4 mouse*. Hum Mol Genet, 2015. **24**(10): p. 2848-60.
243. Song, L., et al., *Bipolar cell reduction precedes retinal ganglion neuron loss in a complex 1 knockout mouse model*. Brain Res, 2017. **1657**: p. 232-244.
244. Yu, A.K., et al., *Rescue of cell death and inflammation of a mouse model of complex 1-mediated vision loss by repurposed drug molecules*. Hum Mol Genet, 2017. **26**(24): p. 4929-4936.
245. Gospe, S.M., 3rd, et al., *Photoreceptors in a mouse model of Leigh syndrome are capable of normal light-evoked signaling*. J Biol Chem, 2019. **294**(33): p. 12432-12443.
246. Quintana, A., et al., *Altered anesthetic sensitivity of mice lacking Ndufs4, a subunit of mitochondrial complex I*. PLoS One, 2012. **7**(8): p. e42904.
247. Ramadasan-Nair, R., et al., *Mitochondrial Function in Astrocytes Is Essential for Normal Emergence from Anesthesia in Mice*. Anesthesiology, 2019. **130**(3): p. 423-434.
248. Quintana, A., et al., *Complex I deficiency due to loss of Ndufs4 in the brain results in progressive encephalopathy resembling Leigh syndrome*. Proc Natl Acad Sci U S A, 2010. **107**(24): p. 10996-1001.
249. Choi, W.S., et al., *Conditional deletion of Ndufs4 in dopaminergic neurons promotes Parkinson's disease-like non-motor symptoms without loss of dopamine neurons*. Sci Rep, 2017. **7**: p. 44989.
250. Villela, D., et al., *Efficient detection of chromosome imbalances and single nucleotide variants using targeted sequencing in the clinical setting*. Eur J Med Genet, 2017. **60**(12): p. 667-674.
251. Civileto, G., et al., *Opa1 overexpression ameliorates the phenotype of two mitochondrial disease mouse models*. Cell Metab, 2015. **21**(6): p. 845-54.
252. Felici, R., et al., *PARP inhibition delays progression of mitochondrial encephalopathy in mice*. Neurotherapeutics, 2014. **11**(3): p. 651-64.
253. Lee, C.F., et al., *Targeting NAD(+) Metabolism as Interventions for Mitochondrial Disease*. Sci Rep, 2019. **9**(1): p. 3073.
254. Johnson, S.C., et al., *mTOR inhibition alleviates mitochondrial disease in a mouse model of Leigh syndrome*. Science, 2013. **342**(6165): p. 1524-8.
255. Johnson, S.C., et al., *Dose-dependent effects of mTOR inhibition on weight and mitochondrial disease in mice*. Front Genet, 2015. **6**: p. 247.
256. Felici, R., et al., *Post onset, oral rapamycin treatment delays development of mitochondrial encephalopathy only at supramaximal doses*. Neuropharmacology, 2017. **117**: p. 74-84.
257. Khan, N.A., et al., *mTORC1 Regulates Mitochondrial Integrated Stress Response and Mitochondrial Myopathy Progression*. Cell Metab, 2017. **26**(2): p. 419-428 e5.

258. Curatolo, P., et al., *mTOR dysregulation and tuberous sclerosis-related epilepsy*. Expert Rev Neurother, 2018. **18**(3): p. 185-201.
259. Jain, I.H., et al., *Hypoxia as a therapy for mitochondrial disease*. Science, 2016. **352**(6281): p. 54-61.
260. !!! INVALID CITATION !!! {Schleifer, 2019 #708}.
261. Jain, I.H., et al., *Leigh Syndrome Mouse Model Can Be Rescued by Interventions that Normalize Brain Hyperoxia, but Not HIF Activation*. Cell Metab, 2019. **30**(4): p. 824-832 e3.
262. Wood, L.D., et al., *The genomic landscapes of human breast and colorectal cancers*. Science, 2007. **318**(5853): p. 1108-13.
263. Waitkus, M.S., B.H. DiPlas, and H. Yan, *Biological Role and Therapeutic Potential of IDH Mutations in Cancer*. Cancer Cell, 2018. **34**(2): p. 186-195.
264. Parsons, D.W., et al., *An integrated genomic analysis of human glioblastoma multiforme*. Science, 2008. **321**(5897): p. 1807-12.
265. Chen, H., et al., *Mutant IDH1 and seizures in patients with glioma*. Neurology, 2017. **88**(19): p. 1805-1813.
266. Dang, L., et al., *Cancer-associated IDH1 mutations produce 2-hydroxyglutarate*. Nature, 2009. **462**(7274): p. 739-44.
267. Losman, J.A., et al., *(R)-2-hydroxyglutarate is sufficient to promote leukemogenesis and its effects are reversible*. Science, 2013. **339**(6127): p. 1621-5.
268. Koivunen, P., et al., *Transformation by the (R)-enantiomer of 2-hydroxyglutarate linked to EGLN activation*. Nature, 2012. **483**(7390): p. 484-8.
269. Shim, E.H., et al., *L-2-Hydroxyglutarate: an epigenetic modifier and putative oncometabolite in renal cancer*. Cancer Discov, 2014. **4**(11): p. 1290-8.
270. Shelar, S., et al., *Biochemical and Epigenetic Insights into L-2-Hydroxyglutarate, a Potential Therapeutic Target in Renal Cancer*. Clin Cancer Res, 2018. **24**(24): p. 6433-6446.
271. Li, H., et al., *Drosophila larvae synthesize the putative oncometabolite L-2-hydroxyglutarate during normal developmental growth*. Proc Natl Acad Sci U S A, 2017. **114**(6): p. 1353-1358.
272. Intlekofer, A.M., et al., *Hypoxia Induces Production of L-2-Hydroxyglutarate*. Cell Metab, 2015. **22**(2): p. 304-11.
273. Oldham, W.M., et al., *Hypoxia-Mediated Increases in L-2-hydroxyglutarate Coordinate the Metabolic Response to Reductive Stress*. Cell Metab, 2015. **22**(2): p. 291-303.
274. Intlekofer, A.M., et al., *L-2-Hydroxyglutarate production arises from noncanonical enzyme function at acidic pH*. Nat Chem Biol, 2017. **13**(5): p. 494-500.
275. Nadtochiy, S.M., et al., *Acidic pH Is a Metabolic Switch for 2-Hydroxyglutarate Generation and Signaling*. J Biol Chem, 2016. **291**(38): p. 20188-97.
276. Hariharan, V.A., et al., *The Enzymology of 2-Hydroxyglutarate, 2-Hydroxyglutaramate and 2-Hydroxysuccinamate and Their Relationship to Oncometabolites*. Biology (Basel), 2017. **6**(2).
277. Martinez-Reyes, I., et al., *TCA Cycle and Mitochondrial Membrane Potential Are Necessary for Diverse Biological Functions*. Mol Cell, 2016. **61**(2): p. 199-209.
278. Wegrzyn, A.B., et al., *Cofactors revisited - Predicting the impact of flavoprotein-related diseases on a genome scale*. Biochim Biophys Acta Mol Basis Dis, 2019. **1865**(2): p. 360-370.
279. Weil-Malherbe, H., *The oxidation of l(-)-alpha-hydroxyglutaric acid in animal tissues*. Biochem J, 1937. **31**(11): p. 2080-94.
280. Duran, M., et al., *L-2-Hydroxyglutaric aciduria: an inborn error of metabolism?* J Inherit Metab Dis, 1980. **3**(4): p. 109-12.
281. Jansen, G.A. and R.J. Wanders, *L-2-hydroxyglutarate dehydrogenase: identification of a novel enzyme activity in rat and human liver. Implications for L-2-hydroxyglutaric acidemia*. Biochim Biophys Acta, 1993. **1225**(1): p. 53-6.
282. Rzem, R., et al., *A gene encoding a putative FAD-dependent L-2-hydroxyglutarate dehydrogenase is mutated in L-2-hydroxyglutaric aciduria*. Proc Natl Acad Sci U S A, 2004. **101**(48): p. 16849-54.
283. Peng, W., et al., *Two novel L2HGDH mutations identified in a rare Chinese family with L-2-hydroxyglutaric aciduria*. BMC Med Genet, 2018. **19**(1): p. 167.

284. Steenweg, M.E., et al., *An overview of L-2-hydroxyglutarate dehydrogenase gene (L2HGDH) variants: a genotype-phenotype study*. Hum Mutat, 2010. **31**(4): p. 380-90.
285. Ullah, M.I., et al., *Identification of novel L2HGDH mutation in a large consanguineous Pakistani family- a case report*. BMC Med Genet, 2018. **19**(1): p. 25.
286. Muntau, A.C., et al., *Combined D-2- and L-2-hydroxyglutaric aciduria with neonatal onset encephalopathy: a third biochemical variant of 2-hydroxyglutaric aciduria?* Neuropediatrics, 2000. **31**(3): p. 137-40.
287. Lee, C., et al., *Hemiconvulsion-hemiplegia-epilepsy syndrome as a presenting feature of L-2-hydroxyglutaric aciduria*. J Child Neurol, 2006. **21**(6): p. 538-40.
288. Rzem, R., et al., *A mouse model of L-2-hydroxyglutaric aciduria, a disorder of metabolite repair*. PLoS One, 2015. **10**(3): p. e0119540.
289. Hunt, R.J., et al., *Mitochondrial stress causes neuronal dysfunction via an ATF4-dependent increase in L-2-hydroxyglutarate*. J Cell Biol, 2019.
290. Fernandez-Aguera, M.C., et al., *Oxygen Sensing by Arterial Chemoreceptors Depends on Mitochondrial Complex I Signaling*. Cell Metab, 2015. **22**(5): p. 825-37.
291. Lee, H.Y., et al., *Isolation and culture of post-natal mouse cerebellar granule neuron progenitor cells and neurons*. J Vis Exp, 2009(23).
292. Chong, J., et al., *MetaboAnalyst 4.0: towards more transparent and integrative metabolomics analysis*. Nucleic Acids Res, 2018. **46**(W1): p. W486-W494.
293. Bolger, A.M., M. Lohse, and B. Usadel, *Trimmomatic: a flexible trimmer for Illumina sequence data*. Bioinformatics, 2014. **30**(15): p. 2114-20.
294. Dobin, A., et al., *STAR: ultrafast universal RNA-seq aligner*. Bioinformatics, 2013. **29**(1): p. 15-21.
295. Anders, S., P.T. Pyl, and W. Huber, *HTSeq--a Python framework to work with high-throughput sequencing data*. Bioinformatics, 2015. **31**(2): p. 166-9.
296. Love, M.I., W. Huber, and S. Anders, *Moderated estimation of fold change and dispersion for RNA-seq data with DESeq2*. Genome Biol, 2014. **15**(12): p. 550.
297. Subramanian, A., et al., *Gene set enrichment analysis: a knowledge-based approach for interpreting genome-wide expression profiles*. Proc Natl Acad Sci U S A, 2005. **102**(43): p. 15545-50.
298. Merico, D., et al., *Enrichment map: a network-based method for gene-set enrichment visualization and interpretation*. PLoS One, 2010. **5**(11): p. e13984.
299. Dietzl, G., et al., *A genome-wide transgenic RNAi library for conditional gene inactivation in Drosophila*. Nature, 2007. **448**(7150): p. 151-6.
300. Weinberg, F., et al., *Mitochondrial metabolism and ROS generation are essential for Kras-mediated tumorigenicity*. Proc Natl Acad Sci U S A, 2010. **107**(19): p. 8788-93.
301. Petruzzella, V. and S. Papa, *Mutations in human nuclear genes encoding for subunits of mitochondrial respiratory complex I: the NDUF54 gene*. Gene, 2002. **286**(1): p. 149-54.
302. Quintana, A., et al., *Fatal breathing dysfunction in a mouse model of Leigh syndrome*. Journal of Clinical Investigation, 2012. **122**(7): p. 2359-2368.
303. Ferrari, M., et al., *Hypoxia treatment reverses neurodegenerative disease in a mouse model of Leigh syndrome*. Proc Natl Acad Sci U S A, 2017. **114**(21): p. E4241-E4250.
304. Lake, N.J., et al., *Leigh Syndrome: Neuropathology and Pathogenesis*. Journal of Neuropathology and Experimental Neurology, 2015. **74**(6): p. 482-492.

CURRICULUM VITAE: Greg McElroy

gregory.mcelroy@northwestern.edu

1800 W Roscoe St. Apt 534

Chicago, IL 60657

201-956-4127

EDUCATION

Northwestern: Feinberg School of Medicine MSTP: Chicago, IL *MD/PhD Student* 2014-2016
 2016 MSTP Heller Award for outstanding academic performance in Feinberg Preclinical Phase 1, Nutrition Club Chair of Academic Nutrition, Admissions Committee Member, Preclinical Curriculum Tutor. Graduate Coursework: Data Science, Carcinogenesis.
 Step 1 Score (2016): 261

Williams College: Williamstown, MA *Bachelor of Arts with Honors in Biology* GPA: 3.89 2008-2012
Academic Honors: Phi Beta Kappa, Sigma Xi, Magna Cum Laude, Honors in Biology
Selected Coursework: The Cell, The Organism, Ecology, Physiology, Animal Behavior, Psychology, Integrative Plant Biology, Genetics, Conservation Biology, Biochemistry, Organic Chemistry I and II, Foundations of Modern Chemical Science, Mechanics, Electromagnetism and Physics of Matter, Statistics and Data Analysis, Multivariable Calculus, Game Theory

RESEARCH EXPERIENCE

Feinberg School of Medicine: Department of Medicine, Division of Pulmonary and Critical Care 2016-
 Working towards dissertation in the laboratory of Navdeep Chandel studying regulation of hypoxic signaling pathways by mitochondria, the impact of mitochondrial dysfunction on aging and cancer, and the role of electron transport chain complex 1 function in the pathogenesis of Leigh Syndrome and other pathologic states of altered cellular metabolism including cancer metabolism and neurodegeneration.

Beth Israel Deaconess Medical Center: Departments of Endocrinology and GI 2013-2014
 Worked with Dr. Mark Herman (Assistant Professor of Medicine, Endocrinologist, Research Director of BIDMC Endocrinology Grand Rounds) and Dr. Sarah Flier (Instructor in Medicine, Gastroenterologist). Responsibilities included managing mouse colonies, metabolic studies, analyzing gene expression, assaying liver glycogen and triglyceride storage, allelic discrimination between SNPs near genes of interest, flow cytometry, cell culture, generation of murine macrophages from bone marrow, extracting murine splenocytes, and western blots.

Boston University Medical Center: Center for Regenerative Medicine, Pulmonary Center 2012
 Worked with Andrew Wilson, M.D. (Director of the Alpha-1 Center, Pulmonologist, Assistant Professor of Medicine). Responsibilities included culture of undifferentiated human iPS cells; directed differentiation of human iPS cells; cloning, preparation, and titering of lentivirus, and mouse surgeries, qPCR, ELISA, flow cytometry, cloning, and cell culture.

Field Research Assistant: Isle Royale National Park, Michigan Summer 2010
 Studied the mechanics of *Sphagnum* spore dispersal by vortex ring and behavior of pollinators on *Cornus canadensis* involving rapid plant movements for pollen dispersal with Professor Joan Edwards. Worked with Professor David Smith studying population genetics of chorus frog populations

Laboratory Research Assistant: Williamstown, Massachusetts, Banta laboratory Summer 2011
 Used PCR to amplify a gene sequence, "Overdrive" from *A. tumefaciens* that is known to interact with the protein VirC2. Used atomic force microscopy to analyze the specific binding topology of this interaction.

Honors Thesis in Biology: Advisor: Professor Lois Banta 2011-2012
 Studied the question of whether the type VI secretion system in *Agrobacterium tumefaciens* delivers effectors that dampen host defenses to increase bacterial virulence and if the type VI secretion system can be recognized by the plant to trigger a second wave of antimicrobial cellular defenses in plants.

TEACHING EXPERIENCE:

Teachers Assistant: Williamstown, MA, 2011
 TA for Ecology lab taught by Professor David Smith – Responsible for compilation, editing, and initial analysis of data collected by students in the field, also helped organize and run a lab section.
 TA for Northwestern graduate school introduction to grant writing course, responsible for leading small group discussion.

Teachers Assistant: Chicago, IL 2017
 TA for Northwestern graduate school introduction to grant writing course, responsible for leading small group discussion, and providing feedback on student grant ideas, organization and style.

PRISM Mentor: Chicago, IL 2018-2019
 Northwestern MSTP student organized outreach program (PRomoting Inner-city youth in Science and Medicine) served as a mentor along with other MSTP students with high-school aged students at the Pederson-McCormick Boys and Girls Club to teach an after-school organ-system, case-based curriculum on medicine and science to promote interest in these areas.

CONFERENCE POSTER PRESENTATIONS:

2018 Cell Symposium: Multifaceted Mitochondria 6/4/18
 2018 Child Neurology Society Annual meeting 10/15/18
 2019 Fusion Conferences: Metabolism in Health and Disease Conference 5/25/19
 2018-2019 intramural conferences: Lewis Landsberg Research Day, MSTP Department retreat, Pulmonary Division Lung Symposium

PUBLICATIONS:

Wilson AA, Kwok LW, Porter EL, Payne JG, **McElroy GS**, Ohle SJ, Greenhill SR, Blahna MT, Yamamoto K, Jean JC, Mizgerd JP, Kotton DN. (2013) Lentiviral Delivery of RNAi for In Vivo Lineage-Specific Modulation of Gene Expression in Mouse Lung Macrophages. *Mol Ther.* 2013 Feb 12. doi: 10.1038/mt.2013.19.

McElroy, G. S., & Chandel, N. S. (2017). Mitochondria control acute and chronic responses to hypoxia. *Exp Cell Res.* doi:10.1016/j.yexcr.2017.03.034

McElroy, G.S. and N.S. Chandel, *Probing mitochondrial metabolism in vivo*. Proc Natl Acad Sci U S A, 2019. 116(1): p. 20-22.

Hunt, R.J., Granat, L., **McElroy, G.S.**, Ranganathan, R., Chandel, N.S., and Bateman, J.M. *Mitochondrial stress causes neuronal dysfunction via an ATF4-dependent increase in L-2-hydroxyglutarate*. *J Cell Biol* (2019) 218 (12): 4007–4016. doi: 10.1083/jcb.201904148

In peer review or preprint:

Martínez-Reyes, I., Cardona, L.R., Kong, H., Werner, M., Kihshen, H., **McElroy, G.S.**, Vasan, K., Weinberg, S.E., Gao, P., Steinert, E., Piseaux, R., Budinger, G.R.S., and Chandel, N.S. *Mitochondrial ubiquinol oxidation is necessary for tumorigenesis*. In press accepted at Nature

McElroy, G.S. D. Mithal, C. Reczek, P. Reyfman, C. Horbinski, N. Chandel. *NAD⁺ regeneration rescues lifespan but not ataxia in a model of mammalian complex I dysfunction in the brain*. In revision.

Kong, H., Reczek, C., **McElroy, G.**, Steinert, E., Wang, T., Sabatini, D., Chandel, N. *Metabolic determinants of cellular fitness dependent on mitochondrial reactive oxygen species*. In peer review.

Romero-Morales, A., Rastogi, A. Temuri, H., Rasmussen, M., **McElroy, G.**, Hsu, L., Almoacid, P., Millis, B., Chandel, N., Cartailier, J., Gama, V. *Human iPSC-derived cerebral organoids model features of Leigh Syndrome and reveal abnormal corticogenesis*. In submission, pre-print available: bioRxiv 2020.04.21.054361; doi: <https://doi.org/10.1101/2020.04.21.054361>